AFOSR Scientific Report
AFOSR 70-1936TR

AD 711400

Project THEMIS

College of Engineering
UNIVERSITY OF UTAH
Salt Lake City, Utah

"1. This document has been approved for public release and sale; its distribution is unlimited."

THERMAL DECOMPOSITION OF HIGH-TEMPERATURE RESISTANT POLYMERS

N. W. Burningham
J. D. Seader

July 1970 UTEC TH 70-085

A Project THEMIS Program

sponsored by
the U. S. Air Force
Office of Scientific Research

Contract #F44620-68-C-0022

M. L. Williams
Project Manager

Department of Chemical Engineering
College of Engineering
University of Utah
Salt Lake City, Utah

ABSTRACT

During this research work, the thermal response of several test materials was characterized by isothermal and dynamic thermogravimetric analysis. Pyrolysis gas analysis, infrared spectra analysis and elemental analysis were employed also to formulate a description of the thermal-degradation reaction. A new, systematic approach to the determination from dynamic TGA data of kinetic parameters describing pyrolysis was developed.

The specific polymeric materials selected for evaluation in this program were chosen from those representing the forefront of high-temperature polymer technology. Samples of linear para-polyphenylene, polybenzimidazole, polyimide, phenylated polyquinoxaline and phenolic resins were tested.

In TGA experiments, material samples ranging in weight from 3 to 9 mg were heated in both flowing and non-flowing helium environments and changes in sample weight were detected by a Cahn automatic-recording electrobalance. Weight measurements were made with an average accuracy of ±0.0015 mg.

In separate experiments, gaseous products of isothermal decomposition were collected and analyzed by the techniques of gas chromatography. Pyrolysis gases were generated in a Vycor chamber and were swept by a steady-flowing helium stream to the gas-sampling inlet of a chromatograph. Thus the gases identified were correlated with the specific exposure times and temperatures of their generation.

Analyses of infrared spectra and elemental analysis of virgin polymer and char residues were combined to further illuminate thermal-decomposition reactions.

In order to overcome the limitations and inaccuracies of generally employed methods of TGA-data analysis, the quasilinearization numerical technique was introduced. This powerful analytical tool used data points directly and computed kinetic parameters based on a least-squares-optimized fit of the data. In this way, pyrolysis kinetic parameters were determined for polyphenylene, polyimide and polyquinoxaline. Similar parameters were not determined for phenolic and polybenzimidazole resins since the analytical method was not sufficiently developed to permit handling of their complex thermograms.

Phenolic polymer was found to have a pyrolysis temperature of about 360°C and to yield 57 percent char at 900°C when heated dynamically at 10°C/min. The gaseous decomposition products were primarily H_2O, H_2, CH_4 and CO. The pyrolysis reaction was reasonably well described by the mechanism of Parker and Winkler in which pendant phenyl groups were eliminated and coalescing structures produced the light gases.

Dynamic TGA tests for polyimide identified the pyrolysis temperature as 480°C and the char yield as 57 percent at 900°C. Polyimide decomposition produced CO and CO_2 as essentially the only products until temperatures became sufficiently high to fragment phenyl rings. At 597°C, CO, CO_2, CH_4, HCN and H_2 were observed. Thermal decay was initiated by scission within the imide ring followed by subsequent elimination of CO. Carbon dioxide resulted primarily from unreacted

polyamic acid groups. Pyrolysis of polyimide in both flowing and non-flowing helium was described by the same apparent kinetics.

Polyphenylene polymer was observed to decompose slowly in dynamic tests at temperatures below 550°C by the elimination of chlorine. At 700°C pyrolysis species were primarily H_2 and CH_4 evolved at a time-constant molar ratio of 9:1, which indicates constant rates of phenyl ring decomposition and dehydration. The char yield at 900°C was a high 82 percent.

Polyquinoxaline polymer decomposed with two major reaction zones at about 540°C and 690°C to yield 66 percent char at 900°C. Pyrolysis at 540°C produced primarily HCN, while at 700°C HCN, $(CN)_2$, CH_4 and H_2 were found. The isothermal decomposition reaction of this polymer went through an induction period during which the rate of weight loss increased. The mechanism was initiated by elimination of pendant phenyl groups followed by fragmentation of the heteroring.

Thermal decomposition of polybenzimidazole produced a complex thermogram with a pyrolysis temperature of 570°C and a char yield of 76 percent at 900°C. At low temperatures HCN, produced by scission and rearrangement in the heteroring, was the only major gas species evolved. At 700°C phenyl-ring fracture led to formation of CH_3NH_2, H_2, CH_4 as well as HCN.

TABLE OF CONTENTS

TABLE OF CONTENTS (continued)

LIST OF FIGURES

LIST OF FIGURES (continued)

LIST OF FIGURES (continued)

LIST OF FIGURES (continued)

LIST OF TABLES

LIST OF TABLES (continued)

CHAPTER I

INTRODUCTION AND OBJECTIVES

Background and Previous Work

With the advent of the aerospace industry, the engineering application of polymeric materials in high-temperature environments has received much attention. Such materials have been effectively used in severe thermal environments like those associated with re-entry heat shields and rocket-nozzle liners. The value of polymers in extreme-temperature conditions was found in their ability to block transfer of thermal energy to temperature-sensitive structures by the ablation process. Under less severe conditions, high-molecular-weight polymers maintained structural mechanical properties at moderately high temperatures, and extended the range of useful operation of many products.

Since the performance of the so-called "thermally-stable polymers" was of great interest, means of evaluation of their ablation properties were sought. Elucidation of char-forming and heat-blocking mechanisms led to the development of new materials having requisite properties for a particular application. Significant advances have been made in recent years in ablation technology by the formulation of new resin systems which are generally characterized by their highly aromatic or heterocyclic nature. Included in this group are the polyphenylenes, polyimides, polybenzimidazoles, polyimidazopyrolones, polyazomethenes, and polyquinoxalenes. Within these class types a large number of specific polymer formulations have been synthesized.

Initially, pure or filled polymers and reinforced composites

were tested in devices designed to simulate the actual environment of application. Over-all performance was the criterion of selection. However, this approach provided little insight into the mechanisms of the degradation process. Therefore, detailed mathematical models have been incorporated into digital computer programs to predict thermal response of materials and, thereby, to permit design optimization for engineering applications.

The attempt to describe the chemical kinetic phenomena occurring during ablation by means of mathematical models has been hindered by the need for values of kinetic parameters. Since this information is not available directly from theoretical considerations with any degree of accuracy, it must be determined for each material by appropriate experimental measurements. A number of laboratory techniques have been employed with success in ascertaining the necessary polymer-degradation properties. These include differential thermal analysis (DTA), thermogravimetric analysis (TGA), mass spectrometry, chromatography, infrared spectroscopy, and elemental analysis. Although the techniques listed have been used singly or in combinations to supply necessary degradation kinetic parameters, a more complete description of the mechanism of reaction requires additional detailed knowledge of the chemistry of the polymer and of the pyrolysis products.

Thermogravimetric analysis

Thermogravimetric analysis probably has been the most widely used experimental tool for the thermal evaluation of materials. It is a technique for continuously measuring and recording the weight of a material as a function of temperature or time. A plot of the resultant data is called a thermogram. Since weight is the primary

measurement made, the method is particularly suited to investigation of the reaction:

$$\text{polymer} \longrightarrow \text{gas} + \text{char residue.}$$

The objectives of TGA experimentation are the generation of thermograms from which a kinetic model can be formulated which describes the thermal decomposition, and the determination of polymeric thermal stability. TGA data are used in formulating and verifying postulated mechanisms of pyrolysis. Even though previous investigators have determined Arrhenius-type power-law rate equations from TGA data, few attempts have been made to correlate these equations with actual decomposition processes. Such a correlation may be made only if elementary reaction steps can be identified.

Madorsky[30] has pointed out that for a complete understanding of the mechanism involved in the thermal degradation of organic polymers, it is essential to know:

1. The change in molecular weight of a polymer as a function of temperature and extent of degradation;
2. The qualitative and quantitative composition of volatile and non-volatile products of degradation;
3. The rates and activation energies of the process.

It is not possible, usually, to obtain these experimental data from pyrolysis work. Compositions of volatile fractions can be obtained by chromatography and mass spectroscopy, and TGA can provide information on activation energies and kinetic rates of the processes involved. In addition, infrared spectra of char residues yield

additional insight into the sites of the degradation processes. Molecular weight determinations usually require solution techniques and residues obtained during pyrolysis, especially of aromatic heterocyclic polymers, are generally insoluble.

Thermogravimetric data have been obtained by two different methods. The dynamic TGA method produces a weight-temperature thermogram, or in some cases a weight-time thermogram for a programmed rate of temperature rise. Isothermal,or static,TGA yields weight data as a function of time at a constant temperature attained after a period during which the sample is rapidly heated. The dynamic method has been overwhelmingly the most popular in recent years because it generates data much more rapidly than the static method, and it requires a smaller quantity of sample to survey thermal response.

The successful utilization of dynamically-obtained thermograms is strongly dependent upon the accuracy of the data. Data scatter or inaccurate data reduction lead to errors which are generally amplified by common analysis procedures, and which may make kinetic-parameter calculations difficult or impossible. In addition, use of a single dynamic thermogram may not be sufficient. Significant changes in curvature of dynamic thermograms may be completely obscured by an inopportune choice of heating rate. Such errors usually result from heating rates which are too large. However, this phenomenon is completely relative, and a heating rate appropriate for one transition might obscure another. Nevertheless, dynamic measurements are still attractive in surveying rapidly the complete thermal behavior, and results yield, among other things, information as to regions which

might be studied dynamically at lower heating rates or by the isothermal method.

Thermogravimetric measurements are subject to errors which have been discussed at length by other authors [15, 36, 38]. Many possible errors have been avoided in the present work by choice of equipment and experimental procedures. Those errors remaining arise generally from convection, flow currents, temperature measurement, the effect of atmosphere, and changes in buoyancy.

Thermograms, especially those dynamically obtained, have been used as qualitative measures of the relative thermal stability of polymers. However, the extraction of kinetic parameters from either type of thermogram is subject to several limitations and sources of error. The dynamic method seems to be adequate for elementary degradation mechanisms, but a successful analysis of complex mechanisms may require use of both methods. Seader [43] has shown the value of combining the methods in the case of the autocatalytic-type decomposition of polystyrene.

The general nature of thermograms may be illustrated by briefly considering several examples. If the degradation process is a simple, irreversible reaction, then the rate may be described by a power-law function:

$$-\frac{1}{w_o}\frac{dw}{dt} = k\left[\frac{w - w_R}{w_o}\right]^n \tag{1.1}$$

or

$$-\frac{dW}{dt} = k\,W^n\,, \tag{1.2}$$

where

w = instantaneous weight of sample during the degradation process,

w_o = initial weight of sample,

w_R = final weight of the residue upon completion of reaction,

$W = W = (w - w_R)/w_o$

t = time,

n = kinetic order of reaction,

k = specific rate constant.

The reaction rate constant, k, may depend on the absolute temperature according to the Arrhenius law:

$$k = A\, e^{-E/RT}, \tag{1.3}$$

where

A = pre-exponential factor,

E = activation energy,

R = universal gas constant,

T = absolute temperature.

Thermal degradation of Teflon 5, polytetrafluoroethylene, seems to be adequately described by Equations 1.2 and 1.3. Calculated dynamic thermograms for this material for linear temperature-time heating rates of 5, 50°C, and 50,000°C per minute are shown in Figure 1. As the heating rate is increased, the degradation process occurs predominantly at higher temperatures and the thermograms become less steep. For power-law degradations with lower activation energies and/or higher kinetic orders, thermogram slope is also decreased.

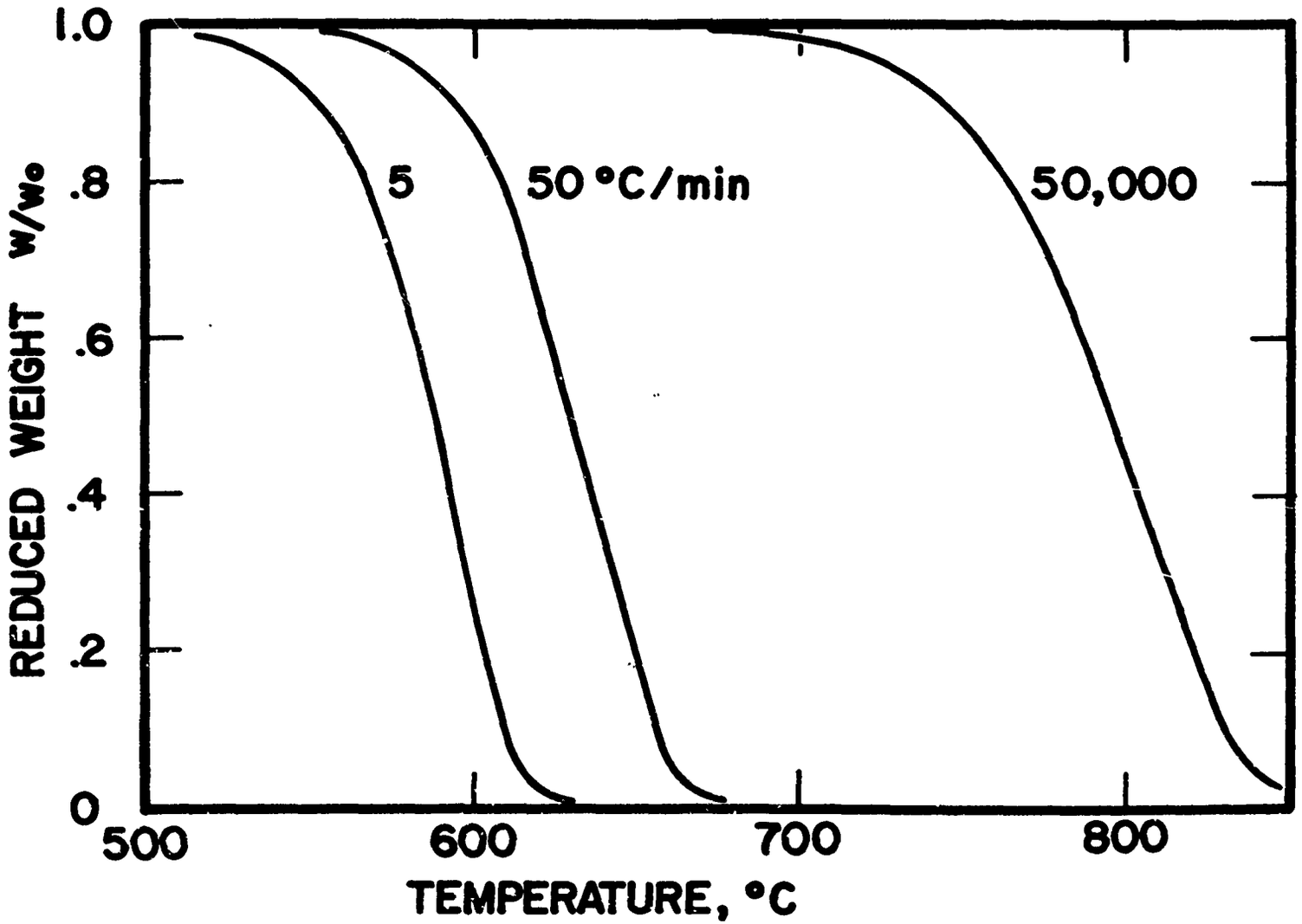

FIGURE 1. Computed Dynamic Thermograms for Teflon

Calculated isothermal thermograms for Teflon 5, shown in Figure 2, exhibit a monotonic decrease in weight as a function of time. In each case a heating rate of 50°C per minute was utilized until attainment of the isothermal temperature. A relatively small amount of weight loss occurred during the heat-up period.

The thermal degradations of many materials are not adequately described by the simple kinetic model of Equations 1.2 and 1.3. Polystyrene has been shown to decompose by an autocatalytic-type mechanism. For this polymer the rate of degradation at a given temperature passes through a maximum. While dynamic thermograms are very similar in nature to those of Teflon, the slopes of isothermal thermograms first increase and then decrease. Thus, static TGA thermograms clearly show the autocatalytic-type nature of the reaction, while dynamic experiments do not. Even though an autocatalytic-type dynamic thermogram may be fitted by a power-law model, the values of kinetic parameters obtained may bear little relation to the actual chemical processes.

A further complex degradation process, not well described by a single power-law model, is a reaction in which the polymer appears to degrade in two or more obvious steps, as detected from a dynamically-obtained thermogram. A fraction of the sample may pyrolyze by an apparent power-law rate function at lower temperatures, with the remainder of the sample pyrolyzing by a seemingly different and independent power-law rate function at higher temperatures. Since there are several chemical reactions proceeding simultaneously, no single rate expression could appropriately account for them, except to consider only a gross average of properties. Phenolic resins are examples

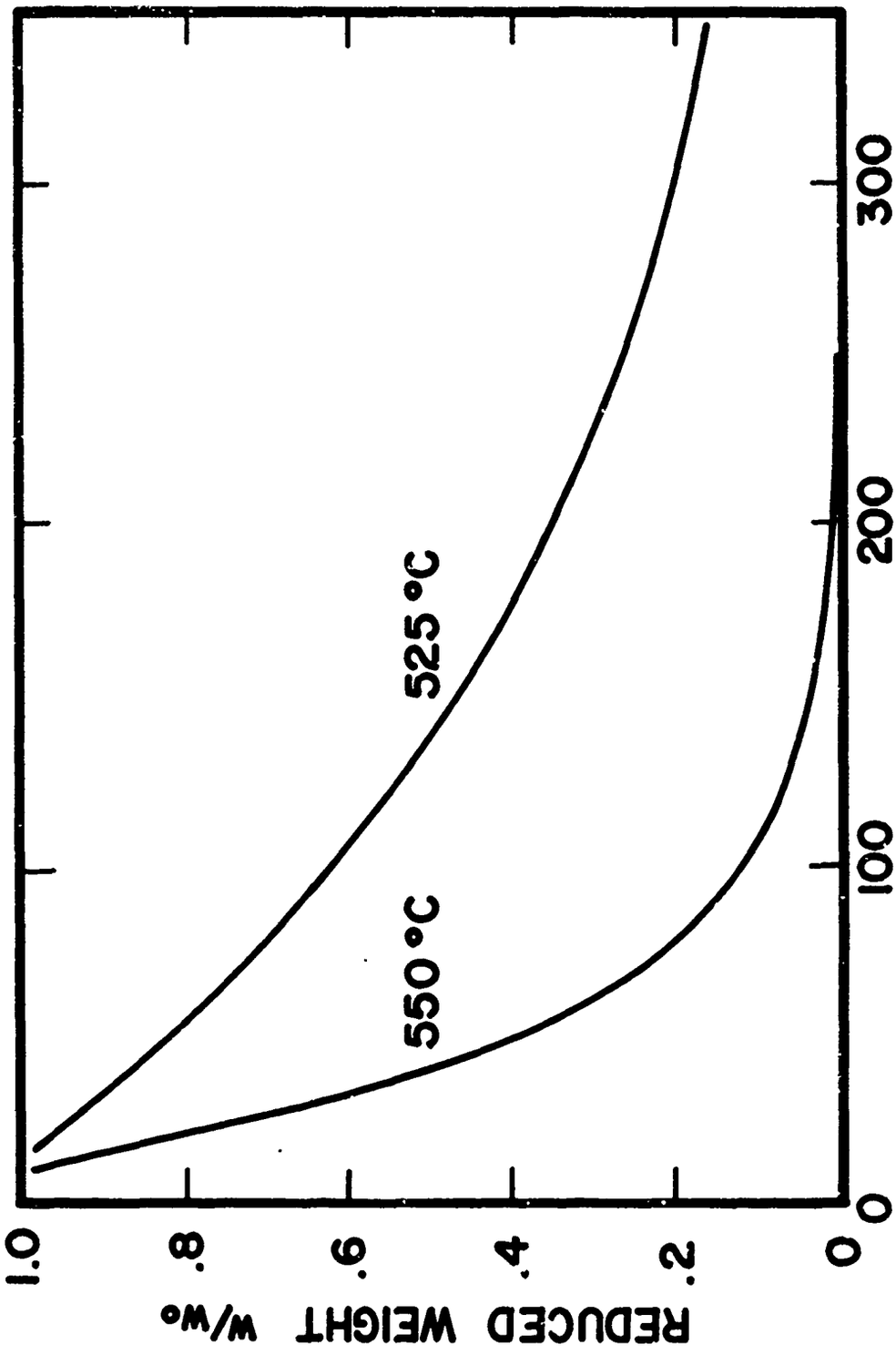

FIGURE 2. Computed Isothermal Thermograms for Teflon

of materials which decompose by at least two different reactions. Attempts to describe the pyrolysis of this material with a single power-law rate expression have been less than successful. Also, kinetic parameters obtained assuming a single rate law have no obvious connection with the physical meanings normally associated with them.

Recently some investigators have used rate laws of the form of Equations 1.2 and 1.3 but have applied them separately to the major reactions observed. Goldstein has fitted data for CTL 91-LD phenolic resin by assuming two independent rate laws[20]. Then,

$$-\frac{dW}{dt} = -\frac{dW_1}{dt} - \frac{dW_2}{dt} = k_1 W_1^{n_1} + k_2 W_2^{n_2} \qquad (1.4)$$

where

$$k_i = A_i e^{-E_i/RT}, \quad i = 1, 2;$$

$$W_i = \frac{w_i - w_{i,R}}{w_{o,i}}, \quad i = 1, 2.$$

After determination of kinetic parameters by this approach, Goldstein was able to predict weight-loss curves with greatly increased accuracy. Kratch and co-workers have extended the idea of multiple applications of a simple rate law to include a description of phenolic pyrolysis by three reaction mechanisms [27].

Dynamic thermograms have been computed from Goldstein's results and are shown in Figure 3 [43]. The two reaction steps are most evident for the lowest heating rate. A trend towards a less obvious distinction between the two reaction steps is apparent as heating rate is increased. The lower heating rate permits sufficient time for the first step to reach near completion before the second step begins.

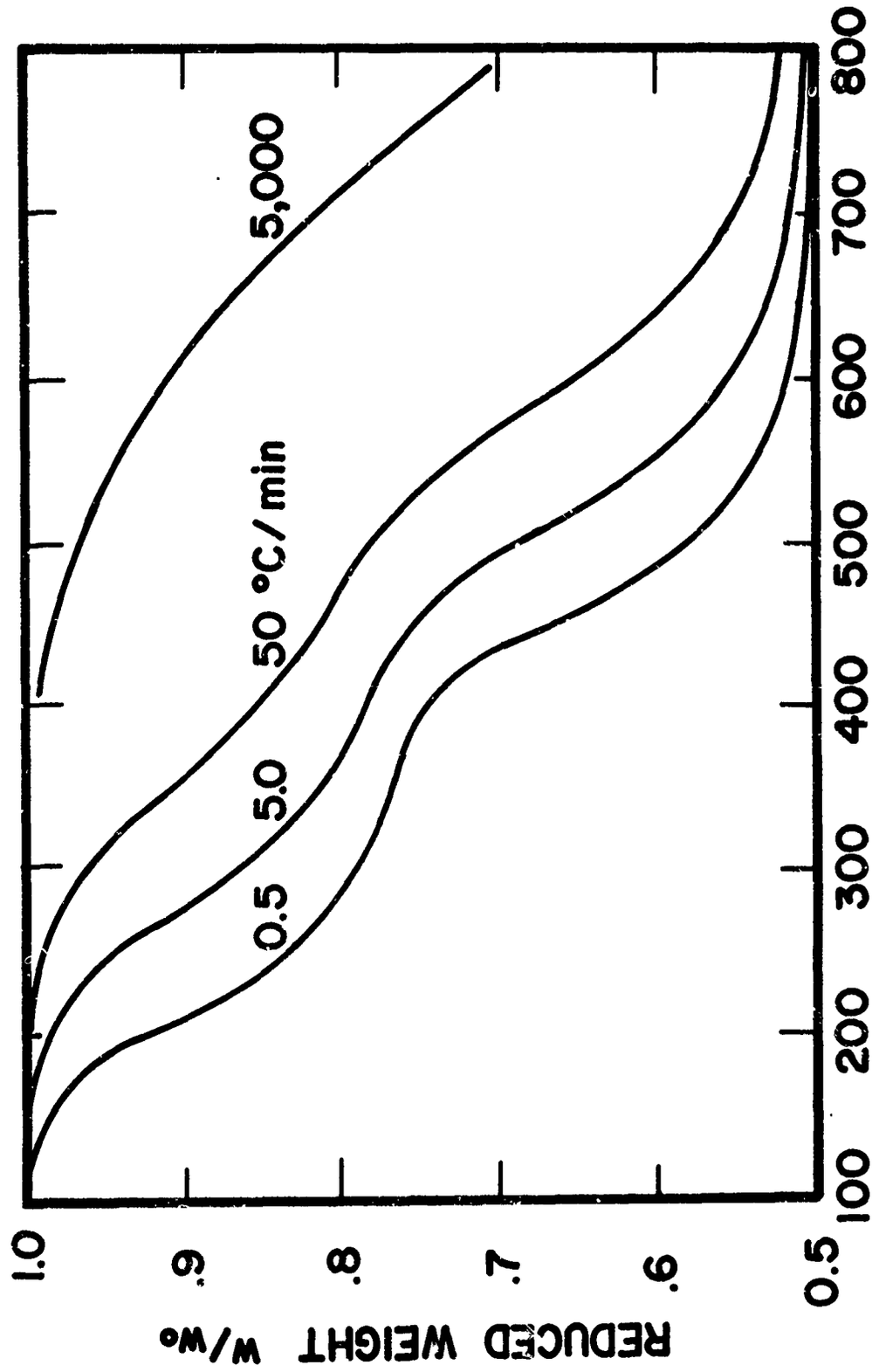

FIGURE 3. Computed Dynamic Thermograms for Phenolic

At the higher heating rate of 5000°C per minute, which is more typical of ablation applications, the predicted TGA curve is again shifted towards higher temperatures and the two reaction steps are not distinguishable. In those cases for which the multiple reaction zones are reasonably separated, both low-heating-rate dynamic experiments and isothermal experiments may be combined to yield kinetic parameters for each separate step.

Question has been raised as to the validity of the use of thermogravimetric data to describe ablation reactions. Thermogravimetric analysis does provide a means for conducting the pyrolysis reaction in an inert environment which simulates actual degradation conditions. Also, the TGA method provides programmed heating yielding a char and permitting volatile products to escape at pyrolysis temperatures with essentially no secondary cracking. Hence it provides a direct measure of primary char formation.

The essential difference between TGA experiments and the actual ablation application is the rate of heating. In usual TGA experiments temperature rise rates are on the order of 1°C to 30°C per minute, while in actual ablation applications rates of temperature rise of 5000°C to 50,000°C per minute can be encountered. As shown in Figure 3, high heating rates can significantly alter the shape of a characteristic thermogram. In addition, some evidence has been presented indicating that for solid rocket propellants, variations in heating rates may alter propellant thermal response [11]. Some authors, therefore, have concluded that TGA data, and kinetic parameters derived therefrom, have no direct connection to material responses in normal ablative

conditions.

Melnick and Nolan [35] have developed a TGA apparatus capable of very high heating rates. They have compared kinetic parameters, assuming a single chemical reaction, obtained at customary TGA heating rates, with those obtained in their high-heating-rate system. Large disagreements in the compared values led them to conclude that no correlation existed between the two types of data and that the normal, low-heating-rate test technique was invalid. However, in reaching this conclusion the authors committed several vital errors which are believed to negate their conclusions.

First, they failed to recognize that several distinct chemical reactions occurred whose cumulative effect was represented in their thermogram. Of particular significance for their tested material, a molded nylon-phenolic composite, was the fact that each of the two constituents decompose essentially independently of the other and over different temperature ranges. Furthermore, the phenolic constituent decomposes by at least two different types of reactions. The authors next compared data from a high-heating-rate, short-duration test, for which it is very unlikely that the sample temperature was either uniform or equal to the programmed temperature, to results of a low-heating-rate, extended-duration test. The tests were compared on the basis of the programmed, not measured temperature. The high-heating-rate test, therefore, strongly emphasized the early portion of the thermogram, giving overwhelming predominance to early reactions. Such reactions may have radically different kinetic parameters than those which describe the effective over-all reaction and represent the entire

thermogram.

On the other hand, other authors have concluded the equivalence of high- and low-heating-rate tests. Parker and Winkler [40] tested a variety of phenolic resins and determined char yields for heat fluxes up to 25 cal/cm^2-sec . They observed that the char yields were essentially the same as those for TGA experiments. It was, therefore, tentatively concluded that primary char-forming processes for phenolics are independent of polymer heating rate for temperature-rise rates from 2°C to 5000°C per minute. However, this significant conclusion is not completely justified by the experimental evidence. While the formation of equal amounts of char is an important observation of great practical value, the final amount of char material formed is not a sufficient measurement or indication of the specific kinetic processes which occurred. It is certainly conceptually possible for the reaction mechanisms to vary and still yield approximately the same amount of char.

As a further complication in isolating heating-rate effects, it must be noted that the kinetics of thermal degradation are strongly affected by the nature of the environment and by the chemical nature of the polymer itself. Thus, it may be difficult, if not impossible, to generalize on the basis of tests on a single or even several polymers. This would particularly be the case for an extrapolation to a fundamentally different chemical structure. Whether or not kinetic mechanisms and rate laws established from TGA experiments are still valid under other conditions is still open to question and discussion.

Kinetic analysis of TGA data

The mathematical analysis of experimental TGA data for the purpose of determining the kinetic parameters of a suitable reaction-rate equation has been the subject of many papers and review articles [15, 12].

The analysis of isothermal TGA thermograms can be carried out by conventional and well-established methods of handling isothermal kinetic data. Ordinarily, integration methods can be used to test assumed power-law rate functions by determining the constancy of the specific rate constant over a suitable range of degradation.

Differential methods utilized with isothermal data have the advantage of determining the reaction order directly when a power-law rate function applies. However, graphically- or numerically-determined slopes are required which cannot always be obtained with sufficient accuracy. Careful consideration must be given to the initial heat-up period when the extent of reaction during this period is not negligible. Values of the activation energy and the pre-exponential factor are determined from several isotherms by plotting the logarithm of the individual values of the determined specific rate constants against the reciprocal temperature.

When the postulated rate function is not readily integrable and/or when it is desired to examine a general rate law of unspecified order, then the recent quasilinearization procedure of Bellman et al. [3] may be of interest. When implemented on a high-speed digital computer, this method utilizes data points directly from the thermogram and applies the method of least squares to obtain a set of kinetic

parameters which best fit the data. Disadvantages of the method include the necessity of supplying initial guesses for the kinetic parameters and the lack of guarantee of convergence. The application of this method is discussed in detail in Chapter V.

Since the initial analytical treatment of dynamic TGA data by van Krevelen, van Heerden, and Huntjens [46] in 1951, a number of papers have been published giving recommended mathematical procedures for determining the kinetic parameters. In general, the methods are more tedious and more uncertain than the methods used with static TGA. Nevertheless, the ability to obtain dynamic TGA data conveniently and rapidly over a wide temperature range has greatly popularized the dynamic technique and corresponding data-analysis methods. The proposed dynamic data-analysis methods may be divided into two groups: those based on a single dynamic thermogram and those based on more than one thermogram (often three). A more common classification, used often in the literature, distinguishes between integral, differential, and difference-differential techniques.

Freeman-Carroll Method

Perhaps the most widely-used method of determining kinetic parameters from a single dynamic TGA thermogram is the difference-differential method of Freeman and Carroll. It can be applied in several different ways, one important modification being that of Anderson and Freeman[1].

One method of application is derived as follows:

It is assumed that the degradation follows the single power-law rate function given by Equation 1.3. A series of operations can be performed on this equation to eliminate the pre-exponential factor, A.

The resulting equation should, when plotted, yield a straight line having an intercept and slope which are related to E and n. The logarithm of Equation 1.3 is taken to obtain

$$\log \left(-\frac{dW}{dT}\right) = n \log W - \frac{E}{2.3\ RT} + \log \frac{A}{\rho} . \tag{1.5}$$

If the derivative with respect to 1/T is taken, the term in A is eliminated to give

$$\frac{d\left(\log \left(-\frac{dW}{dT}\right)\right)}{d\left(\frac{1}{T}\right)} = n \frac{d(\log W)}{d\left(\frac{1}{T}\right)} - \frac{E}{2.3\ R} . \tag{1.6}$$

This equation is readily converted to a difference form suitable for plotting as a straight line:

$$\Delta \left(\log \left(-\frac{dW}{dT}\right)\right) = n\ \Delta (\log W) - \frac{E}{2.3\ R}\ \Delta \left(\frac{1}{T}\right) . \tag{1.7}$$

This equation is applied as follows. From a single dynamic thermogram, such as that shown in Figure 1, slopes of - dW/dT are obtained from graphical, numerical, or other means of differentiation. Then a plot or a table is constructed for values of log (- dW/dT) and log W at corresponding values of 1/T. Successive increments of these two logarithmic quantities are taken at equally-spaced increments of 1/T and plotted as Δ [log (-dW/dT)] vs. Δ (log W). The line passing through the points should be straight if the data are sufficiently accurate and if the power-law rate function applies as initially assumed. The slope of the line is n, and the activation energy can be evaluated from the intercept as

$$E = \frac{2.3\ R}{\Delta\left(\frac{1}{T}\right)}\ \text{x intercept.} \tag{1.8}$$

The pre-exponential factor, A, can be obtained by plotting Equation 1.5 as [log (-dW/dT) - n log W] vs. 1/T. The intercept allows the determination of A from

$$\frac{A}{\rho} = 10^{\text{intercept}}. \tag{1.9}$$

The major disadvantage of the Freeman-Carroll method lies in the need to assume the power-law form for the rate expression. Thus, the order, n, and the activation energy, E, determined may be only empirical constants which best fit the data. In addition, the accuracy of the method is impaired by the need to differentiate twice.

Friedman method

The differential method of Friedman [17], as applied to several thermograms obtained at different heating rates, has received some attention. Initially, the degradation law is stated in terms of an uncommitted concentration function, where the heating rate is grouped with the degradation rate:

$$-\rho \frac{dW}{dT} = A e^{-E/RT} f(W). \tag{1.10}$$

As with the Freeman-Carroll method, the logarithm of the rate equation is taken to give

$$\log \left(-\rho \frac{dW}{dt}\right) = -\frac{E}{RT} + \log [A f(W)]. \tag{1.11}$$

The assumption is then made that the concentration function, f(W), depends only on W and not on temperature. A sequence of values of W is chosen. For each W value and for each thermogram (ρ value), the slope dW/dT is determined. By plotting log (- ρ dW/dT) vs. 1/T with

a parameter of W, lines having slopes of -E/(2.3 R) are obtained. For a single degradation mechanism covering the range of temperature, all lines would have the same activation energy. Because no concentration function has been specified, the activation energy so determined is likely to be of kinetic significance. This figure also gives a family of intercepts, log [A f(W)], for the parametric W values. Thus, by postulating various concentration functions, the remaining kinetic parameters may be determined. For example, if a power-law function is assumed,

$$\log [A\, f(W)] = \log [A\, W^n] \,, \tag{1.12}$$

or

$$\log [A\, f(W)] = n \log W + \log A \,. \tag{1.13}$$

Thus, a plot of log [A f(W)] vs. log W would test this assumed function, and if applicable, permit the determination of the reaction order from the slope and the pre-exponential factor from the intercept.

Although the Friedman method requires several thermograms covering a range of heating rates, it is capable of determining more meaningful values of the activation energy than other commonly-used methods. However, it is still assumed that a single reaction takes place, and that the reaction is unaffected by changes in heating rate. Also, like the Freeman-Carroll method, it suffers from the necessity of determining slopes from the thermograms.

Ozawa method [39].

The recent integral method of Ozawa [39], which also utilizes

several dynamic thermograms, appears to be convenient to apply. It does not involve the inherent inaccuracy of taking slopes. Like the Friedman method, the activation energy is determined without postulating the form of the concentration function. Equation 1C is first put in integral form:

$$-\int_0^W \frac{dW}{f(W)} = \frac{A}{\rho}\int_{T_0}^{T} e^{-E/RT}\,dT \cong \frac{A}{\rho}\int_0^T e^{-E/RT}\,dT \qquad (1.14)$$

However, if $E/RT > 20$, the Doyle approximation [39] gives

$$p\left(\frac{E}{RT}\right) = \int_0^T e^{-E/RT}\,dT \simeq \frac{E}{R}\left[10 - 2.315 + 0.457\,\frac{E}{RT}\right]. \qquad (1.15$$

Substituting Equation 1.15 into Equation 1.14 taking the logarithm of both sides, and rearranging the result yields

$$\log \rho = 0.457\,\frac{E}{RT} - 2.315 + \log\left(\frac{AE}{R}\right) - \log\left(\int_0^W \frac{dW}{f(W)}\right). \qquad (1.16)$$

Thus, if values of T are read from several thermograms of different ρ for fixed values of W and plotted as $\log \rho$ vs. $1/T$ with a parameter of W, an activation energy may be obtained from the slope, $0.457\,E/R$, of each line.

Ozawa also presents master curves for both power-law and autocatalytic-type rate functions which assist in rapidly determining the nature of f(W). For example, Figure 4 shows such master curves for

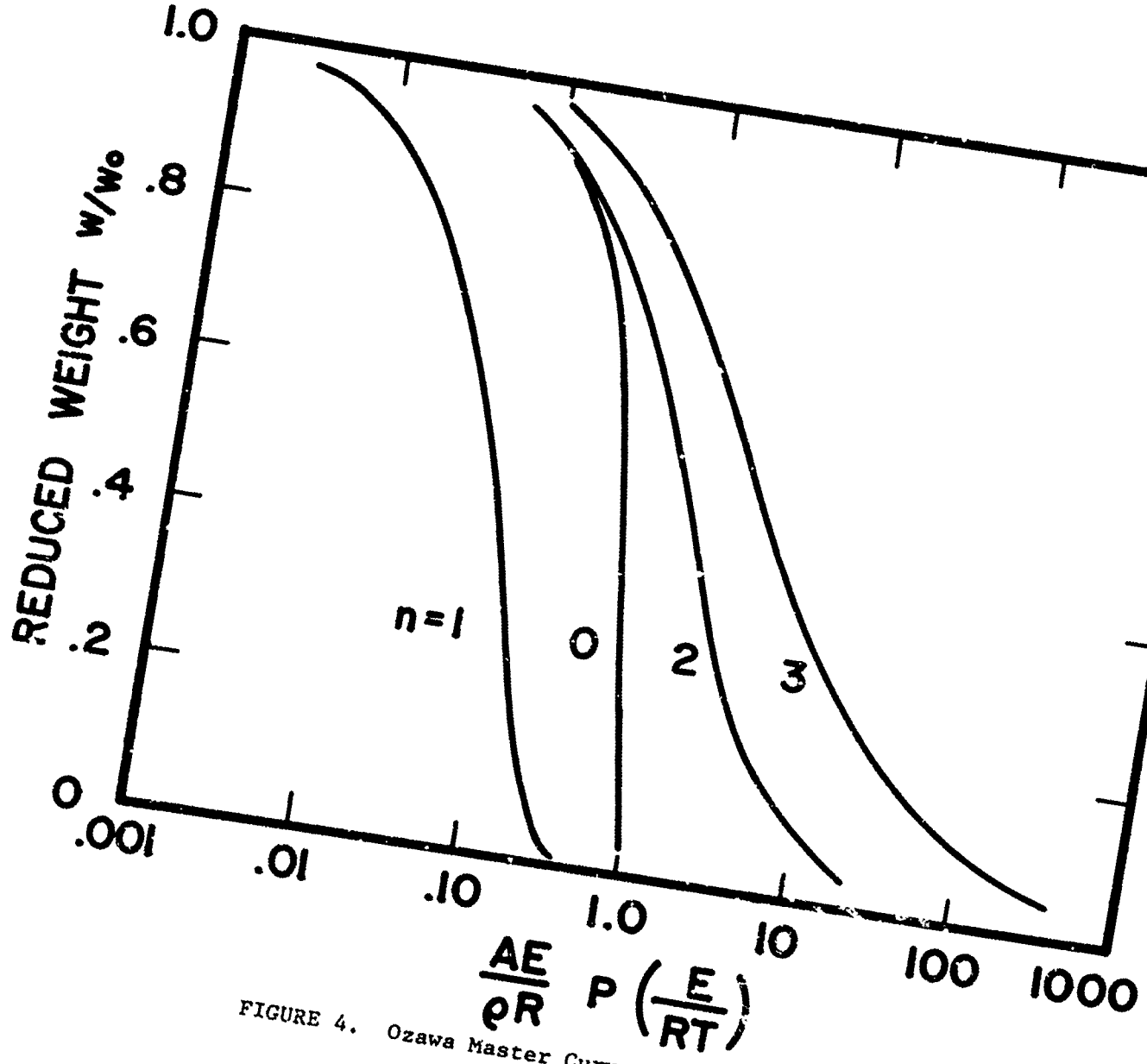

FIGURE 4. Ozawa Master Curves for Kinetic Analysis

zero- to third-order power-law expressions that are based on integrated solutions to Equation 1.14. For example, the zero-order curve is based on the equation,

$$W \cong - \frac{AE}{\rho R} \; p(\frac{E}{RT}) . \tag{1.17}$$

From the value of E, determined as described above, a plot of W vs. log [(E/ρR) p(E/RT)] is made. Superposition of the appropriate master curve permits the computation of A.

Objectives

In light of the foregoing discussion, particularly with reference to the difficulties of thermal analysis, one of the primary objectives of the work reported in this thesis was the generation of reliable TGA data. This required that the problems of the experimental technique be carefully considered and then minimized wherever possible. Part of this objective included the selection, purchase, and assembly of equipment requisite to obtaining accurate TGA measurements. It was intended to characterize the thermal response of several test materials by isothermal and dynamic thermogravimetric analysis and to calculate kinetic parameters for the pyrolysis reaction.

The specific polymeric materials selected for evaluation in this program were chosen from the many possible candidates representing the forefront of high-temperature polymer technology. Samples of polyphenylene, polybenzimidazole, polyimide, polyquinoxaline and phenolic resins were tested. Each of these resins has great potential for use in high-temperature environments. The specific polymers

tested also represent a broad spectrum of chemical types.

A second speciiic goal was the development of a new, systematic approach to the determination of kinetic parameters which avoids the difficulties inherent in the normal techniques previously discussed. The numerical method of quasilinearization appeared to have the desired potential, and the formulation of an approach for its application to dynamic TGA data became a program objective.

Under special circumstances, information derived from TGA experiments may bear a direct relationship to the kinetic mechanism of thermal decomposition. Although generally this relationship is obscured by the complex nature of the decomposition reaction, added information can sometimes be obtained from an analysis of the volatile products of pyrolysis. For this reason, chromatographic gas analysis was included in the program with the anticipation that such information would further illuminate the decomposition reaction.

In addition to chromatography, analysis of infrared spectra and elemental analysis of polymers and char residues helps to characterize pyrolysis reactions by identifying the relative amounts of atomic species and the types of existing molecular bonds. Even though the IR spectra of most high-temperature polymers is very complex, distinguishing structural features can often be observed and followed through the course of a reaction. Infrared analysis and elemental analysis were, therefore, included where desirable.

In summary, the objectives of this thesis project were to characterize the thermal decomposition of selected high-temperature polymers by thermogravimetric analysis, and to provide an engineer-

ing description of the pyrolysis reaction by application of the numerical method of quasilinearization for the determination of kinetic parameters. The results obtained are directly useful in predicting thermal response for environments causing ablation.

CHAPTER II

EQUIPMENT CAPABILITIES AND FUNCTIONS

The equipment components used to obtain the experimental results reported in this thesis are described in the following chapter. The capabilities, as well as the limitations of the equipment, strongly influenced the type and quality of data produced. Therefore, the function of each major component is discussed with emphasis on the primary experimental tool, thermogravimetric analysis.

The items of equipment used in TGA experimentation were a Cahn Electrobalance which measured sample weight; a Marshall tubular furnace which provided heat for thermal degradation of samples; an F & M Scientific Company temperature programmer which controlled furnace temperature; a Mosely X-Y plotter used to record sample weight as a function of time; and a Leeds and Northrup Speedomax W stripchart recorder which records sample temperature as a function of time. Figure 5 shows these items.

Gas analysis experiments were conducted with a tubular, Vycor, pyrolysis chamber mounted horizontally in the Marshall furnace. Evolved gases were analyzed in a Perkin-Elmer Model 154 Vapor Fractometer.

Solid products of thermal decomposition, i.e., residual chars, were analyzed by elemental determinations and by infrared spectroscopy. Infrared absorption spectra were obtained on a Beckman IR-5 spectrophotometer.

Cahn Electrobalance and Gas-Flow System

The system employed in this program for thermogravimetric analysis

Figure 5 View of TGA equipment components

was assembled around a Cahn Model RG Automatic Recording Electrobalance. The electrobalance, shown schematically in Figure 6, is a high-sensitivity, null-point instrument. An electromagnetic D'Arsonval movement supplies the restoring force.

The balance beam has three loops: loop A has a maximum load of 1 gm; loop B load maximum is 2.5 gm; and loop C is used to support tare weights for other loops. The permissible weight change is 0 to 200 mg for loop A and 0 to 1000 mg for loop B. The smallest weight change that can be reliably detected depends on total load, but for small samples it is 2×10^{-7} gm.

As sample weight decreases, the beam tends to rotate and expose more of the photocathode of the vacuum photocell, thus increasing the phototube current. This current is amplified and applied to an electromagnetic coil to restore the beam to the null position. The loop gain of the servo is in excess of 1000, so that the actual beam deflection under load is very small, and the balancing torque is equal to the sample torque. The torque motor used in the balance is linear within the ability to be determined by precision weights. Thus, the balance current is a direct measure of the sample weight to an accuracy of better than $\pm$ 0.05% and a precision of better than $\pm$ 0.01% of full scale sample weight.

Extensive experimentation on the Cahn system has indicated that the zero stability of the instrument is usually consistent with measurements to $\pm$ 0.1μ gm [10]. However, in long-term experiments a steady drift has been observed.

The balance mechanism was mounted in a pyrex vacuum-bottle

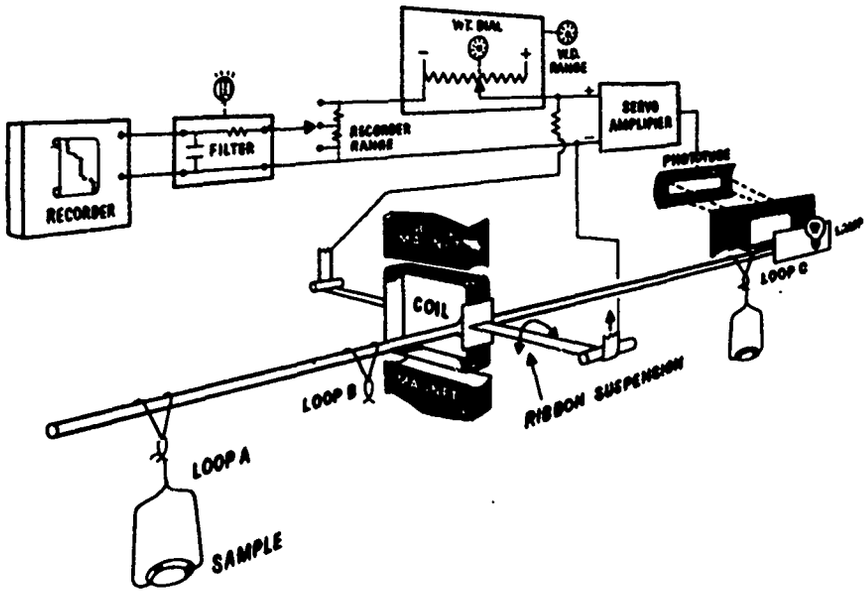

Figure 6. A Schematic Diagram of Cahn Electrobalance

accessory which permitted operation in reduced pressure, or in flow-through environments. The containing vessel was connected to a helium source through a precision control valve and four stages of pressure regulation and control. This gas delivery system was able to provide helium to sweep pyrolysis gases from the region of the decomposing sample at low flow rates. The number of control stages was made necessary by the requirement that the gas flow rate be constant to minimize drag-induced noise on the balance. The direction of gas flow was always from the top of the apparatus to the bottom in order that evolved gases would be prevented from contacting the balance mechanism.

Samples were suspended in hangdown tubes whose size was selected to provide optimum sensitivity and minimum noise for flow-through experiments [10]. Cahn and Schultz [10] observed that peak-to-peak noise diminished with decreasing tube diameter and decreasing pressure. For tubes with diameters less than 19 mm, peak-to-peak noise was less than 1 μ gm in a non-flow environment at atmospheric pressure. The hangdown tubes used in all atmospheric-pressure testing in this project were 19 mm in diameter or less. In tubes of larger diameter, noise levels were reduced to low values by reducing the pressure. Figure 7 illustrates the experimentally-determined peak-to-peak noise resulting from a change in the diameter of the hangdown tube in which the sample was suspended at atmospheric pressure. These data represent a non-flow situation. Figure 8 illustrates how noise in larger diameter tubes was decreased by reducing the pressure in the apparatus [9]. It has also been reported in the literature that a

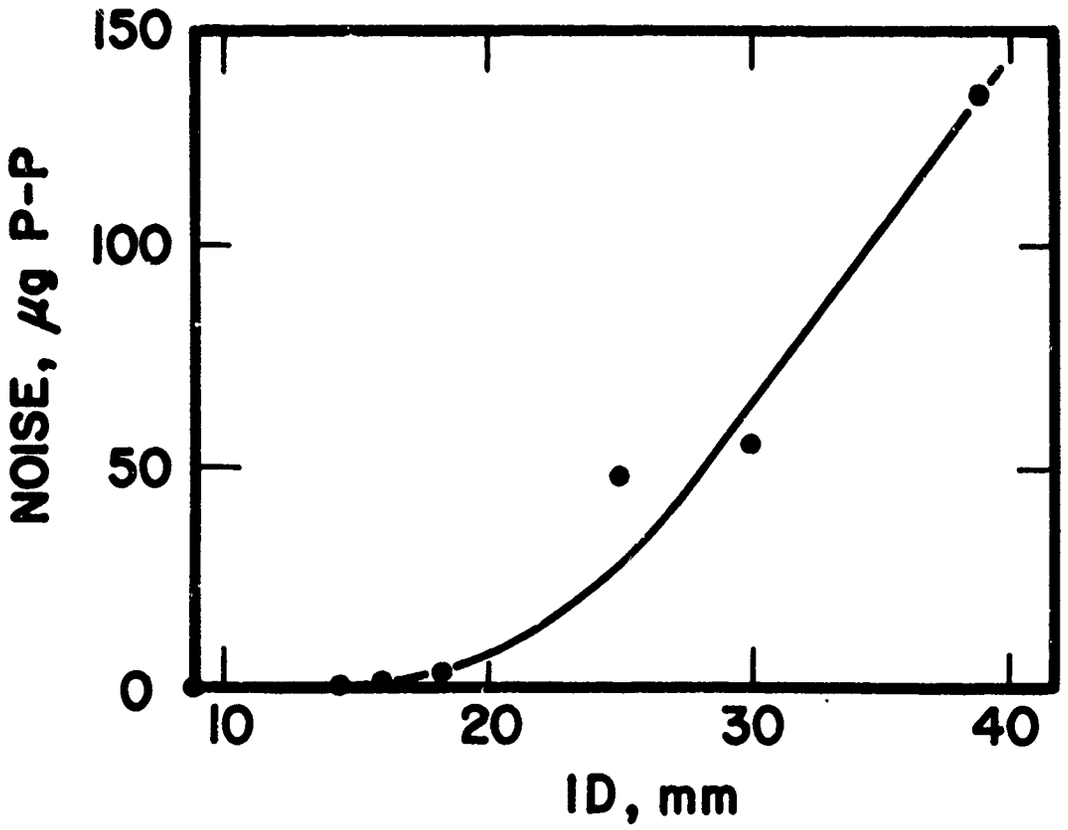

FIGURE 7. The Effect of Hangdown Tube Diameter on TGA Noise at Atmospheric Pressure

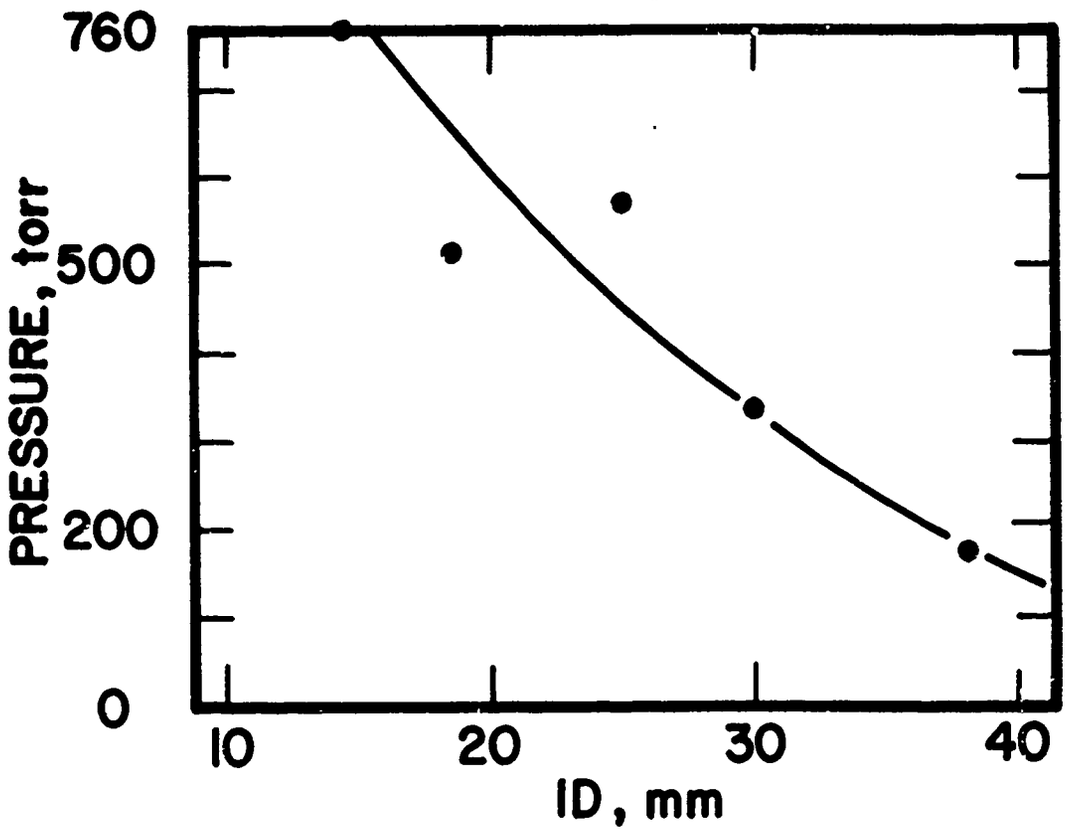

FIGURE 8. The Effect of Pressure on TGA Noise 1μg P-P

flow system exhibits essentially the same noise levels as those shown for a non-flow system if low flow rates are carefully controlled. This conclusion appears to be valid only if the balance mechanism can be isolated from low-frequency vibrations in the surroundings. The Cahn balance system has been used extensively in high precision TGA work and has been shown to be stable in a wide variety of operating conditions.

The temperatures of TGA samples were measured by a ceramic-sheathed, chromel-alumel thermocouple mounted on the pyrex bottle and suspended inside the hangdown tube. The measuring junction of the thermocouple was bared for 3/4 in., and it was suspended approximately five millimeters above the sample pan near the center of the tube. Thermocouple temperature measurements were referenced to a junction in a Dewar flask filled with crushed ice and water. The thermocouple output was calibrated by comparing its generated voltage with an already-standardized thermocouple. Voltage deviations were found to be insignificant with respect to the magnitude of the measurements.

Heating Systems

The furnace used in conjunction with the balance was a Marshall Model No. 1133 tubular, base-metal furnace with a maximum operating temperature of 1200°C. The furnace has a heating zone one-foot long which is provided with shunt taps making it possible to control effectively the temperature profile along the length of the furnace.

The temperature of the Marshall furnace was controlled by an F & M Model 240M-25 temperature programmer. This control device has a true proportional-power output which permits smooth temperature

programming and control from ambient to 1000°C. The solid-state circuitry has a maximum power output of 2500 watts. A temperature sensitivity of less than 0.1°C is possible. The controller can function to provide constant-temperature operation before, after, or between programmed periods. Programming rates of 0.5, 1, 2, 3, 4, 5, 7.5, 10, 15, 20, 25, 30°C/min. are available.

The ability of the programmer to control effectively the temperature of a TGA sample in the furnace is dependent upon the mode of operation, and upon the relative magnitudes of the thermal time constant of the furnace and the electrical time constant of the programmer. For example, the lag of the sample temperature behind the programmed temperature increased as temperature-rise-rate and gas flow rate increased. Also, the temperature overshoot observed when an isothermal plateau had been reached by the programmer was noted to be primarily a function of rate of temperature rise.

Recorders

The output of the Cahn electrobalance takes the form of a DC electrical signal which was the input to a Mosely Model 7001A X-Y plotter. This instrument, handling 11 x 17 in. paper, has input sensitivity ranges from 0.1 mv/inch to 20 v/inch with continuous variable control between calibrated positions. Accuracy of at least 0.2% full scale, linearity of 0.1% on all ranges and an integrated time base applicable to either axis at speeds from 0.01 to 20 in/sec. are all within recorder capability. Because of the great internal voltage suppression capacity of the electrobalance and the breadth of ranges and sensitivities of the X-Y recorder, the visual output

of the recorder is equivalent to a chart many times the 11 x 17 in. size of the chart paper.

It should also be noted that if changes were made during a run in the mass dial range of the Cahn control unit, the calibration of the Mosely recorder was affected unless the recorder was operating in a potentiometric mode. For this reason a switch was installed which allowed performance in and out of potentiometric-mode operation.

Pyrolyzing-sample temperatures were monitored and recorded by a Leeds and Northrup Speedomax W stripchart recorder. The specific model used is designed with variable plug-in range cards. In addition, the precision voltage generated by a potentiometer was used to suppress thermocouple output voltages, and thus extend the range of the recorder while maintaining high sensitivity.

Gas Analysis System

A schematic sketch of the components of the gas analysis system is shown in Figure 9. The principal element was a Perkin-Elmer Model 154 Vapor Fractometer equipped with a thermal-conductivity-cell sensing device. This chromatographic unit was designed to hold two-meter columns and was fitted with a gas-inlet port which permitted sampling of continuously flowing gas streams. There are also provisions for temperature control up to 225°C and for regulation of the flow of helium sweep gas through the unit.

Gases to be analyzed in the chromatograph were generated in a Vycor pyrolysis chamber contained in the Marshall furnace described previously. The sample chamber was swept by a continuous flow of

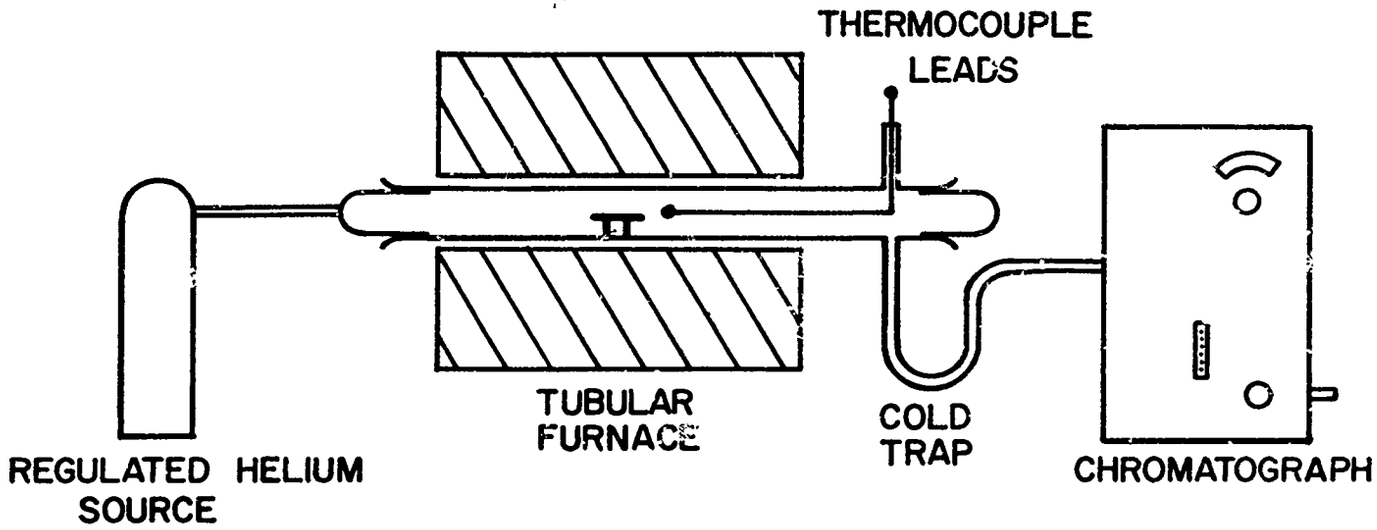

FIGURE 9. A Schematic Diagram of the Gas Analysis System

helium whose flow rate was regulated by the gas-delivery system. Polymer samples to be pyrolyzed were contained in a rectangular, platinum boat supported at the center of the tube by a nichrome framework. Removable caps were attached at each end of the tube to provide easy access. A chromel-alumel thermocouple was supported in the center of the tube such that the bead junction was located 3/8 in. from the center of the furnace when the pyrolysis unit was properly positioned. The displacement from the furnace centerline permitted the sample boat to be centered exactly when placed in contact with the thermocouple.

Decomposition gases, swept from the chamber by the helium flow, passed through a 0°C cold trap before entering the chromatograph. The purpose of the trap was to separate vapors from fixed gases and thereby simplify gas analysis.

Infrared Spectrometer

All infrared spectra were obtained on a Beckman IR5 Spectrophotometer. This unit uses a permanently evacuated thermocouple as a detector, and is capable of sensing spectra in the range of 2 μ to 16 μ. Chart output is linear in wavelength and transmittance. The spectra measured used the full wavelength capacity of the instrument. Samples analyzed were both virgin polymer and char residues. Small quantities of the test sample were dispersed in KBr pellets and absorption spectra were recorded.

CHAPTER III

EXPERIMENTAL TECHNIQUES

Thermogravimetric Analysis

The specific problems encountered and the techniques employed in obtaining the experimental data reported in this thesis are presented in the following chapter. Since the details of several of the employed procedures had important implications with respect to the results obtained, the experimental approach is carefully described. Utilized techniques of thermogravimetry, chromatographic analyses, elemental determination and infrared spectra analyses are presented.

The success or failure of TGA to provide valuable insight into the understanding of polymer degradation is largely dependent upon the care with which experiments are run, and the ability of the researcher to minimize or otherwise account for numerous experimental problems. A brief discussion of difficulties encountered will provide perspective for the experiments and resultant data. Principal experimental difficulties were associated with convection, flow currents, measurement of temperature, the effect of atmosphere, and changes in buoyancy.

Probably the most troublesome problem encountered in the TGA experimentation was that of extraneous noise picked up by the apparatus and superimposed upon desired output. Sources of noise can be either within the detection and recording equipment, or in the environment. Both can be serious. However, noise generated within the Cahn electrobalance was shown to be low and that in the Mosely recorder was held within reasonable limits by careful tuning and maintenance. An electri-

cal filter tuned to eliminate noise in the region of 60 cps helped to reduce vibrational noise levels, and also minimized noise pickup due to electrical ground loops. However, even with these precautions, building vibrations picked up by the sensitive balance mechanism and transmitted to the recorder as noise, completely precluded the use of very small samples and high-sensitivity ranges on the recorder and balance. Isolation of the table supporting the TGA apparatus from the floor by shock-absorbing casters eliminated most high-frequency vibrations. However, low-frequency vibrations, resulting in noise levels up to 50 μ gm, were a significant factor in all experiments.

In addition to electrical and vibrational sources, observed noise levels were also a function of the mode of testing. For example, experiments in which purging gas was swept past the polymer sample had significantly higher noise levels than were observed in non-flow experiments. Only a small part of the increase was attributed to instabilities in gas flow. When a vibration caused a small displacement of the sample pan, the movement was amplified by the flowing gas stream, and noise-inducing oscillations were set up.

Another noise effect, more serious in flow than non-flow experiments, was convection. In a given type of experiment, whether flow or non-flow, noise associated with convection increased with temperature. Also, it seemed to be coupled with building vibrations. That is, vibrations tended to multiply the temperature effects in increasing noise. The use of baffles within the hangdown tube seemed to be of little help, but the reduction of the over-all volume of the system was a positive factor.

It was noted that the size of the exit hole for the gas stream also had an effect on observed noise. Slight pressure pulses attributed to room air currents moving past the exit hole were picked up by the balance. Whenever practicable, a tube connected to the exit was led to a current-insulated dead space.

The build-up of static electricity on the sample holder or on the hangdown tube was another problem which caused the premature termination of a number of early tests. The sample pan was drawn into contact with the wall of the hangdown tube as the result of excessive static charge. Such contact caused intense noise and produced erroneous weight values.

Static could be produced by the handling of hangdown tubes during initial zeroing required by the Cahn balance or by contact with the highly-charged silicone vacuum greases used on ground-glass joints. Some resins, particularly polyquinoxaline, were inherently charged.

Several methods of removing static charges were tried. The system was carefully grounded, glass components were cleaned with sulfuric acid-sodium dichromate solutions, metallic parts, platinum and tungsten were cleaned in oxidizing flames, and several anti-static coatings were applied, all without notable success. Finally, a combination of an acid-cleaned interior and a GTC-59 anti-static coating made by Beaver Laboratories, Inc. was found to permit operation in most cases.

Many researchers who work with large polymer samples have reported an "effective weight gain" in the early part of TGA experiments before significant weight loss occurs. This effect is attributable to changes in buoyancy and can cause appreciable errors in weight measurements.

A null-type instrument, such as the Cahn electrobalance, zeroes buoyancy effects at the beginning of an experiment. However, buoyancy changes as environmental gas reaches increasingly higher temperatures. This error was minimized by using small samples, and by selecting helium as the sweep gas. In addition, a blank thermogram was obtained on an inert material of similar volume, and resulting buoyancy changes were subtracted from later data. The procedure is described in Appendix A.

The precise determination of the temperature of the pyrolyzing sample is a difficulty in all TGA work. The problem of temperature measurement has negated the value of some published experiments. The most frequent discrepancies occur when the recorded temperature does not closely represent the sample temperature or the sample temperature is not uniform.

In all experiments conducted in this effort, temperature uniformity was obtained by using small, finely-divided samples which were spread in a thin layer over the well-conducting platinum container. Suspension of a rapidly-responding thermocouple located very near the resin sample minimized temperature measurement error, which was believed to be small with respect to the magnitude of the temperature.

In order that the strengths and weaknesses of experimental technique might be assessed in light of the problems just outlined, each technique will now be presented in a specific, step-by-step form.

Dynamic-flow experiments

(1) The platinum sample pan was burned to weight-stable cleanliness in an oxidizing flame, and support wires were solvent-cleaned of residual condensates.

(2) The Cahn electrobalance was calibrated and prepared for operation. A detailed discussion of electrobalance calibration is included in Appendix B.

(3) A polymer sample of from 3 to 7 mg was placed on the pan.

(4) Twice the balance chamber was evacuated to 1.8 mm Hg and filled with helium. Internal pressure was maintained above atmospheric when helium filled.

(5) The flow exit was opened and the system flushed at least until helium flow was stable at a flow rate of about 30 cc of helium per minute at atmospheric temperature.

(6) The temperature programmer was set a few degrees below room temperature and with the furnace around the sample the programmer, X-Y recorder and temperature recorder were all turned on.

(7) During the actual run the system functioned automatically. The experimenter needed only to determine and select the form he wished the output to take.

(8) At the conclusion of a run all systems were shut off except the gas flow. Helium purge was maintained during cool-down to preserve cleanliness in the area of the balance mechanism.

Dynamic non-flow experiments

Items (1) through (7) were identical with the corresponding items of the dynamic flow made with the single exception that item (5) was deleted.

(8) At the conclusion of a run the sample hangdown tube was opened to permit flow of helium past the sample. Helium purge was maintained during cool-down to preserve cleanliness in the area of the balance mechanism.

Isothermal flow experiments

Items (1) through (5) were identical with corresponding items of the dynamic flow mode.

(6) The temperature programmer was set to the desired test temperature and with the furnace located below the sample the programmer and temperature recorder were turned on.

(7) When the furnace reached equilibrium at the predetermined temperature, the X-Y recorder was turned on and the furnace was raised to a location around the sample as rapidly as possible by a supporting jack.

(8) During the actual run the system functioned automatically. The experimenter needed only to determine and select the form he wished the output to take.

(9) At the conclusion of a run all systems were shut off except the gas flow. Helium purge was maintained during cool-down to preserve cleanliness in the area of the balance mechanism.

Isothermal non-flow experiments

Items (1) through (8) were identical to corresponding items of the isothermal flow mode with the single exception that item (5) was deleted.

(9) At the conclusion of a run the sample hangdown tube was opened to permit flow of helium past the sample. Helium purge was maintained during cool-down to preserve cleanliness in the area of the balance mechanism.

Analysis of Pyrolysis Products

The purpose of chemical analysis of the products of pyrolysis was to provide additional insight into the thermal decomposition reactions. Analyses included were:

(1) gas chromatography for light gaseous and readily-volatilized products,

(2) absorption infrared spectral identification of char residues, and

(3) elemental determinations of char composition.

A summary of each type of analysis follows.

Gas chromatography

The objective of chromatographic analysis of the decomposition gases was to obtain qualitative identification of gas species, and, if possible, a quantitative measure of their concentration. Because pyrolysis gases had to be swept from the reaction chamber to the chromatograph by a carrier gas, considerable dilution resulted. Therefore, it was necessary to test samples larger than were used in TGA experiments in order to generate sufficient gas for confident identification.

Because of the requirements for larger samples and minimum dilution, a horizontal arrangement of furnace and reaction chamber was selected. In a system horizontally positioned a sample container could be drawn

into a preheated furnace in a simple mechanical way with minimal contamination of oxygen.

Gas chromatographic analysis of pyrolysis gases presented several experimental difficulties. First, because of the broad range of molecular weights of gases involved, no single column was appropriate for all analyses. The wide variety of chemical natures of the gases, e.g., acidic or basic, further complicated the selection of columns. In some cases it was necessary to make multiple runs at a given test condition but with differing columns to make a complete determination. In order to make column changes as infrequently as possible, columns were chosen which had broad applicability. A further consideration in column selection was the elution time of the components being studied. At the same time that gas species had to be sufficiently separated for identification, the retention time had to be reasonably short in order that many samples could be taken during a given experiment. The columns selected were Chromosorb 102, Chromosorb 103, silica gel and Carbowax 1500.

Chromosorb 103 is designed to separate various amines. Thus, it proved useful with basic gases including ammonia. However, Chromosorb 103 is unable to separate sufficiently light gases. Chromosorb 102 is a general-purpose column material suitable for light-gas separation and also appropriate for acidic compounds. Silica gel is also a general-purpose light-gas column which was found to yield poor analysis of low volatility vapors and, of course, water. The Carbowax 1500 column was specifically used to confirm the presence of hydrogen cyanide and cyanogen in some streams.

Chromosorb 102 and silica-gel columns were empirically calibrated for hydrogen, methane, carbon monoxide, and carbon dioxide gases. Samples of each gas with varying concentrations were run through the columns and elution times and peak heights noted. Results of these quantitative calibrations are given in Appendix C. It was prohibitively difficult or unnecessary to calibrate for other gases involved. For example, hydrogen cyanide and cyanogen were not calibrated because pure gases and systems required for their safe handling were unavailable. Calibrations with hydrogen were particularly difficult. Since hydrogen has a higher thermal conductivity than the helium carrier and reference gas, hydrogen might be expected to produce a negative peak in the chromatograph. Yet it was observed that hydrogen could produce a positive peak, a negative and a positive peak, or a positive, negative and positive peak, depending on concentration. Quantitative determinations of hydrogen were certainly far less accurate than values for other gases.

It was also noted that the chromosorb columns needed to be sensitized to some gases before consistent determinations could be made. As an example, it was necessary to pass hydrogen cyanide through Chromosorb 102 before making a qualitative run. It appeared that some of the gas was strongly adsorbed before an effective separation equilibrium was achieved. A stepwise outline of the experimental procedure for gas chromatography follows.

(1) A polymer sample was placed in the platinum sample pan mounted on a nichrome-wire framework. A fine tungsten wire attached to the support was run through the furnace and out

the other end of the pyrolysis chamber. Removable ends on the chamber were replaced and sealed, and the whole mounted in the furnace. The sample pan while in the chamber was outside of the furnace heating zone.

(2) Air was removed from the gas-collection system by evacuation followed by helium flushing, or by flushing alone. Evacuation was more rapid, but also involved the problem of repressurizing without blowing out glass connections. When the flush gas was analyzed to have a very low concentration of air, the next step was begun.

(3) The furnace was driven to the desired test temperature and allowed to stabilize.

(4) The silicone seal on the downstream end of the pyrolysis chamber was removed, allowing access to the tungsten draw wire. The sample was drawn into the furnace to contact with the thermocouple and the silicone cap was replaced. Within approximately 2 to 3 minutes, samples were at furnace temperature. Removing the silicone cap introduced some air into the chamber. However, since air so introduced was downstream from the sample, it is believed that the oxygen had no effect on the decomposing sample. Air continued to appear in the gas analysis as it diffused from the stagnant zone at the chamber's end.

(5) Helium purge gas continually carried pyrolysis products through the cold trap to the gas sampling valve on the chromatograph where samples were periodically taken. Rate of sampling was dependent upon the retention time of the

gas species in the particular column being used.

Liquids condensed in the cold trap were collected in a syringe and identified in a 6-foot silicone-gum-rubber column mounted in an F & M Scientific Corporation, dual-column chromatograph at 100°C. Pyrolysis products which condensed as solids were collected and suspended in acetone. Portions of the suspension were injected for analysis in the dual-column chromatograph. Quantitative analysis of liquid and solid condensed residues was impossible because of the extremely small quantity of material collected.

Infrared absorption spectra evaluation

Infrared absorption spectra were obtained for each of the undegraded polymers and also for the char residues produced during gas-analysis experiments. Even though infrared spectra of polymers are very complex, it was anticipated that they would provide additional evidence as to the regions and functional elements within a polymer which preferentially degraded.

Since the polymers under investigation were essentially insoluble and the residues completely so, small quantities of samples were dispersed in potassium bromide discs which were used for spectral analysis. Since potassium bromide is transparent in the infrared region, absorption patterns observed were those associated with the dispersed sample.

When making KBr disks a small amount of sample was ground into 200-250 mg of KBr in a mortar and pestle. Both the sample and KBr were dessicated to remove as much water as possible. The amount of sample required varied with the color of the material. For the black chars generally produced, a small grain was sufficient. For lighter-

colored specimens up to 20 mg was necessary.

After the mixture was carefully ground to homogeneity, about 200 mg were placed in a pelletizer for three minutes at 24,000 psi. The finished disk, about 1/32 in. thick, was mounted on a spring-loaded sample clip which held the specimen in the infrared beam. After recording the spectra, a standard polystyrene film was placed in the sample slot and the well-known 6.238 μ peak was recorded for calibration reference.

If too much sample is put in a pellet, the intensity of the transmitted beam may be insufficient for proper analysis. However, the Beckman unit uses a comparator circuit for peak generation, and placing a screen in the reference beam may raise the relative intensity of the sample beam into a satisfactory region. Insufficient material in a pellet leads to very weak peaks.

Elemental analysis

As a final analysis to illuminate the thermal decomposition process, the elemental composition of undecomposed polymer and residual chars was determined. Such data provided a check on the assumed chemical structure and indicated the molar composition of volatile pyrolysis products.

Samples used for elemental analysis were both virgin polymers and the residues produced in gas chromatography experiments. Each resin was analyzed as to carbon and hydrogen content. In addition, chlorine was determined for polyphenylene, oxygen and nitrogen for polyimide, oxygen for polyquinoxalene and nitrogen for polybenzimidazole. All analyses were made by M-H-W Laboratories, P. O. Box 326, Garden City, Michigan.

CHAPTER IV

MATERIALS STUDIED

One of the objectives of this work was to investigate the thermal properties of several polymeric materials which represent the forefront of polymer technology and simultaneously exhibit desirable thermal stability and ablation properties. Of the many possible candidates, four chemical types were chosen: polyimide, polyphenylene, polybenzimidazole, and polyquinoxaline. In addition, because of the extensive literature and use of phenolic resins, a well-known high-temperature phenolic was selected as a ready basis of comparison with previous workers.

The specific polyimide evaluated was Monsanto Chemical Company Skybond 700. This resin has wide engineering application and is one of the more promising polyimides. The polyphenylene tested was a linear, para-polyphenylene provided by the Ames Laboratory of NASA. Whitaker Corporation's Imidite 2108 polybenzimidazole resin was selected because it is the most readily available of the small number of commercially distributed polybenzimidazoles. Dr. Wrasidlo of Naval Ordnance Laboratory provided samples of polyquinoxaline resin synthesized by him and designated WJW I-73. The phenolic resin chosen was Monsanto Chemical Company SC-1008.

The basis for selection of each of these resins, founded on their basic chemistry and properties, will now be presented.

Polyimide Polymer

Probably the first recorded synthesis of a polyimide is that of Bogert and Renshaw [5] who observed that 4-aminophthalic anhydride and dimethyl-4-aminophthalate, on heating, eliminated water and methanol, respectively, yielding a polyimide

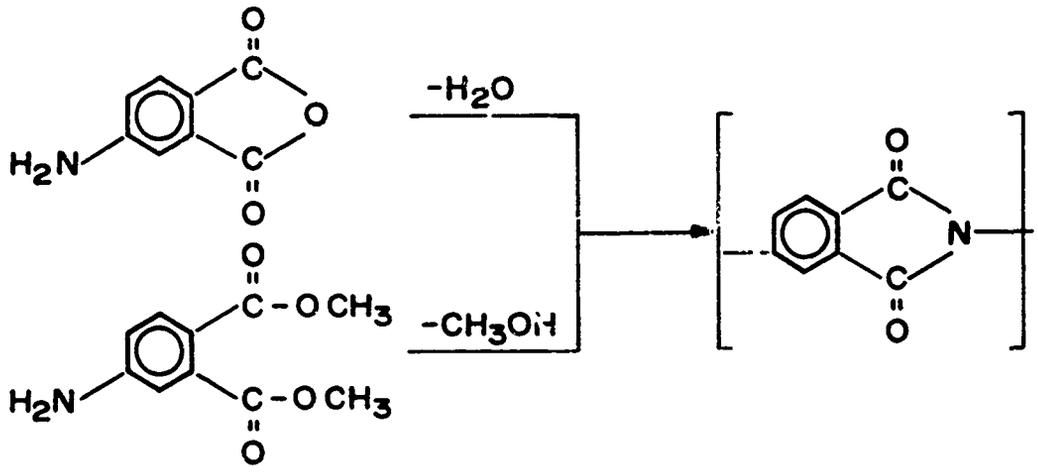

Edwards and Robinson [14] prepared polyimides of high molecular weight by fusing salts of a diamine and a tetraacid or a diamine and a diacid-ester. A low molecular weight polymer was produced in the initial reaction, but subsequent extended heating yielded a high molecular weight product. This melt-flux method was limited to polyimides with melting points sufficiently low that they remained molten under conditions of polymerization.

More modern methods of synthesis of polyimides have been discussed extensively in the literature [2, 16]. The basic procedure for polyimide preparation involves reaction of an aromatic dianhydride with an aromatic diamine in an appropriate solvent to form an inter-

mediate polyamic acid. The soluble polyamic acid polymer is dehydrated by thermal or chemical means to yield insoluble polyimide.

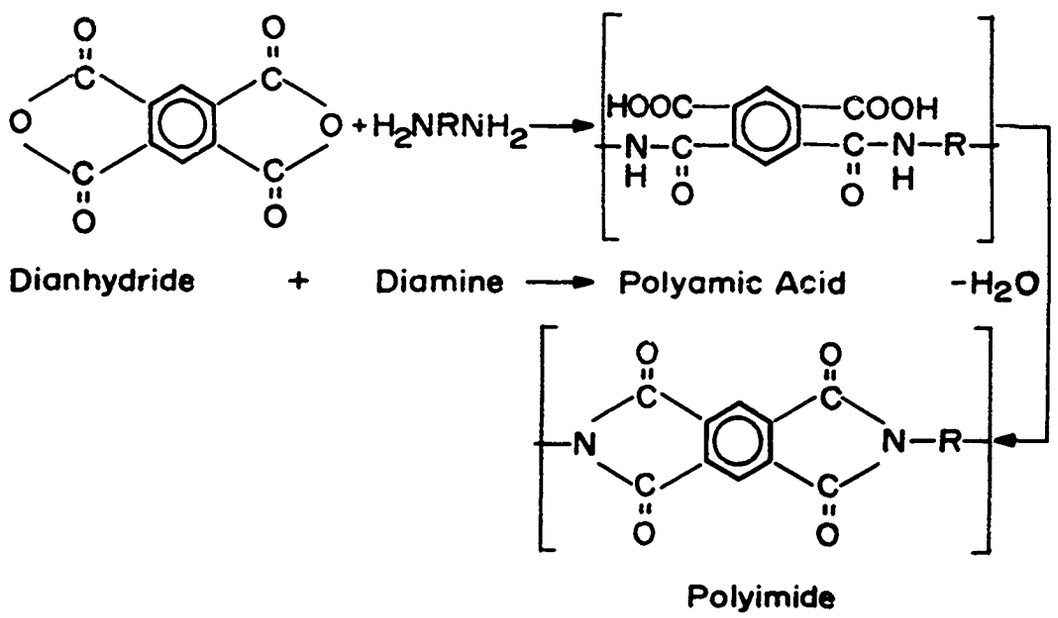

A wide range of organic dianhydride and diamine compounds have been combined to form an extensive family of polyimide polymers. In general, polyimides are highly colored and are characterized by excellent resistance to irradiation and to solvent attack, and by a high degree of thermal stability. The desirable high-temperature properties can be enhanced by increasing the aromaticity of the structure. Frost and Bower [18] investigated possible linking groups and reported the following approximate order of thermal stability: imide > ether, sulfide, direct phenyl-phenyl bond > amide, ester > methylene > isopropylidene.

The details of preparation of polyimides have been discussed at some length in the literature[34]. In general, the synthesis of high-molecular-weight polyimides is dependent upon the use of extremely pure monomers, complete exclusion of water during formation of polyamic

acid, choice of an appropriate solvent, and maintenance of low temperatures. The temperature limitation appears to be related to three reactions which can limit molecular weight [16]. These are:

(1) partial conversion to polyimide releasing water, which could hydrolyze polyamic acid,

(2) extensive conversion to polyimide above 100°C, which in addition to hydrolysis, would result in premature precipitation of low molecular weight polyimide from the reaction mixture, and

(3) possible transamidation with amide solvents upsetting stoichiometry.

In imidization the controlling step is the removal of water. Difficulties associated with water removal can limit the dimensions of a sample and prevent complete ring closure. The conversion is indicated by the disappearance of the NH band at 3.08 μ and the appearance of characteristic imide bands at 5.65 μ and at 13.8 μ. Wrasidlo and coworkers quantitatively followed imide conversion by measuring the increase in the imide carbonyl group in the infrared at 5.65 μ.
In addition, the mechanism of imidization was postulated to proceed through a diol formation.

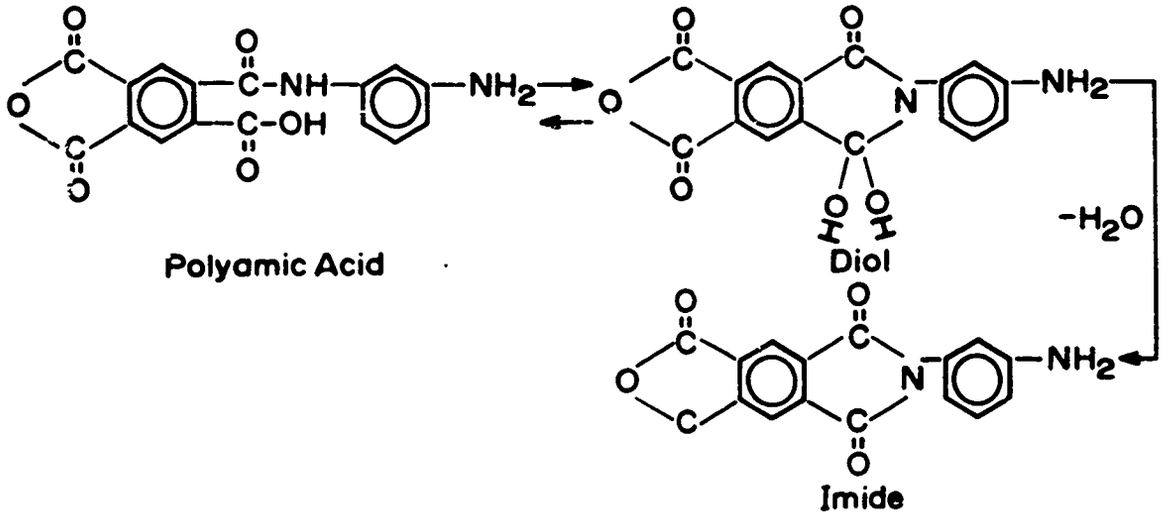

The particular polyimide selected for inclusion in this program, Skybond 700, has moderate usage in coating and other high-temperature applications. However, some confusion exists as to the exact chemical structure of the polymer. Johnson and Gaulin [23] identified Skybond 700 as the condensation product of benzophenone tetracarboxylic dianhydride and 4,4'-oxydianiline yielding the structure:

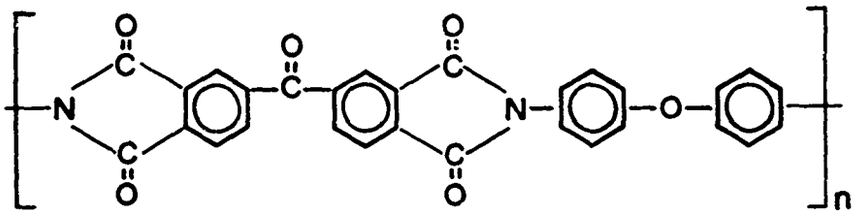

However, analysis of the infrared reflectance spectrum provided by the manufacturer indicates that the reactants are benzophenone tetracarboxylic dianhydride and meta-phenylenediamine which produce the structure:

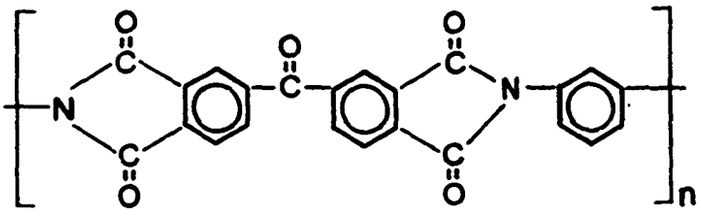

Since either set of reactants is permitted by the patent covering this resin and the manufacturer does not wish to be more specific, infrared spectral analysis was used to distinguish between the two possible forms. Infrared spectra for Skybond 700 are shown in Figure 10.

Some of the adsorption peaks which could differentiate between the two spectra are obscured by other characteristics of the polymer. However, the difference in the out-of-plane hydrogens of each structure provides sound evidence that meta-phenylene diamine was the reactant used. The presence of three out-of-plane hydrogens is indicated by a

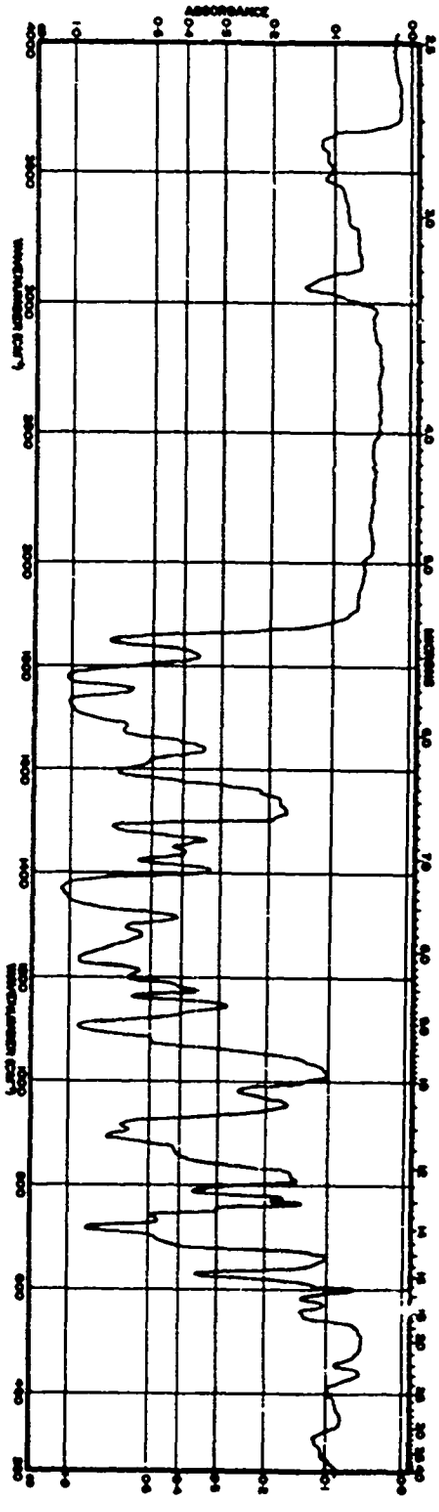

Figure 10. Infrared Spectrum of Skybond 700 Polyimide

moderately strong peak in the range 810-750 cm^{-1}. On the other hand, two out-of-plane hydrogens associated with the bis-oxydianilene structure would show a peak in the region 860-800 cm^{-1}. Evaluation of the spectra leads to a rejection of this latter structure. The polyimide polymer was cured by heating the bulk resin to 177°C at a temperature-rise rate of about 8°C per minute. The temperature was maintained at 350°F for 30 minutes. A 16-hour postcure followed. Two hours were spent in a helium environment at 200°C, 225°C, 250°C, 300°C, 325°C, and 4 hours were spent at 372°C.

Polybenzimidazole Polymer

One method of synthesizing high-molecular-weight polymers which exhibit desirable thermal stability characteristics is to combine benzene ring structures with other aromatic heteracyclic groups to form a totally aromatic structure. With the development of the technique of intramolecular condensation of linear chains of cyclic groups, a large number of polymers have been prepared including the polybenzimidazoles.

Benzimidazole derivatives synthesized from ortho-phenylene diamine and carboxylic acids have been known for some time to possess a high degree of chemical inertness and stability. The extension of this condensation reaction to yield high-molecular-weight products appears to have been first accomplished by Brinker and Robinson [7] who found that bis-ortho-diamines react with aliphatic dioic acids to form linear condensation polymers.

Marvel and Vogel [32] modified the Brinker-Robinson procedure by condensing aromatic tetramines and the phenyl esters of aromatic

dicarboxylic acids to form polybenzimidazoles containing recurring aromatic units. In general,

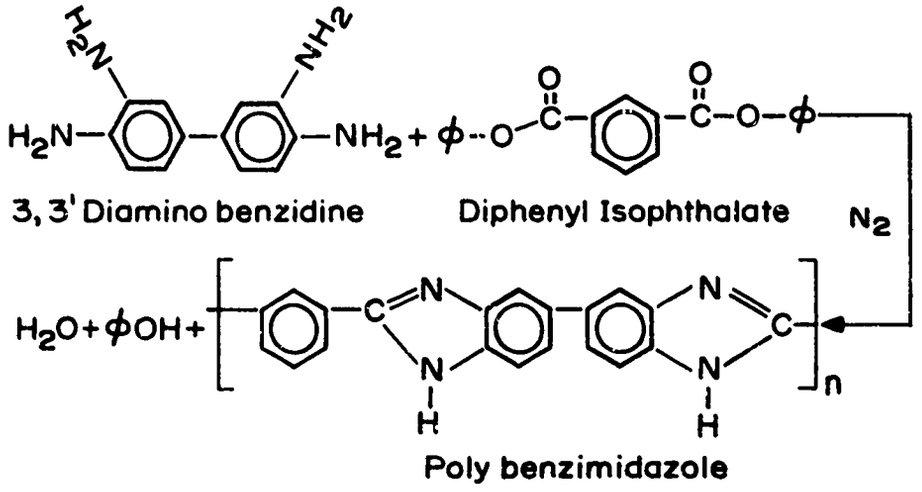

Even though the actual mechanism of reaction is undoubtedly complex, several authors have postulated the reaction steps. Wrasidlo and Levine [48] studying the reaction of diphenyl isophthalate and 3,3'-diaminobenzidene postulated a very complex mechanism in which the final event in the condensation was phenol evolution with the formation of the benzimidazole ring. However, Gray and Schulman [21] found this mechanism was not consistent with their experimental evidence, and proposed that early in the reaction both benzimidazole and hydroxybenzimidazoline structures are present which yield polybenzimidazole by dehydration.

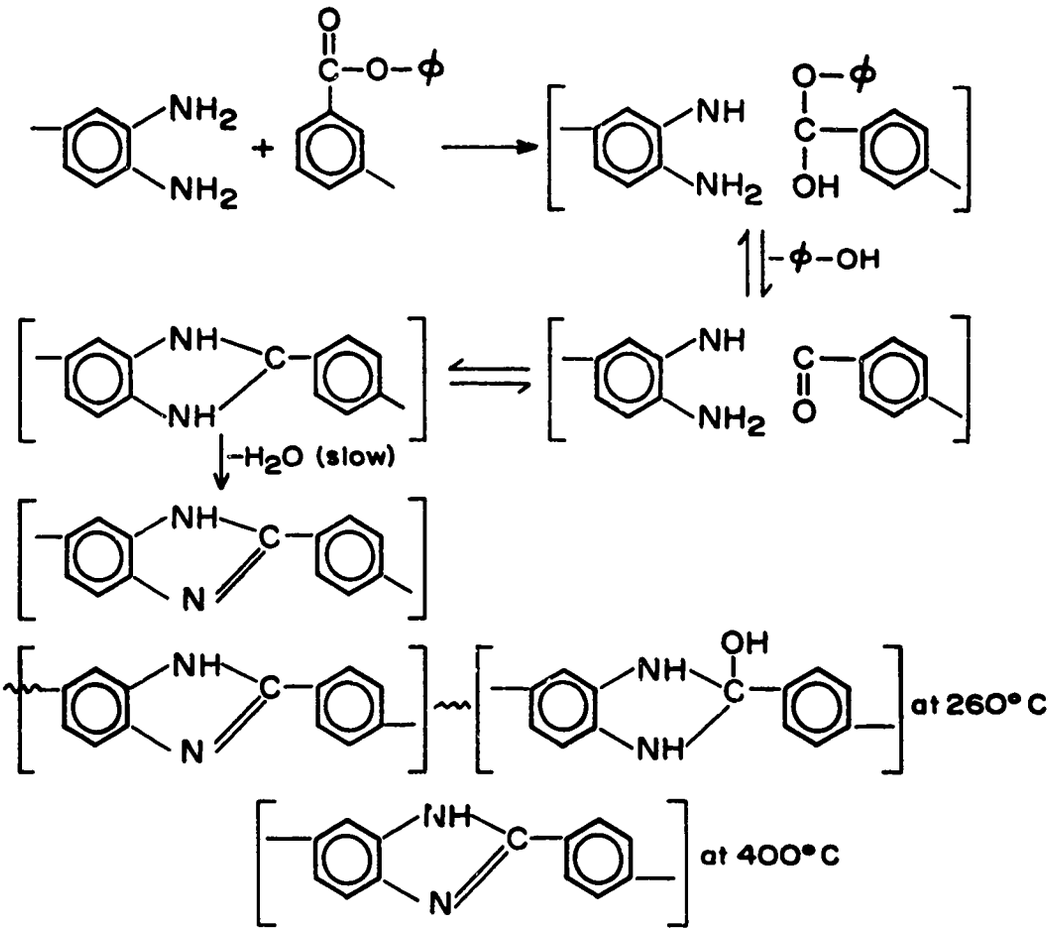

These results appear to be in accord with those of Korshak et al [25]. It appears that dehydration is incomplete below 400°C.

Polybenzimidazoles as a class of materials possess exceptional high-temperature stability both from mechanical and thermal points of view. Marks and Ruben [31] compared eleven resins, including several pherolics, polyimide, branched polyphenylene and polybenzimidazole, in a variety of tests to determine which had the best high-temperature properties. These authors concluded that the over-all performance of the polybenzimidazole, Imidite 2801, was significantly superior

to the other resins evaluated. The primary drawback in the use of polybenzimidazoles is the difficult processing characteristics of the resin.

The specific resin used in this program was Whittaker Corporation Imidite 2801 formed from diphenyl isophthalate and 3,3' diaminobenzidine. Two precured samples were obtained and designated PBI "A" and PBI "B", to differentiate between the different cure cycles associated with each sample. Cured polymer was obtained since equipment capable of providing the necessary temperatures and pressures was not available.

A general cure for polybenzimidazole cannot be given even for a specific resin as optimum conditions have not yet been determined. Because of the present competitive state of benzimidazole development, cure cycles are still considered proprietary. Pressures from 200 psi to 4000 psi and temperatures as high as 510°C have been used. It seems that Imidite 2801, even when cured at 454°C, is still linear with a molecular weight of about 3000 [50]. As the resin is postcured to about 510°C, the active hydrogen in the imidazole ring begins to react leading to branching and crosslinking.

Sample PBI "A" was cured at a pressure of 3500 psi with a maximum temperature of 550°F. Sample PBI "B" was cured at 200 psi to a maximum temperature of 450°C-480°C. The temperature timetable associated with the early part of the cure has not been divulged by the manufacturer. However, a procedure often used is to heat a sample to 350°F in three hours, then to 750°F at a rate of 2°F per minute followed by a postcure. PBI "B" polymer is a very dark brown in color and is very tough. The strength of this sample is probably the result of the high molecular

weight and crosslinking which results from high-temperature cure. By contrast, PBI"A" polymer is a light brown color and has such low strength that it easily crumbled in a mortar and pestle.

Polyphenylene Polymer

In an attempt to utilize the stability of aromatic ring structures in formulating ablative polymers, many investigators have tried to form high molecular weight para-polyphenylene resins. In addition to stability, polyphenylene polymers offer the additional possibility of producing only low-molecular-weight gaseous products upon thermal degradation. Since both of these characteristics are very desirable, polyphenylene resins seem to offer great promise in high-temperature applications.

The first reported synthesis of a para-polyphenylene resin with moderate molecular weight was that of Goldfinger and his associates [19]. They reacted 1,4-dichlorobenzene with metallic sodium in a Wurtz-Fittig reaction to produce a stable product which seemed to be a para-polyphenylene of molecular weight of about 2600. Another successful route has been the dehydrogenation of polycyclohexadienes derived from the polymerization of 1,3-cyclohexadiene

Most recently the synthesis of para-polyphenylenes has been accomplished by the direct polymerization of benzene. Kovacic and Kyriakis [26] found that benzene polymerized readily in the presence of a Lewis acid catalyst-cocatalyst-oxidizing agent to a solid product possessing the properties of para-polyphenylene. For example, benzene was 60% converted at 36°C in fifteen minutes when in the presence of aluminum chloride, water, and cupric chloride.

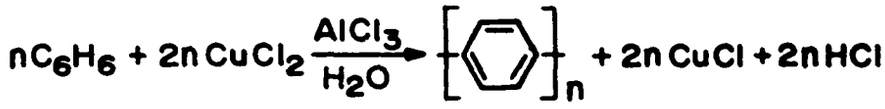

The para-polyphenyl structure was deduced from a number of corroborating tests.

The following reaction mechanism was proposed for the oxidative cationic polymerization.

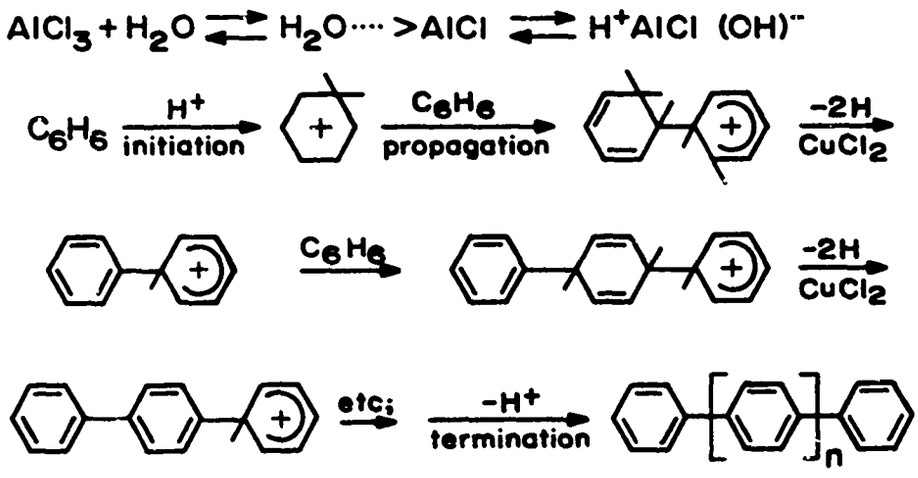

It was noted that if either the Lewis acid, aluminum chloride, or the oxidizer, $CuCl_2$, was omitted, the reaction failed to occur. The suggested initiation entailed the formation of a sigma complex (benzonium ion) which then underwent propagation. The small amount of chlorine left in the polymer could result from a termination reaction involving chloride ion, or from nuclear chlorination by the metal halide.

Industrial preparations of polyphenylene resins employ the techniques of Kavacic and associates almost exclusively when producing para-polymer. A large number of somewhat modified procedures are also available if branched or highly chlorinated structures are desired. As might be expected, branched structures have much enhanced processability but inferior thermal stability when compared with para-structures. Even within the limitations of essentially para linkages, significantly differing properties can be observed in polymers whose methods of preparation are different.

The para-polyphenylene polymer evaluated in this program was supplied by the Ames Research Laboratory of the National Aeronautics and Space Administration. The resin is a black powder and is uncured. Even though testing a cured polymer sample is to be preferred, limitations of available equipment made it impossible. Usually very high pressures, about 25,000 psi, and temperatures from 300°C to 550°C are required to obtain a cure [47]. Cure, in this case, would mean attainment of high molecular weight and would probably also include some crosslinking.

The difficulties in handling para-polyphenylenes, high melting point, absence of suitable solvents and extreme curing requirements, have led one author to say that

> ... fabrication of poly-p-phenylenes into useful products has not been accomplished, and meaningful thermal data on poly-p-phenylenes in applications or in end use tests are not available [47].

The exceptional properties of these resins are presently providing the motivation for the solution of processing problems.

Polyquinoxaline Polymer

Quinoxaline or benzopyrazine compounds are known to exhibit the high melting point, stability, and resistance to chemical attack which is characteristic of aromatic heterocyclics. Preparation of high-molecular-weight polyquinoxalines has been accomplished by the reaction of such tetracarbonyl compounds as 1,4-didiglyoxialbenzene with aromatic bis (ortho-diamines) such as 3,3'-diaminobenzidine by both melt and solution polymerization techniques.

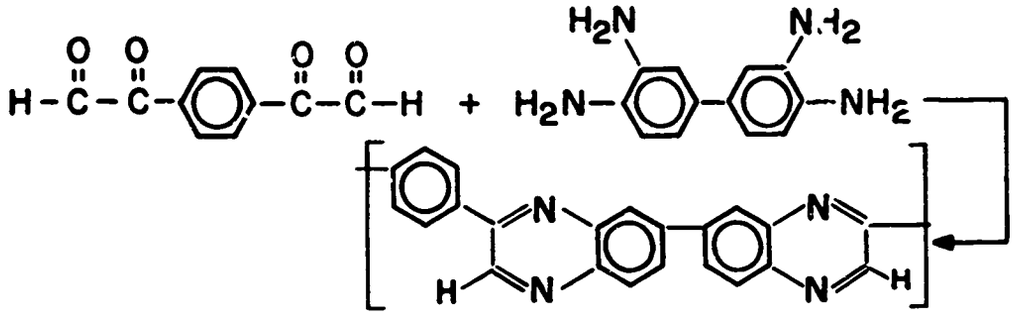

In melt polymerization, the reactants are heated together up to as high as 375°C in a two-step reaction similar to that of the benzimidazoles. The procedure for solution polymerization involves heating the monomers for rather extended periods of time in a suitable solvent to form solutions of polymer which upon crystallization yield product resin.

It has been observed that phenyl-substituted polyquinoxalines have superior thermal and oxidative stability when compared with the unsubstituted structure[49]. The polyquinoxaline resins evaluated in

this program were phenyl-substituted resins prepared by Wrasidlo and Augl of the U. S. Naval Ordnance Laboratory by one-step solution condensation of 3,3' diaminobenzidine with 1,4-bis (phenylglyoxaloyl)-benzene at room temperature. Infrared spectra of this resin showed no carbonyl band (1685 cm^{-1}) and no residual NH band, thus indicating complete cyclization. An example of this spectra is shown in Appendix D.

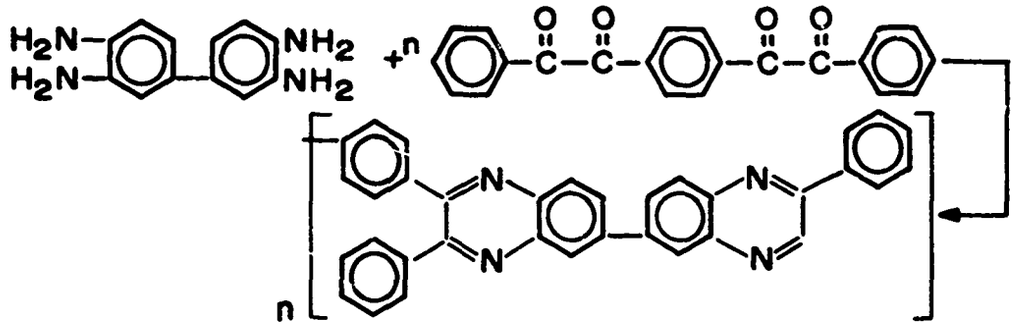

The phenyl substitution of the quinoxaline ring greatly increases solubility characteristics and also enhances molding properties [44].

The resin sample as received was a light yellow flocculant powder. The polymer was tested in the condition as received, and after being advanced by heating at 270°C for six hours in a flowing helium stream. The advancing of this resin does not constitute a full cure as would be required for molding or composite fabrication. The advancing conditions were chosen such that the properties of the resultant polymer could be compared with some literature references [49].

Phenolic Polymer

Perhaps the most important thermosetting resin, both from a historical standpoint and in volume of current commercial application is the condensation product formed by the reaction of phenol and

formaldyhyde. Phenolic resins have a lengthy history beginning with the discovery by Baeyer in Germany in 1872 of the reaction between phenols and aldehydes. The chemistry and technology of phenolics was greatly extended by the work of Baekeland in 1909 who produced the first high-density product.

The phenol-formaldehyde reaction is catalyzed by both bases and acids, and the nature of the final product is greatly dependent upon the type of catalyst and the mole ratio of the reactants. In the presence of alkaline catalysts, with an excess of formaldehyde, methylol phenols are formed which can condense with the elimination of water to yield three-dimensional molecular aglomerates crosslinked by methylene or by ether linkages. In the latter case subsequent loss of formaldehyde may occur with methylene bridge formation. These reactions are illustrated by the following equations:

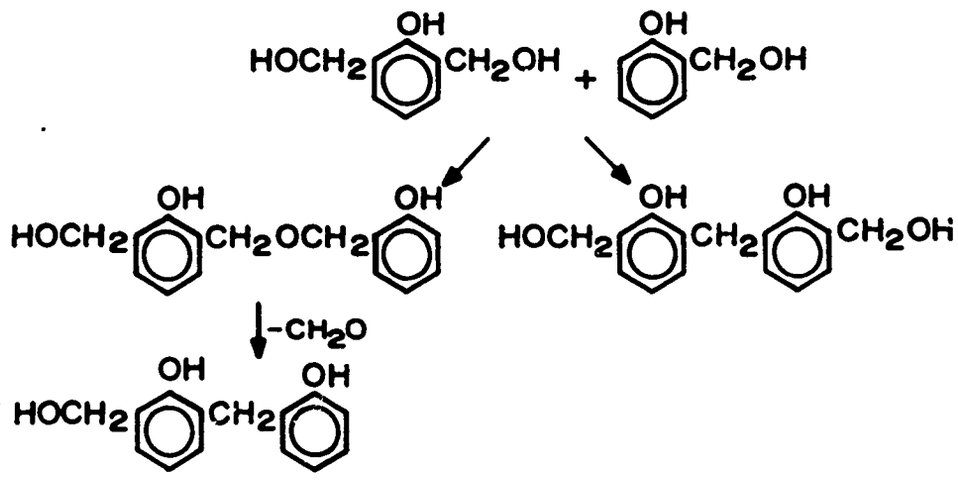

In the presence of acid catalysts, with a mole ratio of less than one, methylol derivatives condense to form linear, low molecular weight polymers, called novolacs, in which random ortho-and para-methylene links occur. Further reaction to form high-molecular-weight products requires addition of more aldehyde or a reactant such as hexamethylene tetramine. It is obvious that a wide variety of end products are possible by variation in reactants and conditions of polymerization. Even though the thermal properties of phenolics are inferior to the other resins evaluated, the extensive literature on their properties and their broad usage made their inclusion in this work worthwhile as a basis of comparison with previous investigators. The specific resin chosen was Resinox SC-1008 produced by Monsanto Chemical Corporation. This resin has extensive industrial use and is representative of phenolics specially formulated for high temperature applications.

Resinox SC-1008 is a base-catalyzed resole in which the ratio of phenol to formaldehyde is about 1.1. The polymer was cured by being slowly raised to 140°C at which temperature it was maintained for 24 hours. It was then heated for 24 hours at 177°C. The polymer was then postcured in helium for 2 hours at both 260°C and 288°C.

CHAPTER V

QUASILINEARIZATION

Several approaches to the mathematical analysis of dynamic thermogravimetric data were summarized in the Introduction. In general, these techniques require a constant rate of temperature rise, and employ one or more graphical techniques for the determination of kinetic parameters. A recently-developed numerical method which avoids these problems and provides a systematic approach to the determination of kinetic constants is the quasilinearization technique of Bellman and Kalaba [4]. This method utilizes experimental data points directly, and selects kinetic parameters by a least-squares-optimization procedure to best fit the data. The method is iterative and requires an initial assumption of the values of the constants. The lack of guarantee of convergence is the primary difficulty with the approach.

Nevertheless, quasilinearization is a powerful analytical tool which offers three significant advantages over most of the presently employed techniques for analysis of TGA data:

(1) It is not necessary to maintain a constant-rate temperature rise during the experiment. A completely flexible temperature history, including periods of differing rates of temperature rise and even isothermal segments, can be successfully handled. The increased analytical flexibility greatly extends the types of experimentation possible.

(2) Multiple experimental runs may be combined in a single data analysis if desired. That is, similar experimental

thermograms for a given material may be collectively analyzed to yield a single set of optimized kinetic parameters.

(3) Inaccurate data handling procedures such as graphical data analysis and slope measurements are completely avoided.

In applying quasilinearization to TGA data, a power law rate function of the type shown in Equation (5.1) is usually assumed.

$$-\frac{1}{w_o}\frac{dw}{dt} = k\left[\frac{w - w_r}{w_o}\right]^n \qquad (5.1)$$

where

w_o = initial weight of polymer

w_r = final weight of residue after complete degradation,

w = instantaneous weight of polymer-residue material during the degradation process,

t = time,

n = kinetic order of the degradation reaction.

Equation (5.1) assumes the degradation process is simple and irreversible and it may be written

$$-\frac{dW}{dt} = k\,W^n \qquad (5.2)$$

where k = specific rate constant and $W = (w - w_r)/w_o$. The rate constant k is assumed to depend on the absolute temperature according to the Arrhenius law

$$k = Ae^{-\frac{E}{RT}} \qquad (5.3)$$

where

A = pre-exponential factor,

E = activation energy,

R = universal gas constant,

T = absolute temperature.

The problem of determining the kinetic constants A, E, and n in Equation (5.2) is transformed to the estimation of the initial conditions for a system of time-dependent differential equations. This is done by assuming that the constants are functions of time such that the following equations are satisfied.

$$\frac{dW}{dt} = - Ae^{-E/RT} W^n \quad , W(0) = 1 - w_r/w_o \; ; \tag{5.4}$$

$$\frac{dA}{dt} = 0, \; A(0) = A_o \; ; \tag{5.5}$$

$$\frac{dE}{dt} = 0, \; E(0) = E_o \; ; \tag{5.6}$$

$$\frac{dn}{dt} = 0, \; n(0) = n_o \; ; \tag{5.7}$$

$$\frac{dT}{dt} = \rho, \; T(0) = T_o \; ; \tag{5.8}$$

where ρ is a known function of time. The latter equation is equivalent to having

$$T = \phi(t) \quad , T(0) = T_o \; .$$

The intent is that all quantities in the equations are functions of time and that the unknowns appear as initial conditions. Equations (5.4) to (5.7) are linearized by converting them into sequences which, hopefully, will rapidly converge to the best values of the kinetic parameters, For example,

$$\frac{dW^{i+1}}{dt} = \frac{dW^{i}}{dt} + \frac{\partial(\frac{dW^{i}}{dt})}{\partial W^{i}} (W^{i+1} - W^{i}) + \frac{\partial(\frac{dW^{i}}{dt})}{\partial A^{i}} (A^{i+1} - A^{i}) +$$

$$\frac{\partial(\frac{dW^{i}}{dt})}{\partial E^{i}} (E^{i+1} - E^{i}) + \frac{\partial(\frac{dW^{i}}{dt})}{\partial n^{i}} (n^{i+1} - n^{i}) + \text{ignored higher-order terms} \qquad (5.9)$$

Thus, if

$$\frac{dW}{dt} = f(W,A,E,n), \qquad (5.10)$$

then

$$\frac{dW^{i+1}}{dt} = f(W^{i}, A^{i}, E^{i}, n^{i}) + \frac{\partial f^{i}}{\partial W^{i}} (W^{i+1} - W^{i}) + \frac{\partial f^{i}}{\partial A^{i}} (A^{i+1} - A^{i}) +$$

$$\frac{\partial f^{i}}{\partial E^{i}} (E^{i+1} - E^{i}) + \frac{\partial f^{i}}{\partial n^{i}} (n^{i+1} - n^{i}), \qquad (5.11)$$

where the i superscripts indicate the particular iteration. In expanded form Equation (5.11) becomes

$$\frac{dW^{i+1}}{dt} = - [A^i d^{-E^i/RT} (W^i)^{n^i} + n^i A^i e^{-E^i/RT} (W^i)^{n^i-1} (W^{i+1} - W^i)$$

$$+ e^{-E^i/RT} (W^i)^{n^i} (A^{i+1} - A^i) - \frac{A^i}{RT} e^{-E^i/RT} (W^i)^{n^i} (E^{i+1} - E^i)$$

$$+ A^i e^{-E^i/RT} \ln W^i (W^i)^{n^i} (n^{i+1} - n^i), \qquad (5.12)$$

$$\frac{dA^{i+1}}{dt} = 0. \qquad (5.13)$$

$$\frac{dE^{i+1}}{dt} = 0, \qquad (5.14)$$

$$\frac{dn^{i+1}}{dt} = 0. \qquad (5.15)$$

The iterative procedure is initiated by assuming values of A°, E°, and n° and solving Equation (5.4) by the Runge-Kutta numerical procedure for $W^\circ(t)$. Setting $i = 0$, the linear differential Equations (5.12) to (5.15) are solved for $W^1(t)$, A^1, E^1, and n^1 by the procedure of forming a particular and homogeneous solution.

The solution of Equation (5.12) can now be represented in the form

$$W^{i+1}(t) = p^{i+1}(t) + \alpha_1^{i+1} h_1^{i+1}(t) + \alpha_2^{i+1} h_2^{i+1}(t)$$

$$+ \alpha_3^{i+1} h_3^{i+1}(t), \qquad (5.16)$$

where α_i^{i+1} are constants to be determined. Thus,

$$\frac{dp^{i+1}}{dt} = - [A^i e^{-E^i/RT} n^i (W^i)^{n^i-1} (p^{i+1} - W^i)$$

$$+ (W^i)^{n^i} A^i e^{-E^i/RT} (-\frac{1}{RT}) (-E^i)$$

$$+ A^i e^{-E^i/RT} (W^i)^{n^i} \ln (W^i) (-n^i)], \qquad (5.17)$$

and

$$p^{i+1}(0) = W(0).$$

also

$$\frac{dh_1^{i+1}}{dt} = - [A^i e^{-E^i/RT} n^i (W^i)^{n^i-1} (h_1^{i+1})$$

$$+ (W^i)^{n^i} e^{-E^i/RT} (A^{i+1})$$

$$+ (W^i)^{n^i} A^i e^{-E^i/RT} (-\frac{1}{RT}) (E^{i+1})$$

$$+ A^i e^{-E^i/RT} (W^i)^{n^i} \ln (W^i) (n^{i+1})]. \qquad (5.16)$$

The following convenient values of initial conditions are chosen.

$$h_1^{i+1}(0) = 0 ;$$

$$A^{i+1}(0) = 1 ;$$

$$E^{i+1}(0) = 0 ;$$

$$n^{i+1}(0) = 0 .$$

Similarly,

$$\frac{dh_2^{i+1}}{dt} = - [A^i e^{-E^i/RT} n^i (W^i)^{n^i-1}(h_2^{i+1})$$

$$+ (W^i)^{n^i} e^{-E^i/RT}(A^{i+1})$$

$$+ (W^i)^{n^i} A^i e^{-E^i/RT} (-\frac{1}{RT}) (E^{i+1})$$

$$+ A^i e^{-E^i/RT} (W^i)^{n^i} \ln (W^i) (n^{i+1})], \qquad (5.19)$$

$$h_2^{i+1}(0) - 0 ;$$

$$A^{i+1}(0) = 0 ;$$

$$E^{i+1}(0) = 1 ;$$

$$n^{i+1}(0) = 0 ,$$

and

$$\frac{dh_3^{i+1}}{dt} = - [A^i e^{-E^i/RT} n^i (W^i)^{n^i-1} (h_3^{i+1}) + (W^i)^{n^i} e^{-E^i/RT}(A^{i+1})$$

$$+ (W^i)^{n^i} A^i e^{-E^i/RT} (-\frac{1}{RT}) (E^{i+1})$$

$$+ A^i e^{-E^i/RT} (W^i)^{n^i} \ln (W^i) (n^{i+1})] \qquad (5.20)$$

$$h_3^{i+1}(0) = 0 \ ;$$

$$A^{i+1}(0) = 0 \ ;$$

$$E^{i+1}(0) = 0 \ ;$$

$$n^{i+1}(0) = 1 \ .$$

With i = 0, Equations (5.17), (5.18), (5.19), (5.20) are solved by the Runge-Kutta 4th order method for $p^1(t)$, $h_1^1(t)$, $h_2^1(t)$, $h_3^1(t)$. The constants α_j^{i+1} are determined for each iteration such that the objective function, Q, is minimized.

$$Q = \sum_{j=1}^{k} (W^{i+1}(t_j) - W_{j,\,DATA})^2 \qquad (5.21)$$

where $W^{i+1}(t_j)$ are the computed points and $W_{j,DATA}$ are the corresponding data points for the particular times.

For i = 0, the objective function becomes

$$Q_1 = \sum_{j=1}^{k} [p^1(t_j) + \alpha_1^1 h_1^1(t_j) + \alpha_2^1 h_2^1(t_j) + \alpha_3^1 h_3^1(t_j) - W_{j,DATA}]^2 \ . \qquad (5.22)$$

For a minimum Q_1

$$\frac{\partial Q_1}{\partial \alpha_1^1} = 0 \ ;$$

$$\frac{\partial Q_1}{\partial \alpha_2^1} = 0 \ ;$$

$$\frac{\partial Q_1}{\partial \alpha_3^1} = 0 \ , \tag{5.23}$$

or

$$\sum_{j=1}^{k} \{[p^1(t_j) + \alpha_1^1 h_1^1(t_j) + \alpha_2^1 h_2^1(t_j) + \alpha_3^1 h_3^1(t_j) - W_{j,DATA}]\, h_1^1(t_j)\} = 0 \ , \tag{5.24}$$

$$\sum_{j=1}^{k} \{[p^1(t_j) + \alpha_1^1 h_1^1(t_j) + \alpha_2^1 h_2^1(t_j) + \alpha_3^1 h_3^1(t_j) - W_{j,DATA}]\, h_2^1(t_j)\} = 0 \ , \tag{5.25}$$

$$\sum_{j=1}^{k} \{[p^1(t_j) + \alpha_1^1 h_1^1(t_j) + \alpha_2^1 h_2^1(t_j) + \alpha_3^1 h_3^1(t_j) - W_{j,DATA}]\, h_3^1(t_j)\} = 0 \ . \tag{5.26}$$

Equations (5.24), (5.25), (5.26) are solved simultaneously for α_1^1, α_2^1, α_3^1 using experimental values of $W_{j,DATA}$ at t_j, and the computed p^1, h_1^1, h_2^1, h_3^1 at the (k) t_j values. The resulting α values are related to the next set of kinetic parameters as follows:

$$\alpha_1^1 = A^1 \ ,$$

$$\alpha_2^1 = E^1 \ ,$$

$$\alpha_3^1 = n^1 \ ,$$

The iterations are continued until the parameters A, E, n converge to within reasonable tolerances. Data from more than one thermogram may be utilized. In this case a set of equations, one for each thermogram, of the form of Equation (5.12) are solved, and the objective function in Equation (5.21) is expanded to include all data sets.

The equivalence of the optimized α's and the kinetic parameters is discussed and proved in detail by Lee [29]. A simplified example may serve to illustrate the proof. In a system of linear equations, such as Equations (5.12) through (5.15), particular solutions may be obtained as shown below:

$$y_p' = f(x), \quad u_p' = g_1(x), \quad v_p' = g_2(x), \quad w_p' = g_3(x),$$
$$y_p(0) = y_p^o, \quad u_p(0) = 0, \quad v_p(0) = 0, \quad w_p(0) = 0.$$

Similarly homogeneous solutions may be obtained.

$$y_{hi}' = f_{hi}(x), \qquad y_{hi}(0) = 0$$
$$u'_{hi} = g_{1h}(x), \qquad \begin{bmatrix} u_{hi}(0) \\ v_{hi}(0) \\ w_{hi}(0) \end{bmatrix} = \delta_{ij}$$
$$v'_{hi} = g_{2h}(x),$$
$$w'_{hi} = g_{3h}(x),$$

Combining these particular and homogeneous equations in the general form for solutions of linear equations gives,

$$y = y_p + c_1 y_{h1} + c_2 y_{h2} + c_3 y_{h3}$$

$$u = u_p + c_1 u_{h1} + c_2 u_{h2} + c_3 u_{h3}$$

$$v = v_p + c_1 v_{h1} + c_2 u_{h2} + c_3 v_{h3}$$

$$w = w_p + c_1 w_{h1} + c_2 w_{h2} + c_3 w_{h3}$$

Direct substitution of initial values gives,

$$u = c_1, \qquad v = c_2, \qquad w = c_3.$$

Convergence of the quasilinearization technique given above is the major difficulty in its application. Realizing that a good initial guess of the values of the constants is necessary for convergence, graphical methods have been used in this study to yield preliminary values. Probability of convergence is also enhanced if one of the parameters is constrained until the others have reached the optimized value. The concept of constrained parameters permits a variety of calculation strategies, each of which should converge to the same result. Of course, the required computer time can vary significantly, depending upon the strategy chosen. Of the three kinetic parameters A, E, and n, the order of reaction n has exerted the greatest influence on convergence. That is, small changes in n have resulted in large changes in the other two parameters. Therefore, n was always the parameter chosen for constraint when convergence requirements made such a limitation necessary. When the order of reaction was constrained the number of homogeneous equations required was reduced by one, and n was not considered as a variable in the linearization procedure. Applying restraints does not alter the basic approach.

Many of the problems associated with convergence in non-linear curve fitting can be reduced through reparameterization. Several different techniques of reparameterization have been published [6, 33] and Kittrell [24] has discussed their application to kinetic analysis. Specifically in the case of a simple Arrhenius model

$$k = A\, e^{-E/RT} \tag{5.27}$$

estimation of the two parameters from experimental data may yield a contour of convergence on a sum-of-squares surface which is very

restricted. Convergence of an iterative routine for such a system may be slow or nonexistent. Experience seems to indicate that kinetic models should be reparameterized by a redefinition of the independent variables. Specifically Kittrell recommends that the exponential parameter

$$k = A\, e^{-E/RT}$$

be redefined as

$$k = \bar{A}\, e^{-\{E/R(1/T - 1/\bar{T})\}} \tag{5.28}$$

where

$$\bar{A} = A\, e^{+E/R\bar{T}} \tag{5.29}$$

These modifications, mathematically equivalent to the original expression, transform the contour of convergence. Parameters $\bar{A}$ and E are obtained more readily, initial estimates are less critical, and convergence is more rapid.

The application of this form of reparameterization to the quasilinearization equations is straightforward. Illustrated below is the case for a constrained n.

Normally it is assumed that

$$-\frac{dW}{dt} = W^n\, A\, e^{-E/RT} = k\, W^n. \tag{5.30}$$

Now we will define

$$-\frac{dW}{dt} = k\, W^n = W^n\, \bar{A}\, e^{-E/R(1/T - 1/\bar{T})}, \tag{5.31}$$

and, therefore,

$$A = \bar{A}\ e^{-E/R\bar{T}} \tag{5.32}$$

The quasilinearization equations resulting from this change are as follows: (for fixed n)

$$-\frac{dW}{dt} = W^n \bar{A}\, e^{-E/R(1/T - 1/\bar{T})} = f(W, \bar{A}, E) \tag{5.33}$$

$$\frac{dW^{i+1}}{dt} = f^i + \frac{\partial f^i}{\partial W^i}(W^{i+1} - W^i) + \frac{\partial f^i}{\partial A^i}(\bar{A}^{i+1} - \bar{A}^i) + \frac{\partial f^i}{\partial E^i}(E^{i+1} - E^i) \tag{5.34}$$

or in expanded form

$$-\frac{dW^{i+1}}{dt} = (W^i)^n \bar{A}^i\, e^{-E^i/R(1/T - 1/\bar{T})} + \bar{A}^i\, e^{-E^i/R(1/T - 1/\bar{T})}$$

$$n^i\,(W^i)^{n-1}\,(W^{i+1} - W^i)$$

$$+ (W^i)^n \bar{A}^i\, e^{-E^i/R(1/T - 1/\bar{T})}\,\left(-\frac{1}{R}(1/T - 1/\bar{T})\right)(E^{i+1} - E^i)$$

$$+ (W^i)^n\, e^{-E^i/R(1/T - 1/\bar{T})}\,(\bar{A}^{i+1} - \bar{A}^i), \tag{5.35}$$

also

$$\frac{dp^{i+1}}{dt} = -\bar{A}^i\, e^{-E^i/R(1/T - 1/\bar{T})}\, n(W^i)^{n-1}\,(p^{i+1} - W^i) \tag{5.36}$$

$$-(W^i)^n\, e^{-E^i/R(1/T - 1/\bar{T})}\,\bar{A}^i\,\left(+\frac{1}{R}(1/T - 1/\bar{T})\right)(+E^i)$$

$$p^{i+1}(0) = W^o\ ,$$

$$\frac{dh_1^{i+1}}{dt} = -\bar{A}^i\, e^{-E^i/R(1/T - 1/\bar{T})}\, n(W^i)^{n-1}(h_1^{i+1})$$

$$- (W^i)^n\, e^{-E^i/R(1/T - 1/\bar{T})}\, (\bar{A}^{i+1})$$

$$+ (W^i)^n\, \bar{A}^i\, e^{-E^i/R(1/T - 1/\bar{T})}\, \left(\frac{1}{R}(1/T - 1/\bar{T})\right)\, (E^{i+1}) \,, \qquad (5.37)$$

$$h_1^{i+1}(0) = 0 \,;$$

$$\bar{A}^{i+1}(0) = 1 \,;$$

$$E^{i+1}(0) = 0,$$

$$\frac{dh_2^{i+1}}{dt} = -\bar{A}^i\, e^{-E^i/R(1/T - 1/\bar{T})}\, n(W^i)^{n-1}\, (h_2^{i+1})$$

$$- (W^i)^n\, e^{-E^i/R(1/T - 1/\bar{T})}\, (\bar{A}^{i+1})$$

$$+ \bar{A}^i\, (W^i)^n\, e^{-E/R(1/T - 1/\bar{T})}\, \left(+\frac{1}{R}(1/T - 1/\bar{T})\right)\, (E^{i+1}) \,, \qquad (5.38)$$

$$h_2^{i+1}(0) = 0 \,;$$

$$\bar{A}^{i+1}(0) = 0 \,;$$

$$E^{i+1}(0) = 1 \,.$$

The solution for values of α_1 and α_2 continues as previously outlined for the regular model. But now,

$$\alpha_1 = \bar{A} ,$$

and

$$\alpha_2 = E .$$

Therefore, A must be calculated. For an appropriate temperature

$$A = \bar{A}\, e^{-E/RT} . \tag{5.39}$$

The initial assumption of the value of $\bar{A}$ is similarly computed. First, values of A°, and E° are assumed for a fixed n, and then $\bar{A}$ is determined from the equation

$$A = A^\circ\, e^{E^\circ/RT} . \tag{5.40}$$

The value of $\bar{T}$ has been taken as the temperature at the point of maximum rate of weight loss.

It is occasionally obvious from inspection of a thermogram that more than a single weight loss mechanism is occurring. The extension of the quasilinearization technique to a two-mode model illustrates in general the procedure for handling multiple modes.

It has been assumed frequently that the total weight loss of a sample is the sum of two independent parallel reaction mechanisms, each associated with a fraction of the original sample weight. Thus,

$$-\frac{dW^{i+1}}{dt} = \frac{dW_1^{i+1}}{dt} + \frac{dW_2^{i+1}}{dt}$$

$$= (W_1^i)^{n_1^i}\; A_1^i\; e^{-E_1^i/RT} + (W_2^i)^{n_2^i}\; A_2^i\; e^{-E_2^i/RT} \tag{5.41}$$

where

$$W = \frac{w - w_r}{w_o} \quad ,$$

$$W_1 = \frac{w_1 - w_{r,1}}{w_{o,1}} \quad ,$$

$$W_2 = \frac{w_2 - w_{r,2}}{w_{o,2}} \quad ,$$

and

$$w_1 + w_2 = w, \qquad w_{o,1} + w_{o,2} = w_o.$$

In this case the approach is to determine independently the particular and homogeneous solutions of each mode and consequently $W_1(t)$ and $W_2(t)$. Using the defining equations, w_1 and w_2 are calculated.

Graphical integration of a reaction peak on a plot of rate-of weight-loss versus temperature yields values of $w_i - w_{r,i}$. In order to obtain values of w_i, an assumption is usually made as to the value of $w_{i,r}$. Generally it is assumed that one reaction produces only gaseous products and the other, therefore, yields all the char residue. Using this assumption, or any other justified by experimental evidences, values of w_i are calculated. The combination of w_1 and w_2 yields $W^{i+1}(t)$, which is used in the calculation of the objective function Q. With these modifications the solution proceeds as outlined for a single mode.

CHAPTER VI

RESULTS AND DISCUSSION

In this chapter the experimental and analytical results of this work are presented, and the implications of these results with respect to the thermal degradation process are discussed. Tables 1 and 2 summarize the types of tests conducted and the specific conditions associated with each experiment. Numerical tabulation of all data. shown graphically in the following sections is included in Appendix F. Each polymer is discussed separately.

A number of different types of thermogravimetric tests were conducted, including combinations of the following conditions: isothermal and dynamic temperature programming; environmental atmospheres of air, helium and vacuum; flow and non-flow gas conditions. Each resin was not evaluated under every possible set of conditions. Test parameters chosen were based on specific experimental objectives. Most preliminary work was done in air with the objective of developing a sound experimental technique, and identifying limitations and idiosyncracies of the equipment. However, since the mechanism of oxidative decay is usually completely different from that of purely thermal decomposition, and since ablation takes place primarily in anaerobic conditions, all results reported herein were obtained in inert or nearly-inert environments.

Initial investigation showed that, for the materials under consideration, programmed temperature-rise rates of 5, 7.5, and 10°C/min. produced thermograms in which changes in thermogram curvature could be determined with equal sensitivity.

TABLE 1. SUMMARY OF TGA EXPERIMENTS

Run No.	Material	Type of Experiment	Environment Condition
1-2-1	SC 1008 Phenolic	Dynamic	He-non-flow
1-2-2	SC 1008 Phenolic	Dynamic	He-non-flow
1-2-4	Phenolic II	Dynamic	He-flow
1-2-5	Phenolic II	Isothermal-590°C	He-flow
1-2-6	Phenolic II	Isothermal-450°C	He-flow
1-2-7	Phenolic II	Isothermal-501°C	He-flow
2-2-1	Polybenzimidazole B	Dynamic	He-flow
2-2-2	Polybenzimidazole A	Dynamic	He-flow
3-2-3	Polyquinoxaline	Dynamic	He-non-flow
3-2-4	Polyquinoxaline	Isothermal-490°C	He-non-flow
3-2-5	Polyquinoxaline	Isothermal-410°C	He-non-flow
3-2-6	Polyquinoxaline	Isothermal-455°C	He-non-flow
3-2-7	Polyquinoxaline	Isothermal-510°C	He-non-flow
3-2-8	Polyquinoxaline	Isothermal-572°C	He-non-flow
3-2-9	Polyquinoxaline	Isothermal-627°C	He-non-flow
3-2-10	Polyquinoxaline	Dynamic	He-non-flow
4-2-1	Polyphenylene	Dynamic	He-non-flow
4-2-2	Polyphenylene	Isothermal-570°C	He-flow
4-2-3	Polyphenylene	Isothermal-600°C	He-flow
4-2-4	Polyphenylene	Isothermal-700°C	He-flow
4-2-5	Polyphenylene	Isothermal-890°C	He-flow
4-2-6	Polyphenylene	Isothermal-900°C	He-flow
4-2-7	Polyphenylene	Isothermal-485°C	He-flow
5-2-1	Polyimide	Dynamic	He-non-flow
5-2-2	Polyimide	Isothermal-490°C	He-non-flow
5-2-3	Polyimide	Isothermal-585°C	He-non-flow
5-2-4	Polyimide	Isothermal-533°C	He-non-flow
5-2-5	Polyimide	Dynamic	He-flow
5-2-6	Polyimide	Isothermal-590°C	He-flow
5-3-7	Polyimide	Isothermal-567°C	Vacuum

TABIE 2. SUMMARY OF GAS ANALYSIS EXPERIMENTS

Run No.	Material	Temp.°C	Column* Used	Time min.	Elemental Char Analysis
PCI-A-1	Polybenzimidazole	588	CS	60	✓
PBI-A-2	Polybenzimidazole	697	CS	98	✓
PQ-1	Polyquinoxaline (unadvanced)	541	CS	56	✓
PQ-2	Polyquinoxaline (unadvanced)	701	CS	60	✓
PP-1	Polyphenylene	585	SG	40	✓
PP-2	Polyphenylene	700	SG	90	
PP-3	Polyphenylene	700	SG	110	✓
PP-5	Polyphenylene	700	SG	60	✓
PP-6	Polyphenylene	700	CS	660	✓
PP-7	Polyphenylene	700	SG	75	
PI-1	Polyimide	480	SG	160	✓
PI-2	Polyimide	597	CS	218	✓

* CS = Cromasorb-102

SG = silica gel

Thereafter, a temperature-rise rate of 10°C/min. was uniformly applied as a matter of experimental convenience. Higher rates tended to obscure minor thermogram-curve inflections clearly detected at rates of 10°C per minute or less.

Elimination of the effects of changes in buoyancy during an experiment was accomplished by the use of blank runs. Pure, high-density graphite of approximately the same volume as used in regular experiments was tested in exactly the same manner as polymer samples. The room temperature weight of the reference sample was the same after testing as it was before. Since the graphite was inert under the test conditions, changes in apparent weight were attributable to buoyancy effect. Figure 11 illustrates this apparent weight change in helium for dynamic temperature experiments, under both flow- and non-flow conditions. The magnitude of the maximum correction was 4.0 per cent in the non-flow case, and was .3 per cent in the case where helium flow was 35 cc per minute. Since the apparent weight change was a function of the helium-sweep rate, a flow-rate of 35 cc per minute was maintained in all TGA experiments. Other flow rates generally led to larger corrections.

Correction curves for isothermal experiments were also determined. However, in this case corrections observed were influenced strongly by the volume of the system, by the size of the exit orifice, and by the extent of baffling used, in addition to the gas-flow rate and steady-state temperature. Therefore, isothermal corrections lack generality, and each was included immediately in the reduction of the data. Isothermal buoyancy corrections were made in a manner similar to the

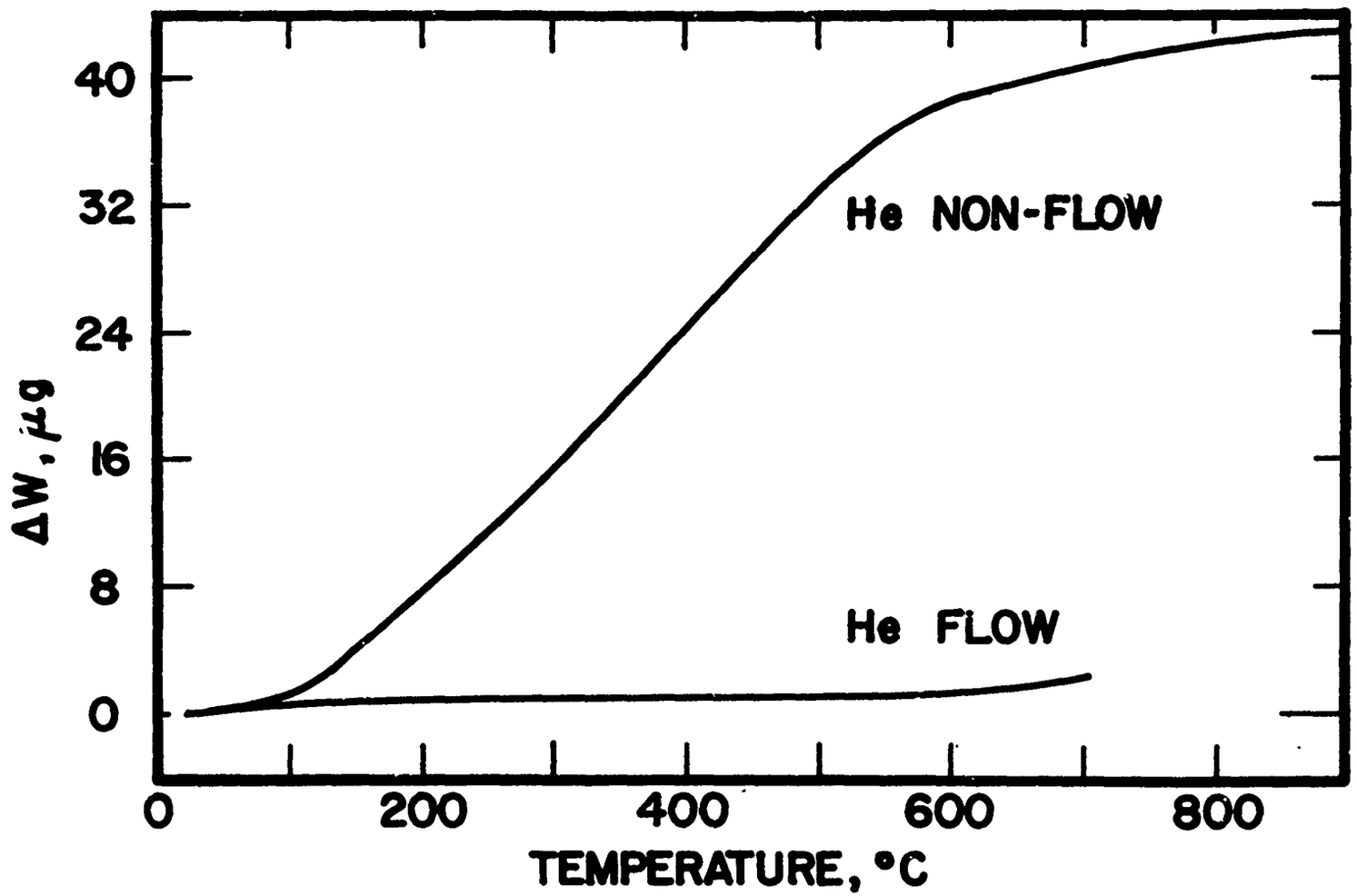

FIGURE 11. Buoyancy Correction for Dynamic Thermogravimetric Analysis in Helium

dynamic corrections. That is, the experiment was duplicated with an inert test material, and the apparent weight changes observed were attributed to buoyancy effects. An example of a buoyancy correction is shown in Appendix A. All data shown in this chapter have been corrected for buoyancy.

The thermogravimetric data for the polymers studied were obtained with a high degree of accuracy. For non-flow experiments, sample weights were measured to within $\pm$ 0.001 mg with initial sample weights varying from 3 mg to 9 mg. In the case of flow experiments, where the control of noise was more difficult, the accuracy of measurement deteriorated, particularly at high temperatures and with small sample weights. In these regions it was necessary to average the oscillations to obtain a mean value representative of the true specimen weight. Usually this averaging was necessary only to determine the final residual weight of the polymer. In the region where weight measurements were critical, the zone used for calculation of kinetic parameters, curves were usually smooth enough to be read directly or with only minor interpolation. In this case, accuracy of measurement was within $\pm$ 0.002 mg or approximately 0.03 per cent for an average sample.

Even though high sensitivities were possible in weight determinations, other subtle errors were encountered. Ever-present static electricity affected apparent weights by as much as 0.01 mg in severe cases. Of course, this extreme was seldom encountered, but to a lesser degree, the effect was always present.

It was observed that the shape and cleanliness of the stirrup on the beam arm of the balance and the hangdown support wire affected weight readings. A high degree of sensitivity and precision in balance

operation required that the hangdown wire, stirrup, and stirrup support all be able to move freely with respect to their points of contact. Condensation of pyrolysis products on these fine wires could restrict free movement, and could lead to small errors in weight measurements, and poor precision between experimental runs. In order to avoid this problem, cleanliness of the entire balance and support system was maintained by periodic washing with methyl-ethyl-ketone. It is also necessary to insure single-point contact between the hangdown wire and the supporting loops. In order to achieve this, the hangdown wire was bent at a sharp angle to form a supporting hook.

Phenolic Polymer

It was not intended in this thesis work to make a detailed investigation of phenolic resin. Because of the extensive literature on this material, it was believed that greater value could be gained by emphasizing newer polymers. However, some data were taken in order to develop sound experimental techniques, to confirm previously obtained conclusions, and to present accurate thermogravimetric information on this polymer. Thermograms obtained from phenolic resin, Resinox SC-1008, in both dynamic and isothermal conditions are presented in Figures 12 through 16. Figure 12 illustrates the dynamic-thermal behavior of the resin in a non-flow, helium environment. Figure 13 is a plot of the rate of weight loss for the same experiment. The complex nature of the derivative curve indicates a complex reaction mechanism. The thermogram exhibits the same characteristic features as have been observed by other investigators [45, 20]. The effect of post-curing this resin is noted by comparing Figures 12 and 13 with

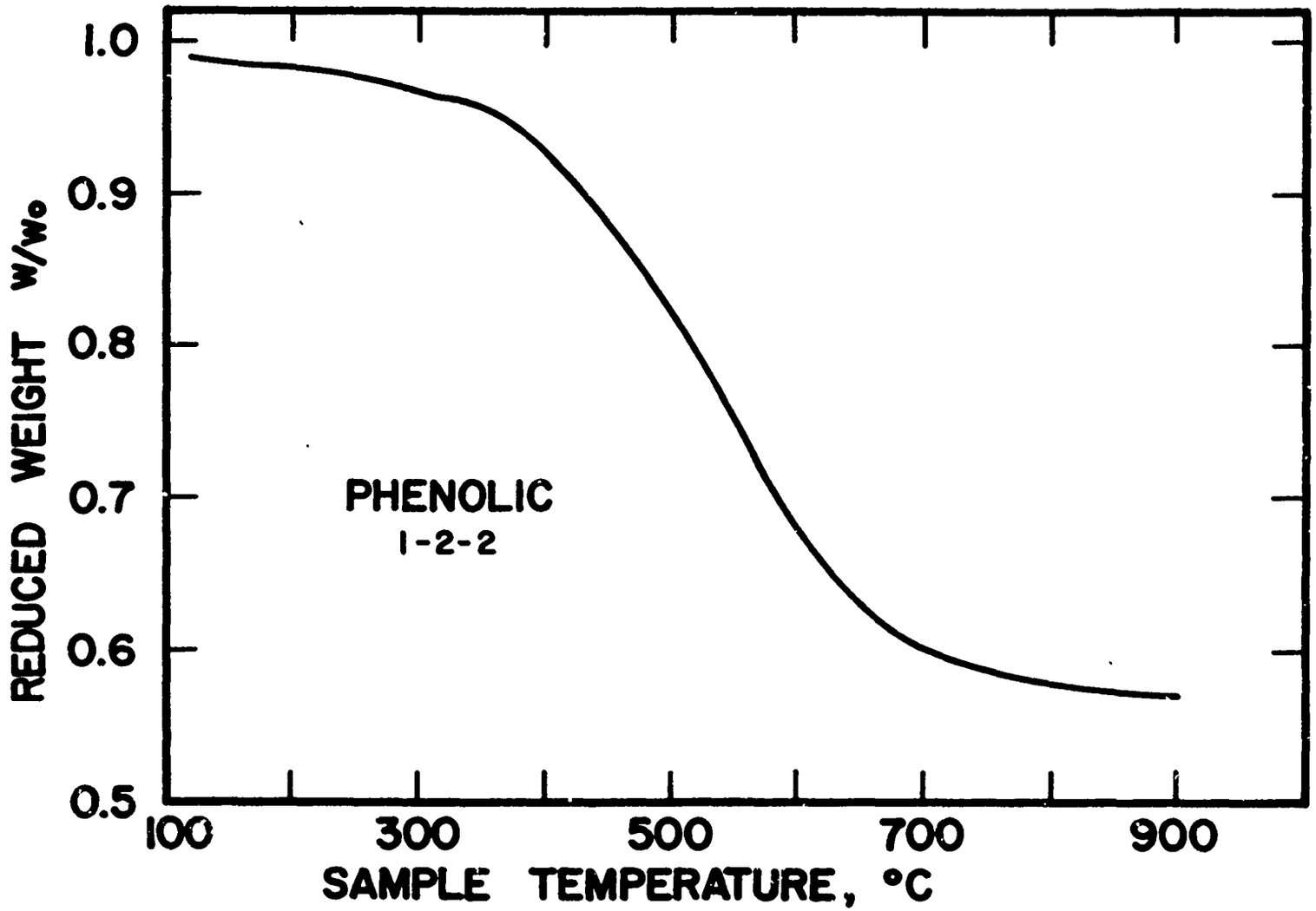

FIGURE 12. Dynamic Thermogram for SC-1008 Phenolic in Non-flowing Helium at 10°C/min

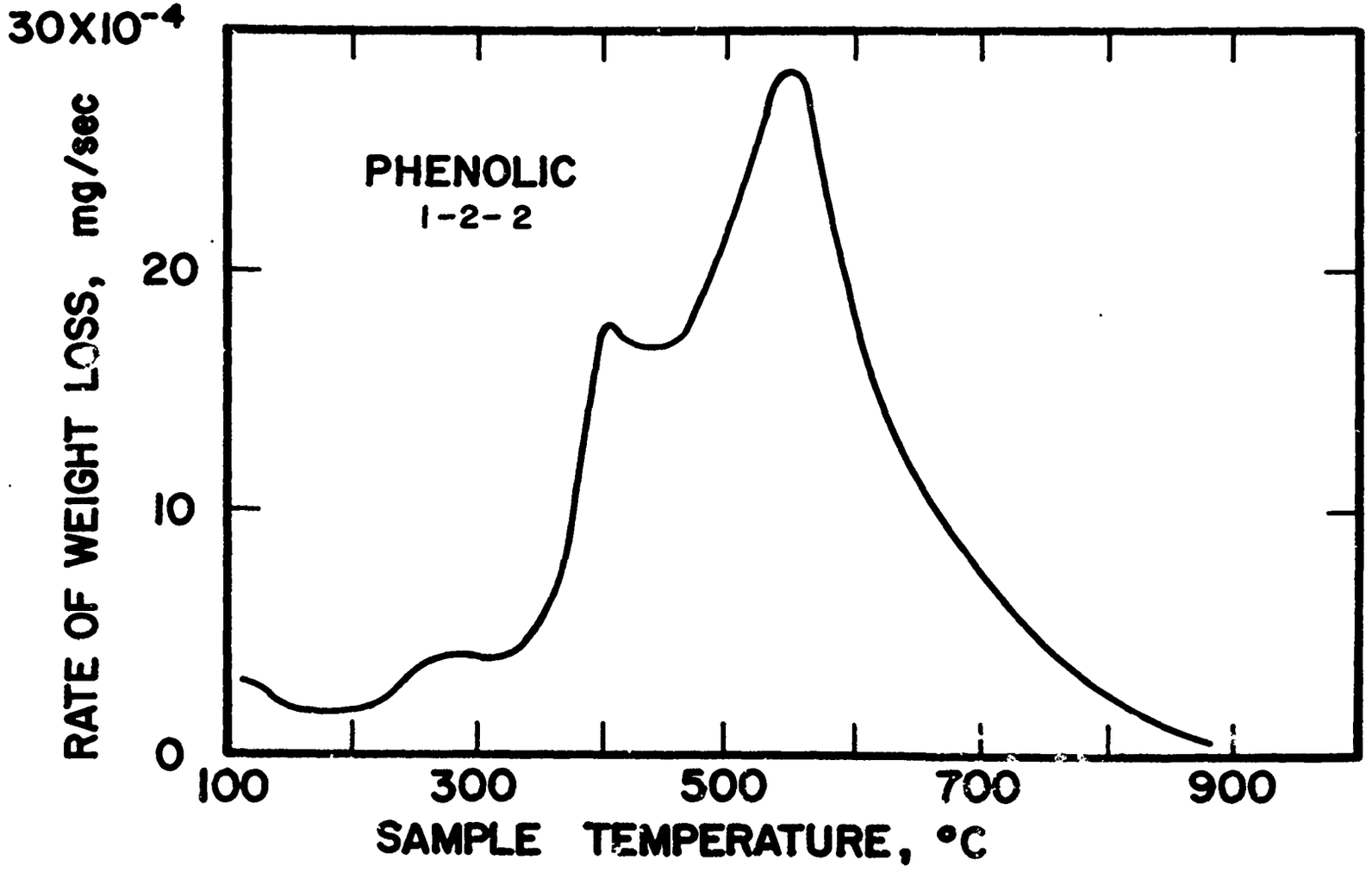

FIGURE 13. Rate of Weight Loss for SC-1008 Phenolic at 10°C/min in Non-flowing Helium

Figures 14 and 15. These latter figures illustrate a dynamic thermogram and a rate-of-weight-loss plot for phenolic II. Phenolic II was the same basic polymer as the original phenolic, but it had been post-cured in helium for two hours at 500°C and for two hours at 600°C. The thermal response indicated in the two cases is very similar. The temperatures corresponding to the major weight-loss peaks are the same in both cases. However, early weight changes, probably resulting primarily from continued cross-linking and condensation, are somewhat smaller for the postcured sample. Also, the postcured resin is slightly more stable in the 500°C to 700°C temperature region, leading to retention of about 4 per cent more of the original weight in the char at 900°C. The curves of rate of weight loss versus temperature shown in this chapter were obtained from numerical differentiation of the data. Since the results of TGA experiments were graphical in form, it was necessary to discretize the thermogram. The number of points determined depended upon the rate of curvature of the thermogram. In all cases enough points were selected that the line through any three consecutive points was essentially linear. The derivative at any point was then calculated from the values of the points equally spaced on either side. In Figure 16 the results of three isothermal experiments are plotted with values of reduced weight as functions of time-of-exposure to the temperatures indicated.

The temperatures of the isothermal experiments represent significant points in the thermogram. At 450°C the first major weight loss peak is totally activated, but subsequent mechanisms are not. The experiments at 501°C and 590°C bracket the largest reaction peak shown in Figure 15.

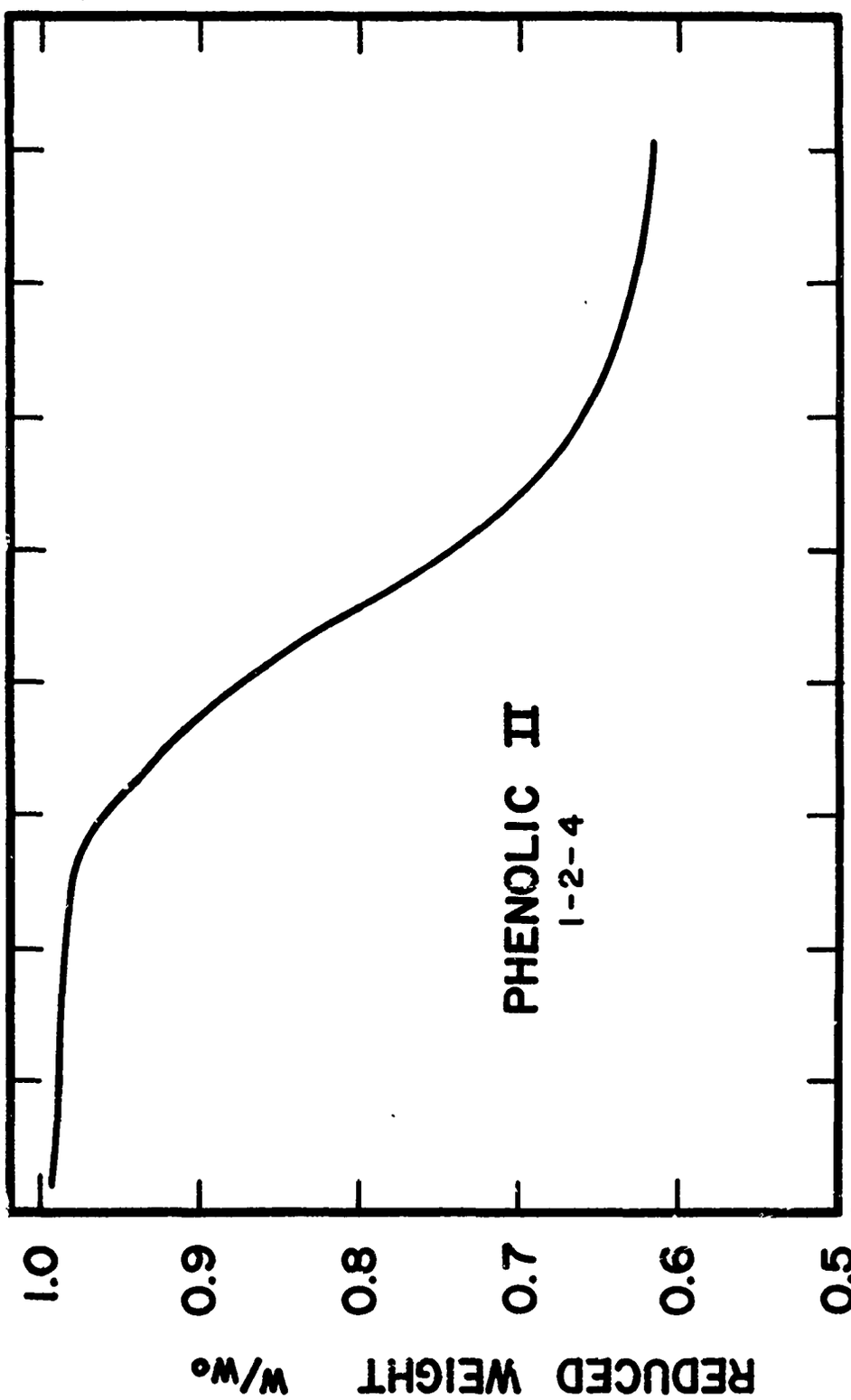

FIGURE 14. Dynamic Thermogram for Phenolic II at 10°C/min in Non-flowing Helium

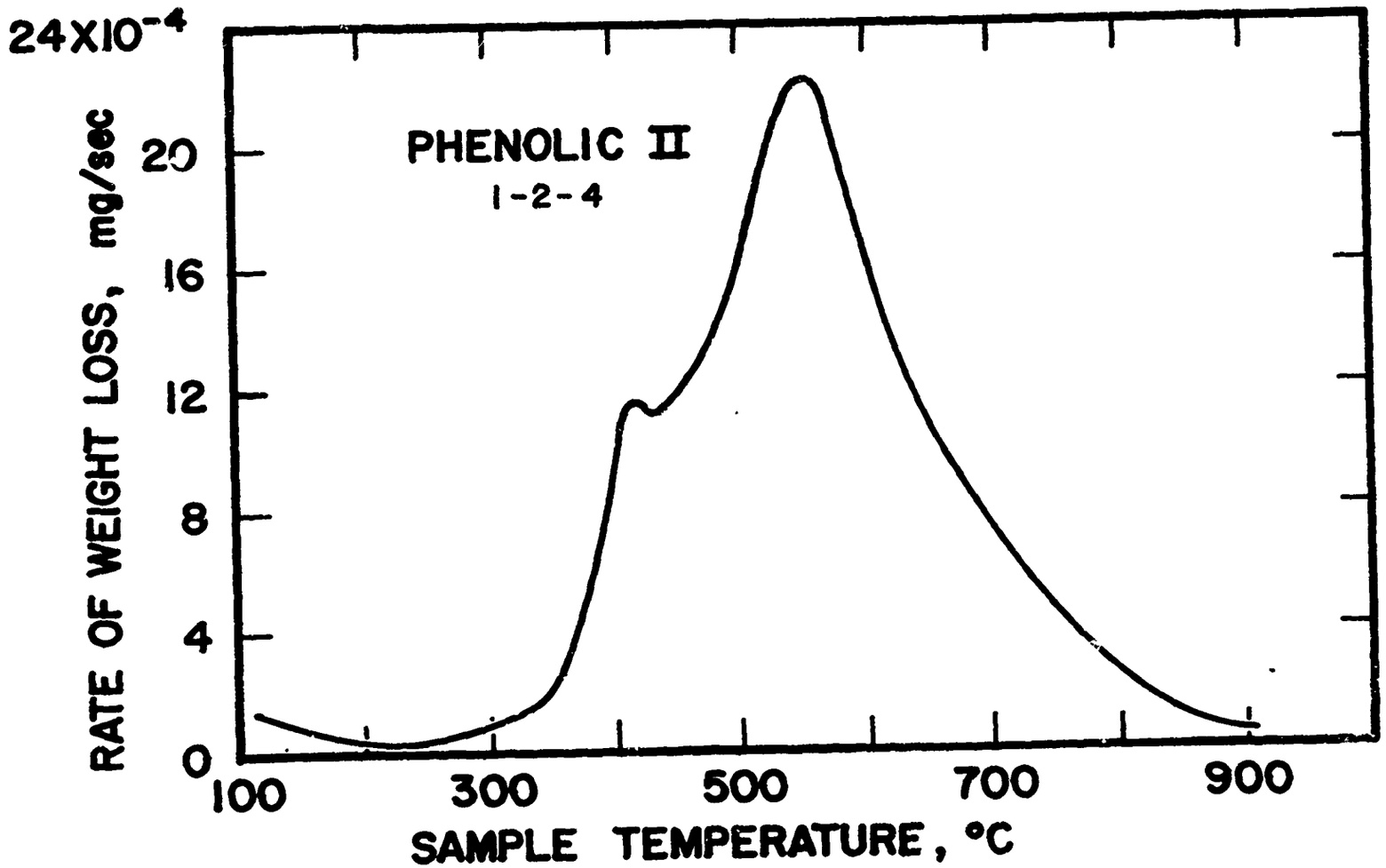

FIGURE 15. Rate of Weight Loss for Phenolic II at 10°C/min in Non-flowing Helium

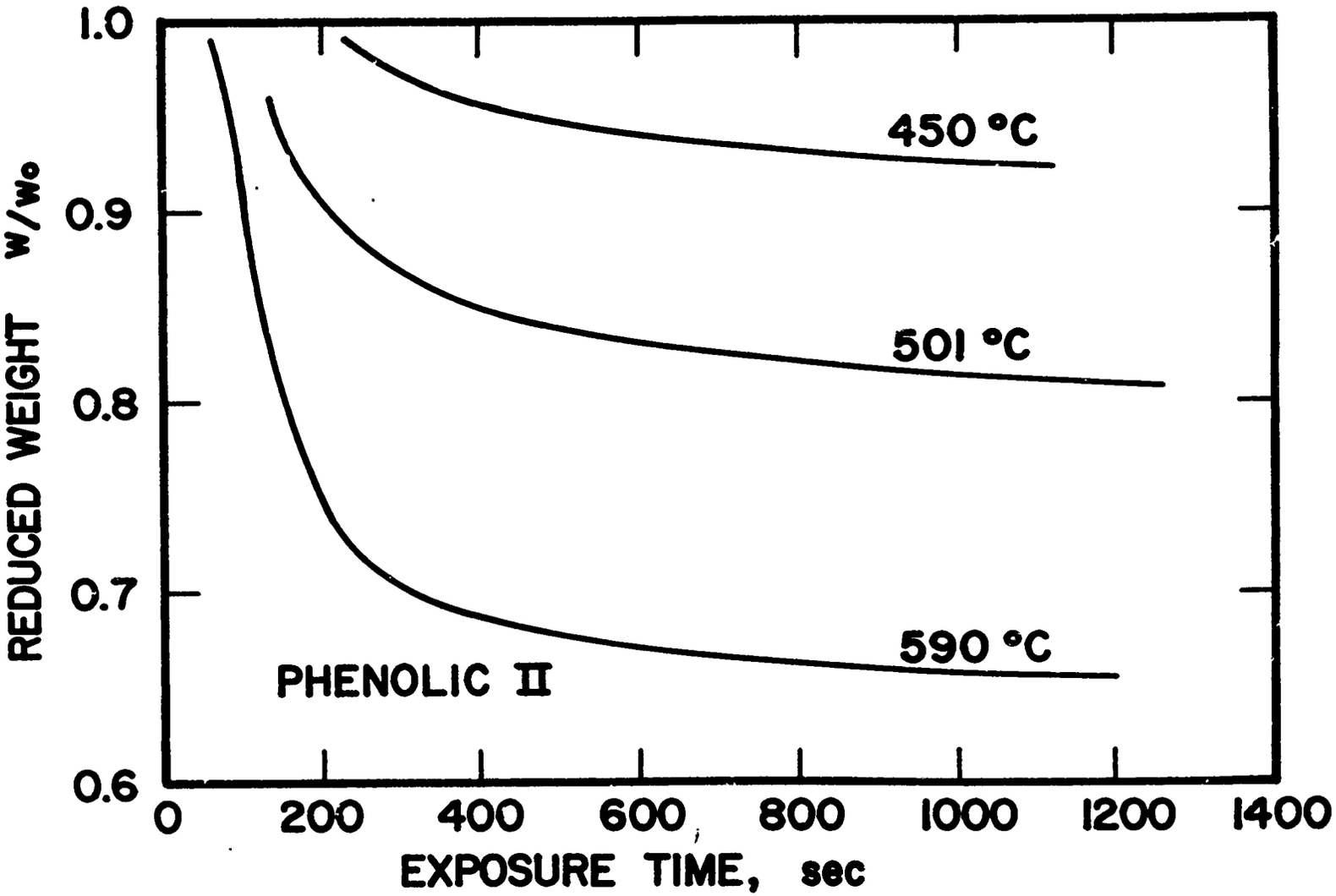

FIGURE 16. Isothermal Thermograms for Phenolic II in Flowing Helium

If the 450°C isothermal experiment represents only that weight lost in the first pyrolysis reaction, then this reaction accounts for the loss of approximately 8 per cent of the original material weight. The dynamic thermogram also is observed to have lost 8 per cent of the original weight of 450°C.

The weight loss in the higher temperature isothermal experiments does not correlate with the dynamic curve as well as the 450°C experiment does. After 1200 seconds exposure at the temperatures of the 501°C and 590°C, the isothermal weight losses were 81 per cent and 65.5 per cent, respectively, while the corresponding dynamic weight losses at these temperatures were 87 per cent and 75 per cent. It seems that at the higher temperatures the activated reaction mechanisms had not yet gone to completion in the dynamic experiment.

In order to determine the reproducibility of thermograms obtained on the Cahn balance, the dynamic evaluation of phenolic resin was duplicated. The dynamic thermogram shown in Figure 12, run 1-2-2, was obtained under exactly the same conditions as for run 1-2-1 conducted eight months earlier. The only significant difference in the two experiments was the initial weight of sample. The data for both of these tests are included in Appendix F, Table F-1, as reduced weight versus temperature. Inspection indicates that the two curves can be directly superimposed with variation only in the third decimal place of reduced weight. The exceptional reproducibility manifested in these two experiments, does not permit the conclusion that such a high degree of precision could always be obtained. Rather, it indicates that when care is taken, the Cahn-balance system is capable of producing high-quality data exhibiting both precision and accuracy.

A further significant conclusion may be possible. The initial weights used in the two experiments were somewhat different, 9.481 mg for run 1-2-1 and 10.529 mg for run 1-2-2. If the thermal decomposition was diffusion dependent, samples of differing initial weights would exhibit differing kinetics. Thus, if the two samples are considered to be sufficiently different, the pyrolysis reaction observed was not diffusion limiting.

The gaseous products of pyrolysis generated during a dynamic TGA flow experiment were analyzed in the Perkin-Elmer chromatograph described previously. The major species were identified as water, hydrogen, carbon monoxide, and methane. It was hoped that pyrolysis gases would be swept from the hangdown tube to the chromatograph in pseudo-plug flow without mixing of the components. Unfortunately, extensive mixing of the pyrolysis gases was observed, caused primarily by convection currents. Therefore, it was impossible to correlate accurately the gases identified and the temperatures of their formation. For this reason, it was decided that pyrolysis-gas-analysis experiments would be conducted under isothermal TGA conditions.

Water was the first detected volatile product of the degradation reaction. It was observed at a pyrolysis temperature of about 150°C, and its presence supports the hypothesis that the early weight-loss reactions shown in Figure 12 were continuations of condensation cross-linking. The quantity of hydrogen in the gas stream was very slight at low temperatures, but it increased significantly as temperature increased. Hydrogen was the dominant product at temperatures greater than 650°C. During the major portion of the decomposition reaction,

methane was the primary pyrolysis product. Similar results were obtained by Friedman [17] and by Schulman and Lochte [42].

Ladacki, Hamilton and Cohz [28] identified the pyrolysis gases of SC-1008 phenolic polymer in their work to calculate the heat of pyrolysis of the resin in a silica-reinforced composite. Approximately 10 to 20 mg of resin was coated on a tantalum wire which was supported in the evacuated inlet tube of a mass spectrometer. The wire was then electrically heated to temperatures of 400°C, 600°C, and 880°C for 45 seconds. The authors did not discuss the problems of attaining or maintaining the test temperature as the resin was heated and pyrolized.

Averaged concentrations of the species collected during pyrolysis were tabulated. These authors found that for the 400°C, 600°C, and 880°C tests, the mole per cents of water in the analyzed gas were 68.5, 18.8, and 6.0. The very high concentration of water in the first test probably indicated that extensive postcuring of the resin had occurred. The still high value observed at 600°C was explained as the result of further condensation plus the occurrence of some pyrolytic reactions. In general, it is believed that the high concentrations of water observed by Ladacki et al. illustrate the difficulty in comparing time-averaged concentrations with instantaneous measurements. For phenolic resin, it seems that time-averaged values must indicate more water than instantaneous determinations do.

A descriptive reaction mechanism postulated by Parker and Winkler [40] for the degradation of phenolic novolac resins in an inert environment is based on several reaction steps occurring predominantly at different temperatures. These steps are in qualitative agreement with the steps observed in the phenolic TGA thermogram of Figure 12 and

are in quantitative agreement with the measured yield of char residue. The gaseous products postulated are also in agreement with the observations made in this thesis.

Parker and Winkler suggest that the thermograms obtained from TGA analysis of phenolics can be explained by assuming that the stable chars observed result from the coalescence of certain benzenoid structures in the principal chains of the polymer. They suggest that the initiation step for the pyrolysis, given as (I) in Figure 17, is the homolytic scission of the carbon-carbon bond connecting the aromatic pendant group to the main chain. Pendant group elimination can occur on either side of the single bonded phenol ring to give both a phenol radical and a cresol radical (III and III-a). Next, a rapid abstraction of hydrogen atoms follows to give phenol and cresol as primary products. The free radical main chain intermediates (II) and (IV) formed are expected to rearrange to give intermediates (VI) and (VII). It is postulated that char formation proceeds through a stable intermediate, shown as (VIII), formed by termination of the main chain radical pairs (VI) and (VII). The formation of this stable bond prevents elimination of those aromatic rings initially bonded by two or more methylene groups in the principal chain. Thus, only those phenolic ring structures,which are multiply bonded in the virgin polymer, are retained in the thermally crosslinked intermediate, which loses methane and carbon monoxide above 500°C to give unstable char. Thermally stable char is depicted as forming by continued crosslinking of the aromatic rings in char (IX) with elimination of hydrogen and water. The final char retains only those aromatic carbons multiply bonded in

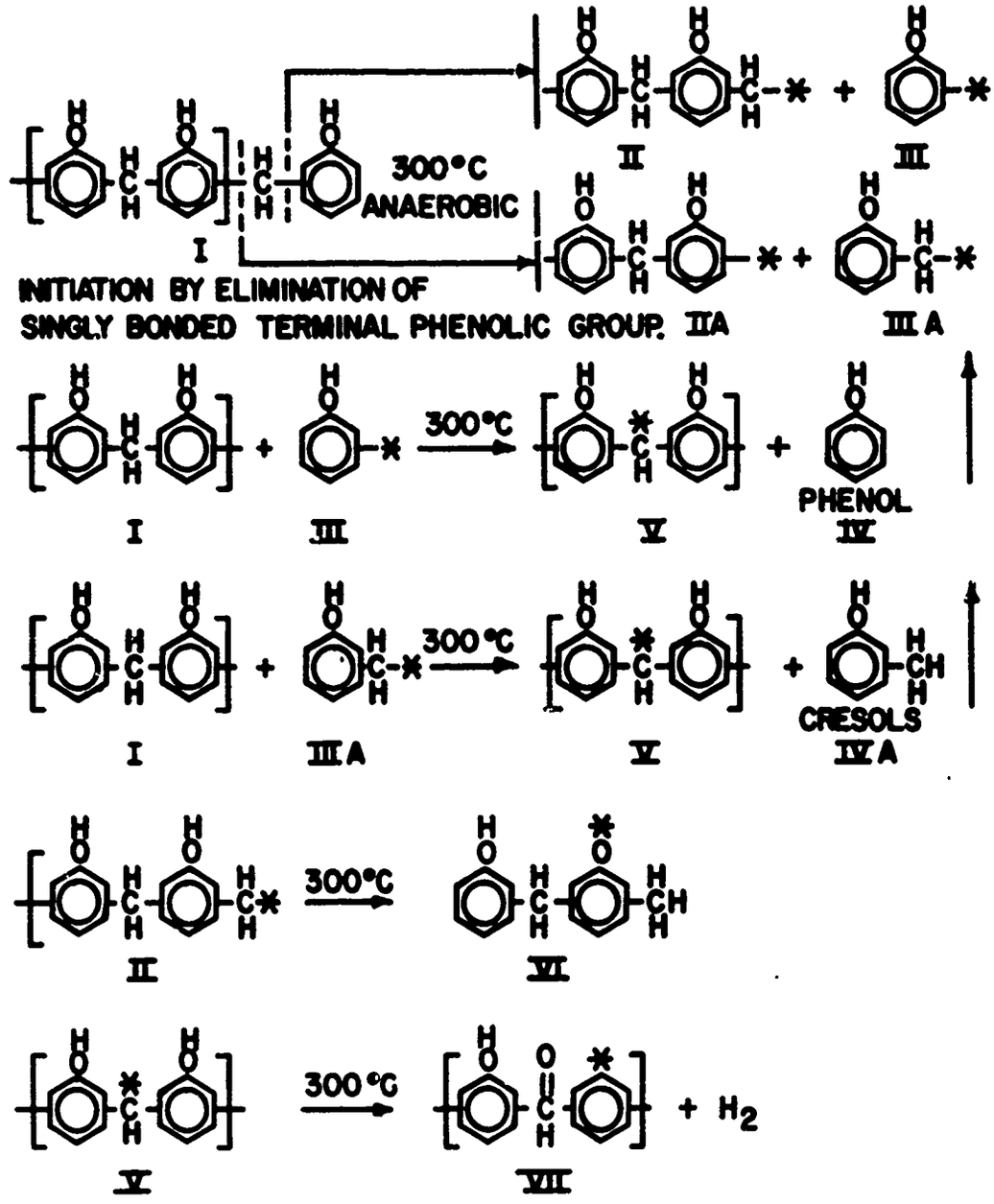

FIGURE 17. Proposed Mechanism of Nonoxidative Thermal Degradation of Phenolic Resins

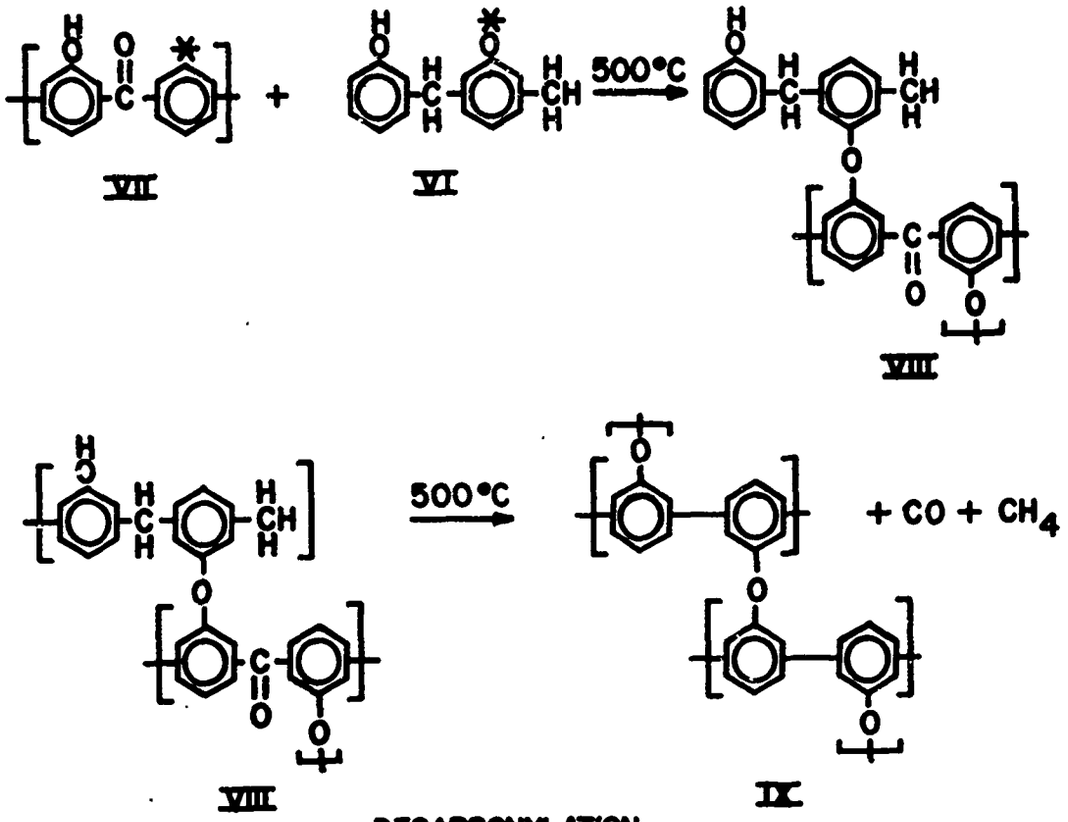

FIGURE 17. Continued

the original polymer. Parker and Winkler applied their proposed mechanism to other published data with considerable success. Certainly the proposed mechanism is an important step in understanding phenolic thermal decomposition.

The mechanism of Parker and Winkler is somewhat different than another porposed by Madorsky [30]. Although Madorsky does not propose a series of detailed reaction steps, he suggested that the primary mechanism of thermal degradation was the scission of bonds as indicated by the dotted line,

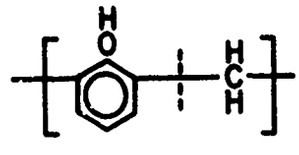

At temperatures of pyrolysis of about 360°C, he determined the main volatile constituents to be acetone, propylene, propanol, and butanol. The compounds, CH_4, CO, CO_2, were thought to result from the complete breakdown of the benzene ring at between 800 and 1200°C. The free radicals resulting from this thermal cracking could either recombine or strip the crosslinked residue of hydrogen and oxygen.

The two mechanisms differ on the location of initial chain scission and on the source of such gases as CO_2, CO, and CH_4. Also, Parker and Winkler detected phenol and cresols which were not observed by Madorsky. The rearrangement proposed by Parker and Winkler yielding char is also another significant difference. Even though the mechanism of Parker and Winkler seems to fit more data better than Madorsky's, neither approach can be completely rejected. The thermal history of phenolic

polymers previous to testing exerts a very strong influence on the nature of pyrolysis gases evolved and the thermogram produced. The early part of a thermogram is particularly affected. Differences in basic polymeric structure and methods of gas analysis also could have easily contributed to some of the differences between the two results.

Parker and Winkler also apply their mechanism to the data reported by Madorsky and point out qualitative agreement between the two. It is interesting to compare the char yields predicted and observed. Madorsky reported a char yield for a phenolic made from 1:1 molar ratio of phenol to formaldehyde as 56 per cent at 800°C. In the results shown in the present work, char yields of 58 per cent and 63 per cent were observed at 800°C for phenolic and phenolic II. Parker and Winkler predicted a char yield of 67.8 per cent, assuming no singly bonded pendant phenol groups, and they, therefore, concluded that the Madorsky resin had five doubly bonded phenol groups for every singly bonded one. If this analysis is correct, the resins tested in this thesis had ratios of doubly bonded to singly bonded phenol groups of 6:1 and 13:1 for the normal phenolic and phenolic II, respectively.

No attempt was made to determine kinetic parameters for Resinox SC-1008 by the application of quasilinearization. Such a calculation would have required extension of the basic equations of Chapter V to include a three-mode model. While this modification is conceptually not difficult, its application would require extensive modification of the experimental approach to provide the necessary data.

Nelson [37] determined kinetic parameters for a phenolic resin by

fitting the dynamic thermogram with three general polynomials. Appropriate mathematical manipulation of the fitted polynomials permitted him to try several schemes for calculating the desired parameters. Although parameters fitting the thermogram reasonably well were finally determined, most methods completely failed because the data being fit were not sufficiently accurate.

Polyphenylene Polymer

Polyphenylene polymer has a structure which was predicted to be ideally suited to ablation applications. It was thought that its totally aromatic structure and simple conformation would produce, upon pyrolysis, the desired attributes of a low-molecular-weight gas, hydrogen, and a stable, highly-carbonaceous char. Some of the expected potential of this polymer is beginning to be realized.

The results of dynamic thermogravimetric analysis of a para-polyphenylene resin are shown in Figures 18 and 19. The exceptional thermal stability of this polymer is indicated by the high char yield of 82% of original weight at 900°C and by the relatively high temperature of occurrence of major weight loss. Another distinguishing characteristic of the thermogram is the gradual loss of weight below 600°C. Above this temperature a more normal appearing region is found. As shown in Figure 19, the rate of weight loss during the early portion of the thermogram seems to be unrelated to later reactions. Evidence for this conclusion was provided by subsequent tests as described below.

Isothermal TGA experiments on polyphenylene were conducted at 485°C and 610°C. The results of the isothermal tests are shown in

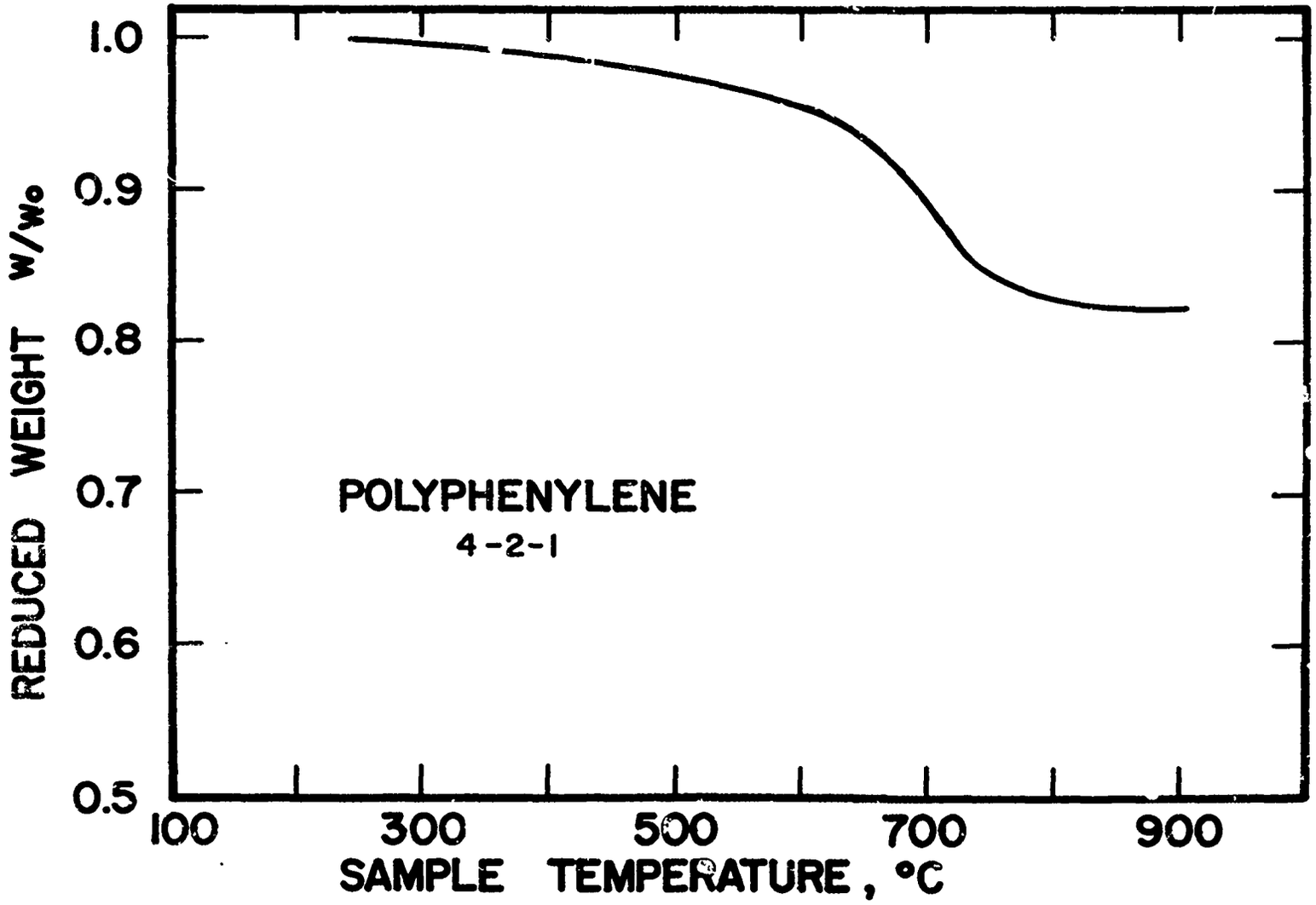

FIGURE 18. Dynamic Thermogram for Polyphenylene at 10°C/min in Non-flowing Helium

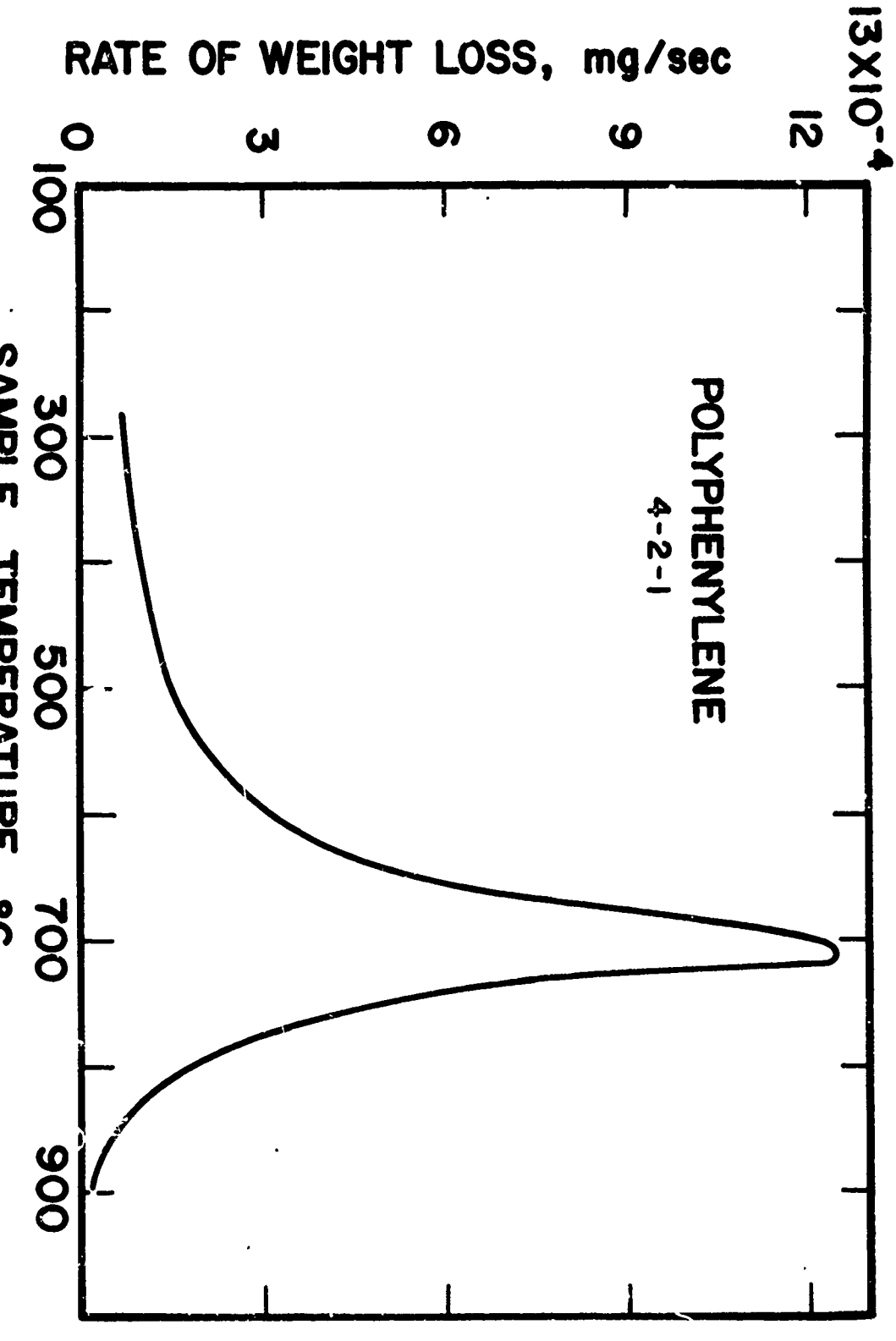

FIGURE 19. Rate of Weight Loss for Polyphenylene in Non-flowing Helium

Figure 20. The temperature of 485°C was chosen as representative of the early pyrolysis reactions of this polymer, while the higher temperature of 610°C is located in the "knee" of the thermogram curve where the major weight-loss mechanism becomes important.

The primary products of pyrolysis were identified as hydrogen and methane. In addition, an undetermined, but probably small amount, of benzene and biphenyl were detected. The benzene was identified as a small, broad, yet distinct peak in the chromatogram. Biphenyl condensed as a white solid on the walls of the pyrolysis chamber which were outside the furnace. Quantities of biphenyl collected were very small. Although biphenyl was noted for each of the samples pyrolized, benzene was only observed for the higher temperature experiments. Benzene was very probably a product of all the experiments, but its presence in small quantities was likely masked.

In all of the results of the analyses of pyrolysis gases reported in this thesis, a distinction must be made between the concentrations of gases measured in the chromatograph and the concentrations evolved within the decomposing polymer. The pyrolyzing resin sample produces gases which are swept from the reaction chamber to the chromatograph by helium carrier gas. If the helium flow rate is constant, the pyrolysis products are continuously and uniformly diluted. At the gas-sampling inlet on the chromatograph, a small sample of the flowing mixture of product and carrier gas is selected for analysis. Thus, the mole fractions reported herein represent diluted product and not the pyrolysis gas as generated. Of course, the measured quantities are directly related to the originally generated compositions by a constant dilution factor, which is a function of the helium flow rate. Further, the

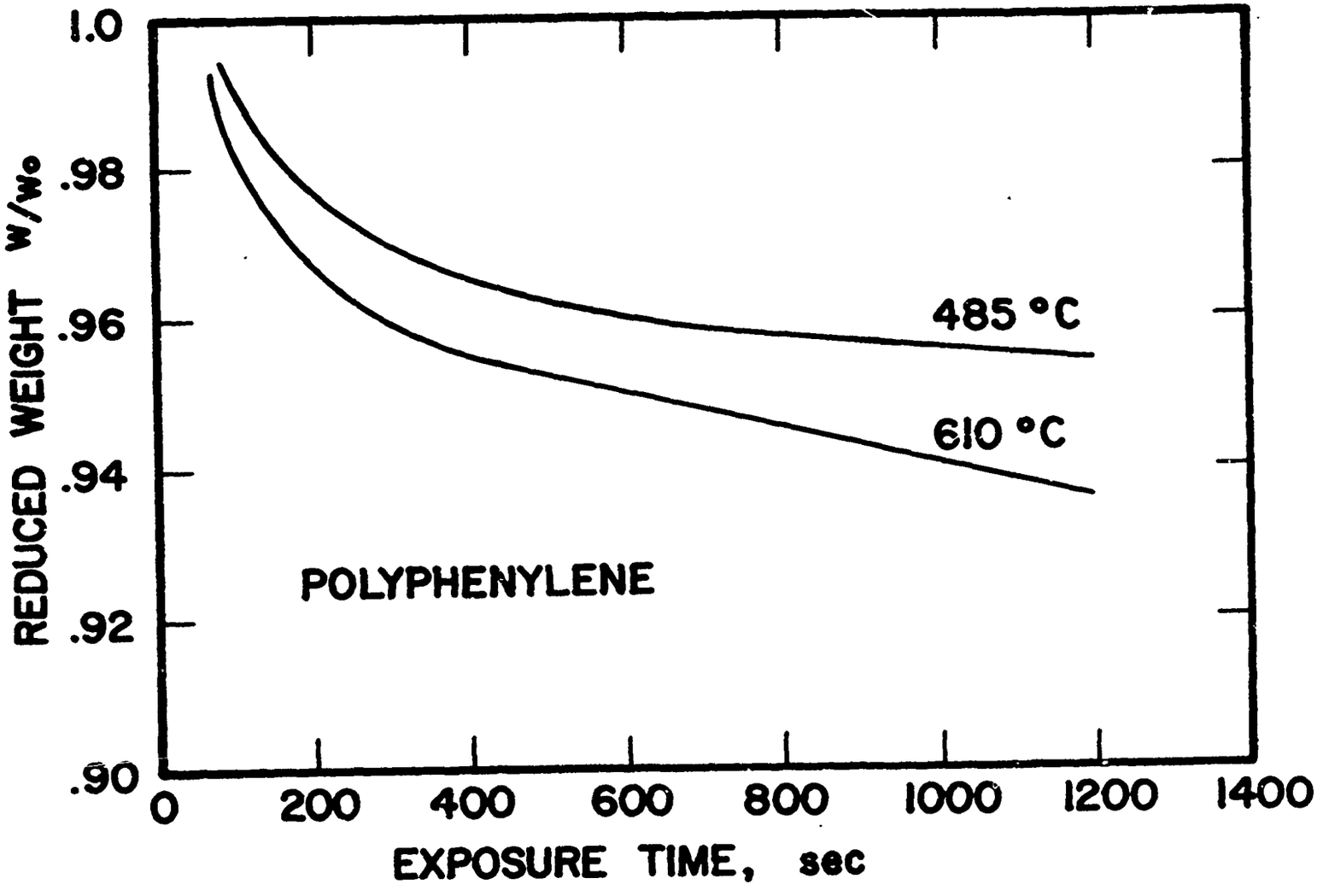

FIGURE 20. Isothermal Thermograms for Polyphenylene in Flowing Helium

measured molar ratios of the gaseous species are the same at the chromatograph as at the point of their evolution if no axial diffusion occurs. Therefore, the experimentally determined molar ratios of pyrolysis gases represent a strong indicator of the decomposition mechanism.

Gas analysis experiments were conducted in such a manner that the pyrolysis gases were identified as they were generated in time. It is believed that this procedure of making instantaneous, sequential analyses is superior to methods commonly employed, which average the compositions over the entire time of decomposition. Certainly instantaneous measurements give far greater insight into the pyrolysis mechanism.

The gaseous decomposition products were predominantly methane and hydrogen at both 585°C and 700°C. Table 3 presents values of concentrations of the diluted gas species as functions of exposure time for an isothermal, 585 °C experiment. Figure 21 shows these same data graphically. Clearly, hydrogen was overwhelmingly the most abundant product. Scatter in the data, probably attributable to inaccuracies in the quantitative hydrogen determinations, make it difficult to deduce trends in the reaction. It seems that in addition to chlorine elimination, the major chemical reaction is the stripping of hydrogen from the aromatic rings. The amount of hydrogen lost represents only about one hydrogen atom for every four phenyl groups. The lack of constancy in the observed molar ratio of hydrogen to methane implies that the reaction mechanism was not constant throughout the decomposition. The results of 700°C pyrolysis are tabulated in Tables 4 and 5

TABLE 3. PYROLYSIS GAS ANALYSIS FOR POLYPHENYLENE AT 585°C, RUN PP#1

Time sec.	H_2		Mole Ratio H_2/CH_4	CH_4	
	Peak Height	Mole Per Cent		Peak Height	Mole Per Cent
240	2.78	.786	42.98	.80	.0183
420	.68	.192	22.58	.37	.0085
660	.47	.133	28.91	.20	.0046
780*	--	--	--	.19	.0044
1020	.12	.0357	5.41	.29	.0066
1320	.03	.0085	--	0	0

*This data point for hydrogen lost by experimental error.

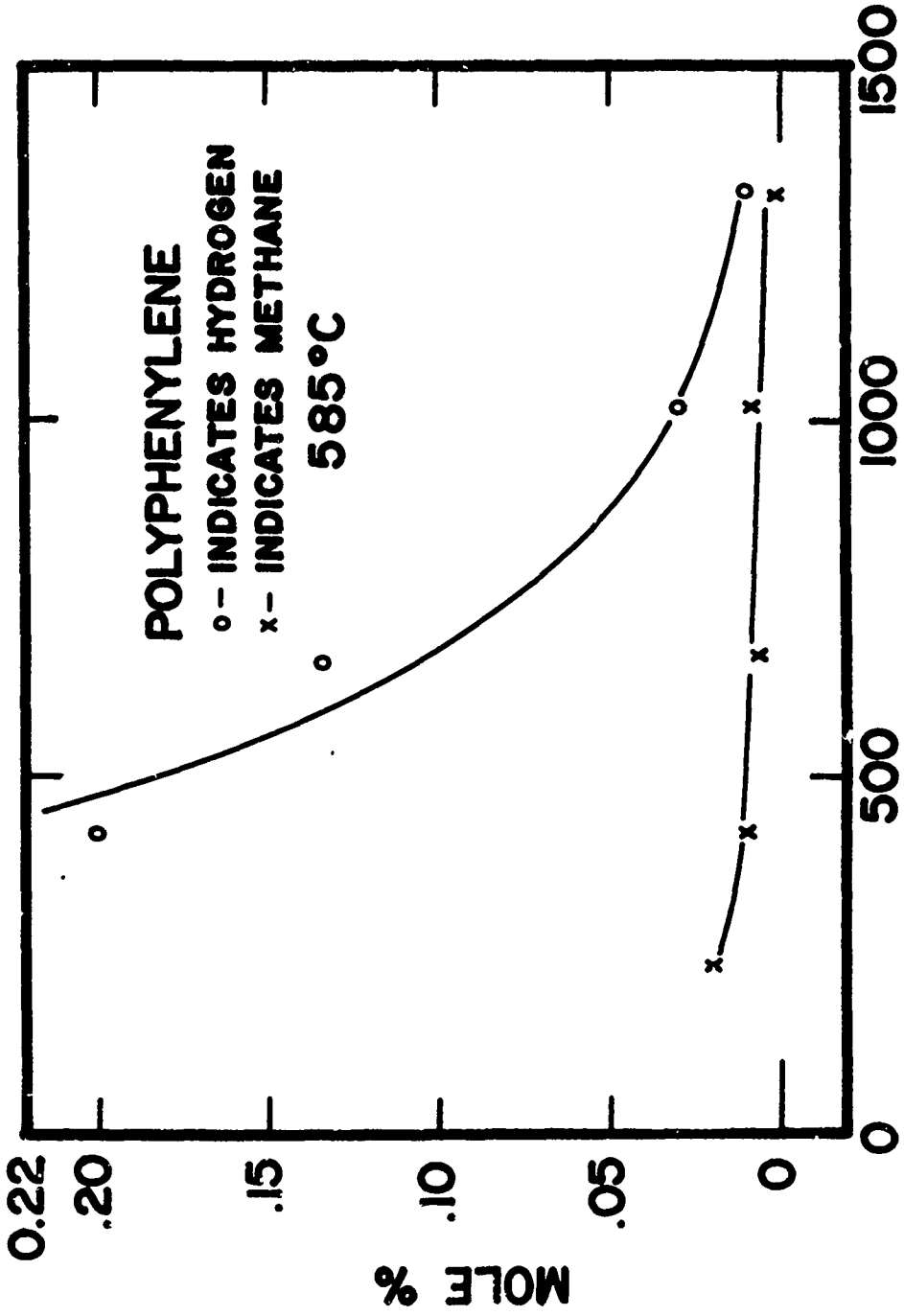

FIGURE 21. Gaseous Pyrolysis Products of Polyphenylene at 585°C in Helium

TABLE 4. PYROLYSIS GAS ANALYSIS FOR POLYPHENYLENE AT 700°C,

RUN PP#3

Time, sec	H_2		CH_4		Mole Ratio H_2/CH_4
	Peak Height	Mole Percent	Peak Height	Mole Percent	
180	.50	.1415	.87	.0199	7.111
330	.47	.1330	.61	.0140	8.071
510	.40	.1131	.50	.0118	9.617
690	.30	.0849	.46	.0158	7.219
900	.22	.0623	.37	.00851	7.321
1080	.21	.0595	.34	.0078	7.628
1320	.22	.0623	.38	.0087	7.156
1560	.23	.0651	.34	.0078	8.344
1740	.24	.0679	.40	.00916	7.414
1980	.18	.0510	.29	.00665	7.669
2340	.11	.0311	.20	.00460	6.767
2730	.15	.0424	.24	.00552	7.690
3000	.09	.0255	.15	.00344	7.404
3480	.10	.0280	.17	.00390	7.179
3960	.17	.0481	.24	.00550	8.707
4800	.12	.0340	.19	.00435	7.816

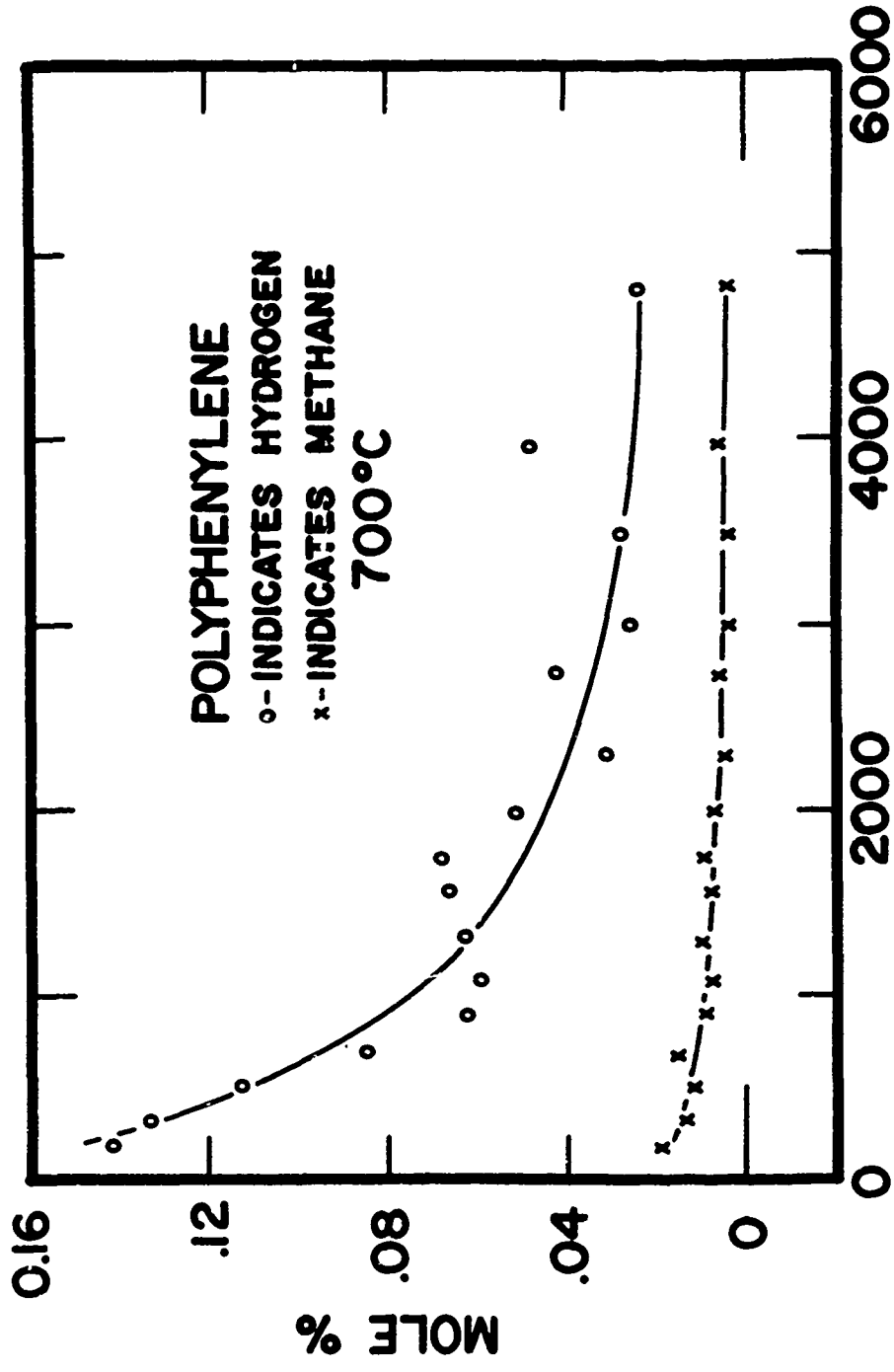

FIGURE 22. Gaseous Pyrolysis Products of Polyphenylene at 700°C in Helium

TABLE 5. PYROLYSIS GAS ANALYSIS FOR POLYPHENYLENE AT 700°C, RUN PP#7

Time, sec	H_2		Mole Ratio H_2/CH_4	CH_4	
	Peak Height	Mole Percent		Peak Height	Mole Percent
240	2.60	.736	9.782	3.4	.0782
420	1.80	.510	7.423	3.0	.0690
600	1.43	.4046	8.796	2.0	.0460
780	1.00	.283	8.226	1.5	.0344
960	0.90	.2547	9.262	1.2	.0275
1140	.65	.1839	7.998	1.0	.0230
1320	.60	.170	8.252	.9	.0206
1500	.50	.1415	9.613	.64	.01472
1680	.50	.1415	9.465	.65	.01495
1860	.40	.113	9.826	.50	.0115
2160	.35	.09905	10.317	.42	.00966
2540	.28	.07924	8.613	.40	.0092
4440	.13	.03679	11.425	.14	.00322

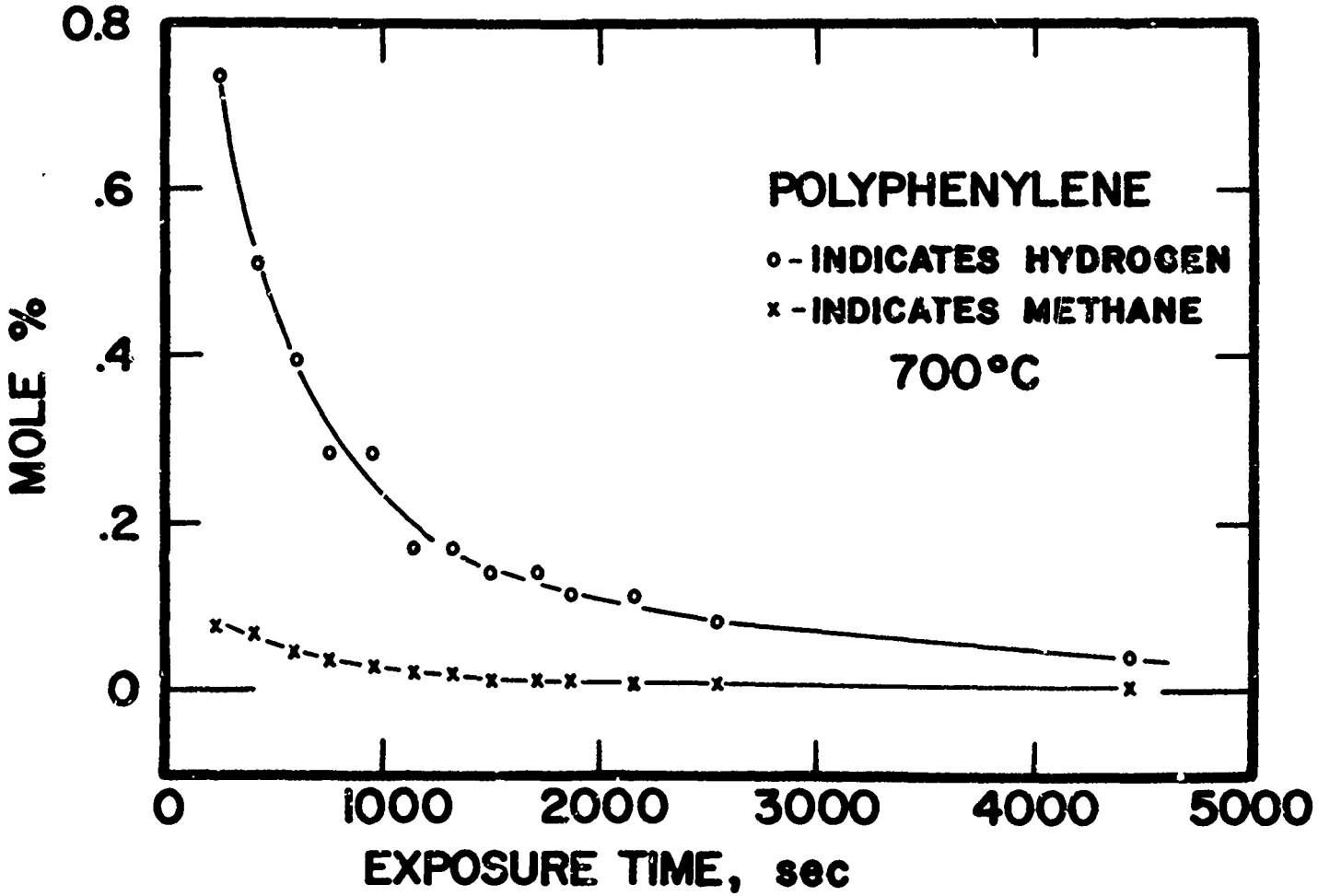

FIGURE 23. Gaseous Pyrolysis Products of Polyphenylene at 700°C in Helium

and are plotted in Figures 22 and 23. The molar ratios of hydrogen to methane in these two 700°C tests, PP#3 and PP#7, were 8:1 and 9:1, respectively, and in each test the ratio was remarkably constant. The small difference between the two ratios is likely attributable to inaccuracies in experimental measurements. The constancy of the molar ratios of the evolved gases during test times up to 4,000 seconds is strong evidence for a hypothesis of constant reaction mechanism.

The ratio of the quantities of hydrogen and methane observed at 700°C were much lower than those found at 585°C. It seems that at the higher temperature a greater number of aromatic rings were fragmented.

The results described and shown above are in agreement with those of Vincent [47]. This author observed the same decomposition products and also showed that the ratio of the quantity of aromatics evolved to that of methane and hydrogen evolved was a function of the chlorine content of the original polymer. For a chlorine content of 2 to 3%, the case with the polyphenylene evaluated here, only a very small percentage of weight loss was expected in the form of aromatics.

It was not possible to identify chlorine-containing gases in the chromatograph columns employed. Yet, it is clear from the results of elemental determinations shown in Tables 6 and 7 that the chlorine is almost completely removed from the polymer at 585°C. The loss of chlorine is, therefore, a major part of the gradual weight loss experienced by the polymer at low temperatures. Its total removal accounts for 82 per cent of the total weight lost at 550°C.

Infrared spectra analysis supports the results of the elemental

TABLE 6. RAW RESULTS OF ELEMENTAL ANALYSIS OF POLYPHENYLENE AND ITS CHARS

Sample	Weight Per cent		
	C	H	Cl
1. Original Polymer	91.82	4.39	2.96
2. Original Polymer	87.07	4.25	2.62
3. 585°C Char	93.31	4.06	0.35
4. 700°C Char	94.71	1.98	0.59
5. 700°C Char	93.36	1.27	Trace
6. 700°C Char	94.96	1.33	Trace

TABLE 7. NORMALIZED ELEMENTAL ANALYSIS OF POLYPHENYLENE AND ITS CHARS

Sample	Weight Per cent			Mole Per cent		
	C	H	Cl	C	H	Cl
1. Original Polymer	92.589	4.427	2.985	63.08	36.23	0.69
2. Original Polymer	92.678	4.524	2.789	62.64	36.72	0.64
3. 585°C Char	95.487	4.155	0.358	65.63	34.29	0.08
4. 700°C Char	97.358	2.035	0.606	79.79	20.03	0.18
5. 700°C Char	98.658	1.342	---	85.96	14.04	--
6. 700°C Char	98.618	1.381	---	85.60	14.40	--

determinations. Spectra of the virgin polymer clearly show a chlorine peak at 805 cm^{-1}. Spectra of char produced at 585°C shows a less intense chlorine peak, which almost completely disappears for 700°C char. Figure 24 shows the chlorine spectral peak for the original polymer and for the 585°C and 700°C chars.

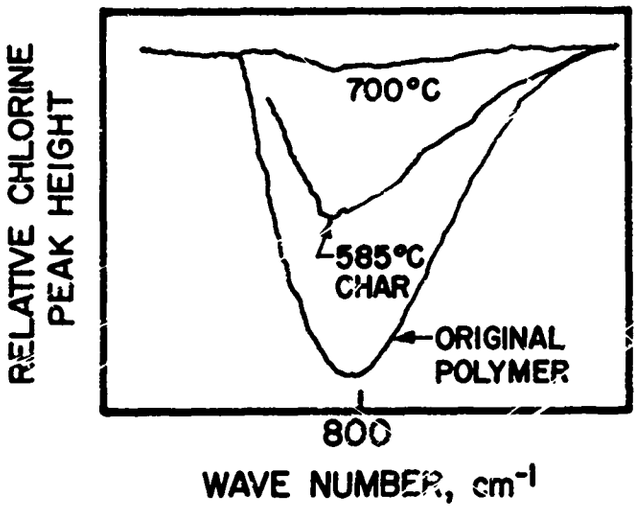

FIGURE 24, Chlorine Spectra for Polyphenylene and Residual Chars

The first stage of degradation, that occurring below temperatures of 550°C or 600°C, appears to be a chlorine-elimination reaction coupled with random scission of the polymer chain and volatilization of the smaller fragments. Vincent [47] has pointed out that the second-stage of reaction, occurring at about 700°C, is very similar for both chlorine-

containing polymer and for relatively pure para-polyphenylene. This result indicates that after elimination of chlorine, further decomposition occurs within the basic aromatic unit of the polymer.

The quasilinearization numerical technique was applied to the determination of kinetic parameters from the thermogram of Figure 18. A single reaction model was assumed and calculations were made as outlined in Chapter V.

In light of the evidence that the thermogram was composed of two basically different reaction zones, the single-reaction-model was first applied only to the major reaction at 700°C. Even with this restriction, it was not possible to achieve convergence in the iterative calculation procedure. Since an accurate initial guess of the parameters was required for convergence, many different values were tried. However, initial values which fit the data quite closely still did not produce a convergent solution. It was necessary, therefore, to formulate a calculation strategy which restrained the computation sufficiently to permit convergence.

Experience indicated that the most sensitive parameter was the apparent order of reaction, n. Thus n was not allowed to change with each iteration, but was constrained to a fixed value. Then, for a specified n, optimized values of A and E were computed. The constrained values of n were arbitrarily selected to be small integers. Graphically, a value of n was determined from isothermal data to be 2.43. However, calculation of n in this way was very sensitive to the value of w_R the final residual weight of the decomposed polymer. Thus, the value of 2.43 for n was taken as an approximate number. Further, the order of

reaction must be a small integer if computed kinetic parameters are to have any real significance with respect to the chemistry of the degradation reaction.

With a constrained value of n = 2.0, a convergent optimized set of values for pre-exponential factor A and activation energy E were found:

$$A = 5.217 \times 10^{11} \text{ sec}^{-1},$$

$$E = 58{,}527 \text{ cal}$$

Vincent obtained $A = 6 \times 10^{10}$ min^{-1} and E = 50,000 cal. by graphical techniques. This relatively close agreement is probably due to the fact that a single, perhaps even quite simple reaction mechanism is occurring. Usually graphical solutions of successive data runs do not agree as closely as the graphical and analytical solutions above.

These parameters fit the part of the data to which they were applied quite well, as shown in Figure 25. Parameters determined on the basis of a single reaction zone come much closer to describing fundamental reaction mechanisms than can parameters averaged to fit a complex curve of many possible reactions. However, it is obvious that only a selected part of the total thermogram has been considered. Inclusion of a broader range of data significantly alters the convergent values. Figure 26 shows the experimental data and curves generated from an initial guess of the parameters and from the convergent values of parameters when all of the thermogram is considered. The initial guesses were n = 2.0, $A = 1.45 \times 10^{12}$ sec^{-1}, E = 60,000 cal, and the convergent values were n = 2.0, $A = 5.45 \times 10^{5}$ sec^{-1}, E = 32,442 cal.

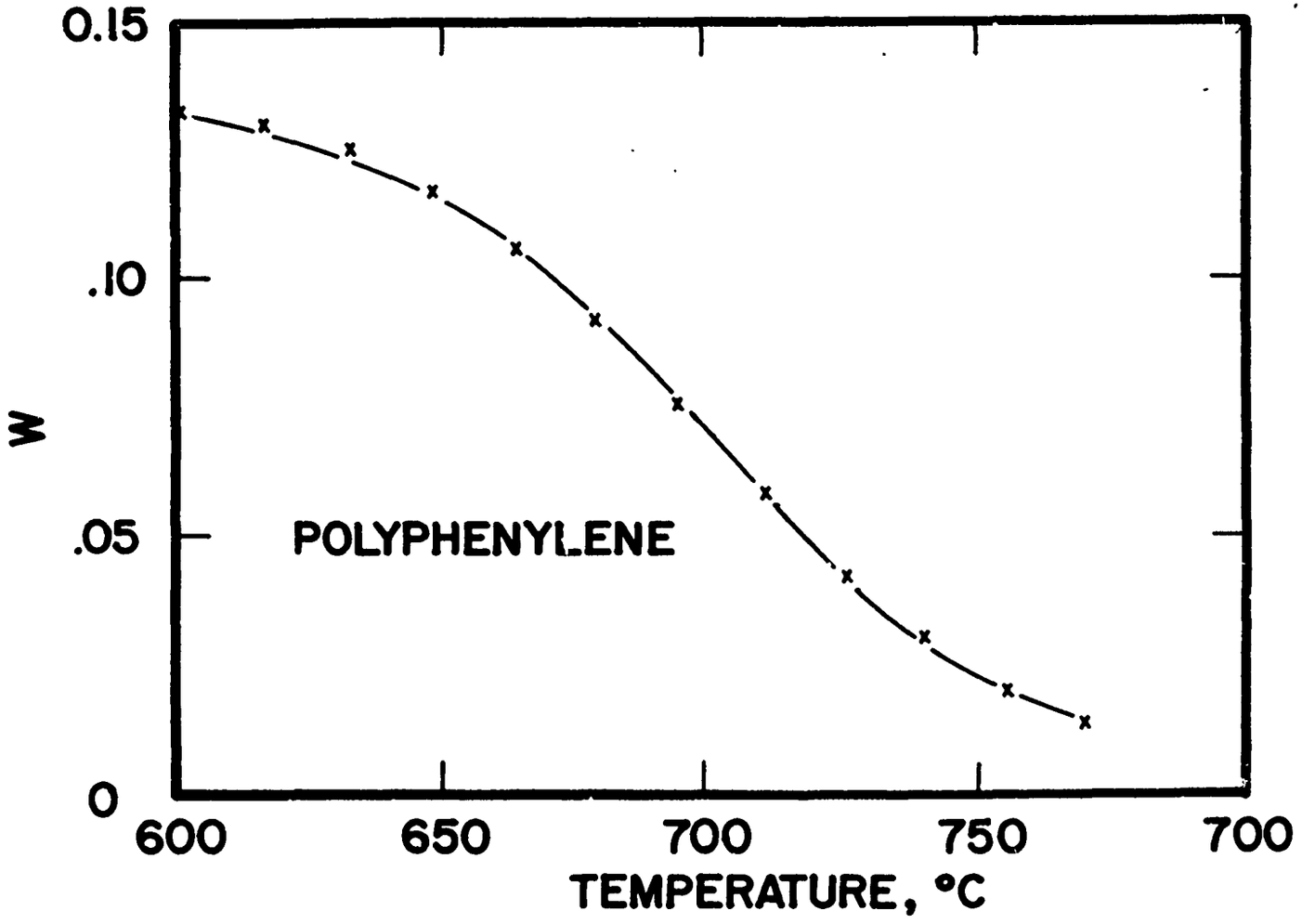

FIGURE 25. A Comparison of Data and Numerically Optimized Results for Polyphenylene

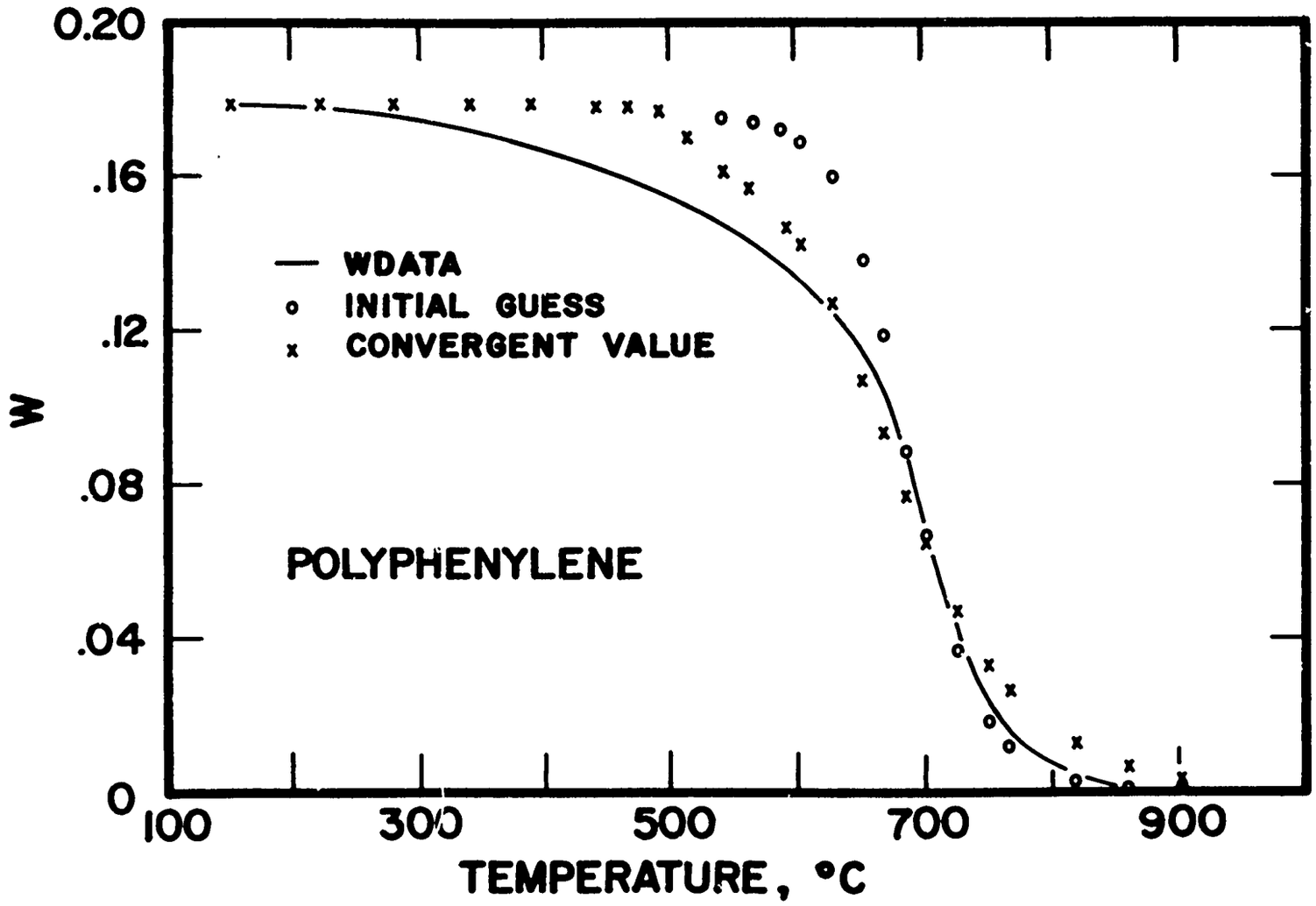

FIGURE 26. A Comparison of Data and Numerically Optimized Results for Polyphenylene

It is necessary to conclude that the number and distribution of data points included in quasilinearization calculations has a strong influence on the results obtained. It is also appropriate to note here that a thermogram may be well described by perhaps an indefinite number of sets of parameters. Indeed, some non-convergent sets which well characterized the curve included negative values of kinetic parameters.

Figure 26 also illustrates that with a constrained value of n, the calculation procedure was able to attain convergence over a moderately extensive range of input.

An attempt to fit the whole thermogram with a two-mode quasilinearization model was made. Convergence was not obtained for this calculation. As shown in Figure 19, the data below temperatures of 600°C did not indicate a distinct reaction peak. The rather nebulous reaction region in the early part of the thermogram was not accurately described by the assumed model. The resultant poor fit created an error sufficiently large that convergence could not be obtained.

A mechanism of thermal degradation can be postulated which accounts for the experimental observations and is consistent with the broader background of organic chemistry. The evolution of hydrogen at 585°C was probably the result of the combination of thermally-excited hydrogen which was found in near proximity on adjacent phenyl groups as shown below.

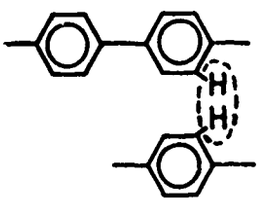

The carbon-hydrogen bond strengths involved are about 81 kcal, and thus hydrogen elimination is much more likely than scission of the phenyl groups and is also probably preferred over chain fracturing. Resulting phenyl radicals may either abstract other hydrogens from any near source or they may combine to bridge the chains. Combination seems very likely energetically. The combination of two hydrogens on the same phenyl group is less expected than the procedure just outlined.

At 700°C the decomposition will still involve hydrogen elimination as described, but the presence of methane must be explained. The phenyl groups in the polymer chain are extremely stable because of the high resonance energy of the ring. Intense thermal excitation is required to open the ring. However, once ring scission occurs, further decomposition probably follows rapidly. The diradical structure illustrated below is very unstable and extracts a nearby hydrogen indiscriminantly to form a triene.

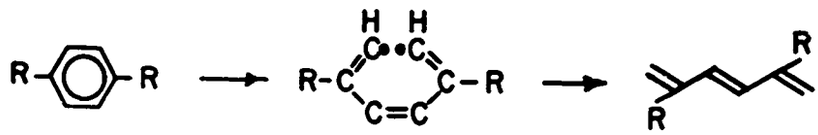

Of course, the triene lacks the delocalization of energy which stabilized the phenyl group and thus, its further decomposition to methyl radicals and finally methane is virtually assured.

The suggested mechanism proposes that the generation of hydrogen and methane proceed by independent reactions. The observed constancy of their molar ratios seems then to result from the relative constancy

of the rates of the two reactions.

Polyimide Polymer

The polyimide family of polymers is a large group of materials, many of which have been evaluated for thermal stability [34]. However, much of the data published were obtained in air and most of the remainder were obtained for polymers whose structures differ from that of Skybond 700, the polymer used in this work. Thus, there are little data available on Skybond 700 resin for the conditions of environment of greatest interest.

A dynamic thermogram for Skybond 700 polymer obtained in a non-flowing helium environment is shown in Figure 27. The numerical derivative of the data in Figure 27 is shown in Figure 28. The appearance of this thermogram suggests that the reaction might be one with a simple mechanism. Because of the apparent simplicity of the thermogram, polyimide polymer was selected for use in experiments designed to illustrate the effects of some experimental variables.

As noted previously, TGA experiments for which the helium environmental gas was not flowing were much easier to conduct than flow experiments. Buoyancy corrections were smaller and noise was greatly reduced. However, in non-flow tests the products of pyrolysis were contained within the region of reaction, and the effect of their proximity was not known.

In order to investigate this effect, a dynamic flow experiment was conducted. The results of this experiment are shown in Figures 29 and 30. The thermograms for the two cases are very similar. The temperature of maximum rate of weight loss was 613°C in both cases.

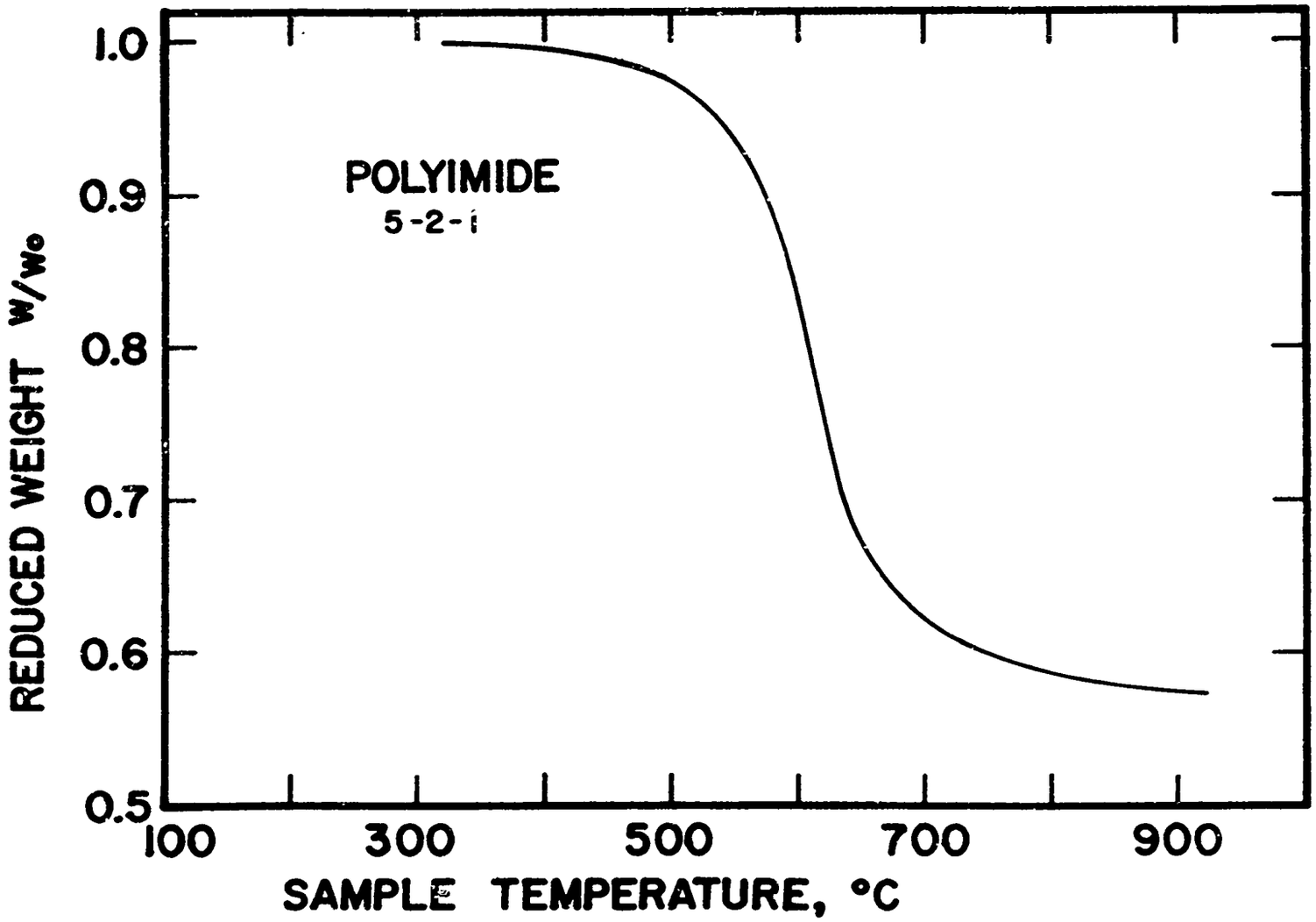

FIGURE 27. Dynamic Thermogram for Polyimide at 10°C/min in Non-flowing Helium

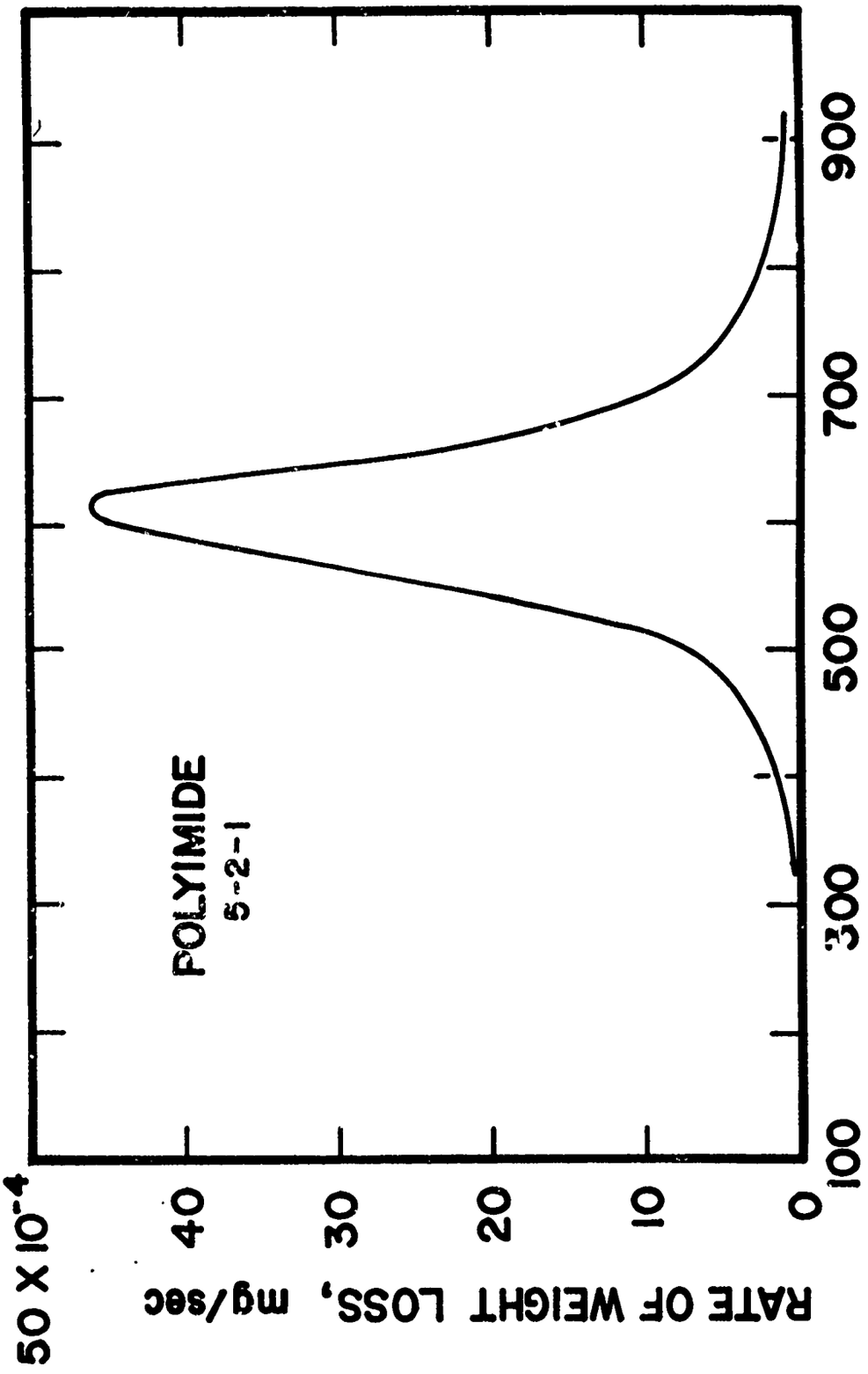

FIGURE 28. The Reduced Rate of Weight Loss for Polyimide in Non-flowing Helium

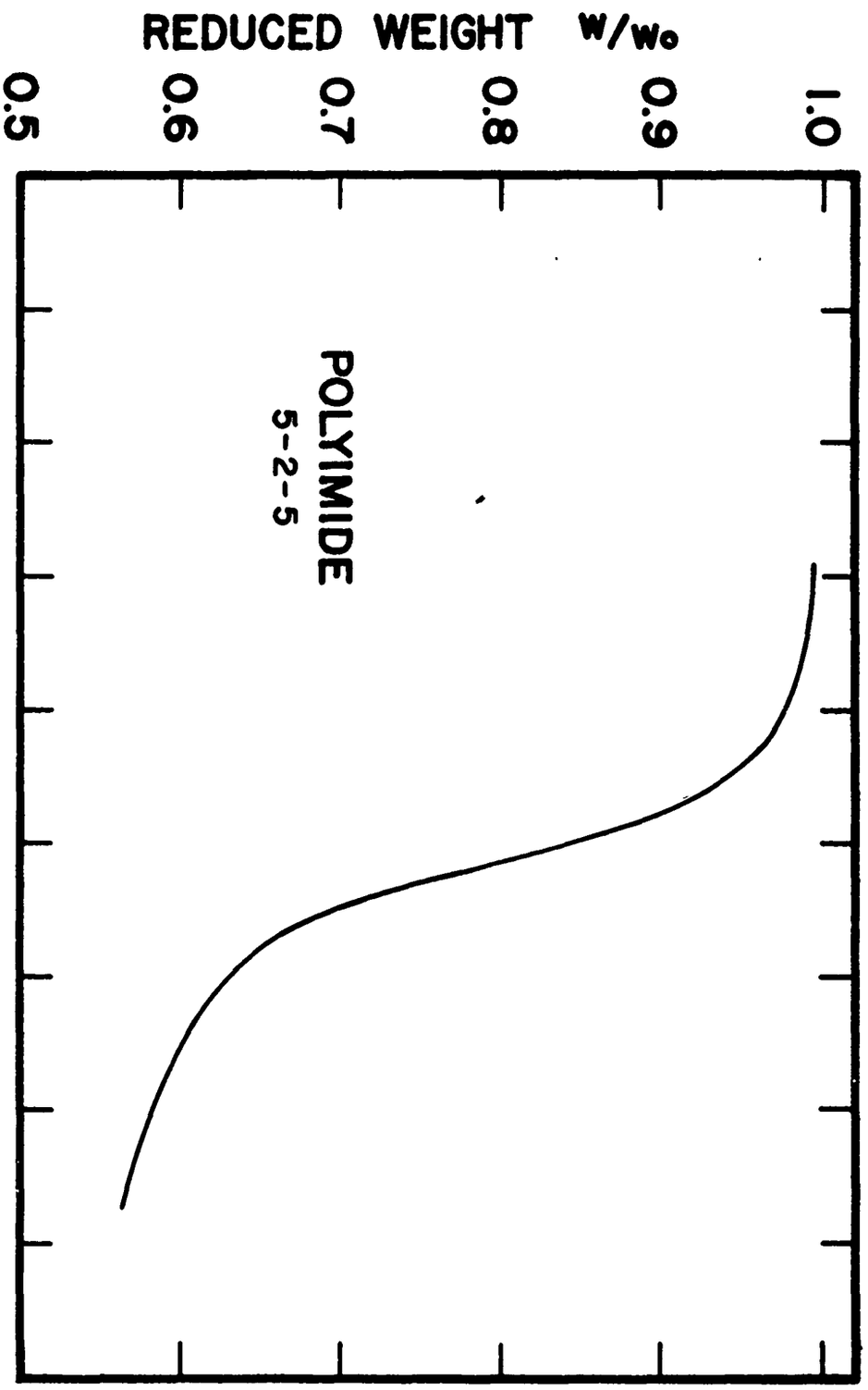

FIGURE 29. Dynamic Thermogram for Polyimide at 10°C/min in Flowing Helium

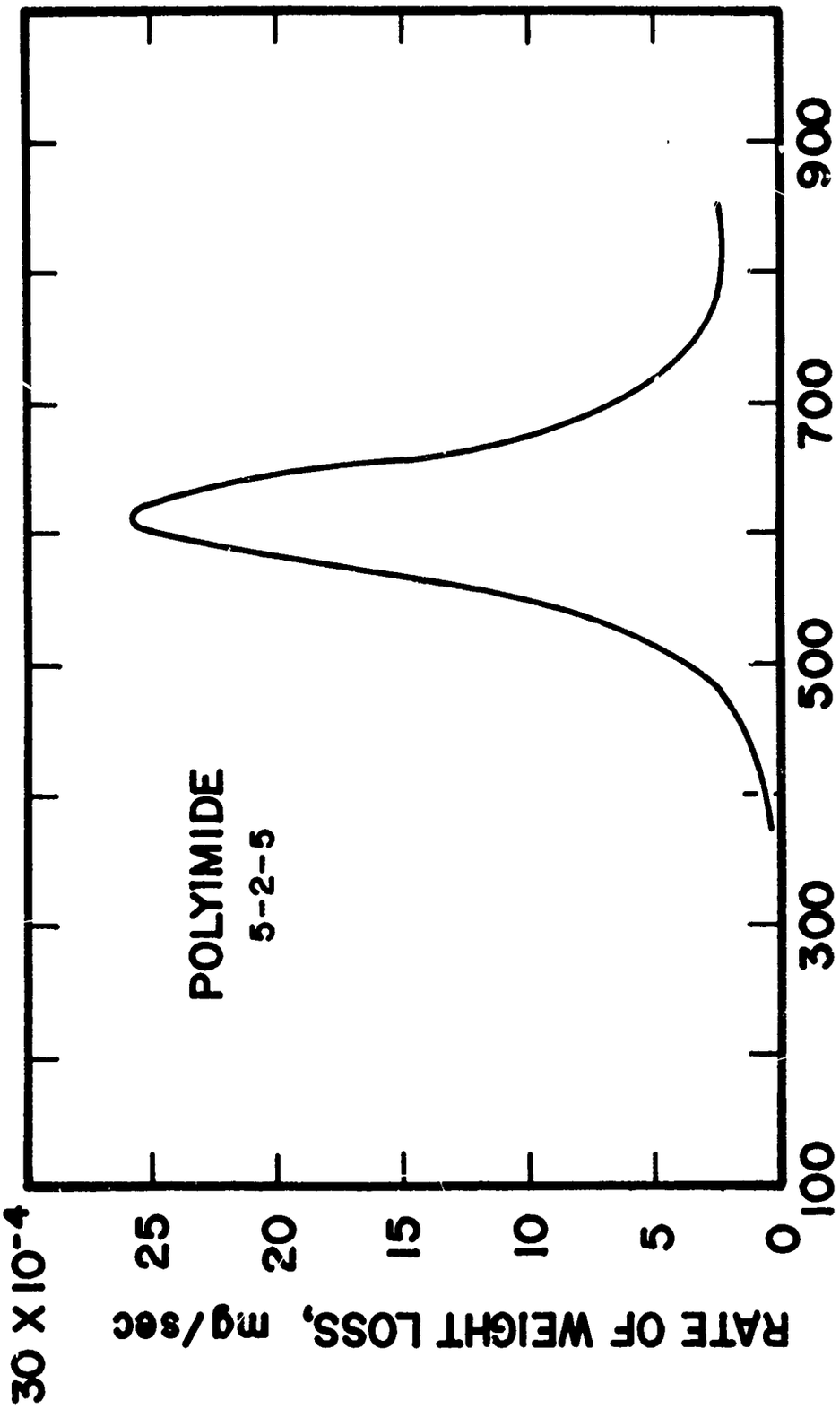

FIGURE 30. Rate of Weight Loss for Polyimide in Flowing Helium

The char yield at 850°C was 58 per cent for the non-flow case and 57 per cent in the flow test. However, a more exact comparison is shown in the reduced-rate-of-weight-loss curves shown in Figures 31 and 32 for non-flow and flow experiments, respectively. It is noted that the differences between the two curves are slight. Polymer tested in a non-flow environment lost weight at a slightly greater rate, passed through a somewhat greater maximum rate, and exhibited a little smaller rate of weight loss at 850°C. Therefore, it seems that within only a small difference, the two types of experiment produce the same results. This conclusion may be dependent upon the size of sample used and the size of the containing volume. The two samples used in this comparison were 9.447 mg and 5.487 mg in weight. If large amounts of polymer had been tested, perhaps the consequently large amount of volatile material might have affected the results.

Isothermal non-flow TGA experiments were conducted at temperatures of 494°C, 533°C and 583°C. Results of these tests are plotted in Figure 33. The temperatures chosen represent the region of increasing rate of weight loss on the thermogram. As might have been expected, the weight losses in the isothermal experiments reflect the increase in reaction rate with increasing temperature. It is also noted that even at 583°C, a temperature quite near that where the maximum reaction rate is observed, the total weight lost is only 31 per cent after exposure for 40 minutes. This represents a char yield of about 11 per cent greater than the dynamic case. It is evident then that the higher temperatures attained in the dynamic experiment drove the pyrolysis further to completion than was possible at 583°C.

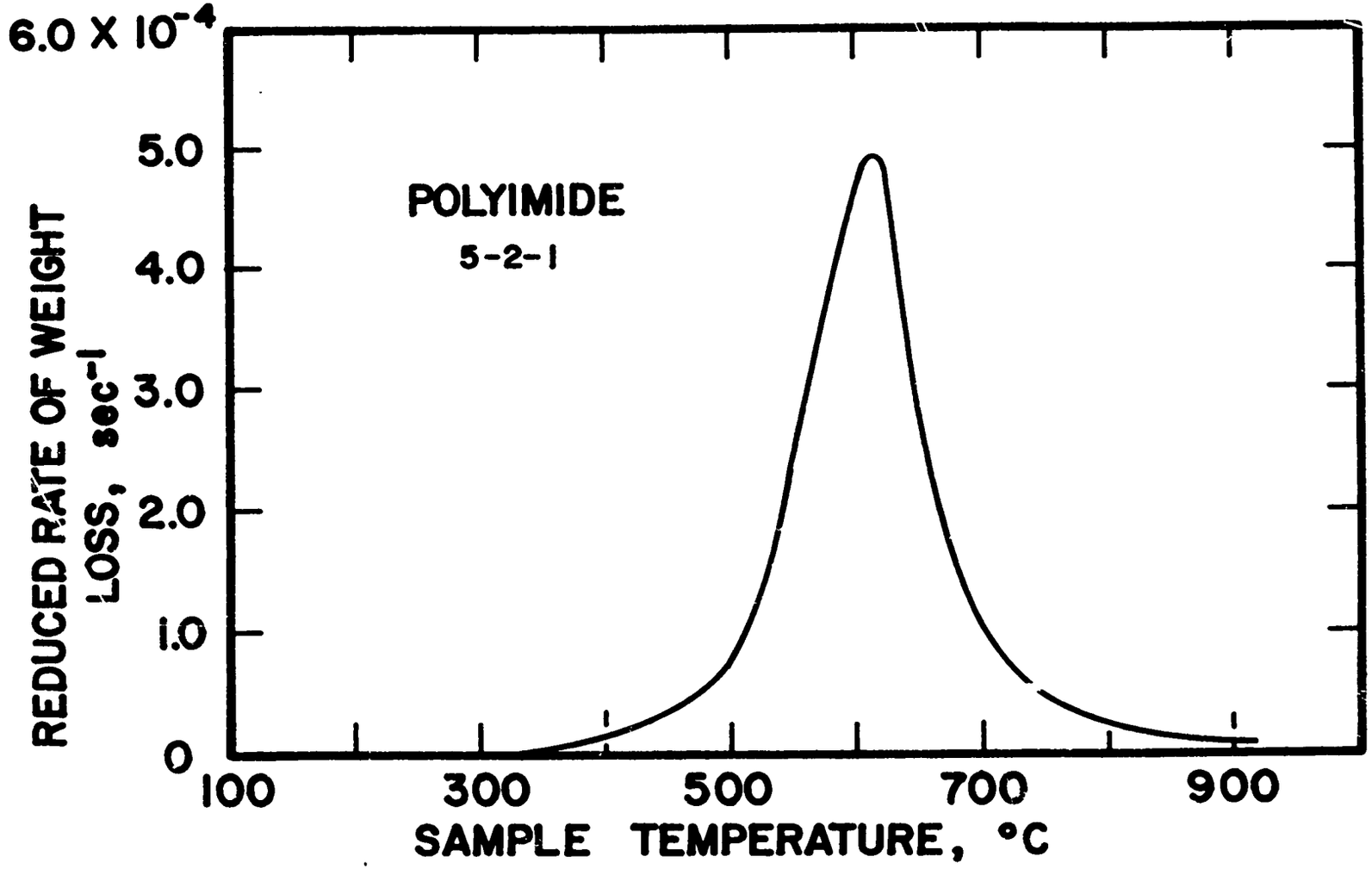

FIGURE 31. Reduced Rate of Weight Loss for Polyimide in Non-flowing Helium

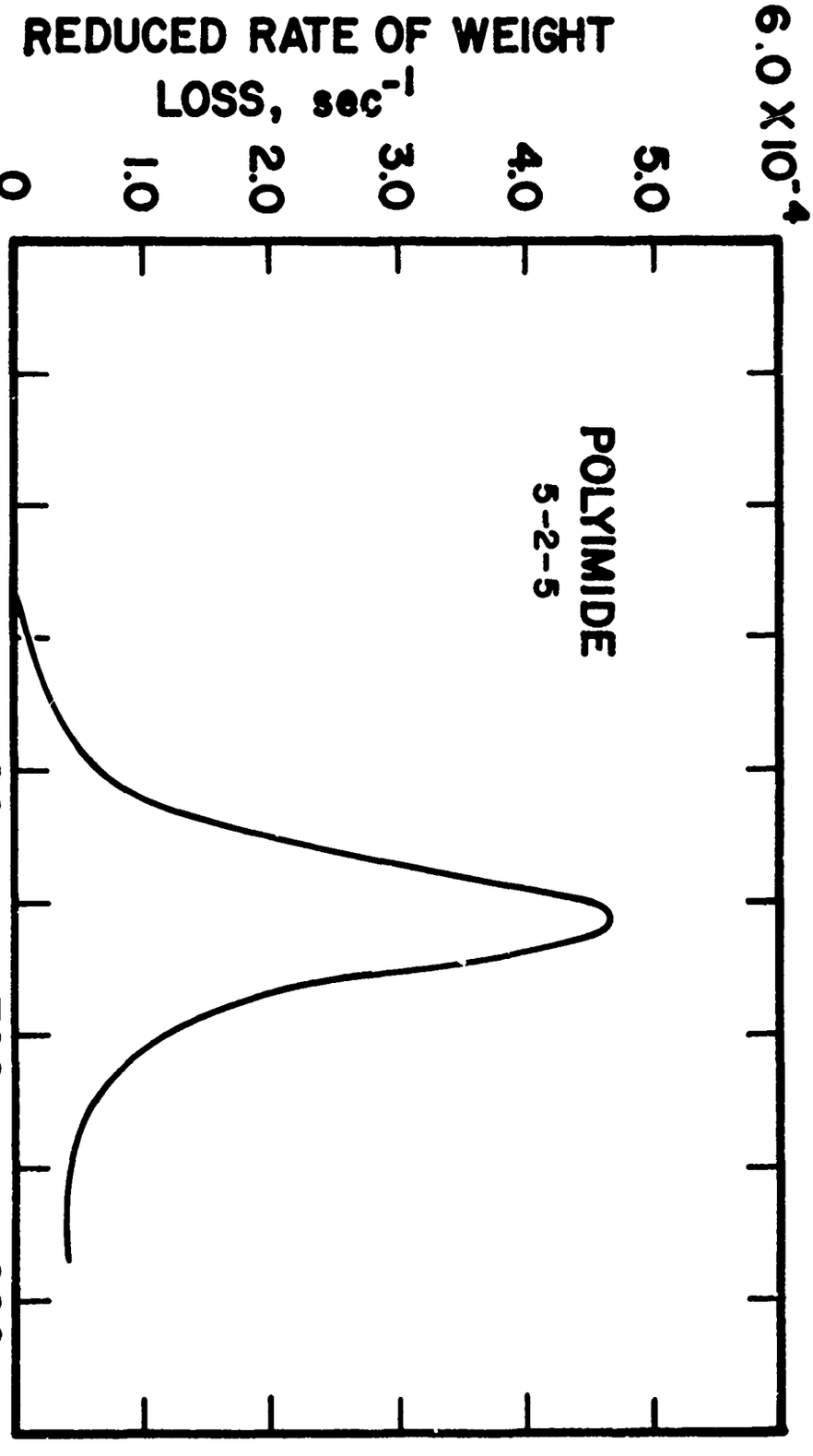

FIGURE 32. Reduced Rate of Weight Loss for Polyimide in Flowing Helium

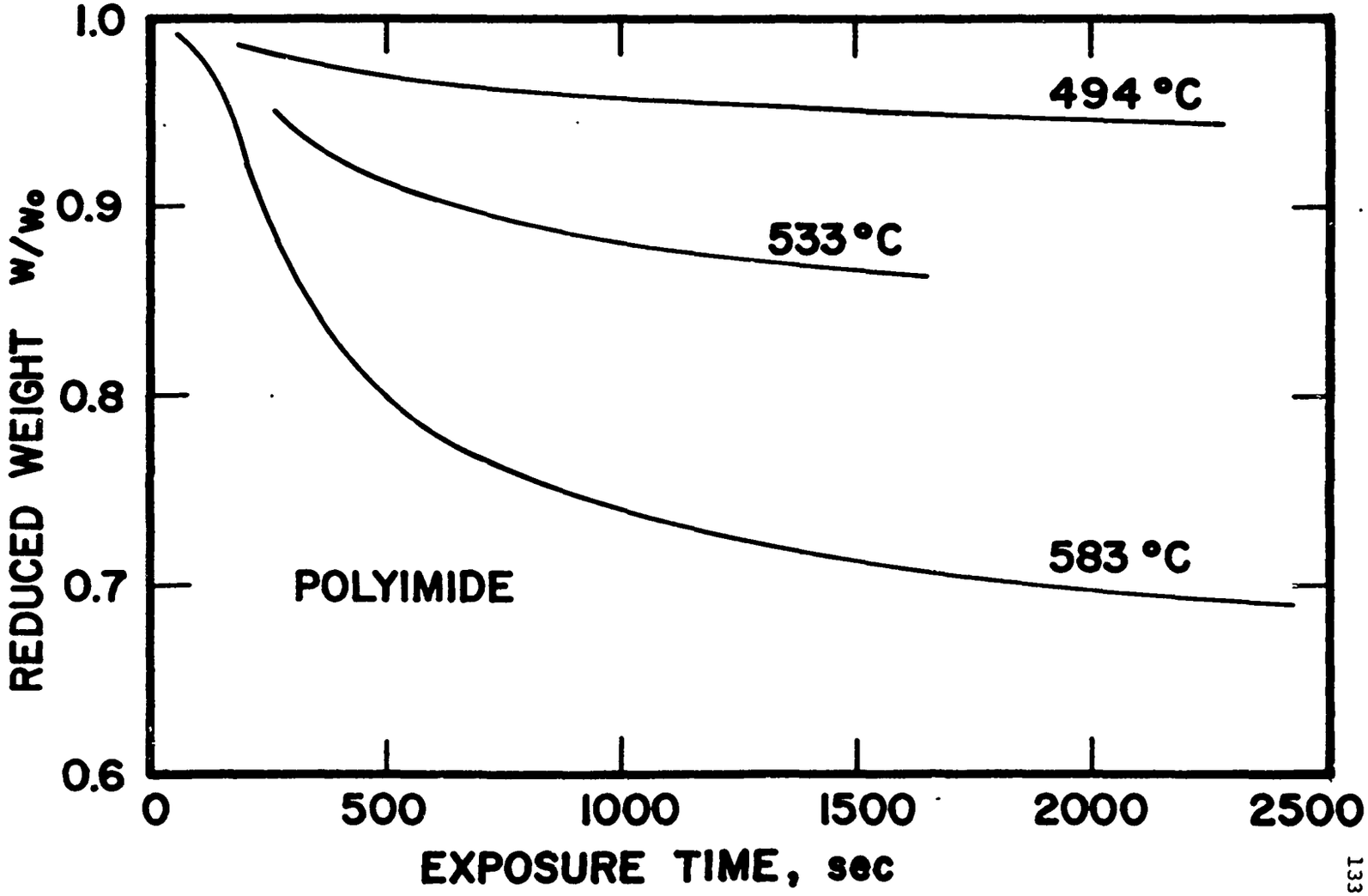

FIGURE 33. Isothermal Thermograms for Polyimide in Non-flowing Helium

Additional isothermal experiments were made to further evaluate the effect of environment on isothermal tests. Figure 34 shows the results of isothermal runs made at a reduced helium pressure of 2 mm Hg at 570°C and in a flowing helium environment at 583°C. The 583°C tests shown in Figures 33 and 34 for non-flow and flow experiments are in reasonably good agreement. Weight loss for the non-flow case was less than a per cent greater than for the non-flow case. The loss in vacuum was slightly less than was expected.

Kinetic parameters were determined from the dynamic non-flow thermogram by quasilinearization. A single power-law reaction model was assumed. An initial guess of the apparent order-of-reaction was determined from an isothermal thermogram as 1.735. It was deemed inappropriate to round this off to a value of 2.0 since that value of n produced a poorer fit of the isothermal data. The computer program yielded convergent values of the parameters as

$$A = 1.886 \times 10^{7}\ \text{sec}^{-1},$$

$$E = 38{,}128\ \text{cal},$$

$$n = 1.735.$$

The value of n was constrained during the calculation. Figure 35 shows a plot of W versus temperature with the data represented as a continuous line and discrete values of calculated W represented by the individually shown points. Good agreement is noted between the computed values, based on convergent kinetic parameters and the data line. The region shown represents the temperature range where the primary pyrolysis reaction occurred. It is generally the fit in this region which yields the best values of kinetic parameters. However, the

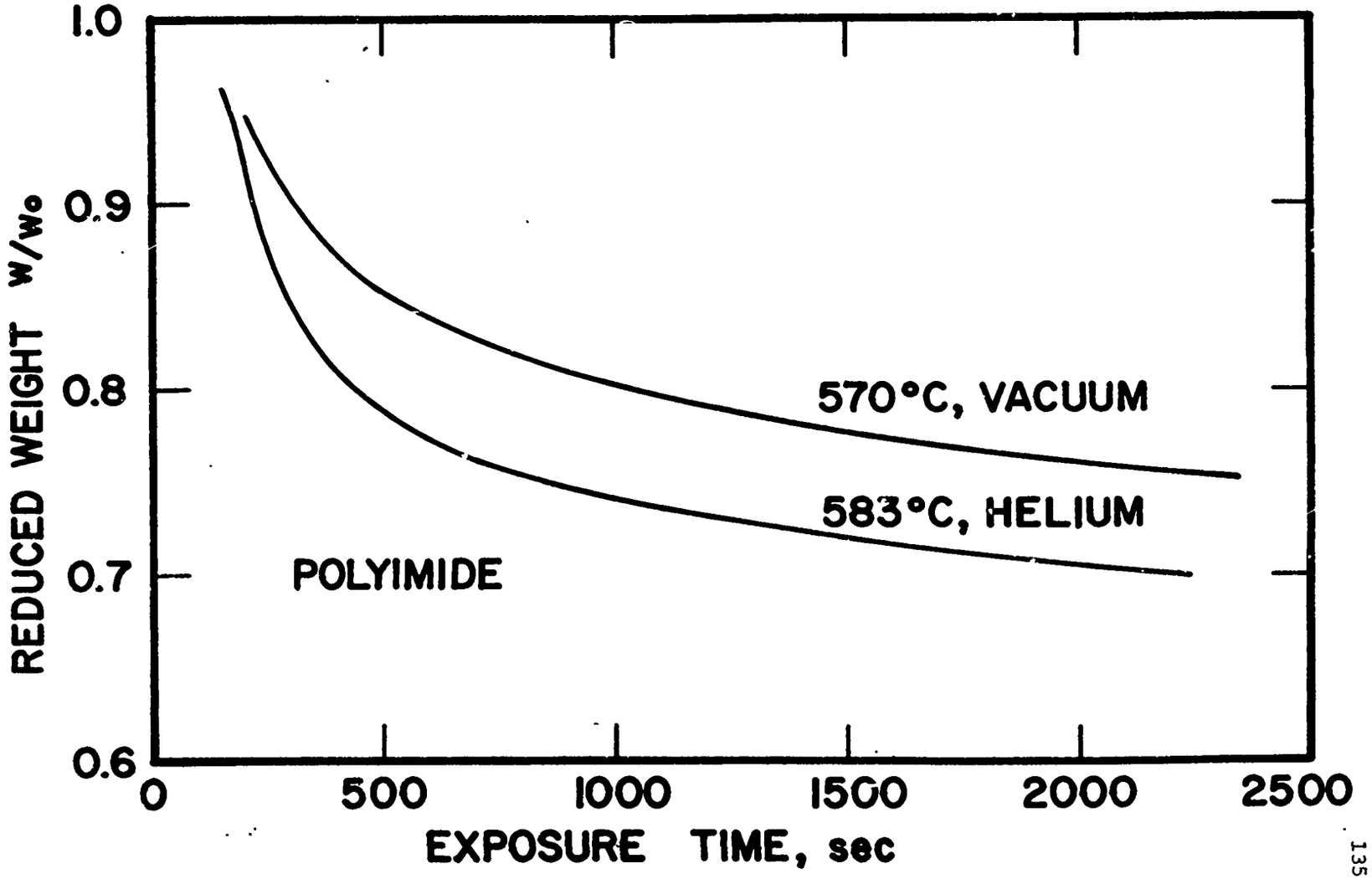

FIGURE 34. Isothermal Thermograms for Polyimide in Flowing Helium and Vacuum

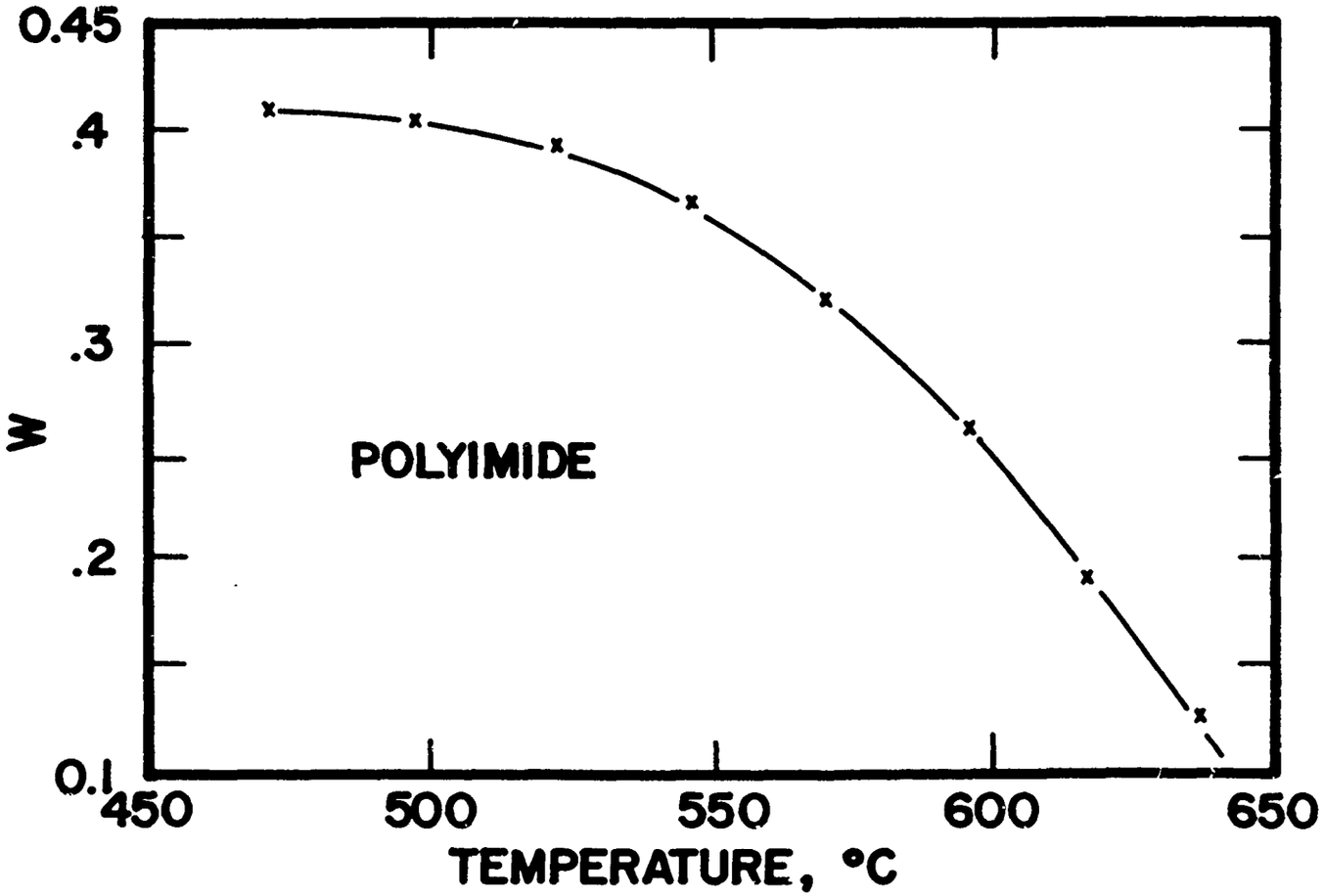

FIGURE 35. A Comparison of Data and Numerically Optimized Results for Polyimide

problems involved in this approach are immediately evident when a comparison is made of data and predicted points based on a fit of only part of the curve. Figure 36 shows the fit over the whole temperature range of the optimized parameters determined from Figure 35. The high temperature region is not well described. Inspection of the curves indicates that the order of reaction should probably be larger for a better fit.

When a value for n of 2.0 was used, resultant values of A and E were 7.105×10^7 and 39,800, respectively. A comparison of the data and points predicted by these values is shown in Figure 37. The fit shown in Figure 37 is indeed somewhat better over-all. However, it is noted that a closer fit at high temperatures is gained only at the expense of greater deviation in the middle temperatures. This trend continues for higher orders of reaction. For n = 3.0, optimized A and E were 1.367×10^{12} and 54,264. Curves are not shown for these values of the parameters, but the fit between data and predicted values was significantly poorer than was the case for n = 2.0.

The magnitude of the activation energy is smaller than was expected. Bruck [8] determined the activation energies for "H"-film polyimide as 31 kcal per mole for degradation in air and as 73 kcal per mole for vacuum pyrolysis.

A significant experimental problem was brought to light when analyzing polyimide thermograms. Since a value of w_R, the final char weight, is required for analysis of both isothermal and dynamic data, it must be assumed that at some point on the thermogram the derivative of weight with respect to time or temperature must be zero. The point

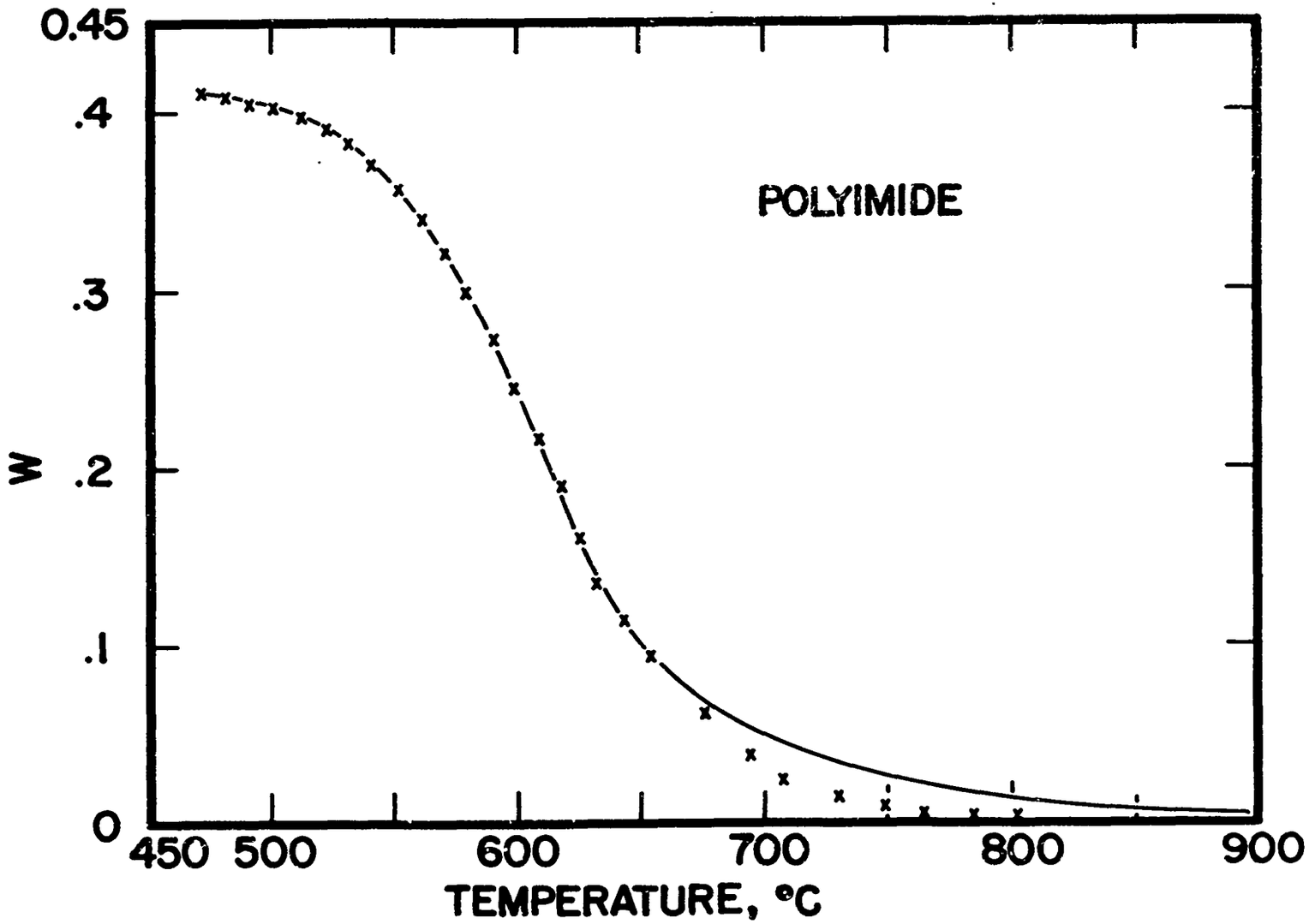

FIGURE 36. A Comparison of Data and Numerically Optimized Results for Polyimide

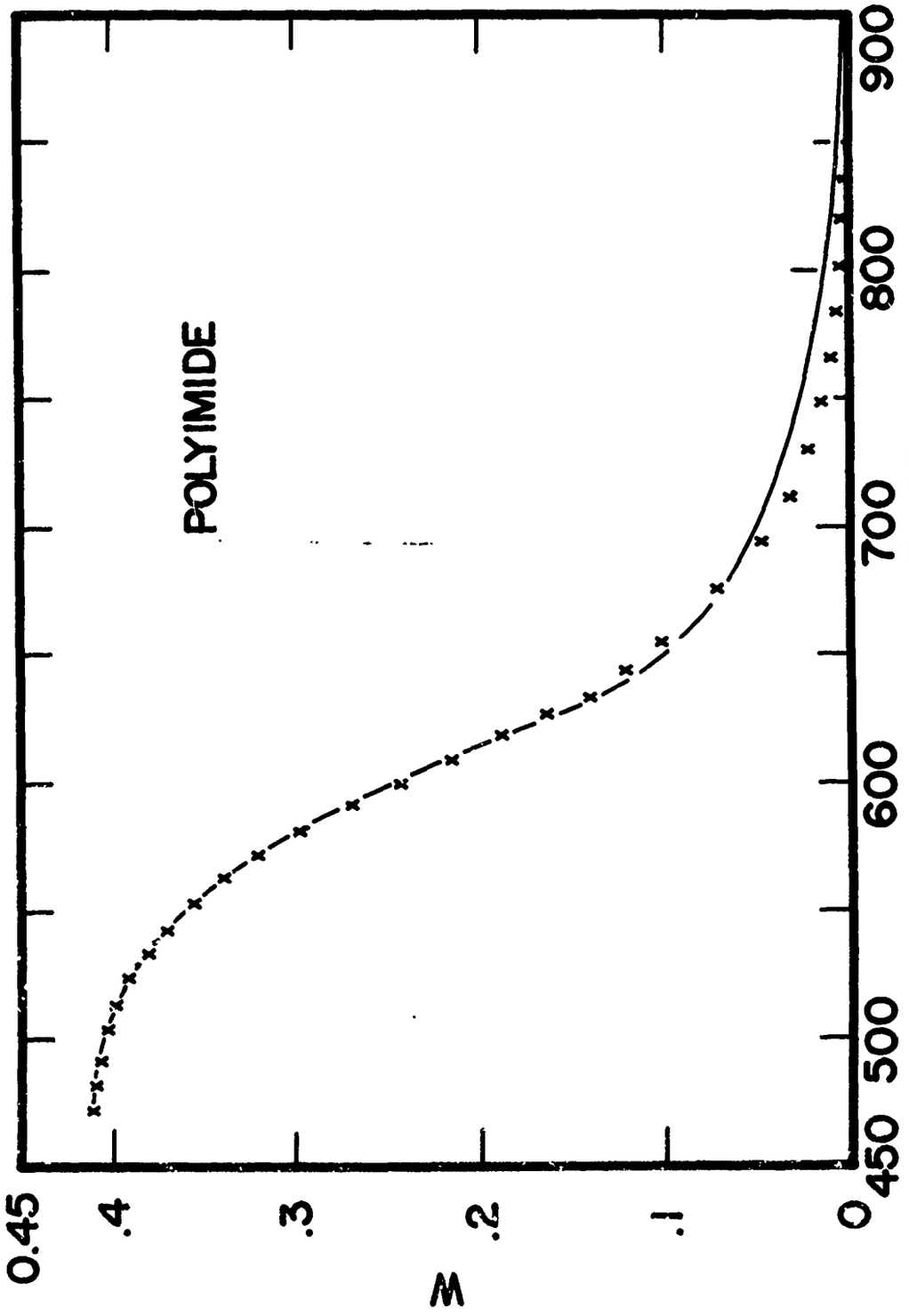

FIGURE 37. A Comparison of Data and Numerically Optimized Results for Polyimide

at which this condition is reached defines w_R.

In practice, when the slope becomes small with respect to the overall changes, a termination point is arbitrarily selected. Parker [40] terminated his experiments when weight loss was less than 1.0 per cent per minute. It was observed that even when the final slope was as small as 1.22×10^{-5} per cent of sample weight per second at 580°C, large variations in determined order of reaction resulted, depending on how long the reaction was allowed to proceed. This problem had some effect on dynamic results but appeared to be particularly critical in isothermal calculations.

While exploring long-exposure time experiments, an experimental error was discovered. In some experiments, if the exposure time was sufficiently long, total volatilization of the sample occurred. It was impossible to explain this result by postulating contaminants in the helium or an air leak during the test. The helium was found to be pure and the system was maintained above atmospheric pressure during the experiment. At temperatures above 800°C some highly carbonaceous material did volatilize from the sample pan and condense on cooler portions of the hangdown tube but the quantity of sample removed in this way was small.

It was finally demonstrated that during the preparation of the system before testing some air was occasionally sucked into the system around the end plate of the containing vessel while filling with helium. Because of the small size of test samples, only a small amount of oxygen was necessary to remove the carbonaceous char.

It appeared that for most of the data collected, this oxygen-inclusion error had not been encountered. Specious results were noted

only after a modification had been made in the apparatus. Those data which were in doubt were repeated.

The effects of this error were evaluated by purposely including some oxygen in the reaction chamber. A normal TGA test was then run with graphite as the sample material. Graphite had already been demonstrated to be inert in a pure nelium environment. No effect was observed until the temperature was approximately 825°C. At this temperature a constant rate of weight loss was superimposed upon the previously-determined thermogram which represented the oxidation reaction. This reaction continued zero order for the char until the sample had totally disappeared.

After discovering this source of possible experimental error, care was taken to ensure oxygen-free environments in subsequent tests. Fittings and attachments were carefully re-sealed whenever they were disturbed and in each experimental set-up sample gas was analyzed for the presence of air before actual testing was begun.

Isothermal gas-analysis tests were made on polyimide at 480°C and 597°C. At 480°C the polymer is just entering the region of decomposition, and at 597°C it is near the temperature of maximum rate of weight loss. Results of analysis obtained at the lower temperature are presented in Table 8 and Figure 38. At this temperature, the only products evolved in sufficient quantities to permit detection were carbon monoxide and carbon dioxide. The measured molar ratios of these gases varies considerably during the early part of the reaction but becomes nearly constant after 1800 seconds of exposure.

This experiment at 480°C was originally conducted in a silica gel

TABLE 8. PYROLYSIS GAS ANALYSIS FOR POLYIMIDE AT 480°C IN HELIUM, RUN PI#1

Time, sec	CO			CO_2	
	Peak Height	Mole Per cent	Mole Ratio CO/CO_2	Peak Height	Mole Per cent
180	3.2	.0672	.466	4.0	.144
320	8.4	.1764	2.033	2.41	.0867
720	4.8	.1008	3.414	.82	.0295
1110	3.8	.080	3.704	.60	.0216
1380	3.4	.0713	4.986	.40	.0143
1800	2.8	.0588	5.495	.30	.0107
2220	2.5	.0525	4.907	.30	.0107
2700	2.21	.0462	6.416	.20	.0072
3120	1.95	.0409	6.691	.17	.0061
3600	2.0	.0420	5.833	.20	.0072
6720	1.45	.0304	7.689	.11	.0039
7680	1.26	.0264	6.682	.11	.0039
9660	1.0	.0210	0	0	0

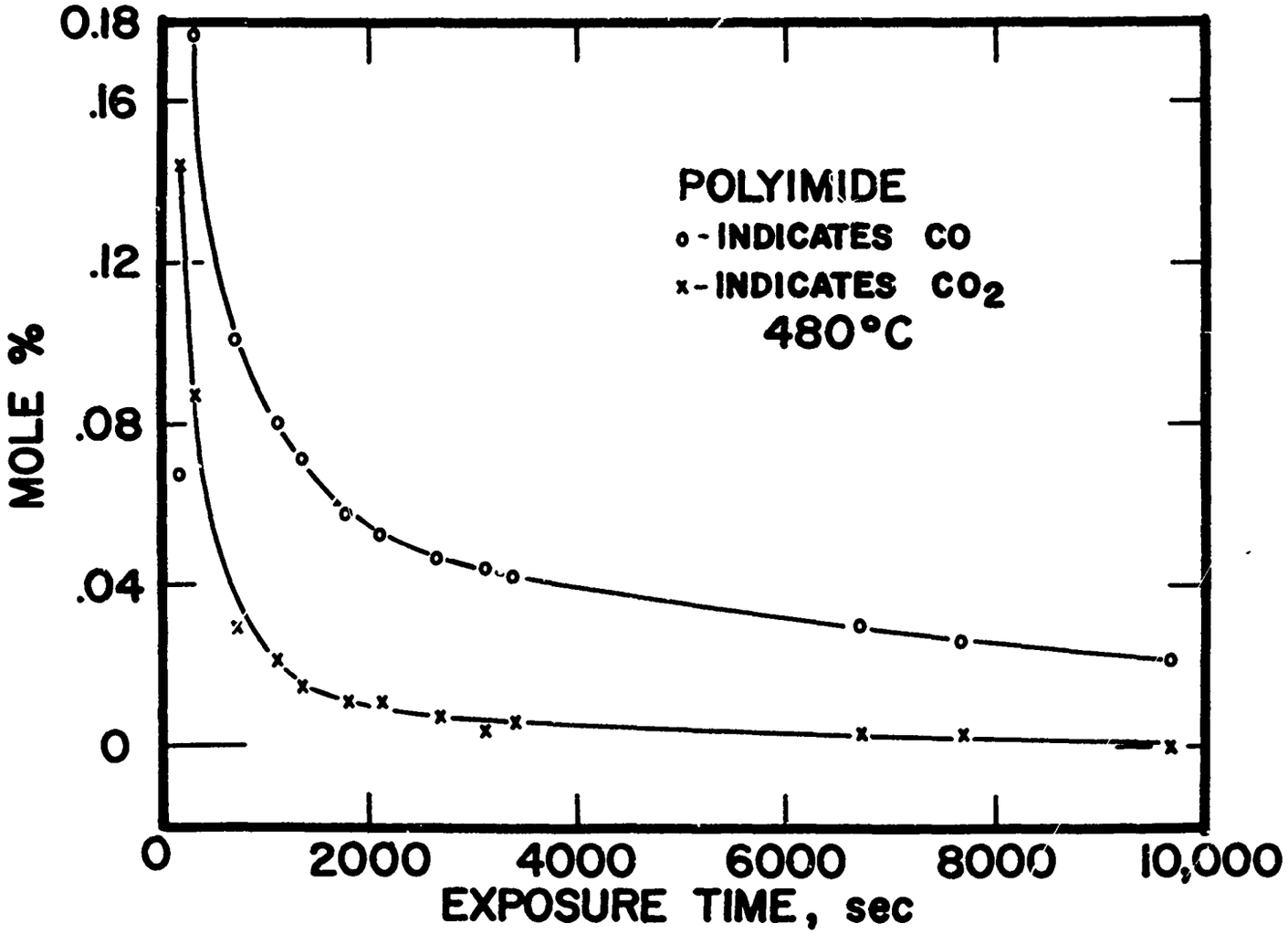

FIGURE 38. Gaseous Pyrolysis Products for Polyimide at 480°C in Helium

column. A repeat of the test in a Chromosorb 102 column indicated the presence of a small amount of water which had not been identified in the earlier test.

Pyrolysis experiments run at 597°C produced gaseous products which were significantly different from those found in the lower temperature test. Hydrogen, hydrogen cyanide, and water were all detected in addition to carbon monoxide and carbon dioxide. The results of this experiment are shown in Table 9 and Figure 39.

The source of the hydrogen is undoubtedly found in the stripping of benzene-type structures in the molecular chain. The test temperature of 597°C was certainly high enough to initiate this reaction, while a temperature of 480°C was apparently too low.

The production of HCN in the decomposition reaction obviously required considerable rearrangement within a partially fragmented imide ring. Since it is essentially impossible to predict the course of the many possible rearrangement reactions which could possibly have occurred, it seems that HCN probably represents a stable form produced by many interactions.

The origin of carbon monoxide could easily have been found in the degradation of the benzophenone substructure, or in the imide groups. Since the imide bond is the most probable site for initial ring fracture, generation of CO probably follows the ring opening with recondensation through the nitrogen atom maintaining the chain structure. It is significant to note in this regard that very little nitrogen-bearing gas was identified and that elemental analysis of char residues contained a high proportion of nitrogen.

TABLE 9. PRVOLYSIS GAS ANALYSIS FOR POLYIMIDE AT 597°C IN HELIUM, RUN PI#3

Time, sec	CO		CO_2		Mole Ratio CO/CO_2	Peak Heights		
	Peak Height	Mole Per cent	Peak Height	Mole Per cent		H_2	H_2O	HCN
300	72.0	1.512	22.0	.792	1.909	0.12	8.1	---
570	21.3	.4473	3.6	.1296	3.451	0.10	3.2	---
900	10.1	.2121	3.6	.1296	1.705	0.10	1.6	0.3
1440	6.1	.1281	2.0	.072	1.879	0.08	0.5	0.2
1920	3.1	.0651	1.2	.0432	1.506	0.07	0.2	0.2
2400	2.5	.0525	0.8	.0288	1.823	0.07	0.1	0.1
3120	1.6	.0336	0.6	.0216	1.556			
3600	1.2	.0252	0.5	.0180	1.400			
4740	0.8	.0168	0.3	.0108	1.556			
6120	0.5	.0105	0.2	.0072	1.458			
7200	0.4	.0084	0.1	.0036	2.333			
9360	0.3	.0063	0.1	.0036	1.750			

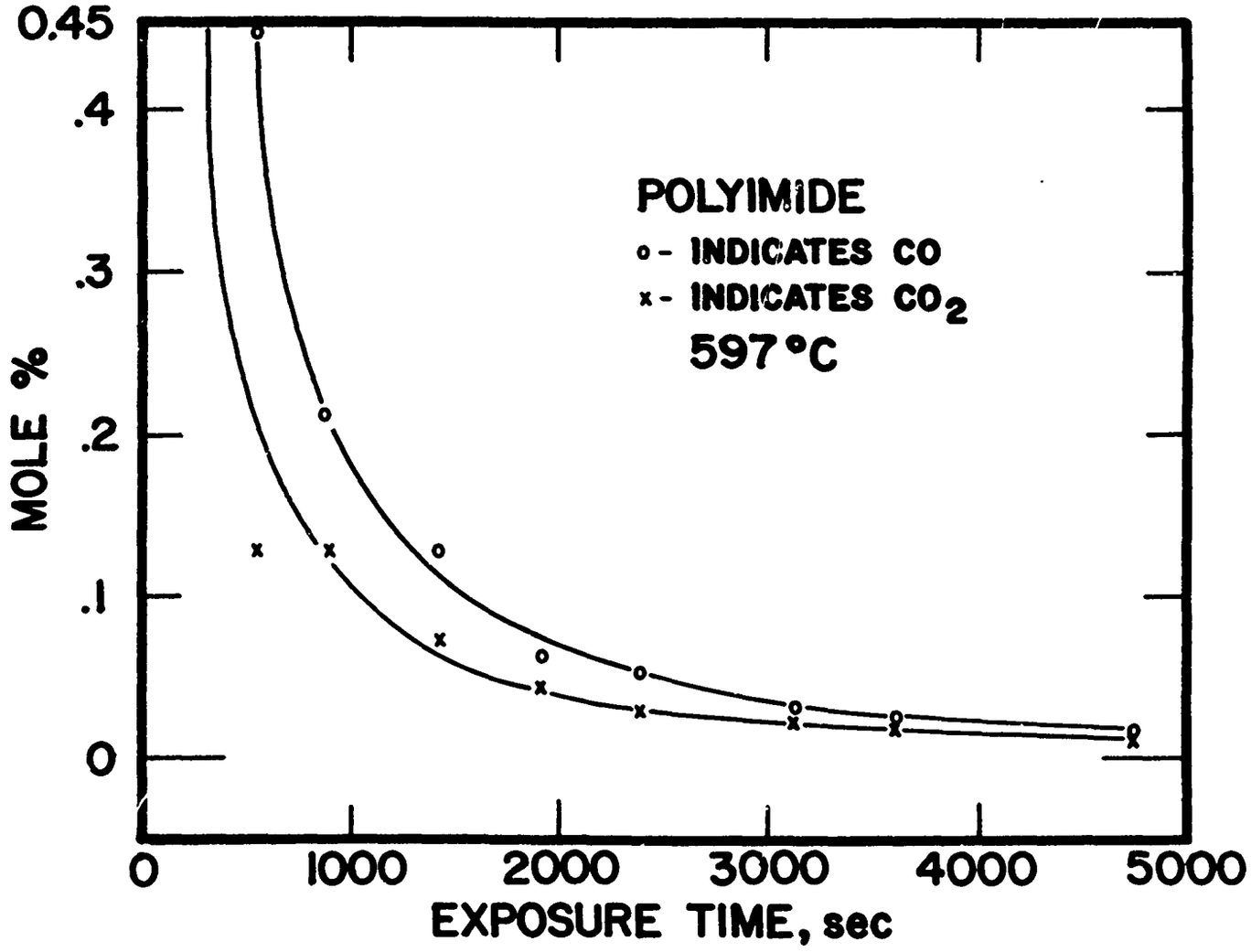

FIGURE 39. Gaseous Pyrolysis Products for Polyimide at 597°C in Helium

The appearance of important amounts of carbon dioxide in the pyrolysis poses several questions concerning its source. Bruck [8] has reported significant amounts of CO_2 in the pyrolysis of "Kapton" polyimide type H, commonly called H-film. Bruck attributed the formation of CO_2 to incomplete ring closure during imide formation. The resultant polymer structure would then have both imide groups and the polyamic-acid intermediate groups as discussed in Chapter V. It was then postulated that the polyamic acid units could decarboxylate at elevated temperatures to produce CO_2 or they could undergo hydrolytic scission and subsequent decarboxylation to form the same gas. In either case production of CO_2 was associated with impurities in the imide structure.

The hydrolytic scission and the thermal decarboxylation steps are shown below.

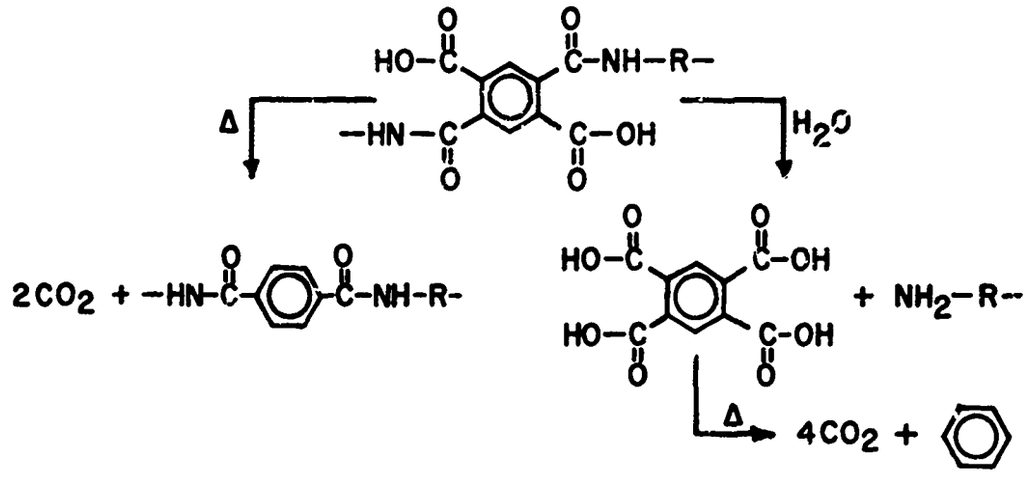

Bruck also expressed the opinion that only catalytic amounts of water would be required to promote the hydrolytic scission process.

On the other hand, Johnson and Gaulin [23] testing Skybond 700 did not observe water as a major element of pyrolysis. They, therefore,

proposed that CO_2 was a primary decomposition product originating in the imide ring. These authors postulated two different mechanisms of CO_2 generation which involved internal oxygen transfer within the imide. Model compounds were used as the source of information.

The results of this investigation tend to support the ideas of Bruck. Evidence in this direction is found in the results of elemental analysis and infrared spectra analysis. A quantitative determination of the elements in the virgin polyimide polymer and in the two chars formed at 480°C and 597°C was made. Table 10 presents the reported data and Table 11 shows the same values normalized to 100 weight per cent.

TABLE 10. REPORTED ELEMENTAL ANALYSIS FOR POLYIMIDE

	Weight Percent			
Material	C	H	N	O
Virgin Polymer	71.79	2.52	6.16	19.63
480°C Char	71.87	2.79	7.37	14.79
597°C Char	86.20	2.77	7.37	0.62
Idealized Structure	70.05	2.54	7.11	20.30

TABLE 11. NORMALIZED ELEMENTAL ANALYSIS FOR POLYIMIDE

	Weight Per cent				Mole Per cent			
Material	C	H	N	O	C	H	N	O
Virgin Polymer	71.72	2.52	6.15	19.61	58.83	24.77	4.33	12.07
480°C Char	74.23	2.88	7.61	15.28	58.54	27.28	5.15	9.03
597°C Char	88.90	2.86	7.60	0.64	66.10	25.49	4.85	3.56
Idealized	70.05	2.54	7.11	20.30	57.50	25.00	5.00	12.50

Taking the idealized repeat unit as the basis of calculation, the virgin polymer has a structure represented by $C_{23}H_{10}O_5N_2$. Elemental analysis of the uncharred polymer corresponds to a structure of $C_{23.5}H_{9.9}O_{4.8}N_{1.7}$. Similar calculations for the two char residues indicate structures of $C_{23.4}H_{10.9}O_{3.6}N_{2.1}$ and $C_{26.4}H_{10.2}O_{1.4}N_{1.9}$ for the 480°C Char and the 597°C Char, respectively.

The elemental analysis confirms the trends shown in the gas analysis. Comparison of the compositions of the original polymer and the 480°C char show an increase in the mole per cents of hydrogen and nitrogen, and a decrease in the mole per cent of oxygen in the char. These observations are consistent with the removal of carbon dioxide and carbon monoxide from the polymer as detected by gas analysis. Further in the 597°C char, the mole per cents of nitrogen, hydrogen, and oxygen show small, moderate and large decreases, respectively These results are consistent with the determinations of small quantities of HCN and H_2, moderate amounts of water, and major quantities of CO and CO_2 observed in gas analysis. Elemental analysis results also support a degradation mechanism in which the imide ring is attacked, carbon/oxygen fragments are expelled, and chain integrity is maintained by recombination through the nitrogen atoms. However, questions as to the source of water and carbon dioxide remain.

The infrared spectrum of Skybond 700 polyimide, cured as specified in Chapter IV, is shown in Figure 40. Several important absorption peaks are evident. First, both of the peaks generally associated with imide structures, at 1780 cm^{-1} and 715 cm^{-1}, are present. However, there is also a strong indication of the presence of an amide structure

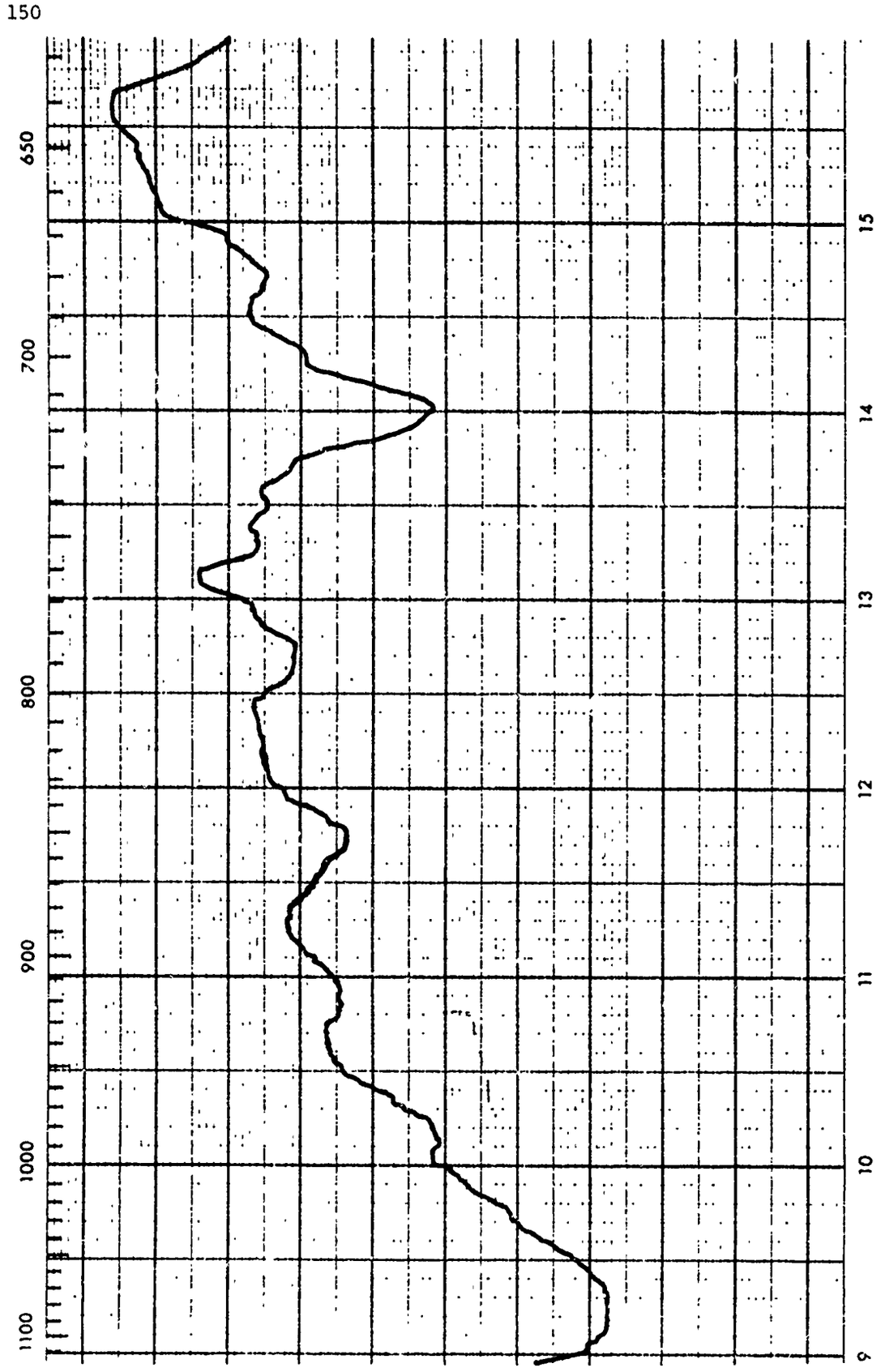

Figure 40 Infrared Spectra of Polyimide in a KBr Pellet

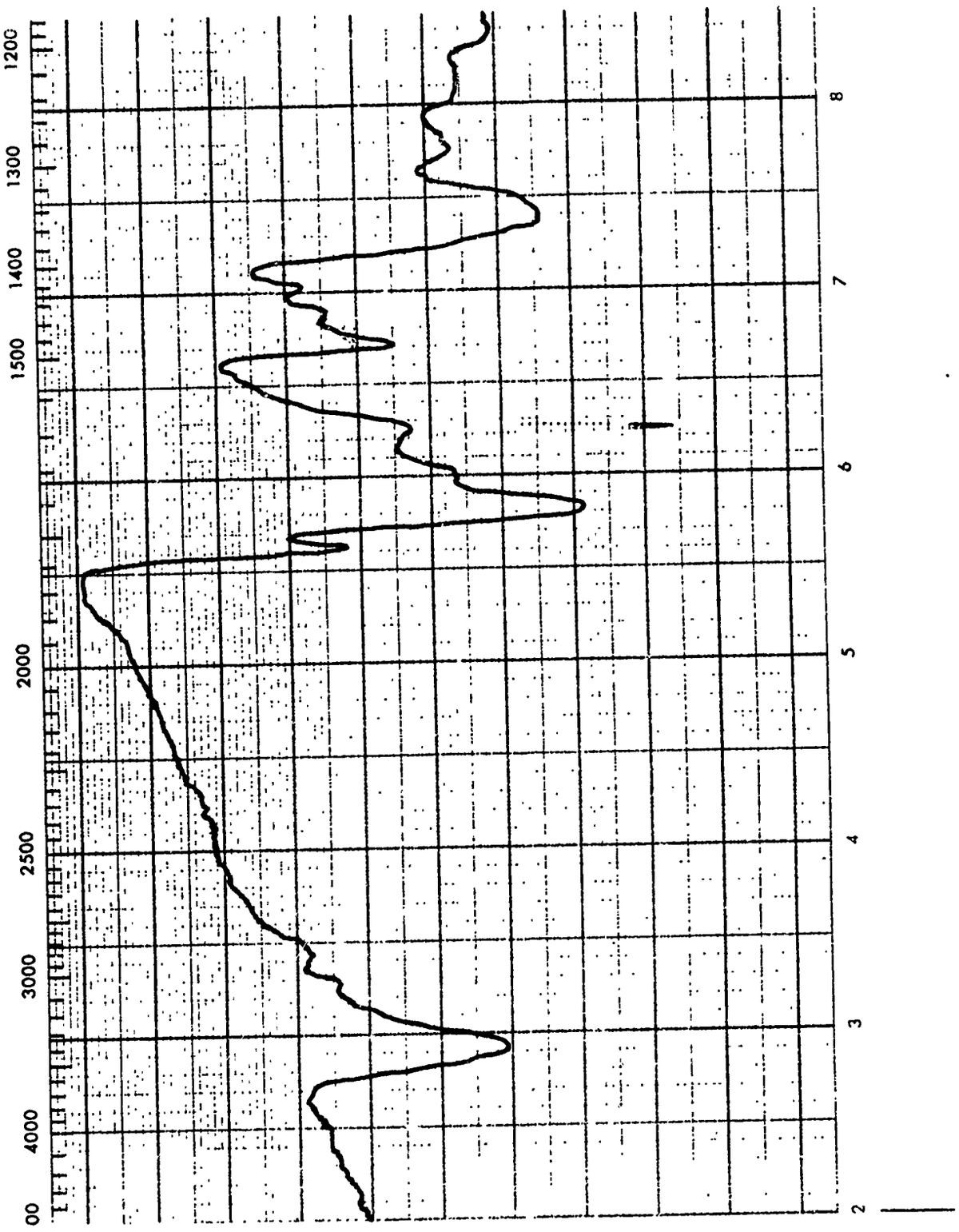

Figure 40 (continued)

because of the -NH stretching band at 3380 cm^{-1}. Of course, this band would not be present if complete conversion to imide had been obtained.

Both the detected presence of substantial water in the pyrolysis gas and the identified presence of amide structures in the polymer support the mechanisms proposed by Bruck. They do not, however, negate the possibility that the Johnson and Gaulin mechanism proceeds simultaneously. In fact, the latter mechanism explains the presence of HCN in the pyrolysis products, whereas Bruck's does not consider it.

The infrared spectra of char residues shown in Appendix D continue to exhibit both imide and amide absorption peaks. In general, the other characteristics of the original polymer are also manifest, although at an apparent lower level of intensity.

A mechanism for the thermal decomposition can be suggested. The most likely site of initial ring scission is in the imide ring between the nitrogen and carbonyl groups. Both of the radicals thus formed are known to be relatively stable because of energy delocalization into adjacent phenyl groups. However, the phenyl-carbonyl radical will rapidly rearrange to yield CO, and the resultant phenyl radical may recombine as shown below.

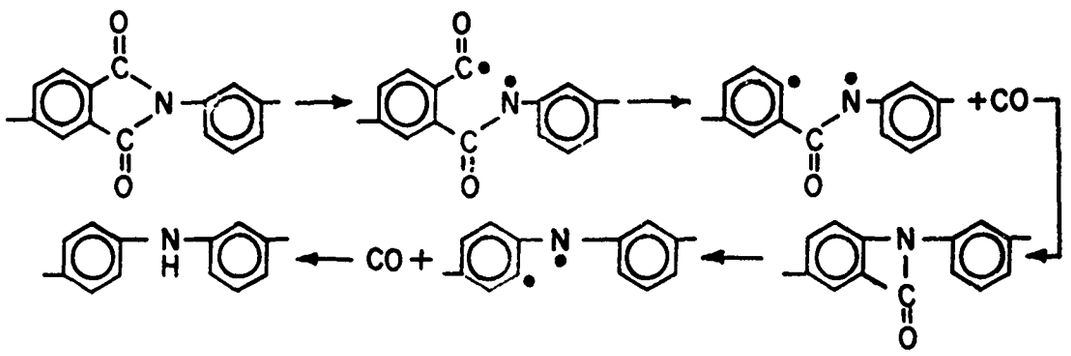

Further rearrangement in the four-membered heteroring with elimination of more CO is very likely. As a final step, the abstraction of nearby hydrogen by the radicals produced, yields a final structure in which nitrogen has become a chain element. This mechanism accounts for the voluminous carbon monoxide produced upon pyrolysis and also predicts the experimentally observed retention of nitrogen in the char. It is believed that the CO_2 and H_2O identified come primarily from polyamic acid decomposition as shown earlier. Hydrogen found during 597°C pyrolysis is the likely product of stripping reactions on phenyl groups as described for polyphenylene. Hydrogen cyanide probably represents the stable product of energetic rearrangements within the heteroring. A mechanism similar to that of Johnson and Gaulin could account for the production of some HCN as shown below.

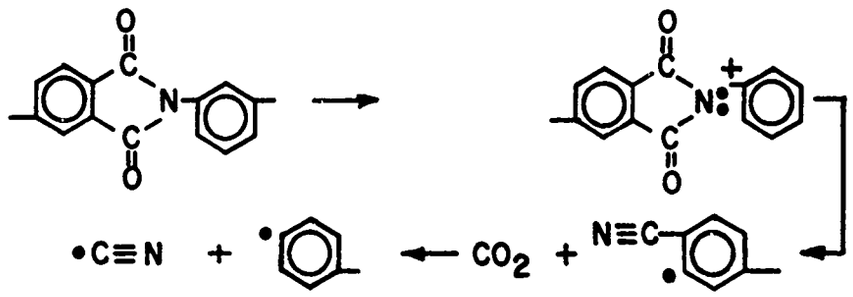

The first step, scission of the nitrogen-phenyl bond, leads to a resonance-stabilized free radical which provides a favorable configuration for internal oxygen transfer. Elimination of CO_2 produces a nitrile grouping which may either form a new chain link or which may be eliminated to eventually yield hydrogen cyanide.

Polyquinoxaline Polymer

Polyquinoxaline polymer is one of the newest of the high-temperature resins. As such, very little has been published about its thermal stability or pyrolysis reaction [16].

A dynamic thermogram obtained on polyquinoxaline in a non-flow helium atmosphere is shown in Figure 41. The temperature-rise-rate employed in this test was 10°C per minute, as was used in all dynamic experiments reported in this thesis. Numerical differentiation of discretized data produced the rate-of-weight-loss curve shown in Figure 42. Inspection of these plots reveals why polyquinoxaline was such an interesting material to study. First, the appearance of two reaction peaks which were reasonably separated presented a good opportunity to distinguish between reactions occurring in each region. Secondly, the reaction zones seemed to be separated sufficiently in temperature that these data might represent a good test case for the application of a two-mode model of the quasilinearization numerical analysis.

The specific polyquinoxaline resin tested in this work was synthesized and donated by W. J. Wrasidlo of the U. S. Naval Ordnance Laboratory. Mr. Wrasidlo recommended that the polymer be advanced before being tested. In order to evaluate the effect of such a procedure, the resin as supplied was heated for 6 hours at 260°C in a helium atmosphere. The resultant polymer had the same bright yellow appearance after being advanced as it had before. It was then tested in helium exactly like the previous sample. Results of this experiment are shown in Figures 43 and 44.

Comparison of the two tests indicates that thermograms for the

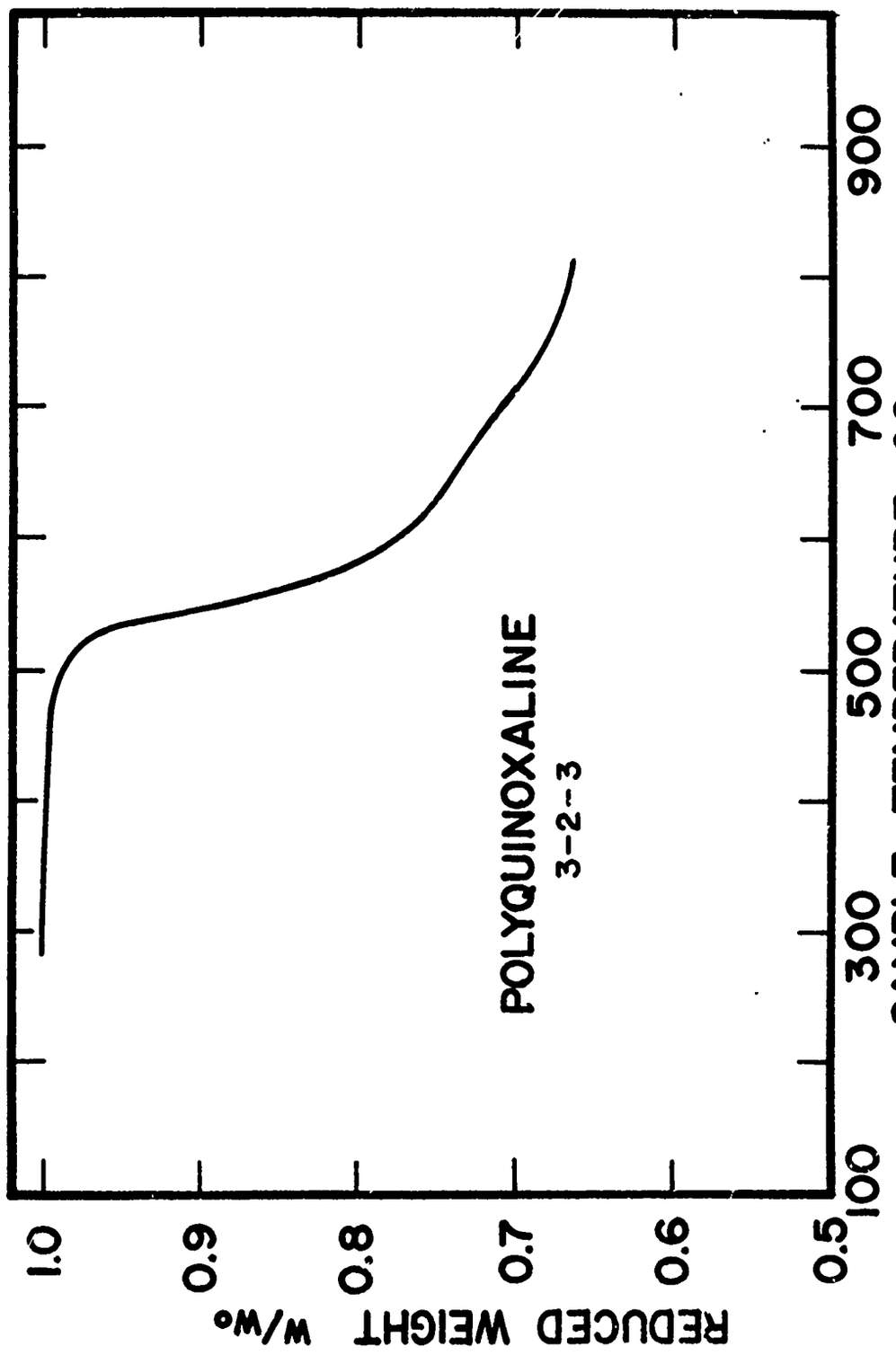

FIGURE 41. Dynamic Thermogram for Polyquinoxaline at 10°C/min in Non-flowing Helium

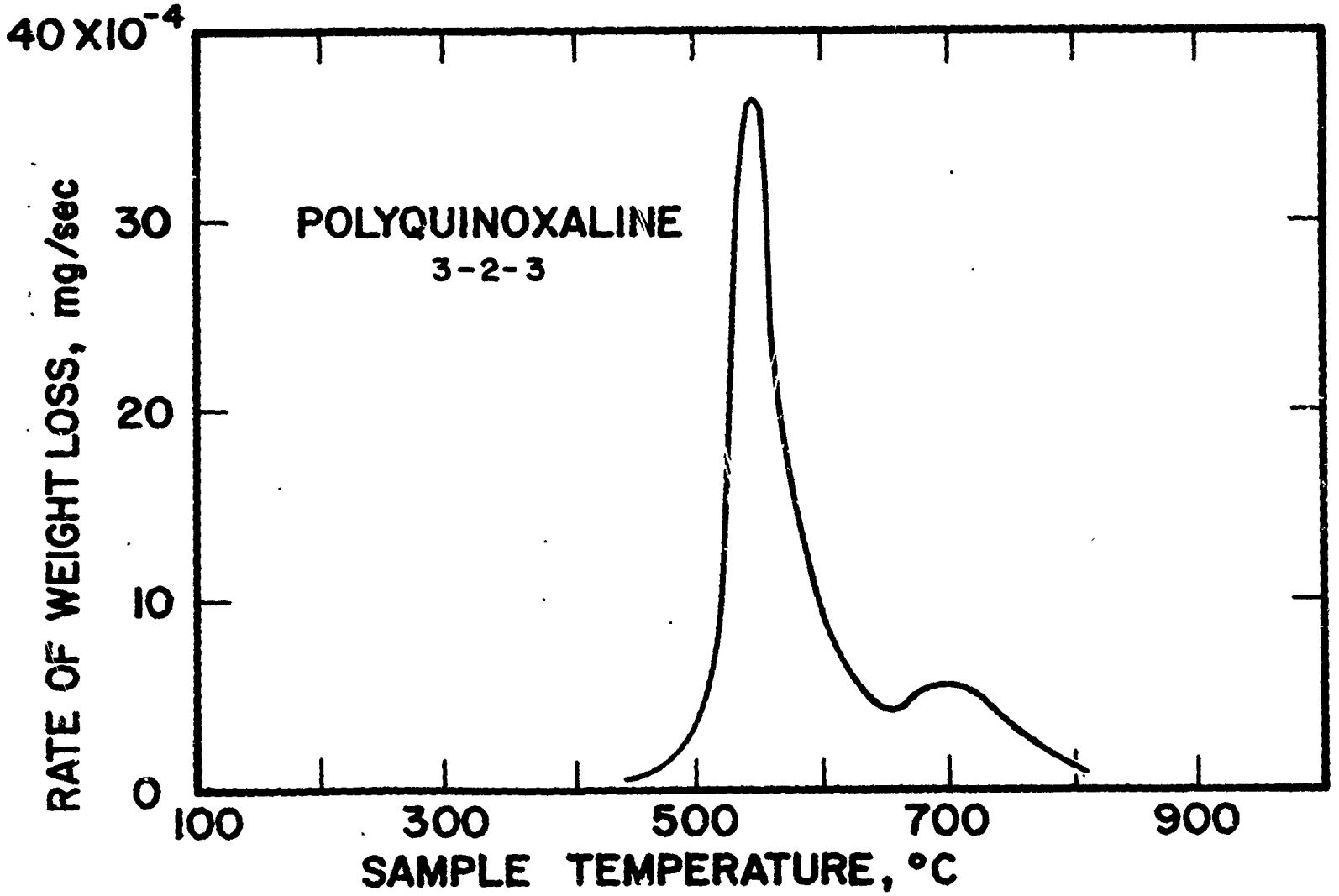

FIGURE 42. Rate of Weight Loss for Polyquinoxaline in Non-flowing Helium

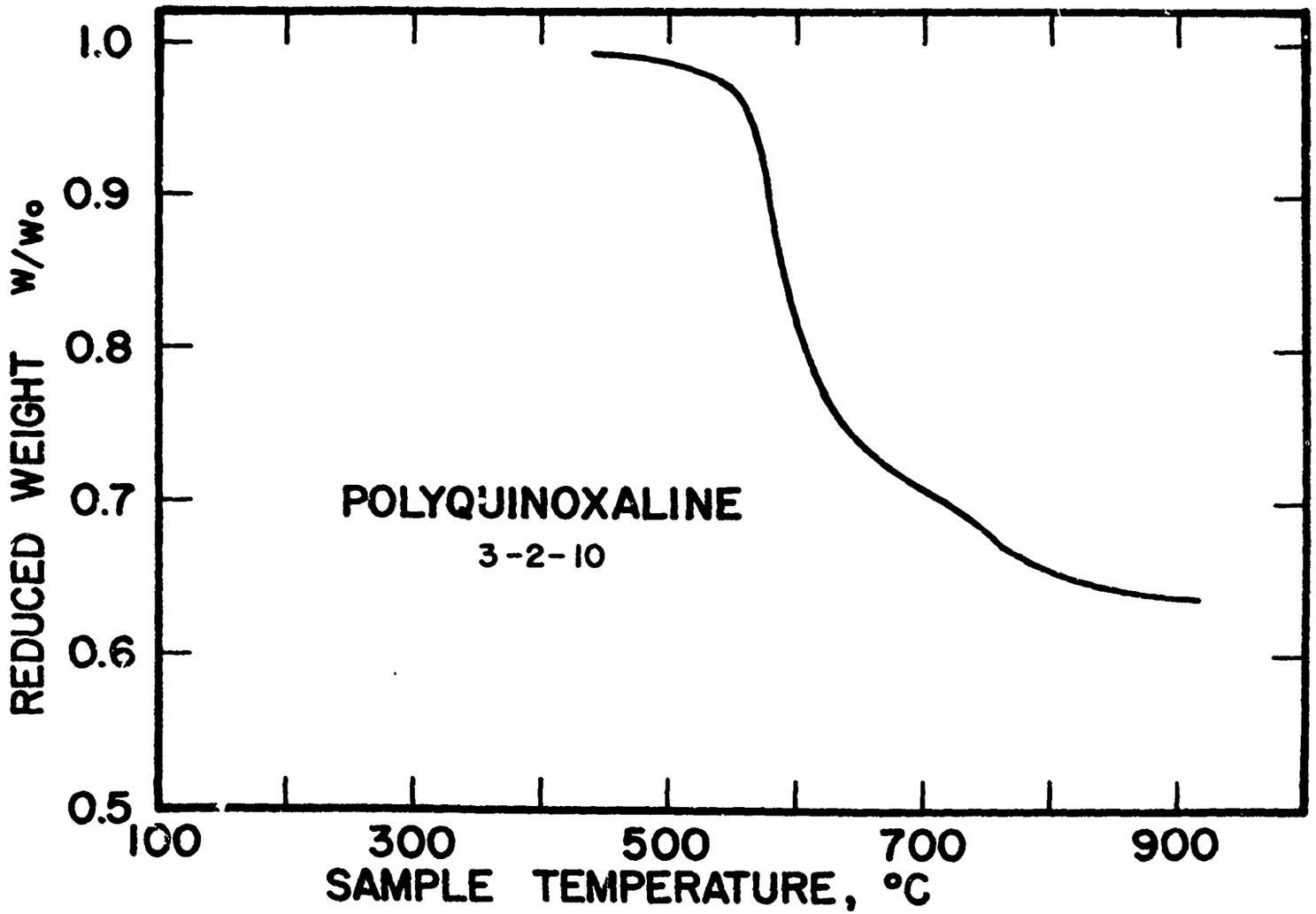

FIGURE 43. Dynamic Thermogram for Advanced Polyquinoxaline at 10°C/min in Non-flowing Helium

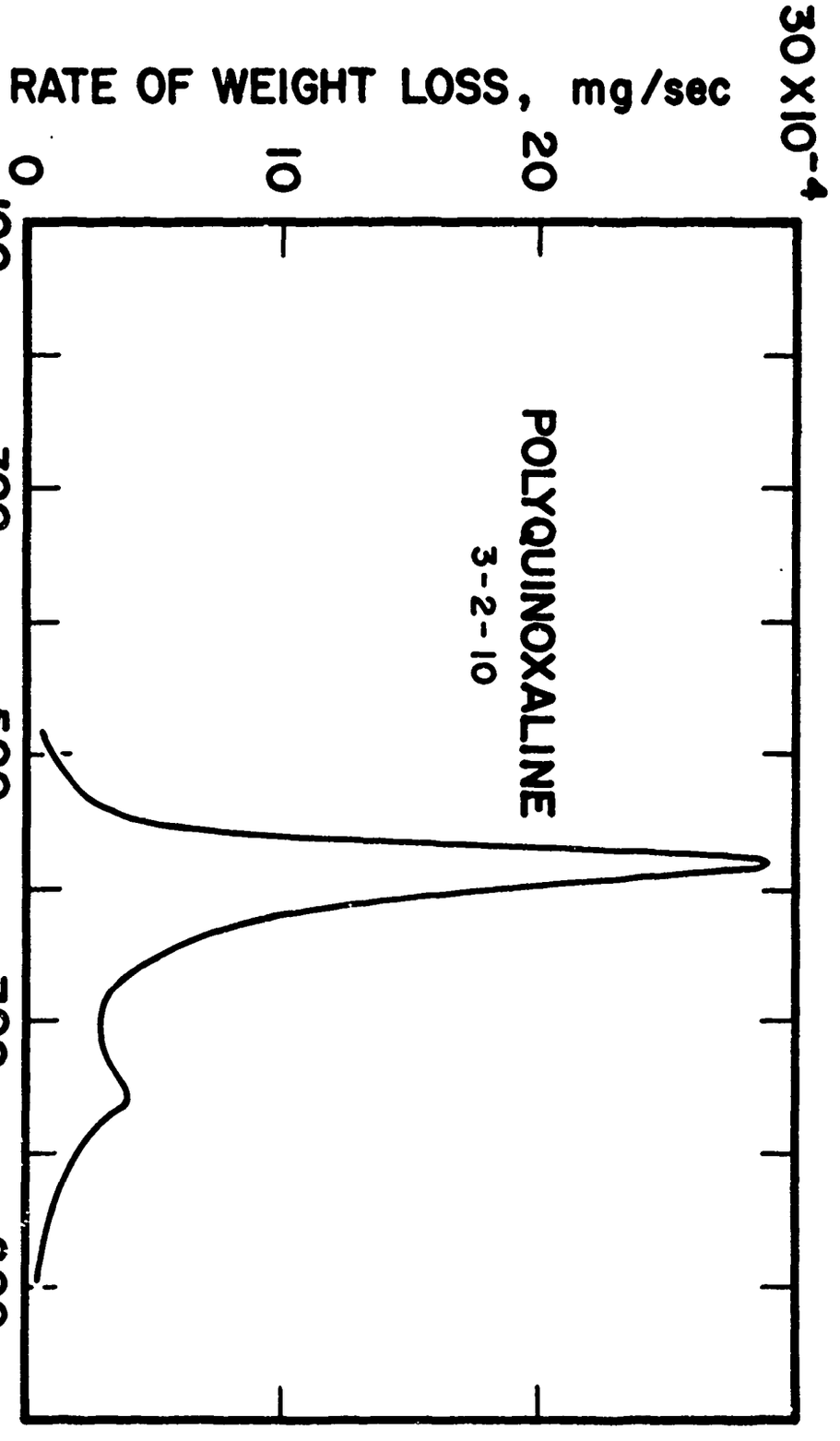

FIGURE 44. Rate of Weight Loss for Polyquinoxaline in Non-flowing Helium

advanced and unadvanced materials are strikingly similar. The principal difference between the two thermograms is the translation of the reaction peaks to about a 30°C higher temperature for the advanced resin. A reasonable explanation of this result is given later in this section after all the pertinent data are presented.

Isothermal TGA experiments on unadvanced polyquinoxaline were conducted at 572°C and 627°C. A temperature of 572°C is approximately 30°C above the maximum-rate temperature and about 30°C below the temperature at which the second mechanism becomes activated. This temperature was chosen in order that only the reaction associated with the first peak would be observed. A temperature of 627°C was in the temperature region of the second peak.

Isothermal results are plotted in Figure 45. The thermograms shown are different from the results of other isothermal pyrolyses presented in this chapter. They definitely seem to indicate an autocatalytic-type decomposition. Particularly in the case of the 572°C test, the isotherm passes through a maximum slope. It is usually very difficult to identify non-monotonic thermograms because the pyrolysis rate increases during the early part of the curve due to the rising temperature of the sample. However, in the case shown in Figure 45, temperatures near the steady-state value were reached in approximately 120 seconds. Therefore, the observed increase in rate of reaction cannot be attributed to increasing sample temperature.

Isothermal experiments were also conducted at 410°C, 455°C, 490°C, and 510°C. Results of these experiments generally confirm the autocatalytic-type nature of the pyrolysis. Because of the relatively small

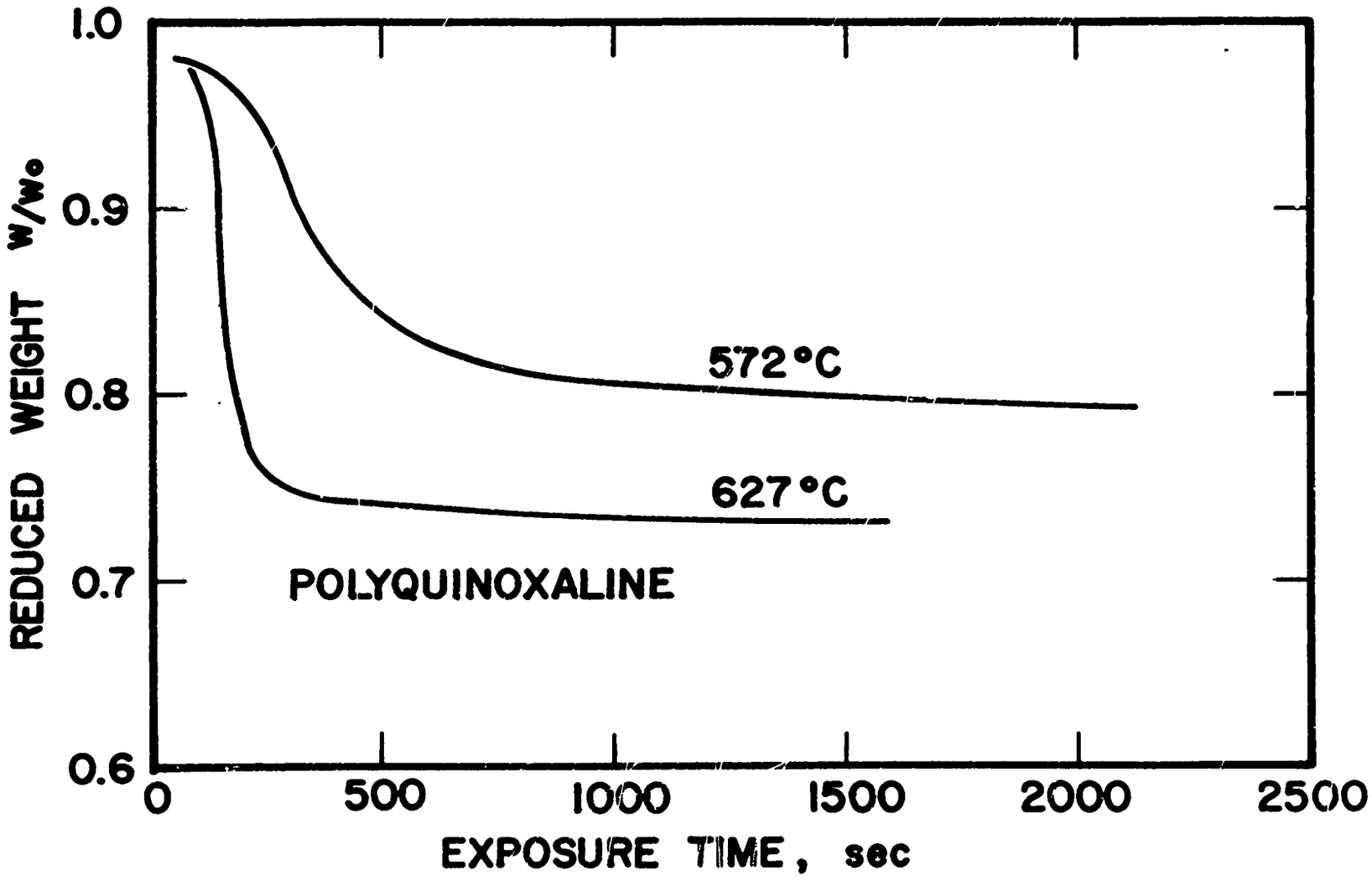

FIGURE 45. Isothermal Thermograms for Polyquinoxaline in Non-flowing Helium

weight losses observed in these tests, they are not included here but are given in Appendix F.

The volatile products evolved during isothermal experiments at 541°C and 701°C were analyzed. At 541°C the overwhelmingly abundant gaseous product found was hydrogen cyanide. Small quantities of hydrogen and methane were also observed. Benzene was the only vapor condensed in the cold trap during the pyrolysis. Even though benzene was identified as a decomposition product, quantitative measurements were impossible because of the minute quantities collected.

The gaseous products of 701°C pyrolysis were cyanogen $(CN)_2$, hydrogen cyanide, methane and some hydrogen. In addition, vapors collected were identified as benzene and a small amount of toluene. Since column calibration was not feasible for cyanogen or hydrogen cyanide because of their extreme toxicity and consequently difficult handling procedures, only peak heights are recorded in Table 12 and Figure 46 for the products identified.

Upon consideration of the products of pyrolysis at 541°C the polymer degradation probably took place almost completely within the quinoxaline ring. Hydrogen cyanide represented the thermodynamically stable product resulting from the thermal scission of the ring. The benzene collected almost certainly came from the removal of pendant phenyl groups from the polymer. The high percentage of the original polymer which remained as char indicated that the quinoxaline unit was fractured in such a way that chain integrity was largely maintained. If the chain cannot maintain continuity by recombining over gaps left by volatilized fragments, total decomposition results. Such is essentially

TABLE 12. POLYQUINOXALENE PYROLYSIS-GAS ANALYSIS AT 701°C

Time sec	Relative Peak Heights			
	H_2	$(CN)_2$	HCN	CH_4
300	0.2	4.2	0.95	3.6
600	0.1	1.6	0.75	0.9
780	0.05	0.9	0.60	1.1
1080	0.04	0.9	0.70	0.7
1290	0.04	0.8	0.60	0.5
1590	0.05	0.6	0.40	0.4
1860	0.05	0.4	0.20	0.4
2160	0.03	0.4	0.10	0.3
2400	0.01	0.5	0.10	0.2
2700	--	0.3	--	0.1
3000	--	0.3	--	--
3300	--	0.2	--	--

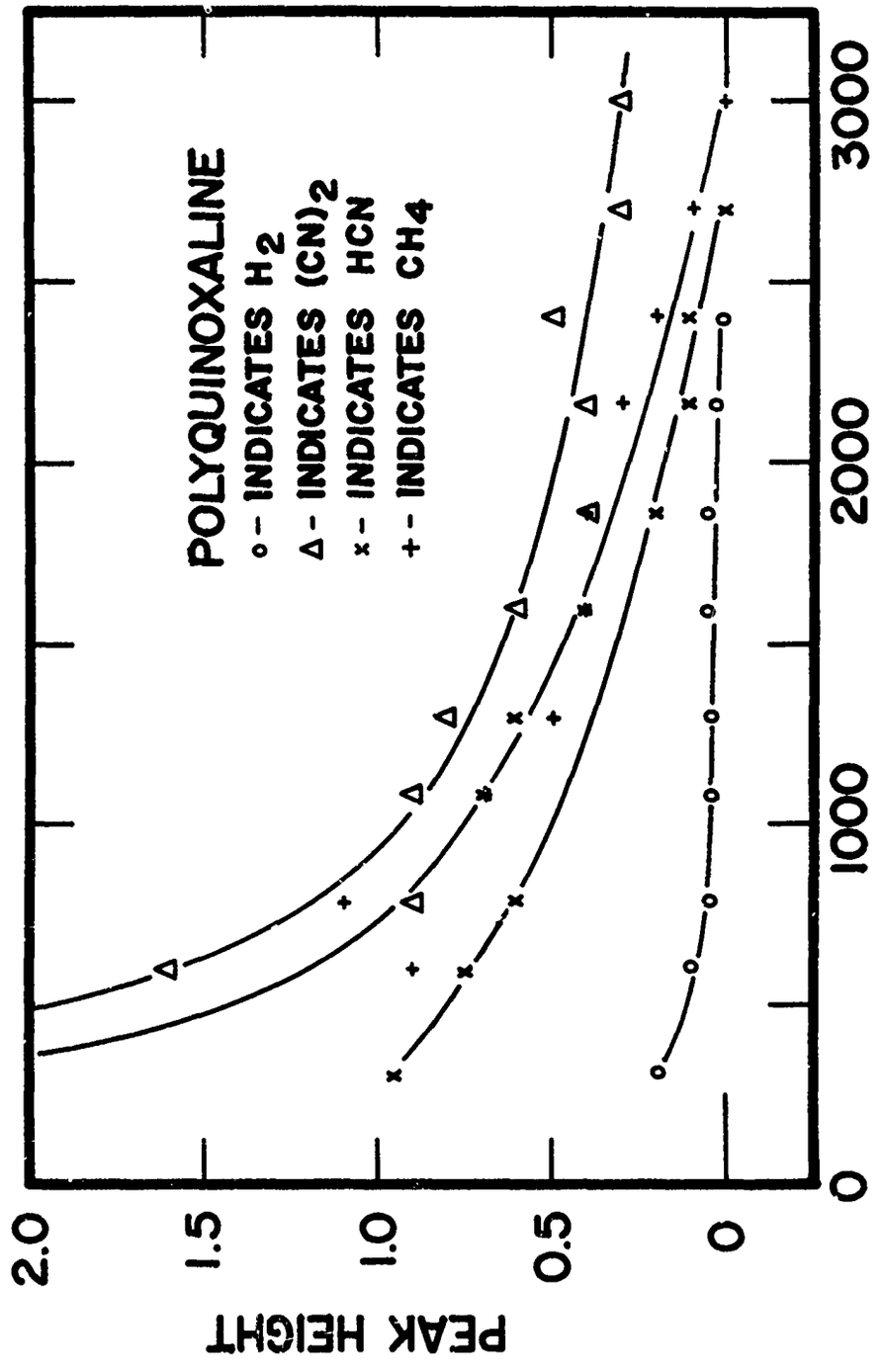

FIGURE 46. Pyrolysis Gas Analysis for Polyquinoxaline at 701°C

the case for the pyrolysis of polyquinoxaline in air where total volatilization occurs.

Pyrolysis of this polymer at 701°C exhibits many of the characteristics of decomposition at 541°C. Again, the quinoxaline ring was the predominant site of attack. Fragmentation of this unit produced both HCN and $(CN)_2$. The high test temperature evidently supplied sufficient energy to tear out large parts of the quinoxaline ring without permitting rearrangement after the initial fracture occurred. This conclusion is indicated since hydrogen cyanide is significantly more stable thermodynamically than cyanogen.

Formulation of a mechanism consistent with the results of polyquinoxaline decomposition is particularly difficult because of the large number of almost equally probable reactions which may take place. The mechanisms proposed here and in other sections of this thesis are presented with an awareness of the shortcomings of any such proposition. However, in spite of difficulties and lack of uniqueness of any unproved mechanism, specific reaction steps are shown which are reasonable and lead to the desired products. Such an explanation does not mean that the reactions are justified solely on the basis of correct predictions of observed products. Many well-known reactions similar and sometimes identical to those presented here are to be found in texts and papers on organic chemistry.

A mechanism consistent with these observations of polyquinoxaline decomposition is shown below. It is proposed that because of ring stabilization in the heteroring, direct attack is less likely than initiation by elimination of the pendant phenyl groups. Stille [44] has observed phenyl group removal on other polyquinoxalines.

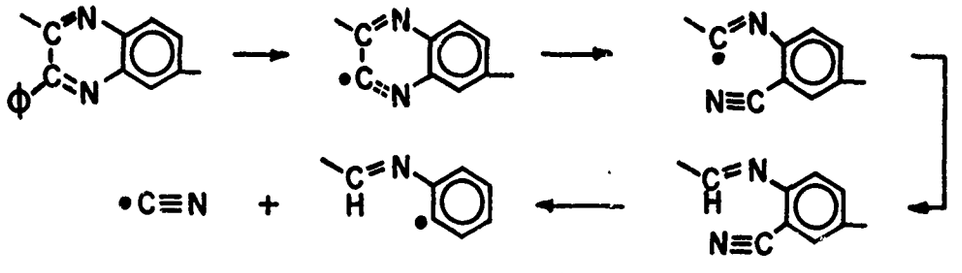

The activated ring may then fracture and rearrange to form a nitrile group which is subsequently eliminated. The radicals produced in the last steps are very unstable and abstract hydrogen from the surroundings very readily.

If the heteroring resonance stabilization is small, a likely reaction is fracture between the two ring carbon atoms. Such a scission could lead to many paths which could account for the products, no one of which seems to be clearly more favorable.

The generation of cyanogen represents a gross fracture of the quinoxaline ring, probably initiated by phenyl removal. Also, at 700°C sufficient energy is available to fracture phenyl groups to produce the methane detected. Hydrogen is again the expected product of stripping reactions.

It is probably not valid to conclude from these tests that the second reaction peak in Figure 42 results only from the generation of cyanogen, even though cyanogen appears to be the major difference between the results of low and high temperature tests. It is more likely that the decomposition of benzene-like units to produce methane accounts for the second peak. Scission with the benzene rings probably

assisted in the generation of cyanogen by reducing the possibilities for stabilizing the activated chain.

The results of elemental analysis of the chars produced during gas analysis are not in disagreement with the above interpretation. Table 13 presents the reported results and Table 14 contains the weight-normalized values.

TABLE 13. REPORTED ELEMENTAL ANALYSIS OF POLYQUINOXALINE

Material	Weight Per cent		
	C	H	N
Virgin Polymer	84.54	4.15	11.35
541°C Char	82.58	3.68	11.56
701°C Char	84.78	1.33	8.07
Ideal Structure	84.30	4.13	11.57

TABLE 14. NORMALIZED ELEMENTAL ANALYSIS OF POLYQUINOXALINE

Material	Weight Per cent			Mole Per cent		
	C	H	N	C	H	N
Virgin Polymer	84.50	4.15	11.35	58.67	34.58	6.75
541°C Char	84.42	3.76	11.82	60.43	32.32	7.25
701°C Char	90.02	1.41	8.57	78.75	14.82	6.43
Ideal Structure	84.30	4.13	11.57	58.62	34.48	6.90

The idealized polymer structure may be represented by $C_{34}H_{20}N_4$, and the anlysis of virgin polymer resulted in a structure of $C_{34}H_{20}N_{3.9}$.

Infrared spectra for polyquinoxaline polymer are included in Appendix D. Spectra obtained did not provide any additional insight into the degradation process.

The observed upward shift of decomposition temperature brought about by advancing the original polymer can be explained in light of the experimental data presented. It is not enough to attribute the temperature shift merely to an increase in molecular weight of the polymer. Since the decomposition was probably randomly initiated and did not proceed through an unzip mechanism, increases in an already large molecular weight would likely have little effect on the temperature of pyrolysis. However, the temperatures at which the decomposition reactions occur could be altered if a greater number of chain fractures were required to produce volatile fragments, or if the number of sites available for initial attack were reduced.

Crosslinking between adjacent polymer chains would increase the number of fractures necessary to yield volatile fragments. Pendant phenyl groups are likely units for crosslinking since the **para**-position of a phenyl group is somewhat activated.

Since the reaction has been identified as being of an autocatalytic-type, reduction of the number of initiation sites effectively would postpone the reaction. Thus, if the reaction was an end-group-initiated autocatalytic-type reaction, as is the case for polystyrene resin, advancement would shift the decomposition to higher temperatures. But another consequence of such a mechanism would be the appearance of the pyrolysis products of the benzene-like units found within the chain. Since these types of products are identified only in small amounts, an

end-group-initiated reaction is not a satisfactory explanation.

Another initiation site was available. If the pendant phenyl groups were eliminated from the polymer, the quinoxaline rings would become activated. Such an initiation step is likely in light of the significant amounts of benzene evolved during decomposition of the resin. Further, phenyl initiation sites would lead directly to scission within the quinoxaline group, and would account for the presence of HCN in the pyrolysis gas at temperatures where little fracturing of the benzene rings is noted.

On the basis of the evidence presented, polymer crosslinking through the phenyl groups may have had some effect, but the predominant influence in the thermal pyrolysis was a phenyl-group initiated, autocatalytic-type decomposition taking place primarily within the quinoxaline unit of the polymer. Thus, removal of phenyl initiation sites through crosslinking brought about by resin advancement could account for the upward shift of reaction temperature. Of course, at high temperatures other mechanisms are likely proceeding simultaneously.

Since isothermal decomposition of polyquinoxaline exhibits some degree of autocatalytic-type behavior, an attempt was made to describe the reaction with an empirical autocatalytic-type model shown below.

$$-\frac{dW}{dt} = A\, e^{-E/RT}(\alpha W + \beta W^2 + \gamma W^3)$$

However, it was found that the model did not produce a consistent interpretation for the isothermal experiments. For example at a value of W = .81, values of A and E computed from the autocatalytic model were 1.03×10^{10} sec^{-1} and 49,300 cal, respectively. At small

values of W values of A became as large as 10^{16} sec^{-1}, and values of E correspondingly increased to about 85,000 cal.

The inconsistency encountered may be the result of several factors. The most likely cause was that the assumptions implicit in the assumed model did not hold. The model assumes a single reaction which is unchanging with temperature. Thermogravimetric analysis indicated that these assumptions were not likely to be true. Therefore, in order to gain a description of the decomposition reaction, numerical analysis techniques were employed.

The dynamic TGA data of polyquinoxaline were analyzed by application of the quasilinearization two-mode model. Several computation strategies were tried before convergence was obtained in the iterative calculations. As a first attempt, graphically-obtained values of kinetic parameters were used in an unrestrained calculation. This calculation failed to be sufficiently stable to permit convergence, apparently because of the very sensitive interaction between the two reaction modes.

As a second trial, it was attempted to optimize the parameters of the second peak with those of the first peak and the order of reaction of the second held constant. The reverse calculation was also tried. While these approaches did lead to some convergent values, the sensitivity of interaction between the parameters made optimization of the combined reaction very laborious.

The third and best approach tried was to optimize the parameters of the first reaction peak using only data taken before the second reaction peak became activated. Of course, it was still necessary to

constrain n_1 during these calculations. Graphical values of n_1 had been obtained which varied from 1.6 to 2.0. Computer calculations seemed to indicate that a value of near 2.0 could best fit the data. In this way values of kinetic parameters for the first reaction mode were found to be 8.212×10^{15} sec^{-1} for A_1 and 66,585 cal. for E_1 with a constrained value of 2.0 for n_1.

For comparison, convergent values of kinetic parameters obtained for other assumed values of the order of reaction are given in Table 15.

TABLE 15. CONVERGENT KINETIC PARAMETERS FOR THE FIRST REACTION PEAK OF POLYQUINOXALINE

Constrained n_1	A_1, sec^{-1}	E_1, cal	Sum of Least Squares
1.0	7.050×10^{9}	46,627	0.1328×10^{-1}
1.6	2.680×10^{13}	58,369	0.6686×10^{-2}
1.7	1.102×10^{14}	60,394	0.5973×10^{-2}
1.9	1.929×10^{15}	64,502	0.4787×10^{-2}
2.0	8.212×10^{15}	66,585	0.4299×10^{-2}
3.0	2.980×10^{22}	88,445	0.1956×10^{-2}

The least squares fit of the data shown in Table 15 seem to justify use of an n even larger than 3.0. However, the convergent parameters for an n of 3.0 predict a greater weight loss at the end of the first reaction than that actually observed. Thus, the interaction of the two reaction zones supports the use of a value of n near

2.0.

Having an indication of the magnitude of the parameters for the first peak, values for the second peak were sought while those for the first were held constant. Combinations of n_1 and n_2 were tried with the result that n_2 was found to be near 2.0. Values of n_2 either greater or less than 2.0 seemed to lead to poor agreement with the data.

As a final step in applying the two-mode model, both reaction peaks were optimized simultaneously. In this case it was still necessary to constrain the values of n_1 and n_2. The results of several combinations are presented in Table 16 to illustrate the trends. Values of 3.1 for n_1 and 2.0 for n_2 appear to be very near to the best fit of the data.

Figure 47 illustrates a comparison of data and points computed from optimized kinetic parameters for $n_1 = 1.9$ and $n_2 = 2.0$. Figure 48 shows a similar plot for $n_1 = 3.0$ and $n_2 = 2.0$. As can be seen in Figure 48, the parameters determined by quasilinearization describe the complex dynamic reaction curve very well. The fit of the parameters shown in Figure 47 is obviously inferior to that shown in Figure 48 and yet the over-all conformity is really quite good. Such an observation emphasizes the need for accurate data for use in determining kinetic parameters, since inconsistencies or scatter would seriously affect the final results.

In all of the quasilinearization calculations thus far presented for polyquinoxaline, it was assumed that the sample was composed of two parts which reacted independently to form both gas

TABLE 16. CONVERGENT KINETIC PARAMETERS FOR POLYQUINOXALINE PYROLYSIS

n_1	A_1, sec^{-1}	E_1, cal	n_2	A_2, sec^{-1}	E_2, cal	Sum of Least Squares
2.0	1.242×10^{22}	84,049	1.9	7.195×10^{11}	62,109	0.1432×10^{-2}
3.0	1.394×10^{22}	87,232	2.1	1.161×10^{13}	66,814	0.1425×10^{-2}
2.9	2.574×10^{21}	84,758	2.0	3.836×10^{12}	65,028	0.1523×10^{-2}
3.0	1.474×10^{21}	87,104	2.0	1.020×10^{13}	64,445	0.1426×10^{-2}
3.1	6.818×10^{22}	89,545	2.0	2.171×10^{12}	63,889	0.1353×10^{-2}

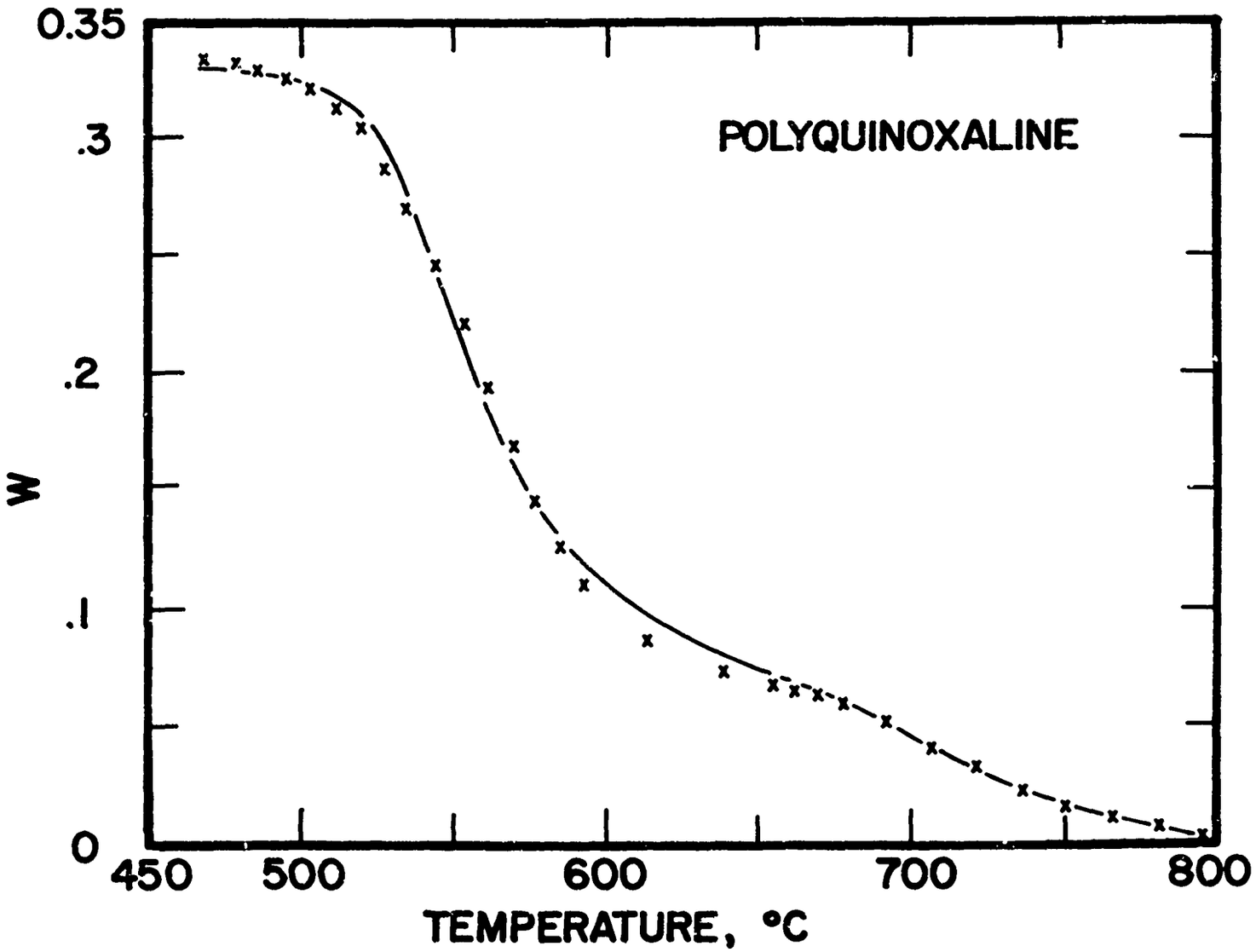

FIGURE 47. A Comparison of Data and Numerically Optimized Results for Polyquinoxaline

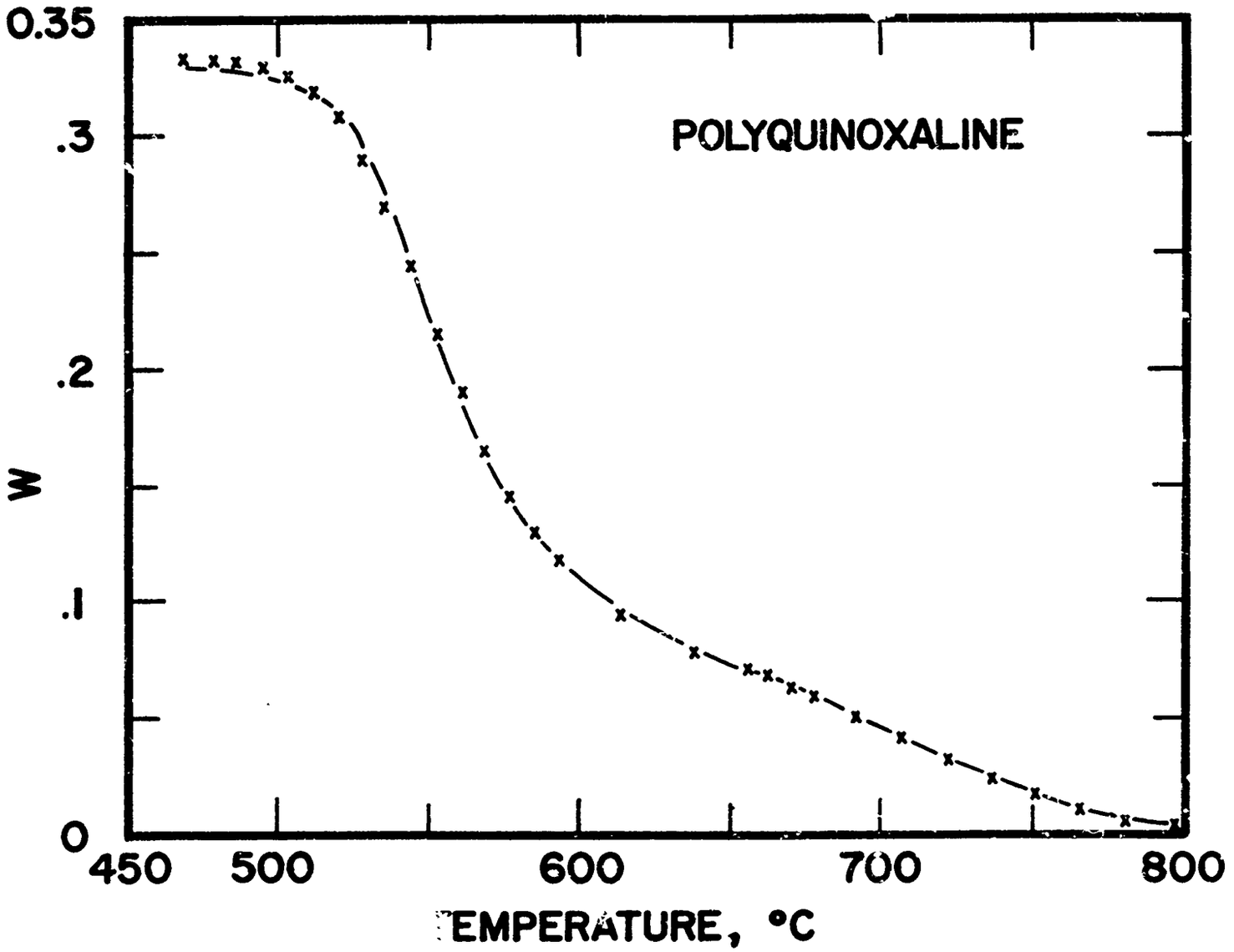

FIGURE 48 Comparison of Data and Numerically Optimized Results for Polyquinoxaline

and char. It was further assumed that the starting material in both reactions produced the same fractional char yield as was determined for the combined reaction from the dynamic thermogram.

Other investigators have assumed for a similar case that one reaction produces only gas and the second produces all the char [20]. Since this assumption seemed far removed from that used in the present work, it represented an opportunity to investigate the affect of a char-yield assumption upon the kinetic parameters computed.

Accordingly, the computer program was modified to consider the case where the second reaction zone produced only gaseous products and did not contribute to char formation. This latter char assumption was called W_R #2 and the former W_R #1. The results of calculations based on both assumptions are presented in Table 17.

The effect of the very different char assumptions can be seen clearly by comparing kinetic paramenters for the case of n_1=3.0 and n_2=2.0. Quite emphatically there was absolutely no modification of calculated parameters as a result of the difference in char assumptions. It seems therefore that any consistent assumptions concerning char yield for the case of a parallel-reaction model are equally acceptable for quasilinearization computations.

Also implicit in the application of the two-mode model as outlined is the assumption of uncoupled reactions. The case of coupled reaction mechanisms was not included in this work.

In light of the above results the value of using polyquinoxaline in high temperature environments may be limited. While the temperature of incipient weight loss is high at about 500°C, corresponding tempera-

TABLE 17. KINETIC PARAMETERS FOR POLYQUINOXALINE CHAR ASSUMPTIONS

Char Assumption	n_1	A_1	E_1	n_2	A_2	E_2
W_R#1	2.0	1.242×10^{22}	84,049	1.9	7.195×10^{11}	62,109
W_R#1	3.0	1.474×10^{21}	87,104	2.0	1.020×10^{13}	64,445
W_R#2	1.9	2.131×10^{14}	62,563	2.0	4.459×10^{15}	71,896
W_R#2	3.0	1.474×10^{21}	87,140	2.0	1.019×10^{13}	64,443

tures for other aromatic materials are equally as high. At temperatures above 500°C the weight loss for polyquinoxaline is rapid and the 64 per cent final char produced at 900°C is not as high as for polyimide, polybenzimidazole or polyphenylene. However, polyquinoxaline is superior to phenolic both in regard to the temperature of pyrolysis and the amount of char produced. Also, the gaseous products of pyrolysis are highly toxic and, therefore, inappropriate for use near living creatures.

The relatively large weight loss observed for polyquinoxaline probably results from an inability of the polymer to bridge gaps in the chain produced by fragmentation within the quinoxaline structure.

Polybenzimidazole Polymer

As in the case of the phenolic resin, two different types of polybenzimidazole resin were tested. As discussed in Chapter IV, PBI-A and PBI-B are the same basic polymer. However, PBI-A material was cured at moderate temperature and high pressure. PBI-B was cured at relatively low pressure and high temperature. The dynamic thermogravimetric response of material PBI-A is shown in Figure 49 and the reduced rate of weight loss is shown in Figure 50. The general nature of PBI curves are somewhat similar to the phenolic curves shown previously. In both figures, low-temperature weight loss results from curing condensation reactions, followed by a double-peaked region of major weight loss. Figures 51, 52, and 53 illustrate the basic dynamic thermogram, the rate of weight loss, and the reduced rate of weight loss for PBI-B resin. The higher temperature cure of this

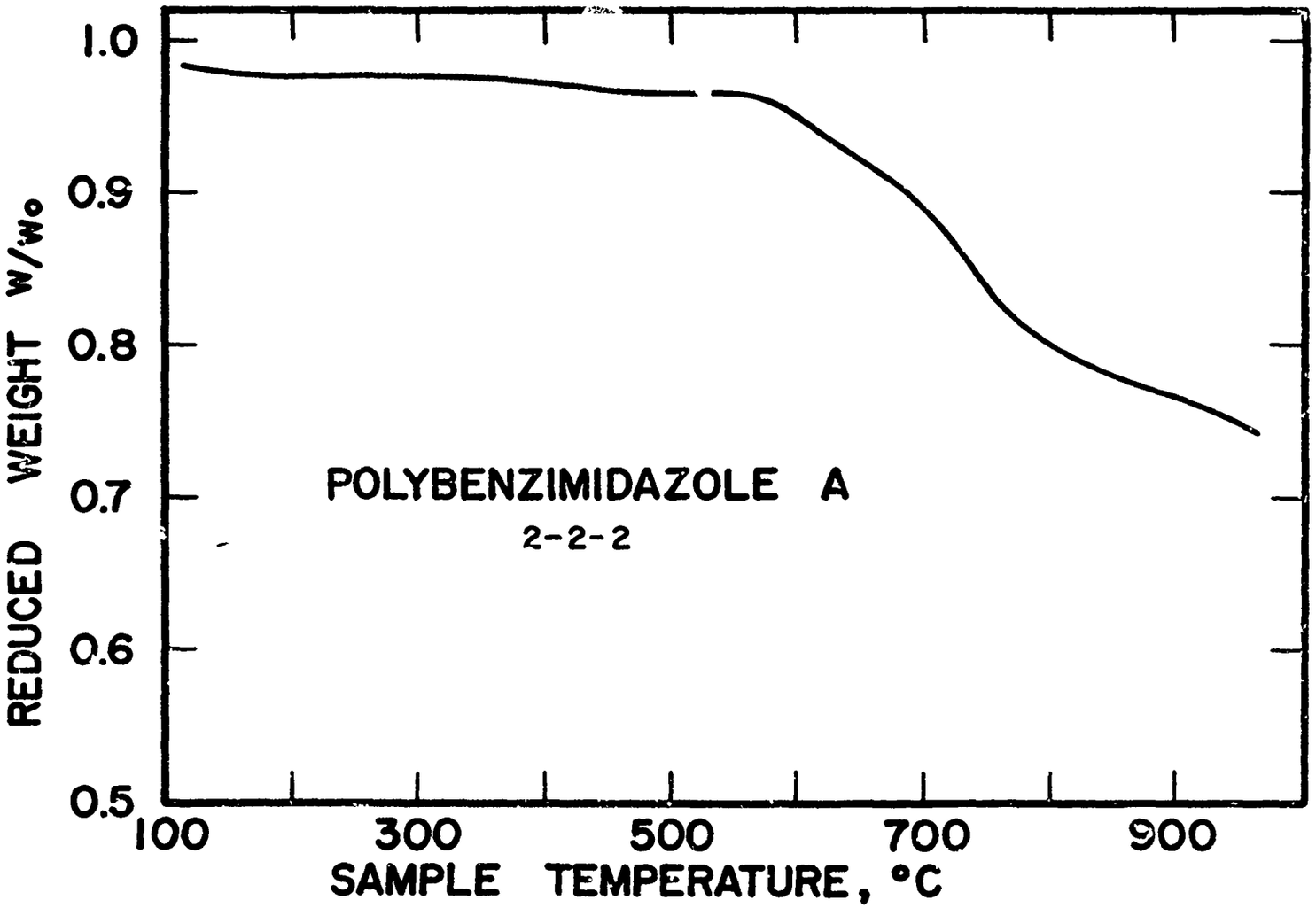

FIGURE 49. Dynamic Thermogram for Polybenzimidazole at 10°C/min in Flowing Helium

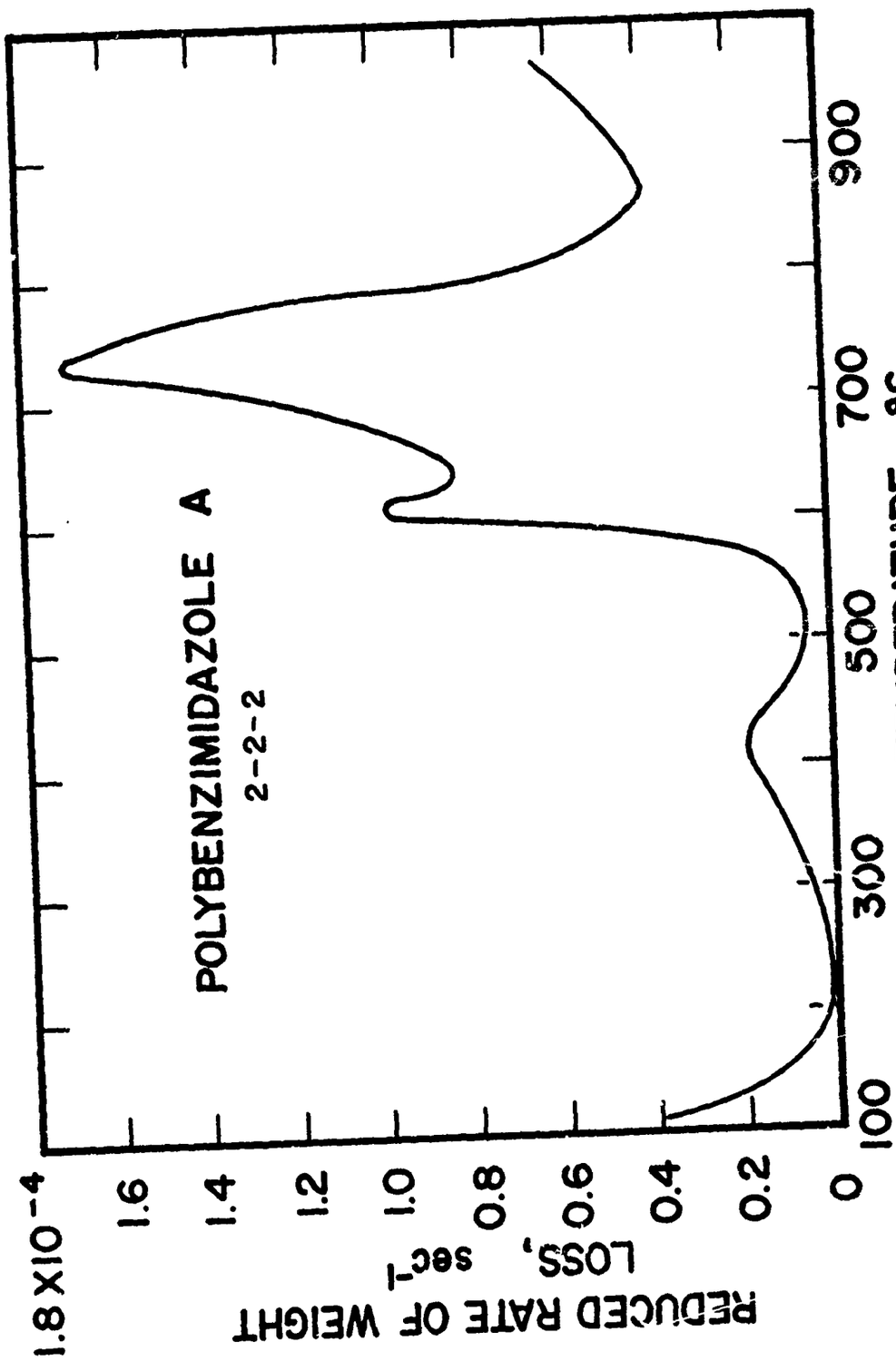

FIGURE 50. Reduced Rate of Weight Loss for Polybenzimidazole in Flowing Helium

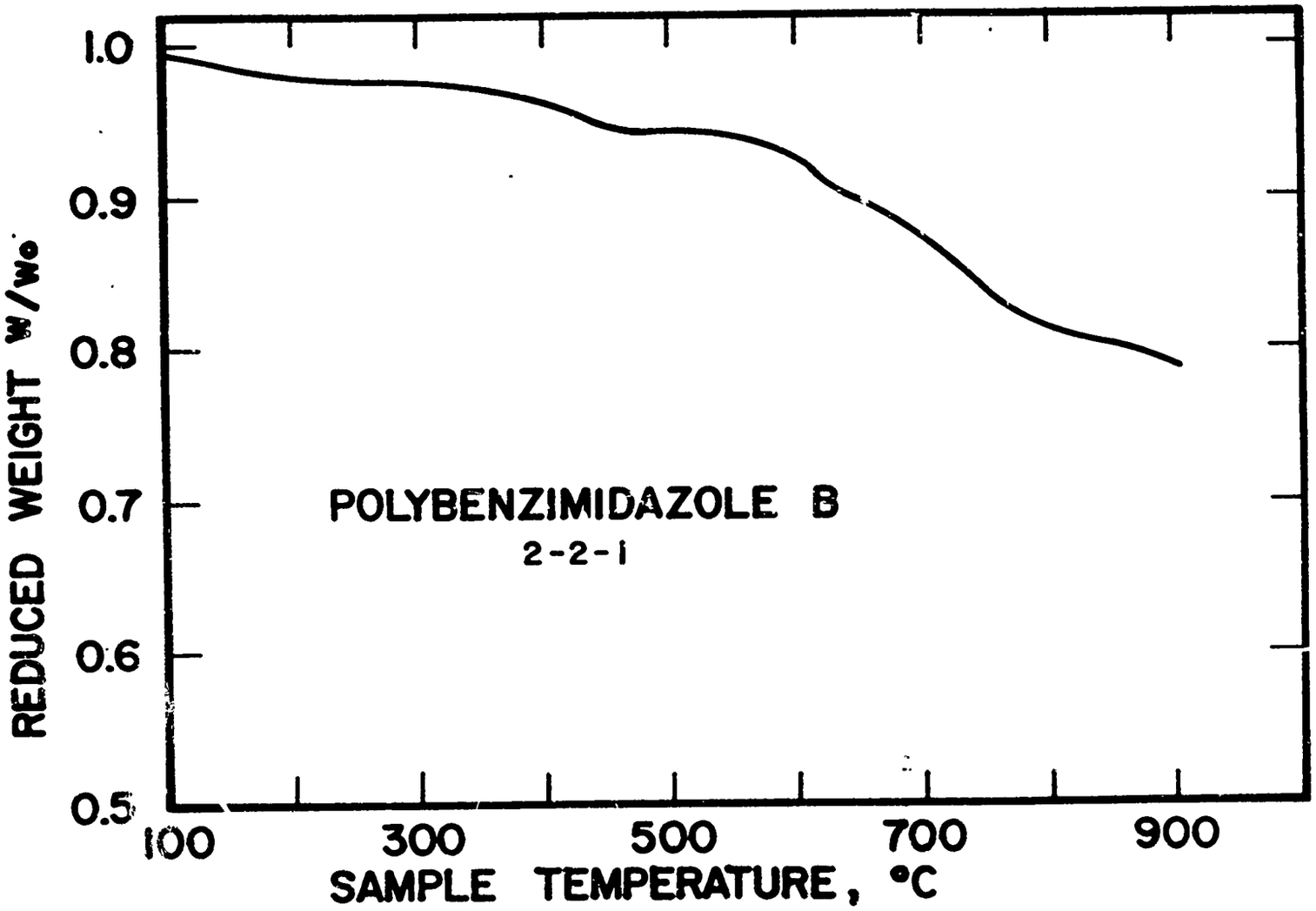

FIGURE 51. Dynamic Thermogram for Polybenzimidazole at 10°C/min in Flowing Helium

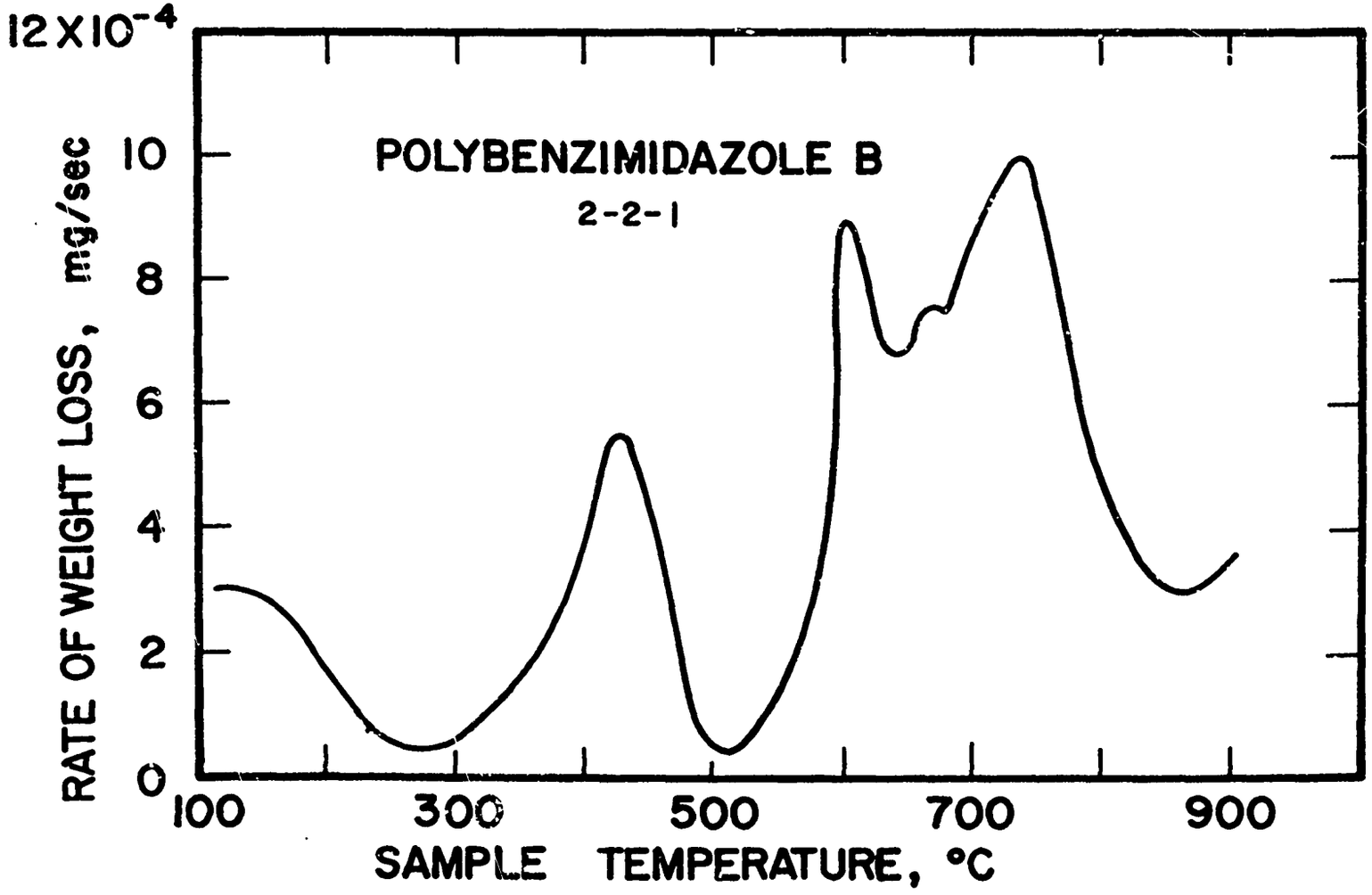

FIGURE 52. Rate of Weight Loss for Polybenzimidazole in Flowing Helium

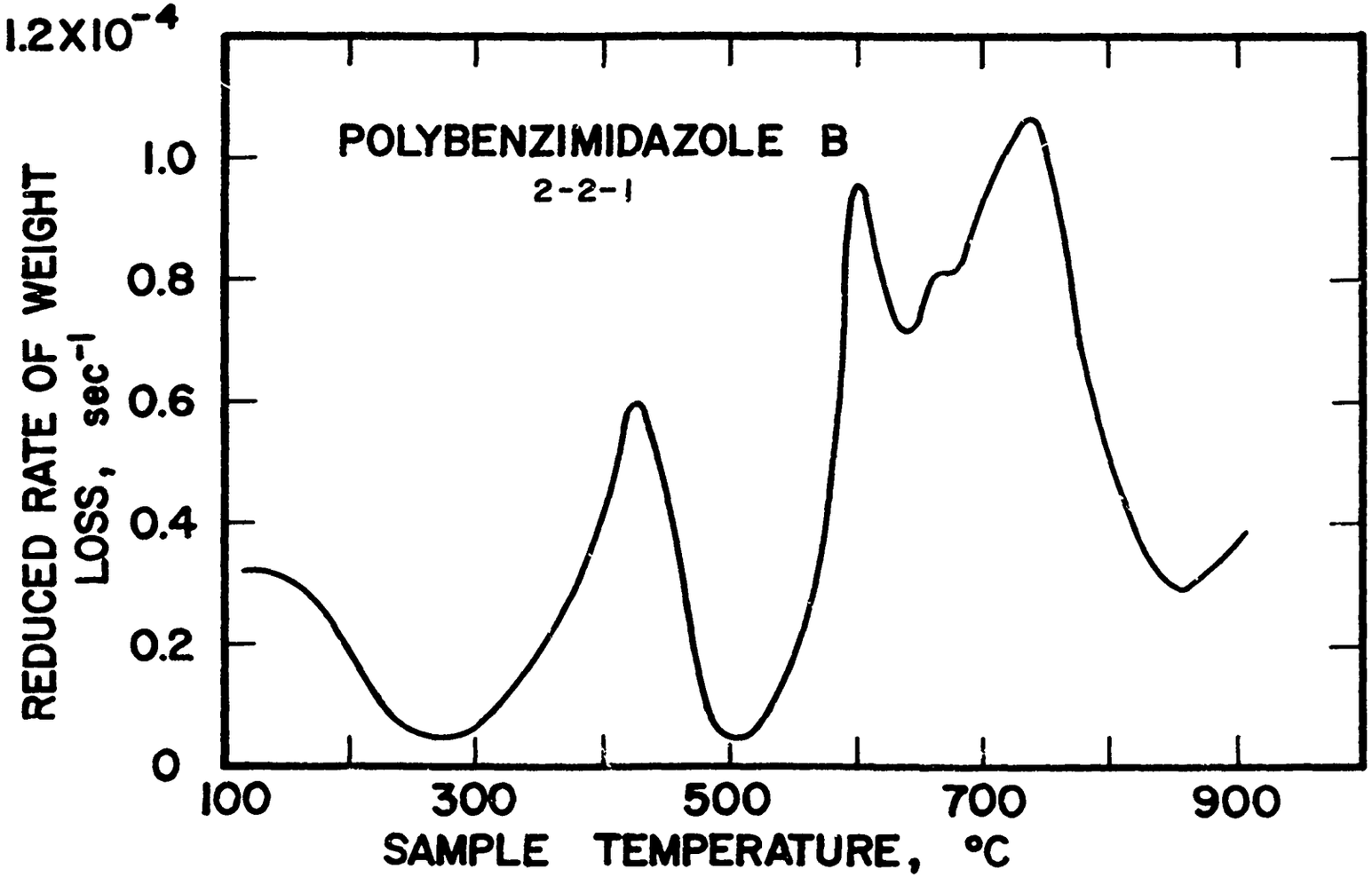

FIGURE 53. Reduced Rate of Weight Loss for Polybenzimidazole in Flowing Helium

resin apparently did not diminish postcuring effects which are observed during the experiment, but altered the magnitude of the principle pyrolysis reactions. Thus, for PBI-B, more weight was lost between 450°C and 650°C but a greater weight of char resulted at 900°C. It was also significant that the decomposition reaction was still proceeding at an appreciable rate at 900°C, indicating that a stable char structure had not been formed.

PBI-A resin also was pyrolyzed under isothermal conditions at 588°C and 697°C for gas analysis. These temperatures were located in regions of major interest for this polymer. The lower of the two temperatures corresponded to the region where the first major weight-loss mechanism began to be activated. The higher temperature corresponded to the beginning of a region where a second major weight-loss mechanism was observed.

At 588°C small amounts of hydrogen, methane and ammonia were observed in early gas samples. The major volatile product of the PBI pyrolysis was hydrogen cyanide. Calibration of the HCN peak on the chromatograph was not practicable. However, the HCN peak was much greater in height and many times the area of the peaks of the other pyrolysis gases. The reaction producing HCN appears to occur rapidly at 588°C with a precipitous decrease in HCN evolution as exposure time increases. The relative heights of the observed chromatographic peaks are presented in Table 18 and plotted in Figure 54 as functions of the time of exposure. Mole fractions of the gases were not plotted since the conversion factor for HCN, the predominant component, was not known. The ratios of the quantities of the identified gases were not

TABLE 18. POLYBENZIMIDAZOLE PYROLYSIS GAS ANALYSIS

at 588°C

Time sec	Relative Peak Heights			
	HCN	NH_3	CH_4	H_2
180	15.2	0.3	2.6	0.4
390	5.5	0.2	2.41	0.25
780	1.4	0.05	1.2	0.1
1260	0.4	---	0.6	0.1
1740	---	---	0.5	0.1
2100	---	---	0.4	---
2460	---	---	0.4	---
3060	---	---	0.4	---

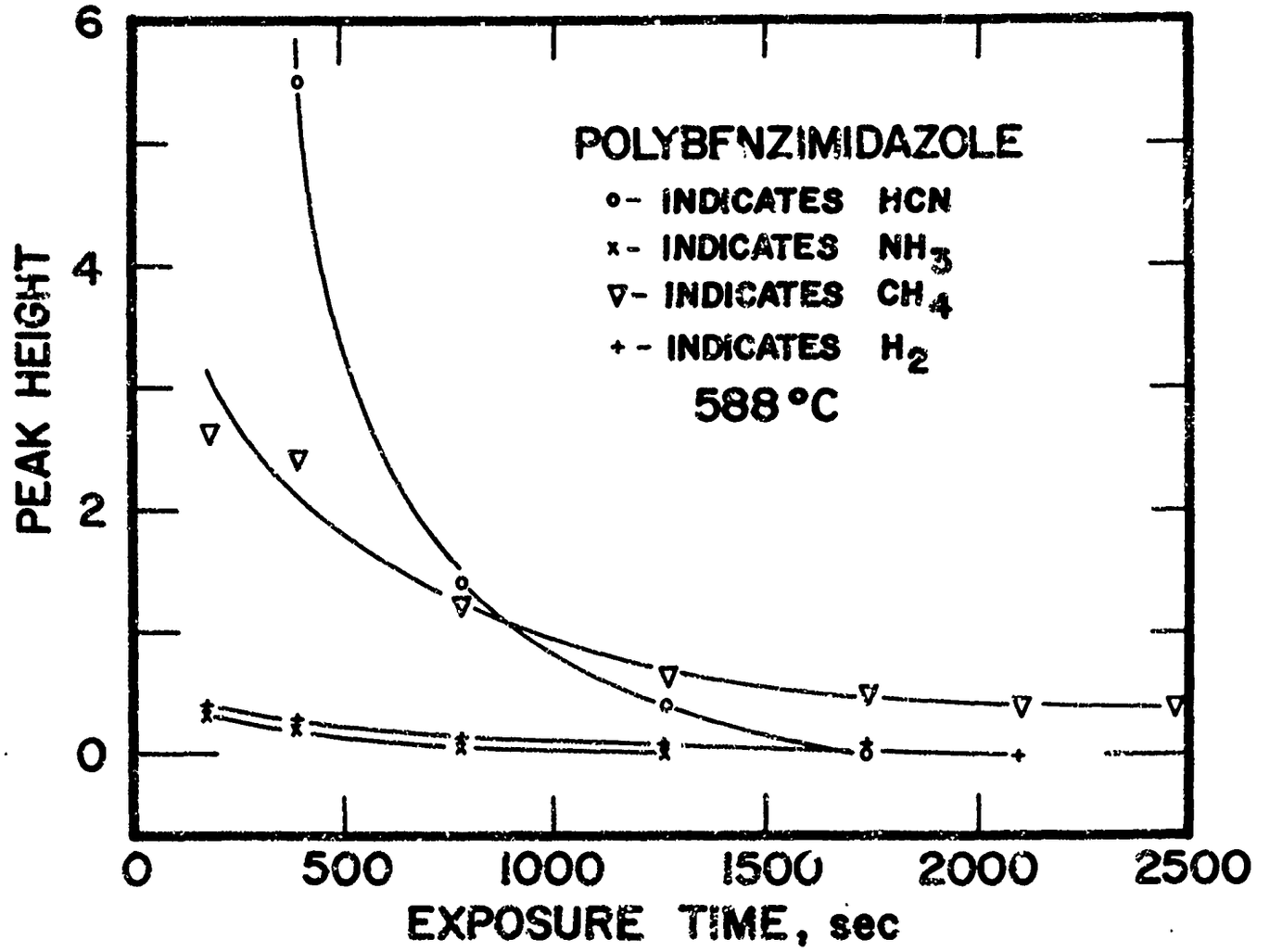

FIGURE 54. Polybenzimidazole Pyrolysis Gas Analysis at 588°C

constant during the experiment. The presence of ammonia seems to be the result of end-group scission which occurs early in the pyrolysis. HCN is almost undoubtedly the result of fragmentation in the imidazole ring. The source of methane may be decomposed phenyl structures, and hydrogen results from the dehydrogenation of benzene type-rings. The predominance of HCN in the product gases indicates that the destruction of the imidazole ring is the primary decomposition reaction.

The results of elemental analysis of the virgin polymer and char residues produced at 588°C and 697°C are shown in Tables 19 and 20. The results of Table 19 and other similar ones reported in this thesis have been weight normalized to 100 per cent. The laboratory analysis of the virgin polymer does not correspond to the idealized structure as closely as might be expected. The deviation in nitrogen content seems particularly large. The idealized structure can be represented as C_{20}, H_{12}, N_4 while the normalized laboratory results represent a structure of $C_{18.3}$, $H_{12.2}$, $N_{3.5}$.

The pyrolysis products at the higher temperature of 697°C were significantly different than those found at 588°C. As shown in Table 21 and Figure 55, the pyrolytic evolution of methane was markedly increased. Simultaneously, production of HCN was much less than at the lower temperature, and a new species, identified as methyl amine, formed a significant fraction of the evolved gas.

The larger quantity of methane probably indicated that a greater number of the phenyl structures were decomposing. Also, the presence of methyl amine may be explained as the product of residual nitrogen combining with fragments of decomposed benzene rings. Before hydrogen

TABLE 19. REPORTED ELEMENTAL ANALYSIS OF PBI-A

Material	Weight Per cent		
	C	N	H
Virgin Polymer	76.41	16.98	4.23
588°C Char	78.33	17.96	3.42
697°C Char	86.16	12.39	1.37

TABLE 20. NORMALIZED ELEMENTAL ANALYSIS OF PBI-A

Material	Weight Per cent			Mole Per cent		
	C	N	H	C	N	H
Virgin Polymer	78.273	17.394	4.33	53.91	10.27	35.82
588°C Char	78.557	18.012	3.430	58.13	11.42	30.45
697°C Char	86.229	12.399	1.371	70.10	9.38	14.52
Ideal Structure	77.92	18.18	3.90	54.53	12.72	32.75

TABLE 21. POLYBENZIMIDAZOLE PYROLYSIS GAS ANALYSIS AT 697°C

Time sec	Relative Peak Heights			
	H_2	HCN	CH_3NH_2	CH_4
198	.3	3.2	5.4	
660	.2	0.7	4.0	7.6
1140	.1	0.4	2.9	0.8
1560	.1	0.2	2.1	0.3
2040	--	0.1	1.6	0.2
2520	--	0.1	1.2	0.1
2940	--	0.1	1.1	0.1

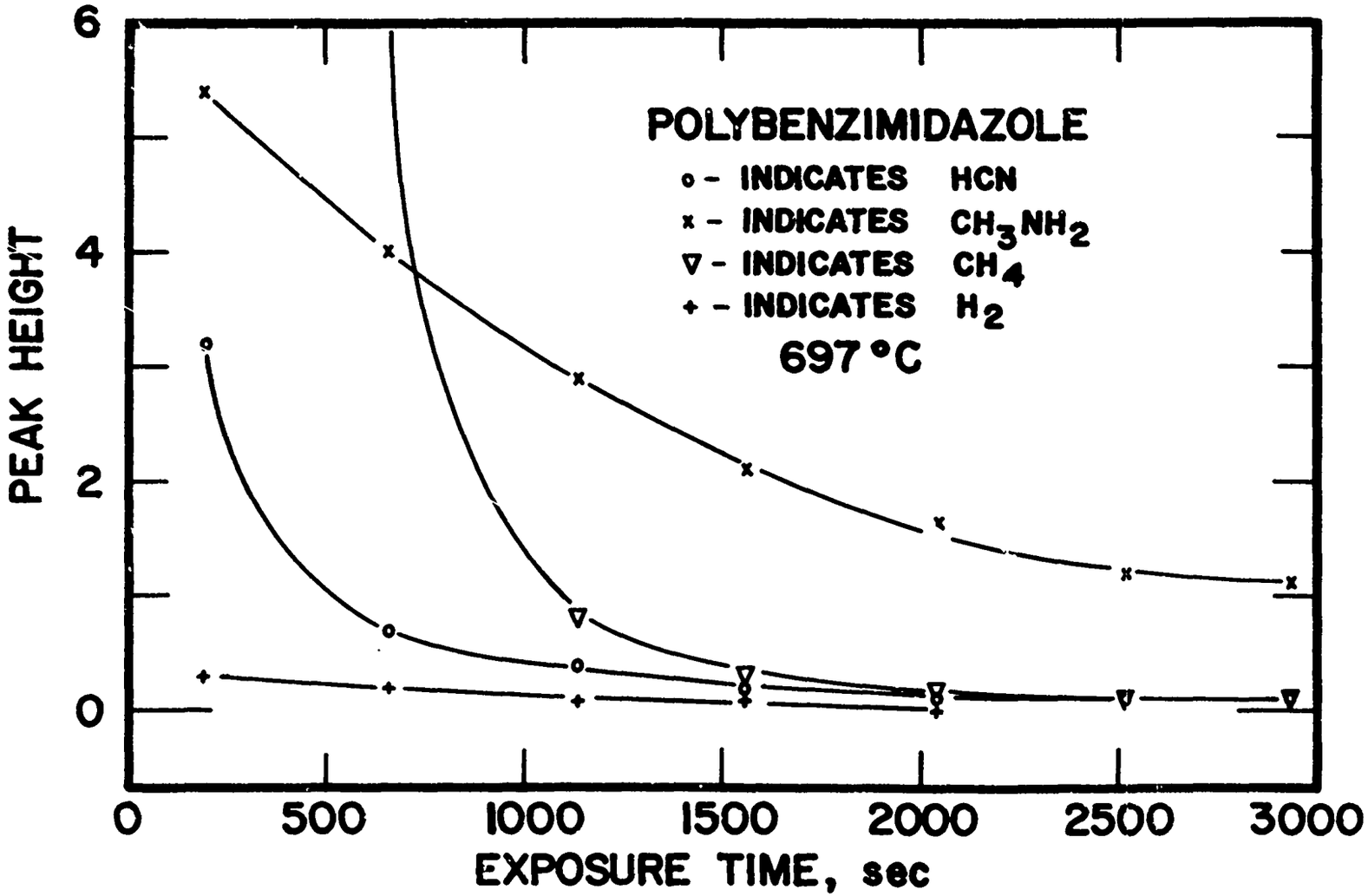

FIGURE 55. Polybenzimidazole Pyrolysis Gas Analysis at 697°C

cyanide could be identified as one of the products of pyrolysis, it was necessary to determine an elution time for this gas in the chromatographic columns of interest. Therefore, HCN was generated from potassium cyanide and acid and was allowed to flow through the gas sampling port of the chromatograph for determination of elution times.

An attempt was made to correlate the results of elemental analysis, gas analysis and TGA experiments by making a mass balance on the reacting system for each of the isothermal runs. All calculations were based on a mer unit of polymer represented as C_{20} H_{12} N_4. Since isothermal TGA data were not available for the conditions of the gas generation experiments, the amount of weight loss at each temperature was estimated by interpolation from existing data. Then, values of the carbon, hydrogen, and nitrogen ratios for the char residues were calculated from the results of the elmental analyses. Next, the relative molar loss of each element was compared with the pyrolysis gas species identified in the chromatograph, and the amounts of each gas which best described the total weight loss were computed. Calculated concentrations were then compared with experimental gas concentrations. An example of such a mass balance for the data shown in Table 19 is shown in Appendix G. The agreement between calculated and observed gas concentrations was quite poor. In fact, the mass balance, computed as outlined, led to a negative generation term for hydrogen.

It should be noted that the results of the mass balance were very sensitive to slight errors in elemental determinations. An error of one or two per cent in elemental weight fractions is sufficient to completely alter the conclusions. When consideration is given to the

inherent difficulties in making elemental determinations of very small quantities of material, and to the errors introduced by non-homogeneities in samples and by metallic contamination, it seems reasonable that an error of several per cent might be encountered. As a further indication, the weight-per cents of Table 19 for virgin polymer summed to only 97.62 per cent before normalization. Thus, this obvious error strongly influenced mass balance calculations for both chars.

Schulman and Lochte [42] attempted a similar calculation in order to determine gaseous products from a material balance. These authors were able to draw only the most general conclusions and relied on experimental measurements for gas analysis.

The dynamic thermograms for the polybenzimidazole resins shown in Figures 49 to 53 exhibit several interesting characteristics which can be related to the chemistry of the polymer. The loss of weight observed at temperatures below 550°C are very probably continuations of the cure mechanism plus a small contribution by end-group reactions. By recalling the chemistry of polybenzimidazoles discussed in Chapter IV, end group reactions would tend to produce ammonia and phenol. Support for the correctness of this conclusion was found in the observation that both water and phenol were identified as volatile products in this temperature region. These compounds are indeed those expected from the ring-closure condensation reactions of PBI formation. Schulman and Lochte made similar observations.

In a comparison of Figure 50 and 52 it is noted that the weight loss peak at 425°C is significantly larger for PBI-B than for PBI-A. This observation might be considered contrary to expectation in light

of the higher temperature cure and, therefore, the greater thermal stability which usually follows. Since water was the primary material lost for the peak in generation, it probably represents either a continuation of the condensation reaction or a product of a previous condensation. It is believed that both explanations are valid. The very porous structure of PBI-B, cured in a closed mold, probably retained water produced during previous cure. The evolution of retained water plus the loss of continued condensation products could account for the large weight-loss peak at 425°C.

A properly cycled cure involving high pressures produces a much more dense polymer which is less likely to retain water. There is also evidence that heating the polymer in the presence of the volatile by-products can lead to several side reactions in which water takes part.

The foregoing discussion serves to emphasize the fact that the thermal properties of a polymer are normally strongly dependent on its previous thermal history.

A number of investigators have studied the stability of polybenzimidazoles. In particular, several have evaluated a polymer chemically the same as that studied in this work, namely, poly [2,2'-(m-phenylene)-5,5'-bibenzimidazole] [41, 22]. Those data available which are comparable to those shown here manifest many of the characteristics illustrated in Figures 49 through 53. In each case the temperature of incipient decomposition was between 550°C and 600°C. Significant decomposition reactions were noted even in the temperature range of 900°C to 1400°C. Weight loss in

helium at 900°C was approximately 23 per cent to 25 per cent of the original sample weight. Published data are not presented in sufficient detail or with sufficient accuracy to evaluate further comparisons.

Schulman and Lochte [42] investigated the nature of the volatile products of pyrolysis by means of gas chromatography and mass spectrometry. The cure of the material they studied was similar to that of PBI-B except the maximum temperature reached was only 400°C (750°F) compared to 470°C for PBI-B. They reported that in the range of 550°C to 625°C, principal degradation products were water, with some ammonia and phenol. At somewhat higher temperatures, from 600°C to 850°C, hydrogen cyanide, hydrogen, methane and carbon dioxide were also observed. The averaged mole per cents of the major gaseous species were:

HCN	30%,
H_2O	38%,
NH_3	13%,
H_2	13%,
CO	4%,
CH_4	1.5%.

Hydrogen cyanide represented the major product detected over essentially the entire decomposition range.

In the degradation of another sample, which was aged as a film in air, ammonia and carbon monoxide were not observed. In a third sample, which was cured as a powder in argon, hydrogen cyanide, methane, and hydrogen were the postulated products. Thus, conditions of cure are again noted to affect markedly the nature of decomposition products.

The results of this thesis are in general qualitative agreement with the data of Schulman and Lochte. Two important differences exist. First, in this work significantly less ammonia was found and somewhat more methane was noted. The second, and more important, difference was the observation in this work of appreciable amounts of methyl amine.

The chromatographic detection of methyl amine in a Chromosorb 102 column was problematic. This particular column was designed for use with acidic gases, such as HCN, and it had been sensitized to acidic gases. The introduction of methyl amine in such a column apparently initiates reactions within the column which make difficult accurate measurement of its elution time. It is believed, however, that the sample was characterized well enough to justify the identification of methyl amine as a component of the pyrolysis gas.

A mechanism of PBI decomposition which depends upon hydrolytic ring opening has been proposed [48]. However, utilization of basic organic chemical concepts and known reactions suggests a more straightforward approach. It is likely that initial attack on the polymer begins with heteroring opening as illustrated below.

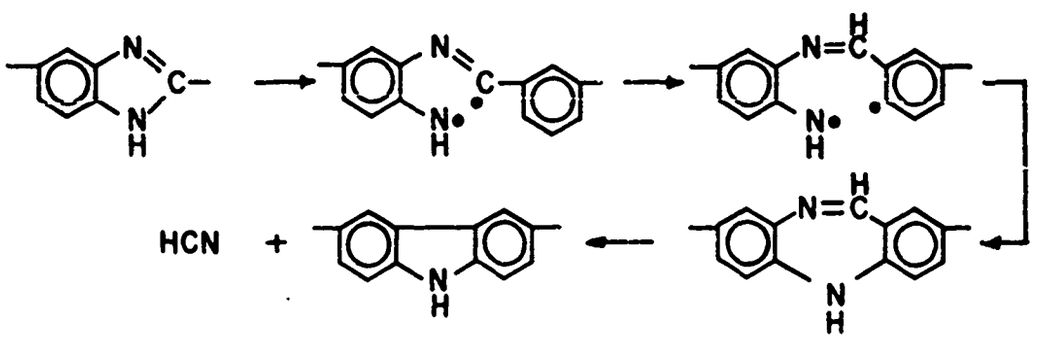

The fracture is shown at the single nitrogen-carbon bond whose breaking is energetically the most likely. The resultant radical formed on a carbon atom possessing a double bond is very unstable and it will quickly abstract a near-by hydrogen atom. The hydrogen on the adjacent phenyl group is a likely candidate. It is then possible to form a new ring unit which further condenses with the elimination of HCN.

The final structure postulated is very stable and further degradation will only occur at temperatures sufficiently high to fracture the phenyl group. Continued reaction would then yield methane and possibly methyl amine. Another source of methyl amine may be found in the nitrogen radical shown above in the first reaction step. Since the radical enjoys some stabilization because of its attachment to a phenyl ring, an energetic decomposition which fractures both the imide and phenyl rings could yield methyl amine directly.

Infrared absorption spectra for virgin PBI-A polymer and for char residues produced at 588°C and 697°C were recorded and are shown in Appendix D. The destruction of the benzimidazole ring is indicated by the decreased intensity of imide peak at 3300 cm^{-1}. The general loss of aromaticity was also noted. However, even after exposure to 697°C for 90 minutes, some imide structure remained. These spectra, in general, support the assertion that the major decomposition occurs in the imidazole ring, and that at 697°C significant fragmentation of the phenyl structures leads to a further loss of aromaticity in the polymer.

As in the case of phenolic resin, quasilenearization numerical techniques were not applied to the complex thermogram of polybenzimidazole. Prerequisite to such an application would be an extensive experimental program to determine with great accuracy the exact shape of the dynamic thermogram. Based on the experience of fitting a two-mode model for polyquinoxaline, the extensive overlap of PBI reaction zones will make absolutely necessary the use of very fine data. In additon, further development of the numerical technique will likely also be required.

Based on the results shown here, polybenzimidazole appears to be a prime candidate for some high temperature and ablative applications. The high-temperature threshold of major decomposition and the high char yield are very desirable properties. However, the molecular weights of gaseous pyrolysis products are not as small as would be hoped, but they are not excessively large either. Of course, TGA work and pyrolysis gas analysis do not give insight into the other important requisite properties of ablators, such as strength of char and processability of the polymer. Yet the structural properties are amenable to improvement in many ways, if the requisite thermal properties are available. The primary negative feature of PBI degradation is the poisonous nature of the evolved gases.

CHAPTER VII

CONCLUSIONS

The results of thermogravimetric analyses presented in Chapter VI of this thesis represent an accurate description of the thermal response of the polymers tested to both isothermal and dynamic heating conditions. As a result of these studies, experimental values of the primary char yields, the temperatures of pyrolysis and the nature of pyrolysis gases were obtained.

The use of dynamic TGA data for the determination of kinetic parameters was explored by numerical analytical methods. The parameters determined were able to describe the dynamic thermograms accurately. However, there was some question as to the meaning of the parameters thus determined. Activation energies computed were lower than would be expected for simple bond-breaking reactions. Apparently low activation energies were understood when the thermal degradation was recognized as a complex reaction network. Therefore, the over-all activation energy for the pyrolysis network was expected to be lower than the energies involved in breaking aromatic bonds. The kinetic results of thermogravimetric analysis represent, then, an averaged set of parameters describing the over-all effect of a complex reaction mechanism. Only in the case of an elementary reaction will thermogravimetric analysis results directly describe the magnitudes of the chemical kinetic parameters of the reaction.

It is of interest to compare the various degradations. Even

though polyimide apparently reacted in a simple way from TGA evidence, gas analysis indicated a rather involved series of reactions really occurred. In the case of polyquinoxaline, the observation of two major reaction zones could have suggested a two-step series reaction. A more correct explanation proposes that the second reaction zone indicates that a new mechanism is activated, i.e., the fragmentation of the phenyl ring.

In all of the gas analysis experiments conducted, temperatures of approximately 650°C seemed to be associated with the destruction of phenyl groups with the production of methane. At lower temperatures little methane was observed except for the pyrolysis of phenolic which contains methylene bridges.

For polybenzimidazole it seems possible to correlate in a general way, the major reaction peaks and gas species observed in light of the mechanism of pyrolysis proposed in Chapter VI. The first reaction peak, occurring at 612°C, produced HCN, and may be described by the imide-ring fracture and rearrangement shown in the proposed mechanism. The second and larger reaction peak, occurring at 730°C, probably represented a combination of three parallel reactions. First, the HCN reaction described above likely continued. Second, phenyl group fragmentation yielded the observed methane. Third, as a consequence of phenyl group destruction, nitrogens attached to carbon fragments collected hydrogen to yield methyl amine.

The pyrolysis of polyphenylene seems to be the least complex decomposition studied. However, even the simplest explanation of the observed reaction suggests two parallel reactions, dehydrogenation and phenyl scission. It is again noted that phenyl ring destruction

occurred at about 630°C.

In spite of the difficulties encountered in interpreting TGA-determined kinetic parameters, there is nevertheless a need for an empirical description of how polymers degrade even if a theoretical one is presently unattainable. Quasilinearization numerical technique provided a systematic approach to thermogram analysis which has produced a fit of the data superior to that attained by other methods. The kinetic parameters so determined have important use in ablation computer programs for the prediction of ablation performance of materials.

Based on the results of the thermal analysis reported in Chapter VI, the relative ablation performance of the materials tested can be evaluated. Ablative materials may be compared and ranked on the basis of the following properties: (1) char yield, (2) molecular weight and properties of gaseous decomposition products, (3) temperature of pyrolysis, (4) heat of pyrolysis, (5) mechanical strength of virgin polymer and char residues, and (6) fabricability. Although all of the criteria are not equally important, efficient performance in each area is required. The tests conducted in this research provide some of the necessary information, but they give no indication as to the mechanical properties or the heats of pyrolysis.

Table 21 presents a comparison of the five resins tested with respect to temperatures of pyrolysis, primary char yield, desirability of gaseous products, and an indication of the fabricability of the polymer.

TABLE 22. A COMPARISON OF THE ABLATION PROPERTIES OF POLYMERS

Material	Pyrolysis Temp °C	Char Yield	Pyrolysis Gases	Fabricability
Phenolic	360	57	Moderate Molec. Wt Low Toxicity	Very good
p-Polyphenylene	600	82	Low Molec. Wt. Non-toxic	Poor
Polyimide	480	58	Moderate Molec. Wt. Toxic	Fair
Polyquinoxaline	520	66	High Molec. Wt. Very toxic	Good
Polybenzimidazole	570	76	Moderate Molec. Wt. Toxic	Poor

The temperatures of pyrolysis shown in the table directly measure the stability of the polymer chain. Phenolic resin with its aliphatic linkages is significantly less stable than the other resins, each of which possesses some degree of aromaticity. As the delocalization of bond energy increases, the stability of the associated ring structures similarly increases. Thus we note the great stability of polyphenylene which directly reflects its high degree of aromaticity, and in descending order of stability find polybenzimidazole, polyquinoxaline, and polyimide. The complex interaction of the various structures in the aromatic polymers prohibits exact prediction of pyrolysis temperatures, but the approximate values for the polymers were predictable a priori.

The yield of char during thermal decomposition is probably the most important thermal property identified in Table 21. It is also interesting to note the correlation between pyrolysis temperature and char yield. Probably a more profitable interpretation of char forma-

tion can be found in the mechanism of pyrolysis. Those resins which produce high char yields all seem to undergo crosslinking and coalescent reactions. Both phenolic and polyimide resins are relatively poor char producers and in the pyrolysis of both materials breaking of the polymer chain is probable. Thus increased fracturing of the chain makes more likely the elimination of volatile fragments. Polyquinoxaline produced a relatively high fraction of char, but its pyrolysis offers opportunity to remove large fragments in the form of cyanogen. Polybenzimidazole, a step better as a charring ablator than polyquinoxaline, likely undergoes ring condensation during pyrolysis to produce a structure more stable than that of the starting material. Polyphenylene decomposition seems to produce as much crosslinking as fragmentation and the chain coupling early in the reaction undoubtedly aids in char retention.

No attempt was made in this research work to investigate post-pyrolytic reactions. Experimental conditions were selected specifically to minimize or remove altogether the possibility of such reactions. However, in actual applications post-pyrolytic reactions are of real importance. These problems are presently being investigated by Pike and co-workers are Louisiana State University from a thermodynamics point of view, and by Benson and co-workers at Stanford Research Institute from a kinetics point of view.

REFERENCES

1. Anderson, D. A. and Freeman, E. S., "The Kinetics of the Thermal Degradation of Polystyrene and Polyethylene," *Journal of Polymer Science, 54,* 253-360, (1961).

2. Angelo, R. J., U. S. Patent 3,073,785, (June 1963).

3. Bellman, R., Jacquez, J., Kalaba, R. and Schwimmer, S., "Quasi-linearization and Estimation of Chemical Rate Constants from Raw Kinetic Data," *Mathematical Biosciences, 1,* 71-76, (1967).

4. Bellman, R. and Kalaba, R., *Quasilinearization and Non-linear Boundary-Value Problems.* New York: American Elsevier, 1965.

5. Bogert, T. M. and Renshaw, R. R., "4-Amino-o-Phthalic Acid and Some of its Derivatives," *Journal of the American Chemical Society, 30,* 1140, (1908).

6. Box, G. E. P., "Fitting Empirical Data," *Annual of the New York Academy of Science, 86,* 792, (1960).

7. Brinker, K. C. and Robinson, I. M., U. S. Patent 2,895,948 (June 1959).

8. Bruck, S. D., "Thermogravimetric Studies on an Aromatic Polyimide in Air and in the Vacuum Region of 10^{-2} to 10^{-3} Torr Using the Cahn RG Electrobalance," *Vacuum Microbalance Techniques, 4,* 247-278, (1965).

9. Cahn, L. and Peterson, N. C., "Conditions for Optimum Thermogravimetric Analysis at Atmospheric Pressure," *Analytical Chemistry Reviews, 39,* 403-404, (March 1967).

10. Cahn, L. and Schultz, H., "Aerodynamic Forces in Thermogravimetry," *Analytical Chemistry, 35,* 1729-1731, (1963).

11. Cheng, J. T., Ryan, N. W. and Baer, A. D., "Oxidative Decomposition of PBAA Polymer at High Heating Rates," *Twelfth Symposium (International) on Combustion,* 525-532, (1969).

12. Coats, A. W. and Redfern, J. P., "Thermogravimetric Analysis, A Review," *Analyst, 88,* 906-924, (1963).

13. Edwards, W. M., U. S. Patent 3,179,614 (April 1965).

14. Edwards, W. M. and Robinson, I. M., U. S. Patent 2,867,609 (January 1959).

15. Flynn, J. H. and Wall, L. A., "General Treatment of the Thermogravimetry of Polymers," *Journal of Research of the National Bureau of Standards--A. Physics and Chemistry, 70A,* 487-523, (1966).

16. Frazer, A. H., *High Temperature Resistant Polymers,* New York: Interscience Publishers, 1968.

17. Friedman, H. L., "Kinetics of Thermal Degradation of Char-Forming Plastics from Thermogravimetry. Application to a Phenolic Plastic," *Journal of Polymer Science, Part C, 6,* 183-195, (1964).

18. Frost, L. W. and Bower, G. M., "Aromatic Imide Polymers for Electrical Insulation," *Conference on Electrical Insulation, Annual Report,* 45-46, (1963).

19. Goldfinger, O., "Polyphenyl," *Journal of Polymer Science, 4,* 93-95, (1949).

20. Goldstein, H. E., "Pyrolysis Kinetics of Nylon 6-6, Phenolic Resin and their Composites," paper presented at the 155th National Meeting of the American Chemical Society, San Francisco, California, April 1968.

21. Gray, D. N. and Schulman, A. P., "The Mechanism of Polybenzimidazole Formation by Condensation of Aromatic Tetramines and Esters," *American Chemical Society, Division of Polymer Chemistry Preprints, 6,* 778-785, (1965).

22. Iwakura, Y., Uno, K. and Imai, Y., "Polybenzimidazoles," *Journal of Polymer Science, A2,* 2605-2608, (1964).

23. Johnson, T. H. and Gaulin, C. A., "Thermal Decomposition of Polyimides," paper presented at the Polymer Conference Series, Wayne State University, May 1968.

24. Kittrell, J. R., "Mathematical Modeling of Chemical Reactions," paper presented at the Process Design Conference, Oklahoma State University, Stillwater, Oklahoma, March 1968.

25. Korshak, V. V., Frunze, T. M., Kurashev, V. V., and Izyneev, A. A., "Mechanism of Formation of Polybenzimidazole Polymer," *Journal of the National Academy of Science of the U.S.S.R., 60,* 9366-9372, (1964).

26. Kovacic, P., Kyriakis, A., "Polymerization of Benzene to p-Polyphenyl by Aluminum Chloride-Cupric Chloride," *Journal of the American Chemical Society, 85,* 454-458, (1963).

27. Kratch, K. M., Hearne, L. F., and McChesney, H. R., "Thermal Performance of Heat Shield Composites During Planetary Entry," paper presented at AIAA-NASA National Meeting, Palo Alto, California, September 1963.

28. Ladaki, M., Hamilton, J. V., and Cohz, S. N., "Heat of Pyrolysis of Resin in Silica-Phenolic Ablator," *AIAA Journal, 4,* 1796-1802, (1966).

29. Lee, E. S., *Quasilinearization and Invariant Imbedding, Vol. 41,* Mathematics in Science and Engineering. New York: Academic Press, 1968.

30. Madorsky, S. L., *Thermal Degradation of Organic Polymers.* New York: Interscience Publishers, 1964.

31. Marks, B. S. and Rubin, L., "Ablative Resin for Hyperthermal Environments," paper presented at 155th Meeting of the American Chemical Society, San Francisco, California, April 1968.

32. Marvel, C. S. and Vogel, H. A., "Polybenzimidazoles, New Thermally Stable Polymers," *Journal of Polymer Science, 50,* 511-516, (1961).

33. Mizaki, R. and Kittrell, J. R., "Mathematical Modeling of Chemical Reactions," *Industrial and Engineering Chemistry, 59,* 63-68, (1967).

34. Milek, J. T., *Polyimide Plastics. A State-of-the-Art Report.* Report on Contract AF33(615)-2460 for the Air Force Materials Laboratory; Culver City, California: Hughes Aircraft Company 1965.

35. Melnick, A. M. and Nolan, E. J., "The Design and Development of a High Heating Rate Thermogravimetric Analyzer Suitable for Use with Ablative Plastics," paper presented at 155th Meeting of the American Chemical Society, San Francisco, California, April 1968.

36. Murphy, C. B., "Thermal Analysis Techniques," *Analytical Chemistry Reviews, 36,* 1558-1564, (1960).

37. Nelson, J. B., *Determination of Kinetic Parameters of Six Ablation Polymers by Thermogravimetric Analysis.* NASA Technical Note, NASA TN D-3919; Washington, D. C.: National Aeronautics and Space Administration, 1967.

38. Newkirk, A. E., "Thermogravimetric Measurements," *Analytical Chemistry Reviews, 32,* 1558-1561, (1960).

39. Ozawa, T., "A New Method of Analyzing Thermogravimetric Data," *Bulletin of the Chemical Society of Japan, 38,* 1881-1886, (1965).

40. Parker, J. A. and Winkler, E. L., *The Effects of Molecular Structure on Thermochemical Properties of Phenolics and Related Polymers.* NASA Report TR R-270; Sunnyside, California: National Aeronautics and Space Administration, 1967.

41. Phillips, R. and Wright, W. W., "Polybenzimidazoles," *Journal of Polymeric Science, B2,* 47, (1964).

42. Schulman, G. P. and Lochte, H. W., "Thermal Degradation of Polymers. II. Mass Spectrometric Thermal Analysis of Phenol-Formaldehyde Polycondensates," *Journal of Applied Polymer Science, 10,* 619-635, (1966).

43. Seader, J. D., "Use of Thermogravimetric Analysis in Polymer Degradation Studies," paper presented at the 1969 Polymer Conference Series, University of Detroit, Detroit, Michigan, May 1969.

44. Stille, J. K. and Williamson, J. R., "Polyquinoxalines," *Journal of Polymer Science A, 2,* 3867-3875, (1964).

45. Strauss, E. L., Lochte, H. W. and Conley, R. T., "The Thermo-oxidative Degradation of Phenol-Formaldehyde Polycondensates: Thermogravimetric and Elemental Composition Studies of Char Formation," *Journal of Applied Polymer Science, 9,* 2799-2810, (1965).

46. van Krevelen, D. W., van Heerdin, C., and Huntjens, F. J., "Physico-chemical Aspects of the Pyrolysis of Coal and Related Organic Compounds," *Fuel, 30,* 253-259, (1951).

47. Vincent, D. N., "Thermal Degradation and Cure of Polyphenylene," paper presented at 155th Meeting of the American Chemical Society, San Francisco, California, April 1968.

48. Wrasidlo, W. J. and Levine, H. H., "Polybenzimidazoles. Reaction Mechanism and Kinetics," *Journal of Polymer Science, A2,* 4795-4808, (1964).

49. Wrasidlo, W. J. and Augl, J. M., "Phenylated Polyquinoxalines from Bis(Phenylglyoxaloyl)-Benzene," *Journal of Polymer Science A1, 12,* (1969).

50. Zanowick, R., Personal Communication, April 1970.

APPENDIX A

BUOYANCY CORRECTIONS

This appendix presents the results of a dynamic thermogravimetric analysis experiment in tabular form, and illustrates, for selected data points, the procedure used for making buoyancy corrections in the data. Table A-1 presents raw experimental data, the magnitude of the buoyancy correction factor for each data point, and the final corrected data as plotted in Chapter VI of this thesis.

TABLE A-1. BUOYANCY CORRECTIONS FOR POLYPHENYLENE RESIN, RUN 4-2-1

Temperature °C	Weight mg	Buoyancy Correction µgm	Corrected Weight mg
150.0	6.406	4.1	6.410
245.0	6.393	11.0	6.404
359.0	6.335	20.0	6.355
455.0	6.261	29.2	6.290
551.8	6.159	37.1	6.196
599.3	6.084	37.9	6.122
650.0	5.966	39.0	6.005
701.8	5.960	40.1	5.701
750.0	5.370	41.2	5.411
804.5	5.267	42.3	5.309
849.0	5.233	43.6	5.277
904.0	5.220	44.8	5.265

In the case shown above the volume of displacement of the sample corresponded closely to that of the carbon used in the blank run plotted in Figure 11. Therefore, the weight corrections were directly applicable. In cases where the volume of the sample is not the same as used in the blank run, the correction factors are correspondingly proportioned.

APPENDIX B

CALIBRATION PROCEDURE FOR CAHN ELECTROBALANCE

This appendix outlines in detail the balancing procedure required before use of the Cahn balance.

1. Connect the weighing assembly control unit of the Cahn balance and the X-Y recorder. Select appropriate recorder ranges and control settings for porper display of the experimental results.
2. Set the recorder to 0% with its own zero control. At any time in the future you can return the recorder range switch to the Z position to check the stability of the recorder zero. In the Z position the balance output is zero, independent of sample weight.
3. Plan your experiment. Decide which sample loop you wish to use. Loop A is more sensitive and less affected by environmental conditions, and should be used whenever possible. It has a maximum rated capacity of 1 gram, and maximum range of measurement of sample weight change of 200 mg. If your sample weighs more than one gram, or will change by more than 200 mg during the run, use loop B. Set the tabs on the MASS DIAL RANGE control and the RECORDER RANGE control to the letter corresponding to the loop you select, A or B.
4. Decide what range you want to use for the MASS DIAL RANGE. In general, it should be the next range larger than the maximum sample weight <u>variation</u> expected during operation. If the

sample may disappear completely, it would be the next range larger than the sample weight. Decimal ranges are most convenient; 1,10,100 and 1000 mg. Set the MASS DIAL RANGE switch to the value selected (it reads in milligrams). Note that the switch knob has a smaller pointer on its back, which points to a value labeled MINIMUM RECORDER RANGE. It means just that; do not use recorder ranges finer than this value.

5. Place a stirrup and pan on the loop you have selected. Suspend the stirrup from the bottom of the ring. If using a sample container in addition to the pan, place it on the pan. Place a calibrating weight on the pan equal in value to one half of the mass dial range selected; e.g., a 5 mg weight for a 10 mg MASS dial range.

   If your sample will not vary by its full weight, also place a weight on the pan at least 0.1 mg less than the minimum value the sample is expected to have during the run (0.5 mg on loop B). Call this the substitution weight. It may be either a precision weight or one of the tare weights, or a suitable mass of any inert material. For the highest absolute accuracy, use precision weights. The sum of the substitution weight and the mass dial range must exceed the maximum value the sample is expected to reach during the run; if not, change one or the other of these two.

6. Set the MASS dial to 0.5000. Set the RECORDER RANGE switch to a fairly high value, not less than the MASS Dian Range or 10 mg, whichever is least.

7. Place a stirrup and pan on loop C, the counterweight loop at the right hand end of the beam. A suspension wire terminating in a hook may be used instead, if preferable. Add weight to this loop until the recorder is near zero. The tare weights supplied with the balance are for this purpose. Any other material known to be constant in weight under the conditions of your experiment may be used as well. Loop A is at about the same radius as loop C; loop B is at 1/5 the radius. If the recorder reads below zero, you must remove weight from loop C, or add more to the sample loop. One way to remove weight from loop C is to trim the pan with scissors, or remove it entirely. Beyond this you might replace the stirrup with a length of the wire supplied. If you add weight to the sample loop, leave it on during operation.

   Turn the RECORDER RANGE control down until the recorder is near full scale, and continue adjusting the weight until the recorder is near zero again. Continue this process until the recorder is near zero on the minimum recorder range indicated by the back of the pointer on the MASS DIAL RANGE control. For increments of weight below 1 mg you may also adjust the recorder indication by means of the mechanical COARSE ZERO control on the torque motor.

8. Zero the recorder (set the pen to 0%) with the SET 5 control. If this is not possible, continue adjusting the net tare weight or the COARSE ZERO control as described in 7.

9. Remove the calibrating weight, and set the MASS dial to 0.0000. Zero the recorder with SET 0/10.

10. Replace the calibrating weight and set the MASS dial back to 0.5000. Repeat steps 8, 9 and 10 until no change is noted in going back to 8.

11. Leaving the calibrating weight on, set the MASS dial to 0.4000. Set the recorder to 100% with the CALIBRATE RECORDER control.

    If you cannot, the recorder span is incorrect; set the CALIBRATE RECORDER control to the midpoint of its travel, 150° from either stop, and by reference to your recorder instruction manual, set the recorder to 100% with its own span adjustment.

12. Remove the calibrating weight and the substitution weight from the sample pan. Place the sample on it.

APPENDIX C

CALIBRATION OF CHROMATOGRAPHIC COLUMNS

Chromatographic columns utilized in gas-analysis experiments in this work were characterized as to the elution times of some materials whose presence was expected in test gases. In addition, relative peak heights were measured for various concentrations of test gas wherever practicable. The results of column calibration for Chromosorb 102 is shown in Table C-1. The data apply for a temperature of 60°C and a pressure of 30 psig at the entrance of the two-meter-long column.

The results for a two-meter-long column filled with silica gel are presented in Table C-2 for conditions of 60°C and 30 psig at the entrance of the column.

TABLE C-1

CALIBRATION OF CHROMOSORB-102 COLUMN

Material	Mole Per cent	Elution time sec.	Relative Peak Height
H_2	2.35	32	13.5
	10.85	32	23.3
Air		35	
CO	13.7	35	1100
	21.3	35	1560
	28.9	35	2250
	39.4	35	3180
CH_4	11.2	40	820
	28.9	40	2048
	39.9	40	2820
CO_2	13.7	56	1200
	21.3	56	1790
	28.9	56	2300
	39.4	56	2970
NH_3	~50	88	435
H_2O	~50	162	51
C_6H_6		243	
CH_3NH_2		313	

TABLE C-2

CALIBRATION OF SILICA GEL COLUMN

Material	Mole Per cent	Elution Time	Relative Peak Height
H_2	2.35	42	4.0
	3.0	42	14.8
Air		57	
CO	13.7	65	652
	3.0	65	352
CH_4	3.0	80	221
CO_2	13.7	366	383
	3.0	366	224
C_2H_6		230	
C_2H_4		409	

APPENDIX D

The infrared spectra obtained on the polymers and char residues are shown for reference in this appendix. The difficulties encountered in obtaining good spectra on a single sample are reflected in the lack of distinctness of some of the absorption peaks. These data were used for qualitative information only.

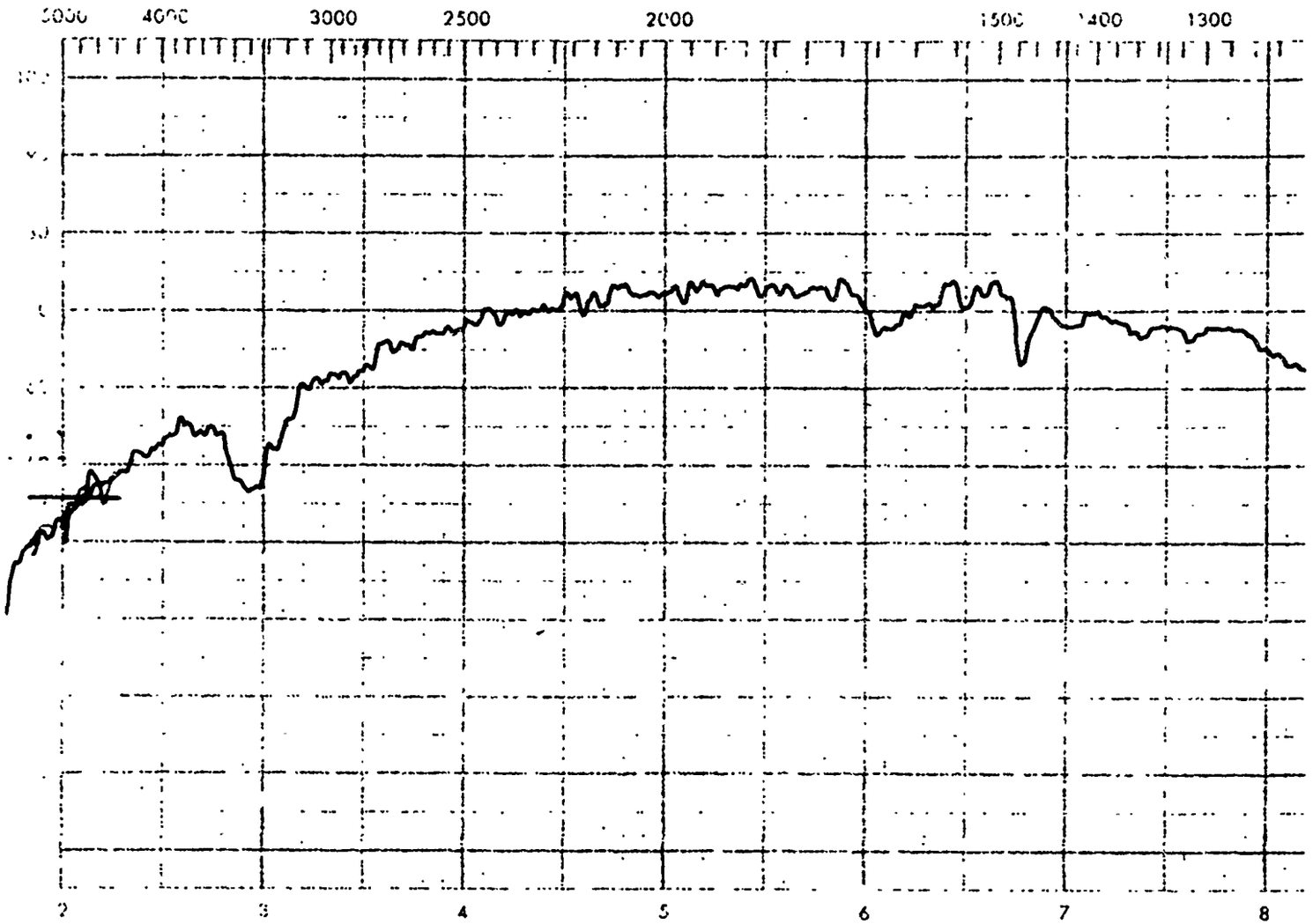

FIGURE D-1. Infrared Spectra: Virgin Polyphenylene

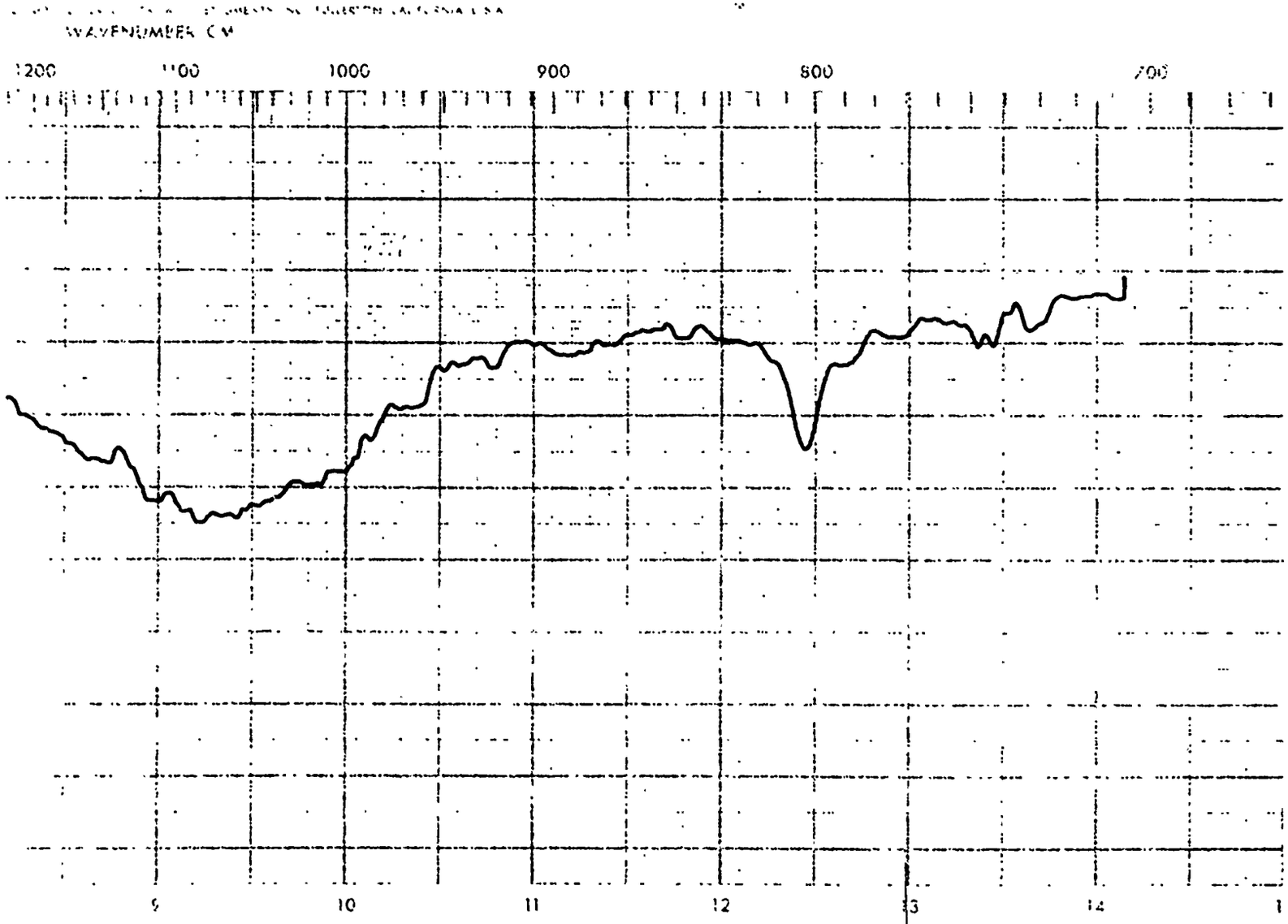

FIGURE D-1 (Continued). Infrared Spectra: Virgin Polyphenylene

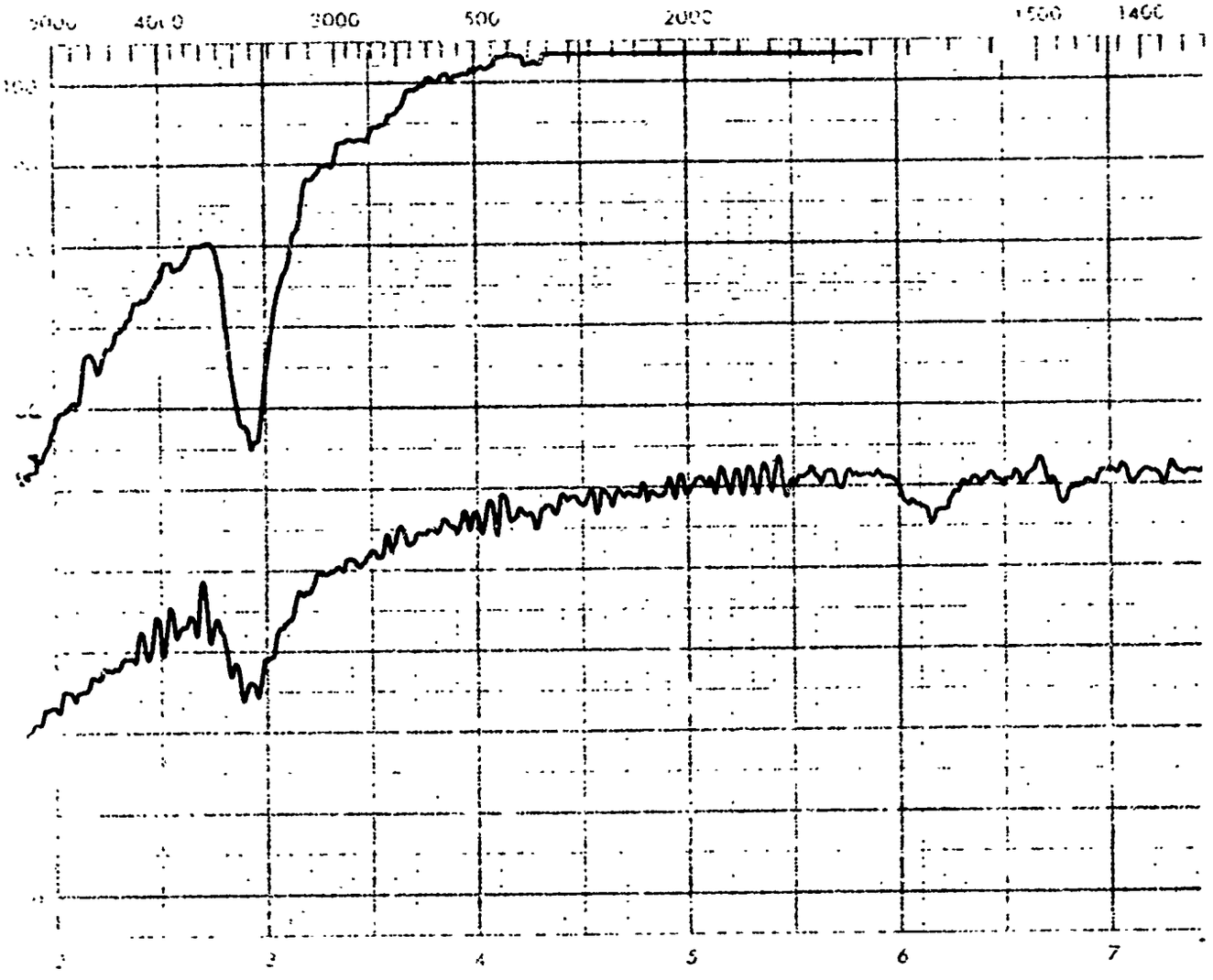

FIGURE D-1 (Continued). Infrared Spectra: Polyphenylene 500°C Char

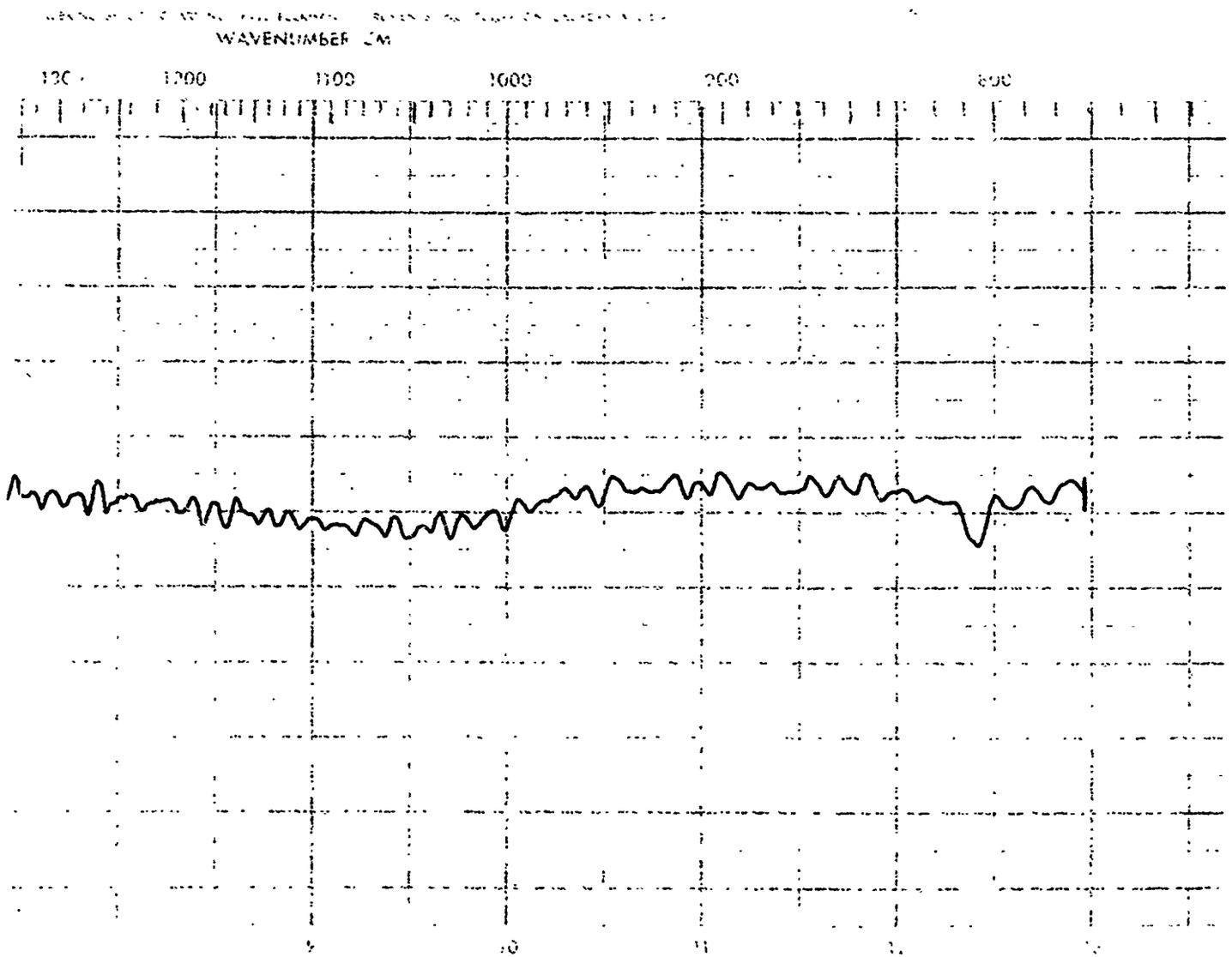

FIGURE D-1 (Continued). Infrared Spectra: Polyphenylene 500°C Char

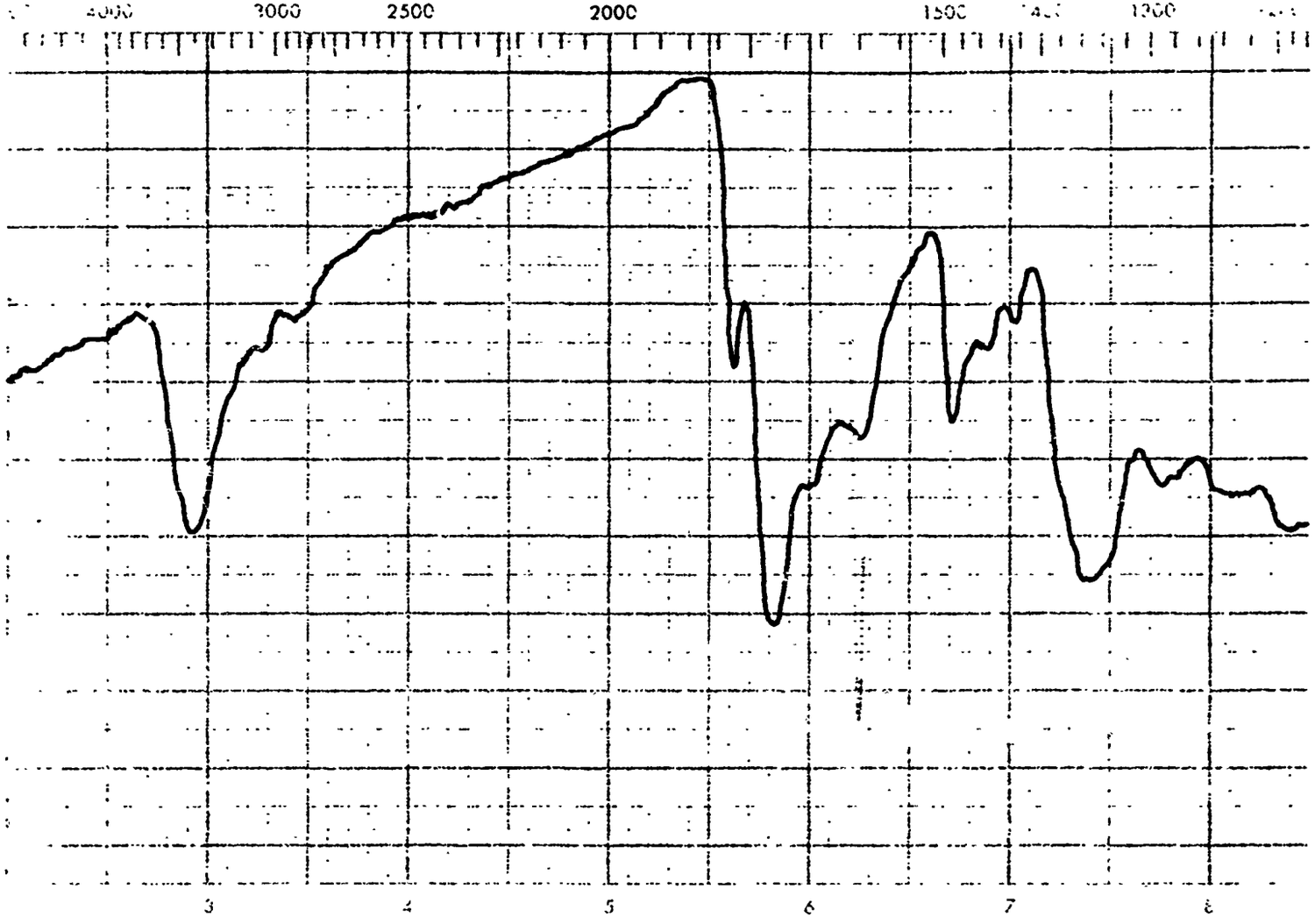

FIGURE D-1 (Continued). Infrared Spectra: Virgin Polyimide

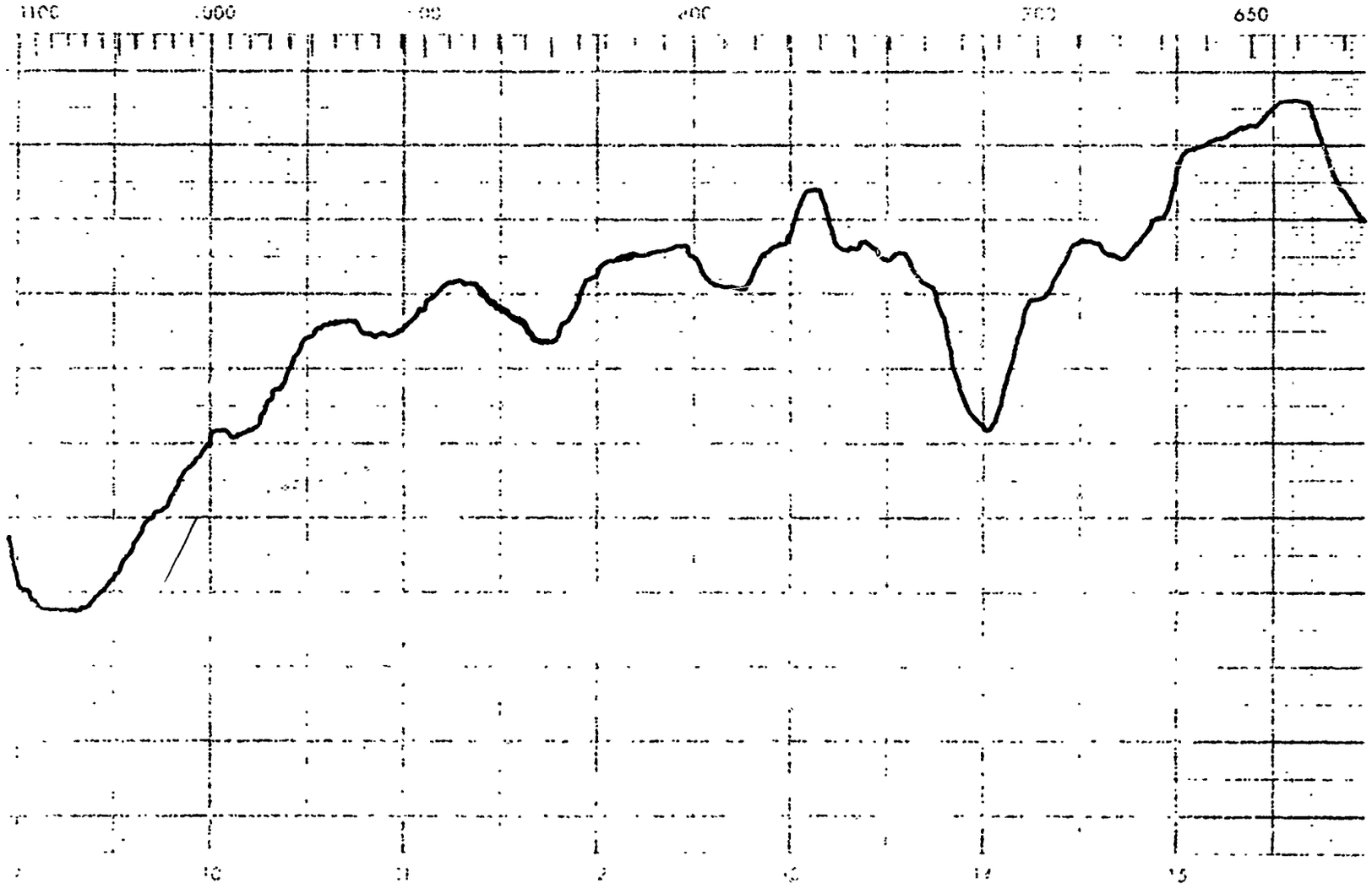

FIGURE D-1 (Continued). Infrared Spectra: Virgin Polyimide

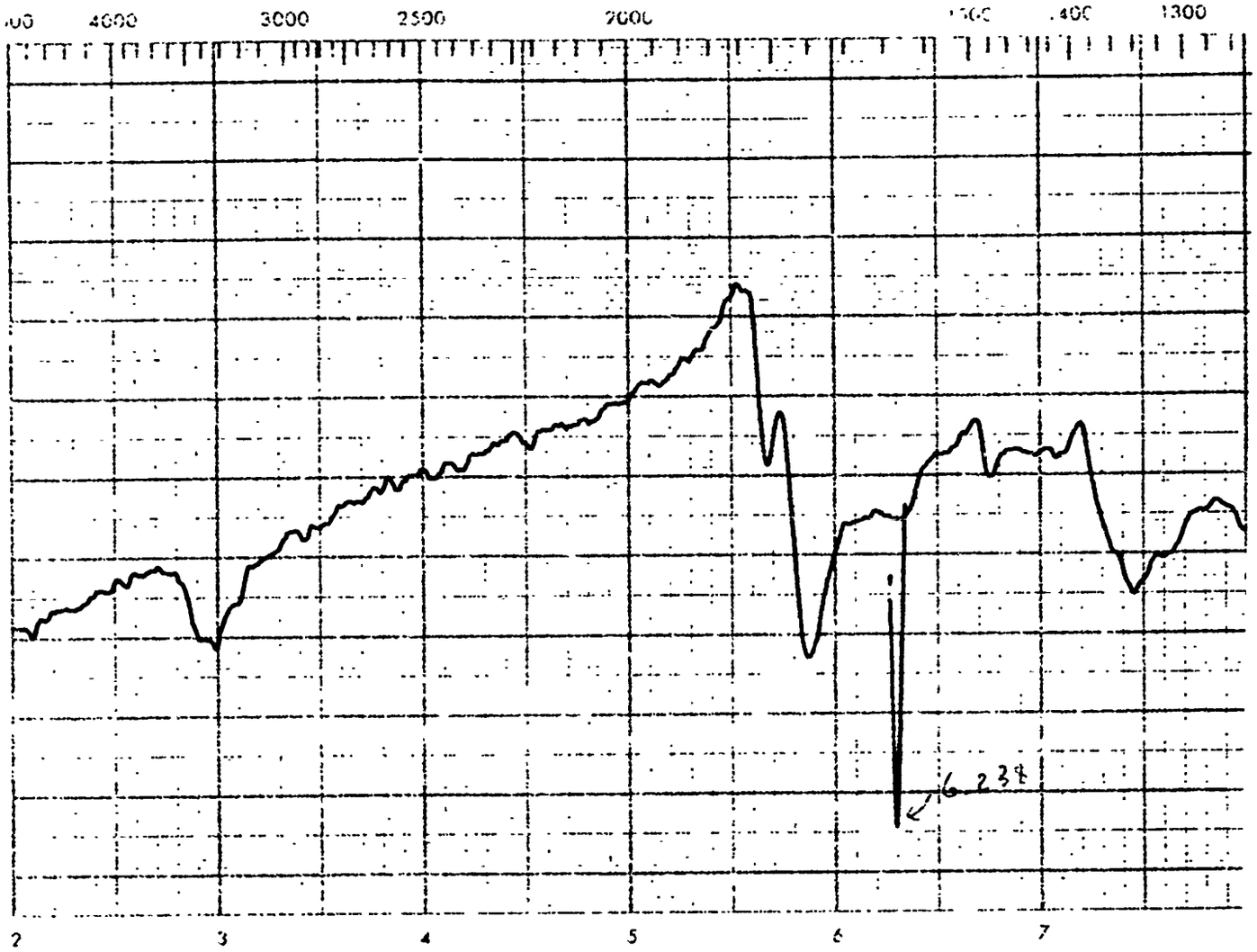

FIGURE D-1 (Continued). Infrared Spectra: Polyimide Char 480°C Char

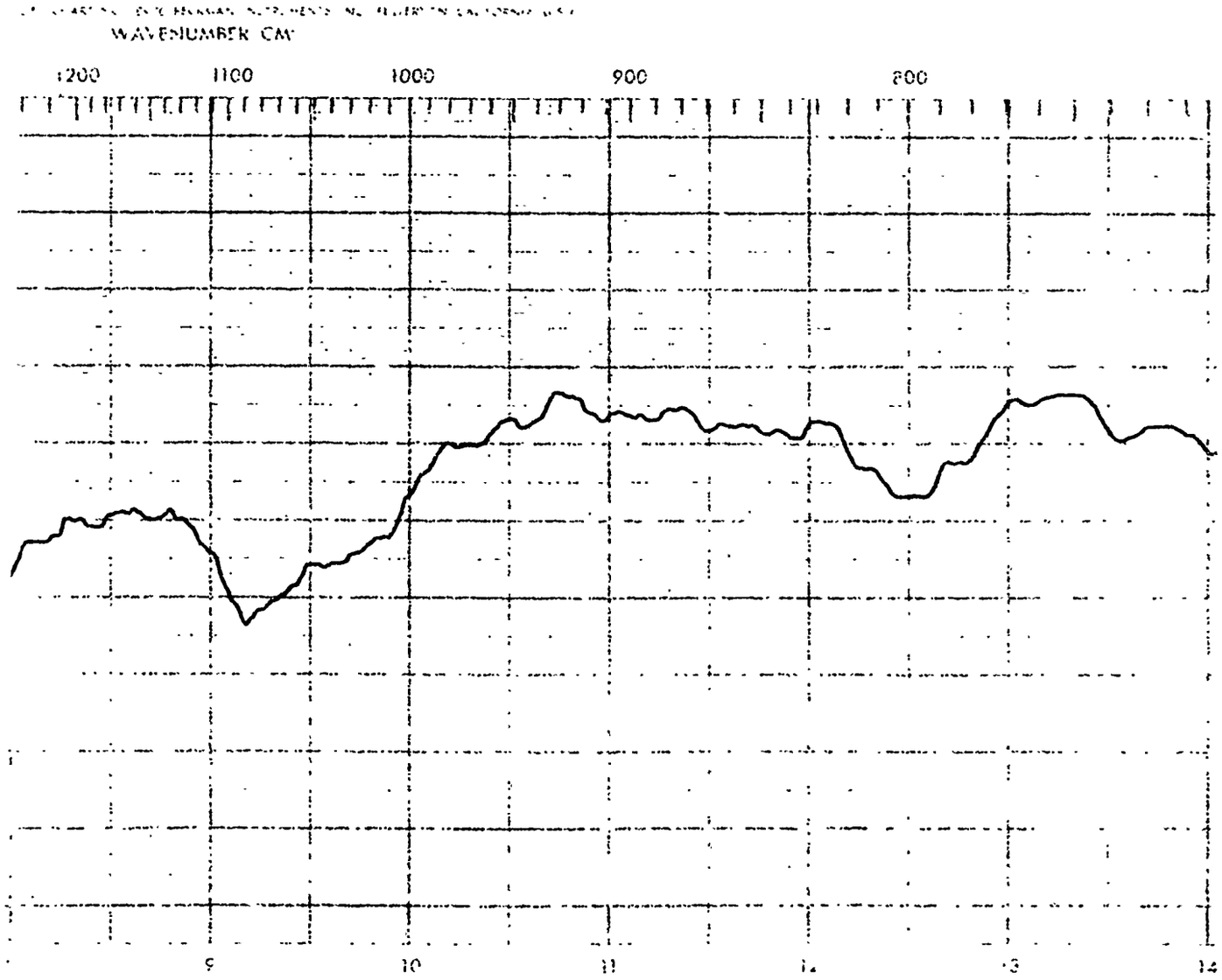

FIGURE D-1 (Continued). Infrared Spectra: Polyimide Char 480°C Char

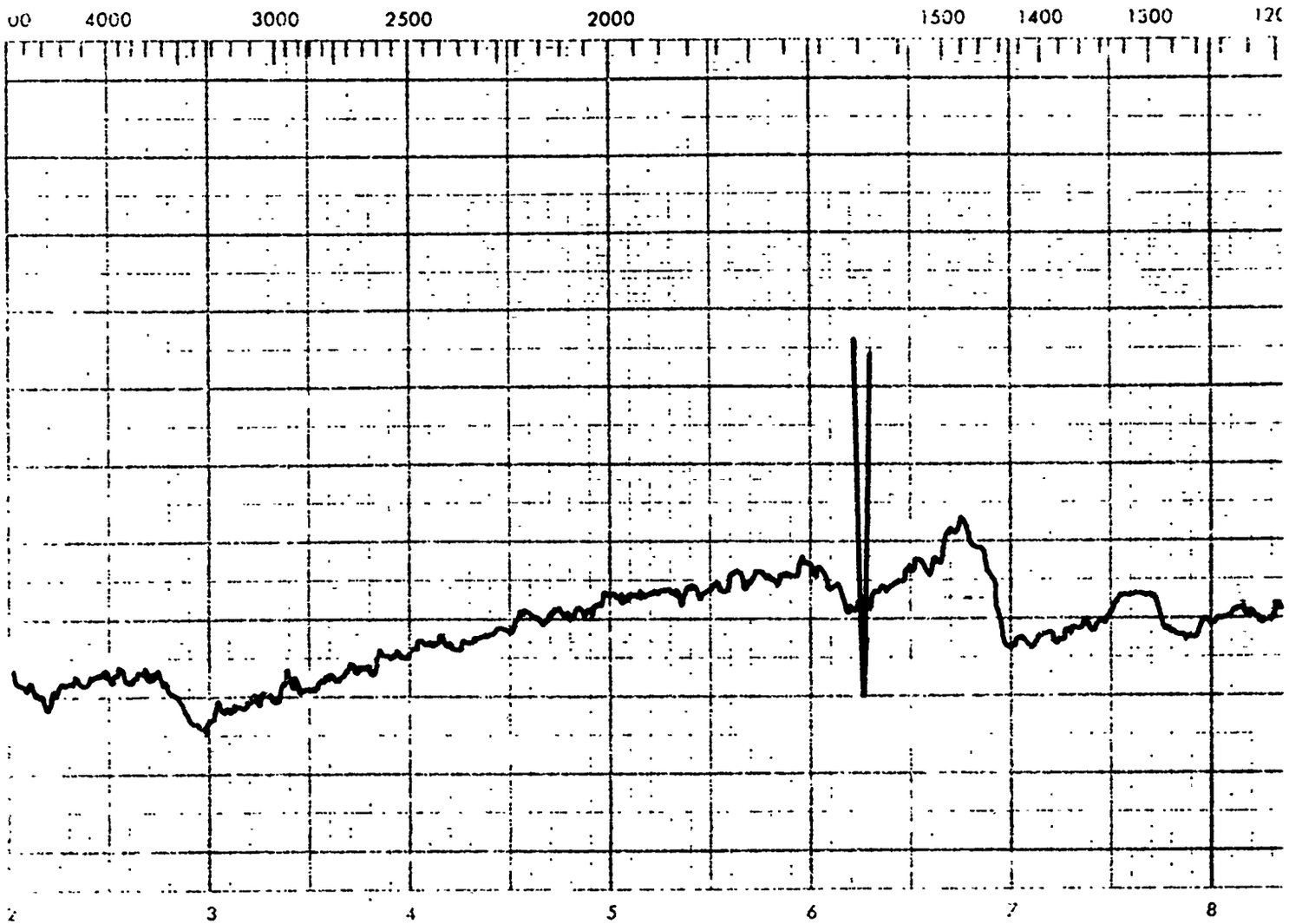

FIGURE D-1 (Continued). Infrared Spectra: Virgin PBI-A

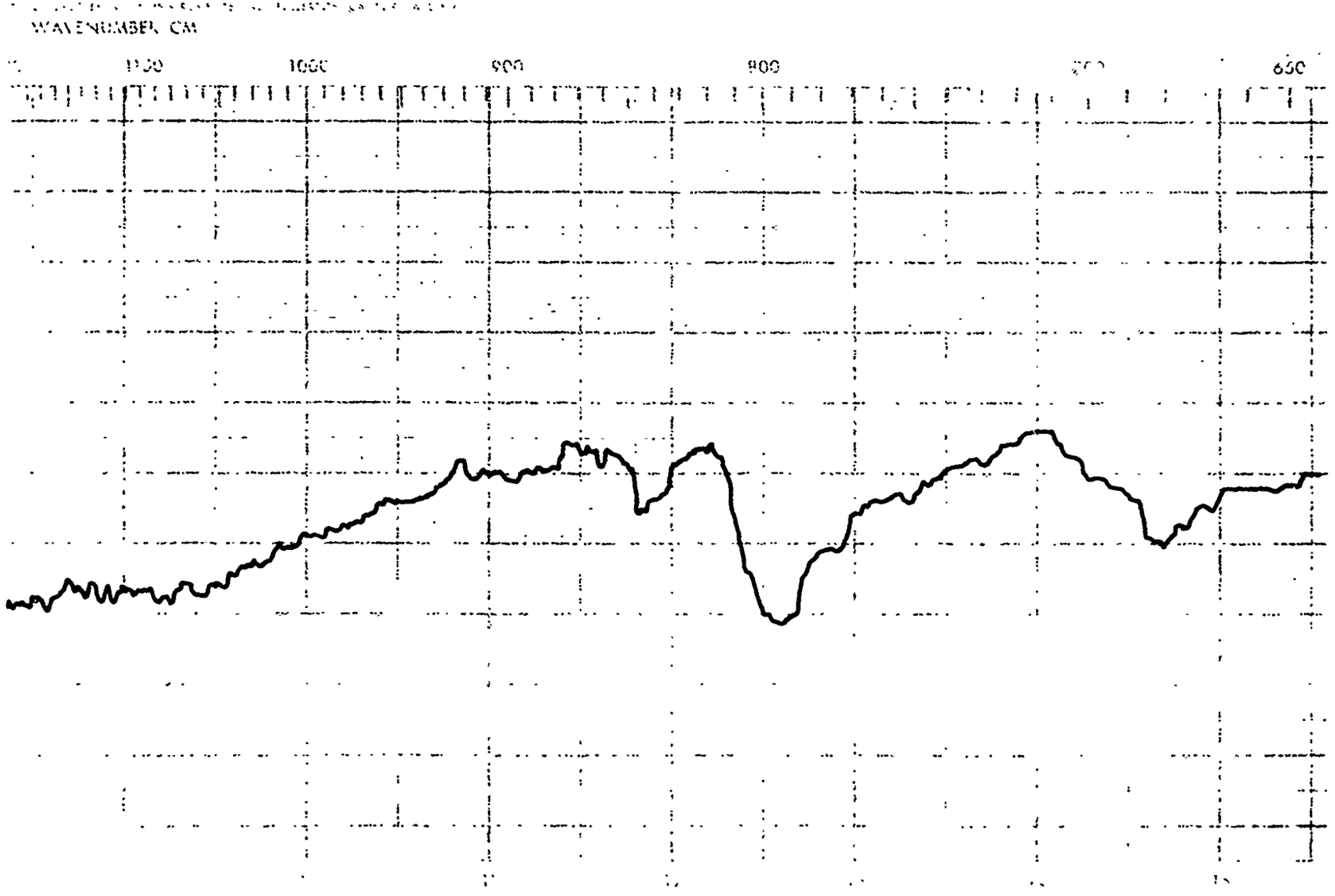

FIGURE D-1 (Continued). Infrared Spectra: Virgin PBI-A

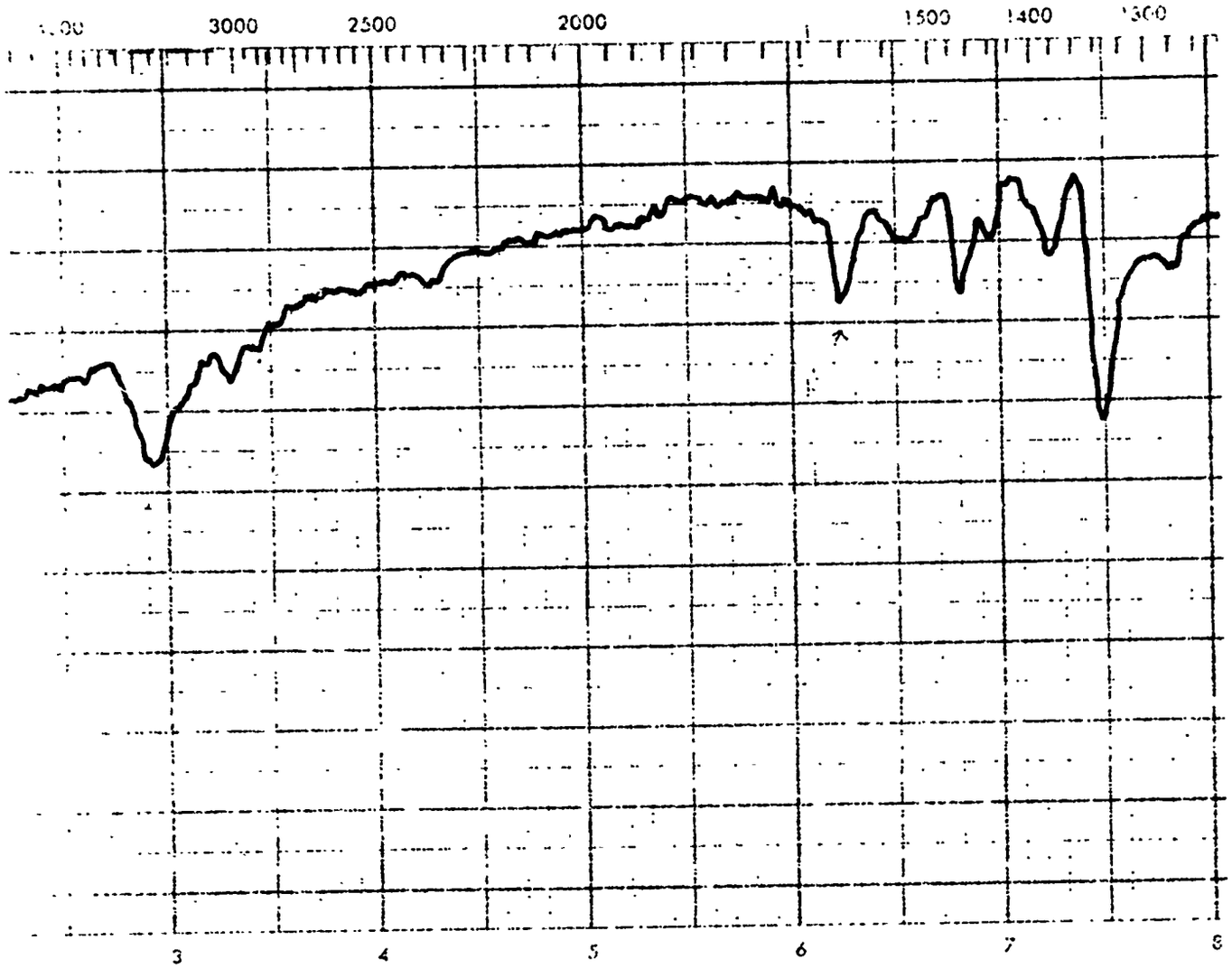

FIGURE D-1 (Continued). Infrared Spectra: Virgin Polyquinoxaline

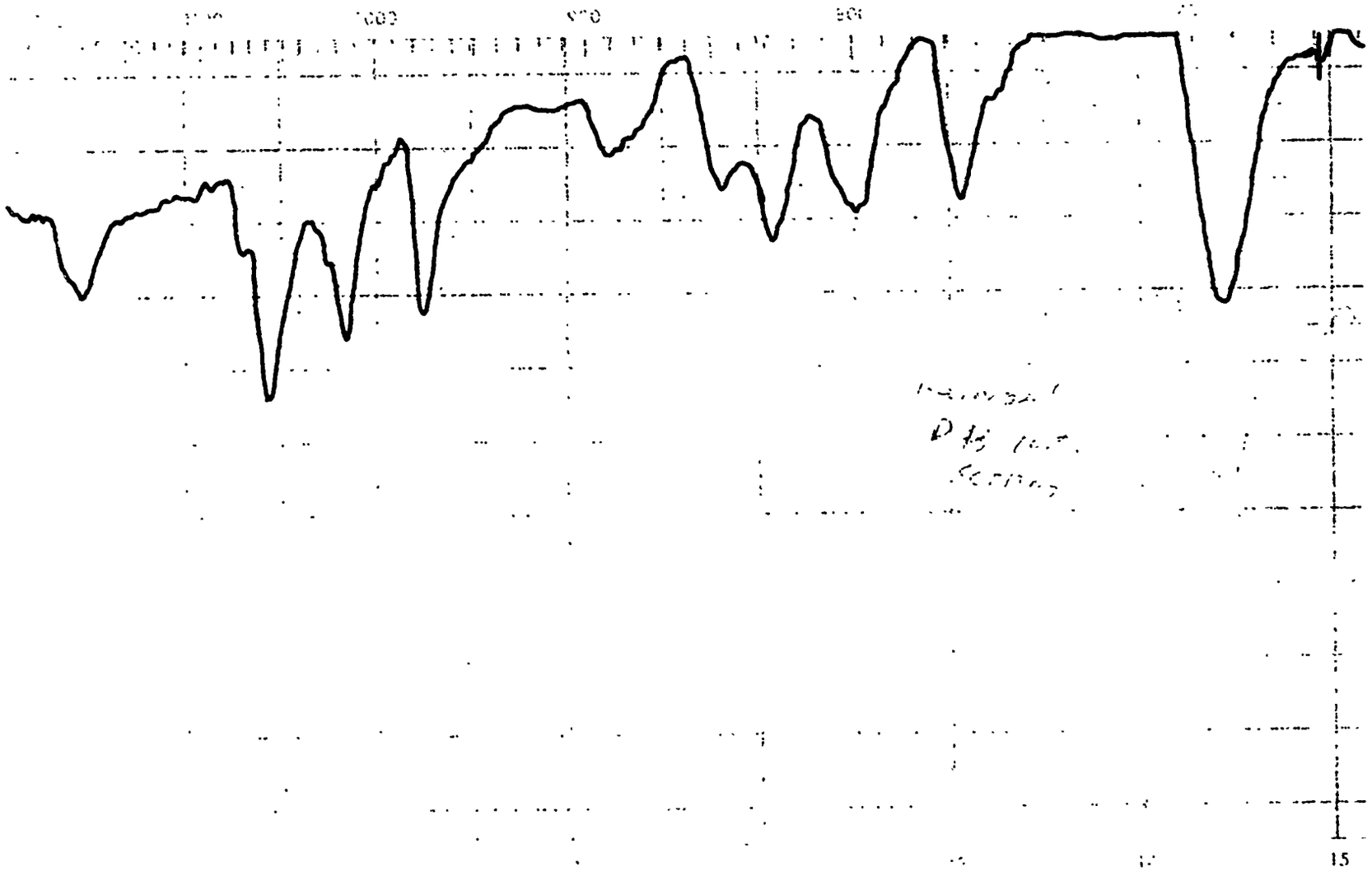

FIGURE D-1 (Continued). Infrared Spectra: Virgin Polyquinoxaline

APPENDIX E

QUASILINEARIZATION COMPUTER PROGRAM

The total computer program used in the computation of kinetic parameters for the two-mode reaction model is included in this appendix. The program is in the form used for computations on polyquinoxaline data.

The values of input information shown in the early part of the program may be called in by read statements similar to those for data input if desired. Definitions of the defined symbols are listed below followed by the program listing.

Input Variables

K: Number of data points

NOI: Number of intervals

SAA(I): Starting time for interval (I)

NPP(I): Number of calculated points in interval (I)

HH(I): Time increments for interval (I)

WO: Initial weight of sample (mg)

WR: Residual weight of sample (mg)

TB(LL): Temperature at which dw/dt = maximum

A(LL): Frequency factor (sec^{-1})

E(LL): Activation energy (cal/mole)

N(LL): Order of reaction

ITRTNS: Number of iterations

WR1: Residual weight associated with the first reaction peak

WO1: Initial weight associated with the first peak

WR2: Residual weight associated with the second peak

WO2: Initial weight associated with the second peak

Main Program Notation

KKK: Number of calculated points

R: Gas constant, 1.987 cal/g mole°K

W(LL,I): Calculated reduced weight for the LL-th peak and the I-th calculated point

WT(I): I-th data point weight value (mg)

TEE(I): I-th data point temperature (°C)

TI(I): I-th data point time (sec)

TEM(I): I-th data point temperature (°K)

TE(I): Temperature corresponding to the I-th calculated point

Y(1,I): Variable in DIFFEQ corresponding to W(LL,I)

X(1,I): Variable in DIFFEQ corresponding to time

JIND: Variable to direct the calculations in FUNCT

KPT: An indexing parameter

WDATA(I): Reduced weight of the I-th data point

WTTT(LL,I): Calculated reduced weight for the LL-th peak corresponding to the I-th data point

WOV(I): Combined reduced weight of the two peaks corresponding to the I-th data point

XLSQR: Sum of the squares of the differences between WDATA(I) and WOV(I)

m: Indexing variable

P(LL,I): Calculated particular solution value for the LL-th peak and the I-th point

H1(LL,I): Calculated homogeneous solution value

H2(LL,I): Calculated homogeneous solution value

PT(LL,I): Calculated particular solution value

HIT(LL,I): Calculated homogeneous solution value

H2T(LL,I): Calculated homogeneous solution value

AMATRX(I,J): Augmented matrix used for solution of simultaneous equations.

```
      QUASILINEARIZATION

C     DETERMINATION OF KINETICS BY QUASILINEARIZATION
      COMMON/555/L(2500),KPT
      DIMENSION WT(250),TLE(250),TI(2500),XX(4),H1T(2,250),H2T(2,250),
     1W(2,2500),P(2,2500),H1(2,2500),H2(2,2500),ST(1),      X(1,2500),
     2Y(1,2500),XDATA(250),F(1),AMATRX(4,5),      YT(1),S(5,1),X(1,5),
     3TEM(250),  PT(2,250),SAA(8),NPP(8),HH(8),
     4WTTT(2,250),A(2),E(2),R(2),          WOV(250),XT(5,250),PN(2)
      COMMON /522/M,E,N,LL,W,R,L,JIN,I,X,TB
      REAL N
      K=194
      ITRTNS=4
      NO1=7
      TB(1)=318.
      TB(2)=973.
      WO=5.225
      WR=3.515
      A(1)=2.98E+22
      E(1)=87015.
      N(1)=3.
      WO1=4.195
      WR1=2.791
      A(2)=4.1E+12
      E(2)=60980.
      N(2)=2.1
      WR2=.724
      WO2=1.09
      SAA(1)=600.
      SAA(2)=800.
      SAA(3)=900.
      SAA(4)=1020.
      SAA(5)=1800.
      SAA(6)=2040.
      SAA(7)=2100.
      NPP(1)=11
      NPP(2)=11
      NPP(3)=11
      NPP(4)=781
      NPP(5)=61
      NPP(6)=51
      NPP(7)=1011
      HH(1)=24.
      HH(2)=36.
      HH(3)=12.
      HH(4)=1.
      HH(5)=3.
      HH(6)=3.
      HH(7)=1.
      KKK=4*10-9
      R=1.987
C     READ IN DATA
```

```
      READ 1, (WT(I),TFE(I),Ti(I),I=1,K)
      DO 99 I=1,K
      TFM(I)=TFE(I)+273.16
   99 CONTINUE
    1 FORMAT (2(1X,3G13.5))
      N1=K-1
      N2=1
C     INTERPOLATE TEM
      DO 88  I=1,N1
      T1=TEM(I+1)-TEM(I)
      T2=T1/10.
      TF(N2)=TEM(I)
      DO87 I2=1,9
      N2=N2+1
      TF(N2)=TEM(I)+T2*I2
   87 CONTINUE
      N2=N2+1
   88 CONTINUE
      TF(N2)=TEM(K)
      DO 77 I=1,K
      WDATA(I)=(WT(I)-WR)/W0
   77 CONTINUE
      W(1,1)=1.-WR1/W01
      W(2,1)=1.-WR2/W02
      R1=W01/W0
      R2=W02/W0
      PRINT 44, (A(LL),E(LL),N(LL),LL=1,2)
   44 FORMAT (//3E20.6//)
      DO 100 LL=1,2
C     CHANGE THE REAL A TO THE DUMMY A USED IN REPARAMETERIZATION
      A(LL)=A(LL)*EXP(-E(LL)/R/TL(LL))
      Y(1,1)=W(LL,1)
      JIND=1
      KPT=0
      DO 21 J=1,W01
      SA=SAA(J)
      NP=NPP(J)
      H=HH(J)
      CALL DIFFEW (SA,JIND,NP,M,7,X,Y,F,XT,IT,S,0)
      DO 3 I=2,NP
      W(LL,I+KPT)=Y(1,I)
    3 CONTINUE
      Y(1,1)=Y(1,NP)
      KPT=KPT+NP-1
   21 CONTINUE
      II=0
      DO 500 I=1,NNK,10
      II=II+1
      WTT(LL,II)=W(LL,I)
  500 CONTINUE
  100 CONTINUE
```

```
      DO 87A I=1,K
      WOV(I)=R1*WTTT(1,I)+R2*WTTT(2,I)
  87A CONTINUE
      XLSQR=0.
      DO 88A JJ=1,K
      XLSQR=XLSQR+(WOV(JJ)-WDATA(JJ))*(WOV(JJ)-WDATA(JJ))
  88A CONTINUE
      PRINT 817
      PRINT 816, XLSQR
      PRINT 818
      PRINT 815,(TEE(KK),WDATA(KK),WOV(KK),WTTT(1,KK),WTTT(2,KK),
     1KK=1,K)
  818 FORMAT (//15H           TEE ,15H          WDATA ,
     1 15H          WOV ,15H          R1 ,15H          R2 //)
  815 FORMAT (5G15.5)
      DO 10 L=1,IIRTNS
      DO 101 LL=1,2
      JIND = 2
      M = 0
      Y(1,1)=X(LL,1)
      KPT=0
      DO 22 J=1,NO1
      SA=SAA(J)
      NP=NPP(J)
      H=HH(J)
C     CALCULATE THE PARTICULAR SOLUTION USING VALUES OF A, E, AND N
C     FOR BOTH PEAKS
      CALL DIFEQ (SA,1,NP,M,.7,X,Y,F,XT,IT,S,0)
      DO 11 I=1,NP
      P(LL,I+KPT)=Y(1,I)
   11 CONTINUE
      Y(1,1)=Y(1,NP)
      KPT=KPT+NP-1
   22 CONTINUE
      II=0
      DO 666 I=1,KKK,10
      II=II+1
      PT(LL,II)=P(LL,I)
  666 CONTINUE
C     CALCULATE THE FIRST HOMOGENEOUS SOLUTION USING VALUES OF A, E, AND
C     N FOR BOTH PEAKS
      JIND =3
      M=0
      Y(1,1)=0.0
      KPT=0
      DO 23 J=1,NO1
      SA=SAA(J)
      NP=NPP(J)
      H=HH(J)
      CALL DIFEQ (SA,1,NP,M,.7,X,Y,F,Y1,YT,S,0)
      DO 12 I=1,NP
```

```
      H1(LL,I+KPT)=Y(1,I)
   12 CONTINUE
      Y(1,1)=Y(1,NP)
      KPT=KPT+NP-1
   23 CONTINUE
C     CALCULATE THE SECOND HOMOGENEOUS SOLUTION USING VALUES OF A, E, AND
C     N FOR BOTH PEAKS
      JIND =4
      M=0
      Y(1,1)=0.0
      KPT=0
      DO 24 J=1,NOA
      SA=SAA(J)
      NP=NPP(J)
      H=HH(J)
      CALL DIFFEQ (SA,1,NP,H,7,X,Y,F,XT,YT,S,G)
      DO 13 I=1,NP
      H2(LL,I+KPT)=Y(1,I)
   13 CONTINUE
      Y(1,1)=Y(1,NP)
      KPT=KPT+NP-1
   24 CONTINUE
      IT=0
      DO 777 I=1,KKK,10
      IT=IT+1
      H1T(LL,IT)=H1(LL,I)
      H2T(LL,IT)=H2(LL,I)
  777 CONTINUE
  101 CONTINUE
C     OPTIMIZE A(1), E(1), A(2), AND E(2) HOLDING N(1) AND N(2) CONSTANT
C  SOLVE LINEAR SIMULTANEOUS EQUATIONS
      DO 18 J=1,4
      DO 18 KK=1,5
      AMATRX(J,KK)=0.
   18 CONTINUE
      DO 19 I=1,K
      XY(1,I)=R1*H1T(1,I)
      XY(2,I)=R1*H2T(1,I)
      XY(3,I)=R2*H1T(2,I)
      XY(4,I)=R2*H2T(2,I)
      XY(5,I)=WDATA(I)-R1*PT(1,I)-R2*PT(2,I)
   19 CONTINUE
      DO 20 J=1,4
      DO 20 KK=J,5
      DO 20 I=1,K
      AMATRX(J,KK)=AMATRX(J,KK)+XY(J,I)*XY(KK,I)
   20 CONTINUE
      DO 210 J=2,4
      J21=J-1
      DO 210 KK=1,J21
      AMATRX(J,KK)=AMATRX(KK,J)
  210 CONTINUE
```

```
      CALL GAUSS (AMATRX,XX,4)
      A(1)=XX(1)
      E(1)=XX(2)
      A(2)=XX(3)
      E(2)=XX(4)
      DO 15 LL=1,2
      DO 15 I=1,KKK
      W(LL,I)=P(LL,I)+A(LL)*W1(LL,I)+E(LL)*W2(LL,I)
      IF (W(LL,I).LT.1.E-5)  W(LL,I)=0.
   15 CONTINUE
      DO 778 LL=1,2
      II=0
      DO 778 I=1,KKK,10
      II=II+1
      WTIT(LL,II)=W(LL,I)
  778 CONTINUE
      DO 801 LL=1,2
      A(LL)=A(LL)*EXP(E(LL)/R/TB(LL))
      PRINT 16, A(LL),E(LL),B(LL)
      A(LL)=A(LL)*EXP(-E(LL)/R/TB(LL))
  801 CONTINUE
   16 FORMAT (//3G15.5//)
      DO 800 I=1,K
      WOV(I)=R1*WTIT(1,I)+R2*WTTT(2,I)
  800 CONTINUE
      XLSQR=0.
      DO 814 JJ=1,K

      XLSQR=XLSQR+(WOV(JJ)-WDATA(JJ))*(WOV(JJ)-WDATA(JJ))
  814 CONTINUE
      PRINT 817
      PRINT 816, XLSQR
  817 FORMAT (/20H      LEAST SQUARES     ,20H      LEAST SQUARES
  816 FORMAT (//1G20.8//)
      PRINT 818
      PRINT 815,(TLE(KK),WDATA(KK),WOV(KK),WTIT(1,KK),WTIT(2,KK),
     1KK=1,K)
   10 CONTINUE
  104 FORMAT  (10H      WDATA     ,13H      WOV       ,
     113H       TI       ,13H       TLE       )
   45 FORMAT (4G15.5)
  227 FORMAT  (8G10.5)
      END


END OF UNIVAC 1106 FORTRAN V COMPILATION.      0 *DIAGNOSTIC* MESSAGE(S)
```

```
      SUBROUTINE DIFFEQ(SA,NE,NP,H,METHOD,X,Y,F,XT,YT,K,KK)
      COMMON/533/TE(2500),KPT
      DIMENSION X(NE,NP),Y(NE,NP),F(NE),XT(NE),YT(NE),K(5,NE),KK(NE,5)
      REAL K,KK
      DO 5 J=1,NE
    5 X(J,1)=SA
      DO 10 L=2,NP
      DO 10 J=1,NE
   10 X(J,L)=X(J,L-1)+H
   90 A2=0.5
      A3=0.5
      B3=0.0
      C3=0.5
      A4=1.0
      B4=0.0
      C4=0.0
      D4=1.0
      AA=1./6.
      BB=1./3.
      CC=BB
      DD=AA
   95 DO 120 L=2,NP
      JJ=KPT+L-1

      CALL FUNCT(F,X(1,L-1),Y(1,L-1),TE(JJ))
      DO 100 J=1,NE
      K(1,J)=H*F(J)
      XT(J)=X(J,L-1)+A2*H
  100 YT(J)=Y(J,L-1)+A2*K(1,J)
      TTT=.5*(TE(JJ)+TE(JJ+1))
      CALL FUNCT(F,XT,YT,TTT)
      DO 105 J=1,NE
      K(2,J)=H*F(J)
      XT(J)=X(J,L-1)+A3*H
  105 YT(J)=Y(J,L-1)+B3*K(1,J)+C3*K(2,J)
      CALL FUNCT(F,XT,YT,TTT)
      DO 110 J=1,NE
      K(3,J)=H*F(J)
      XT(J)=X(J,L-1)+A4*H
  110 YT(J)=Y(J,L-1)+B4*K(1,J)+C4*K(2,J)+D4*K(3,J)
      TTT=TE(JJ+1)
      CALL FUNCT(F,XT,YT,TTT)
      DO 120 J=1,NE
  120 Y(J,L)=Y(J,L-1)+AA*K(1,J)    +BB*K(2,J)+CC*K(3,J)+DD*H*F(J)
  500 RETURN
      END
```

```
      SUBROUTINE FUNCT (F,X,Y,TE)
      DIMENSION F(1),X(1),Y(1),TE(1),W(2,2500),A(2),E(2),N(2),TB(2)
      COMMON /S22/A,E,N,LL,W,R,L,JIND,I,M,TB
      REAL N,NN
      TFB=(TE(1)*TB(LL))/(TB(LL)-TE(1))
      AB=ABS(E(LL)/R/TEB)
      IF (AB. .60.) PRINT 10,E(LL),TE(1),TB(LL),TFB
   10 FORMAT (4G15.5)
      GO TO (1,2,3,4,5), JIND
    1 F(1)=-(Y(1)**N(LL))*A(LL)*EXP(-E(LL)/R/TEB)
      RETURN
    2 M=M+1
      XM=M
      NX=.99+XM/4.
      C=W(LL, X)
      NN=N(LL)-1
      F(1)=-(A(LL)*EXP(-E(LL)/R/TEB)*N(LL)*(C**NN)*(Y(1)-C)+(C**N(LL))
     1*A(LL)*EXP(-E(LL)/R/TEB)*(E(LL)/R/TEB))
      RETURN
    3 M=M+1
      XM=M
      NX=.99+XM/4.
      C=W(LL,NX)
      NN=N(LL)-1
      F(1)=-A(LL)*EXP(-E(LL)/R/TEB)*N(LL)*((C**NN)*Y(1)-(C**N(LL))*EXP(
     1-E(LL)/R/TEB)
      RETURN
    4 M=M+1
      XM=M
      NX=.99+XM/4.
      C=W(LL,NX)
      NN=N(LL)-1
      F(1)=((C**N(LL))*A(LL)*EXP(-E(LL)/R/TEB))/R/TEB
     1-A(LL)*EXP(-E(LL)/R/TEB)*N(LL)*(C**NN)*Y(1)
      RETURN
    5 M=M+1
      XM=M
      NX=.99+XM/4.
      C=W(LL,NX)
      NN=N(LL)-1
    7 RETURN
      END
```

```
      SUBROUTINE GAUSS(A,X,N)
      DIMENSION A(4,5),X(4),RES(4)
      M=N+1
      L=N-1
      DO 12 K=1,L
      JJ=K
      BIG=ABS(A(K,K))
      KP1=K+1
      DO 7 I=KP1,N
      AB=ABS(A(I,K))
      IF(BIG-AB) 6,7,7
    6 BIG=AB
      JJ=I
    7 CONTINUE
      IF(JJ-K)8,10,8
    8 DO 9 J=K,M
      TEMP=A(JJ,J)
      A(JJ,J)=A(K,J)
    9 A(K,J)=TEMP
   10 DO 11 I=KP1,N
      QUOT=A(I,K)/A(K,K)
      DO 11 J=KP1,M
   11 A(I,J)=A(I,J)-QUOT*A(K,J)
      DO 12 I=KP1,N
   12 A(I,K)=0.
      X(N)=A(N,M)/A(N,N)
      DO 14 NN=1,L
      SUM=0.
      I=N-NN
      IP1=I+1
      DO 13 J=IP1,N
   13 SUM=SUM+A(I,J)*X(J)
   14 X(I)=(A(I,M)-SUM)/A(I,I)
      DO 16 J=1,N
      DO 15 I=1,N
   15 RES(J)=A(J,I)*X(I)+RES(J)
   16 RES(J)=A(J,M)-RES(J)
      PRINT 17, (RES(J), J=1,N)
   17 FORMAT (6G20.8)
      DO 18 J=1,N
   18 RES(J)=0.
      RETURN
      END
```

APPENDIX F

Numerical tabulations of the thermogravemetric analysis data are presented in this appendix. Because of the very large number of data points taken from the data output, only selected points are included here.

TABLE F-1

RESULTS OF THERMOGRAVIMETRIC ANALYSIS

Phenolic Run 1-2-1

Time sec	Temp °C	Weight mg	Time sec	Temp °C	Weight mg
0	20.0	9.381	1800	357.0	8.976
160	39.5	9.378	1860	367.0	8.937
220	49.0	9.374	1920	377.0	8.885
280	61.0	9.368	1980	387.0	8.815
350	74.1	9.358	2040	397.0	8.698
420	88.0	9.345	2100	407.2	8.600
480	100.0	9.330	2160	417.5	8.503
550	114.0	9.311	2220	427.5	8.416
600	124.0	9.298	2280	437.5	8.326
660	135.1	9.283	2340	447.3	8.238
720	147.0	9.270	2400	457.0	8.146
780	159.2	9.259	2460	967.0	8.049
860	175.7	9.249	2520	477.0	7.946
920	188.1	9.242	2580	484.0	7.836
970	198.6	9.237	2640	501.0	7.717
1040	213.1	9.229	2700	511.3	7.592
1100	225.4	9.220	2760	521.5	7.465
1160	237.2	9.209	2820	531.2	7.324
1200	245.0	9.199	2880	541.0	7.165
1260	256.1	9.183	2940	551.0	7.018
1320	268.0	9.164	3000	561.0	6.875
1380	278.7	9.145	3120	579.0	6.015
1440	289.5	9.117	3240	597.0	6.402
1500	301.2	9.094	3360	616.0	6.243
1560	313.0	9.071	3600	654.0	5.970
1620	324.0	9.048	3720	673.0	5.861
1680	335.0	9.025	3840	691.0	5.766
1740	346.0	8.997	3960	709.5	5.686

TABLE F-1 (continued)

RESULTS OF THERMOGRAVIMETRIC ANALYSIS

Phenolic Run 1-2-1

Time sec	Temp °C	Weight mg
4080	728.0	5.618
4200	747.0	5.564
4320	764.0	5.521
4440	783.0	5.489
4560	801.5	5.465
4680	820.5	5.447
4800	839.0	5.433
4920	857.0	5.424
5040	876.0	5.415
5160	894.0	5.408

TABLE F-1 (continued)

RESULTS OF THERMOGRAVIMETRIC ANALYSIS

Phenolic Run 1-2-2

Time sec	Temp °C	Weight mg	Time sec	Temp °C	Weight mg
0	20.0	10.539	2580	486.2	8.860
240	52.74	10.521	2700	506.5	8.603
480	99.5	10.458	2820	526.5	8.317
600	123.7	10.424	3000	555.5	7.808
720	147.5	10.396	3120	574.2	7.500
840	171.0	10.376	3240	593.5	7.238
960	195.5	10.359	3360	612.5	7.026
1080	220.0	10.338	3480	631.5	6.854
1200	241.8	10.308	3600	650.0	6.709
1340	271.2	10.259	3720	667.0	6.581
1460	294.3	10.210	3900	696.0	6.420
1590	217.5	10.158	4020	715.0	6.331
1740	345.0	10.093	4140	733.0	6.257
1900	372.3	9.985	4320	760.5	6.172
2000	388.3	9.866	4500	788.0	6.114
2100	405.0	9.704	4800	834.5	6.059
2220	427.0	9.495	5100	879.0	6.031
2340	442.0	9.293	5250	900.9	6.021
2460	466.0	9.087			

TABLE F-1 (continued)

RESULTS OF THERMOGRAVIMETRIC ANALYSIS

Phenolic II Run 1-2-4

Time sec	Temp °C	Weight mg	Time sec	Temp °C	Weight mg
0	23.0	8.474	2880	534.4	7.055
480	95.0	8.428	3000	556.6	6.786
720	141.0	8.397	3120	579.0	6.538
960	191.0	8.380	3240	597.8	6.315
1200	238.1	8.370	3360	616.6	6.135
1440	284.5	8.355	3480	635.4	5.980
1620	317.2	8.338	3600	654.2	5.849
1860	359.6	8.297	3840	693.6	5.630
2100	401.35	8.150	4020	724.5	5.503
2280	430.9	7.948	4260	766.0	5.386
2400	450.6	7.810	4500	800.0	5.311
2520	470.3	7.662	4800	842.5	5.270
2640	490.0	7.490	5100	885.8	5.244
2760	512.2	7.295	5220	903.5	5.236

TABLE F-1 (continued)

RESULTS OF THERMOGRAVIMETRIC ANALYSIS

Phenolic II Run 1-2-5

Time sec	Temp °C	Weight mg	Time sec	Temp °C	Weight mg
1560	22.0	8.849	1900	588.0	6.140
1620	374.0	8.763	1910	588.0	6.125
1680	572.0	7.625	1920	588.0	6.112
1690	572.0	7.435	1930	588.0	6.100
1700	572.0	7.270	1940	588.0	6.090
1210	572.0	7.130	1950	588.0	6.077
1726	572.0	7.010	1960	588.0	6.070
1730	572.0	6.890	1970	588.0	6.059
1740	573.0	6.785	1980	589.0	6.047
1750	573.0	6.696	1990	589.0	6.039
1760	573.0	6.620	2000	589.0	6.032
1770	573.0	6.551	2010	589.0	6.024
1780	573.0	6.492	2020	589.0	6.016
1790	573.0	6.440	2030	589.0	6.008
1800	586.0	6.395	2040	590.0	5.989
1810	586.0	6.355	2070	590.0	5.983
1820	586.0	6.318	2100	591.0	5.964
1830	586.0	6.286	2130	591.0	5.948
1840	586.0	6.257	2160	592.0	5.933
1850	586.0	6.233	2190	592.0	5.921
1860	588.0	6.211	2220	592.0	5.909
1870	588.0	6.190	2250	592.0	5.897
1880	588.0	6.172	2280	590.0	5.888
1890	588.0	6.155	2310	590.0	5.879
			2340	589.0	5.870

TABLE F-1 (continued)

RESULTS OF THERMOGRAVIMETRIC ANALYSIS

Phenolic II Run 1-2-6

Time sec	Temp °C	Weight mg	Time sec	Temp °C	Weight mg
1350	412.0	6.625	1530	454.0	6.210
1360	421.0	6.594	1540	454.0	6.200
1370	427.5	6.555	1550	454.0	6.190
1380	433.0	6.516	1560	455.0	6.181
1390	437.0	6.480	1570	455.0	6.173
1400	441.0	6.446	1580	455.0	6.164
1410	444.0	6.415	1590	455.0	6.153
1420	447.0	6.388	1600	455.0	6.148
1430	449.0	6.365	1610	455.0	6.142
1440	450.0	6.342	1620	455.0	6.134
1450	450.0	6.324	1650	455.0	6.116
1460	451.0	6.301	1680	455.0	6.098
1470	451.0	6.289	1710	454.0	6.083
1480	452.0	6.274	1740	454.0	6.072
1490	452.0	6.259	1770	453.0	6.059
1500	453.0	6.245	1800	452.5	6.047
1510	453.0	6.235	1830	452.5	6.037
1520	453.0	6.221	1860	452.5	6.028

TABLE F-1 (continued)

RESULTS OF THERMOGRAVIMETRIC ANALYSIS

Phenolic II Run 1-2-7

Time sec	Temp °C	Weight mg	Time sec	Temp °C	Weight mg
1380	22.0	5.879	1700	504.5	5.074
1500	433.5	5.705	1710	505.0	5.064
1520	457.0	5.583	1720	505.0	5.051
1540	473.0	5.474	1730	506.0	5.043
1560	483.0	5.385	1740	506.0	5.033
1570	487.0	5.346	1750	506.0	5.023
1580	491.0	5.313	1760	506.0	5.016
1590	494.0	5.284	1770	506.0	5.006
1600	496.5	5.255	1780	506.0	4.999
1610	498.0	5.230	1790	506.0	4.991
1620	500.0	5.204	1800	506.0	4.984
1630	501.0	5.185	1830	506.0	4.965
1640	501.0	5.166	1890	505.0	4.930
1650	502.0	5.148	1920	505.0	4.916
1660	502.0	5.132	1950	505.0	4.903
1670	503.5	5.116	1980	504.0	4.891
1690	504.5	5.085	2010	504.0	4.879
			2040	504.0	4.870

TABLE F-1 (continued)

RESULTS OF THERMOGRAVIMETRIC ANALYSIS

PbI-B Run 2-2-1

Time sec	Temp °C	Weight mg	Time sec	Temp °C	Weight mg
0	22.0	9.369	2640	488.0	8.829
240	49.0	9.362	2760	508.0	8.824
360	71.0	9.343	2880	528.0	8.817
480	94.0	9,313	3000	547.0	8.805
600	117.0	9.277	3120	565.0	8.786
720	142.0	9.241	3240	584.0	8.744
840	165.0	9.207	3360	602.0	8.660
960	189.0	9.18	3480	619.5	8.556
1080	212.5	9.161	3600	639.0	8.475
1200	236.0	9.149	3720	658.0	8.390
1320	260.0	9.143	3840	677.0	8.30
1440	283.0	9.137	3960	695.0	8.206
1560	305.0	9.129	4080	713.5	8.102
1680	327.0	9.117	4200	731.0	7.987
1800	348.0	9.1	4320	749.0	7.868
1920	369.0	9.078	4440	766.5	7.702
2040	389.0	9.047	4560	785.5	7.681
2160	409.5	9.00	4680	803.5	7.620
2280	429.0	8.960	4800	822.0	7.570
2400	449.0	8.88	4920	839.0	7.530
2520	468.5	8 843	5040	856.5	7.496
			5370	904.0	7.387

TABLE F-1 (continued)

RESULTS OF THERMOGRAVIMETRIC ANALYSIS

PBI-A Run 2-2-2

Time sec	Temp °C	Weight mg	Time sec	Temp °C	Weight mg
0	22.5	5.935	3900	689.0	5.332
300	59.	5.915	4020	707.0	5.246
600	118.0	5.831	4110	729.0	5.172
780	154.0	5.811	4200	734.2	5.086
1500	290.0	5.802	4290	747.5	4.997
2100	399.5	5.769	4380	761.0	4.910
2580	478.0	5.724	4500	780.0	4.815
2940	539.0	5.716	4590	793.0	4.761
3210	580.7	5.688	4680	806.8	4.720
3420	614.0	5.595	4860	834.0	4.659
3600	640.5	5.500	5220	887.0	4.570
3720	660.5	5.438	5340	905.0	4.538

TABLE F-1 (continued)

RESULTS OF THERMOGRAVIMETRIC ANALYSIS

Polyquinoxaline Run 3-2-4

Time sec	Temp °C	Weight mg	Time sec	Temp °C	Weight mg
1290	533.0	5.518	1470	516.5	5.467
1310	531.0	5.500	1490	515.0	5.465
1330	529.0	5.496	1510	513.5	5.463
1350	527.0	5.490	1530	512.0	5.461
1370	525.0	5.485	1550	510.3	5.459
1390	523.0	5.481	1570	508.6	5.457
1410	521.0	5.477	1590	507.0	5.455
1430	519.5	5.474	2010	480.0	5.436
1450	518.0	5.472	4230	474.0	5.399

TABLE F-1 (continued)

RESULTS OF THERMOGRAVIMETRIC ANALYSIS

Polyquinoxaline Run 3-2-3

Time sec	Temp °C	Weight mg	Time sec	Temp °C	Weight mg
60	280.0	5.285	1890	608.3	4.053
900	444.5	5.268	2010	626.5	3.976
1230	501.7	5.226	2170	652.4	3.903
1350	521.5	5.148	2330	675.5	3.834
1430	533.5	5.000	2450	693.1	3.779
1470	540.3	4.875	2530	704.5	3.739
1510	547.3	4.739	2610	716.0	3.700
1550	554.3	4.590	2710	731.5	3.657
1590	560.8	4.494	2850	751.8	3.601
1630	567.0	4.400	2970	770.3	3.567
1670	573.4	4.320	3270	814.3	3.516
1730	583.0	4.223			
1790	592.5	4.147			

TABLE F-1 (continued)

RESULTS OF THERMOGRAVIMETRIC ANALYSIS

Polyquinoxaline Run 3-2-6

Time sec	Temp °C	Weight mg
1170	24.0	3.921
1380	449.0	3.822
1440	463.0	3.819
1500	466.0	3.817
1560	466.0	3.816
1620	466.0	3.815
1080	465.0	3.814
1740	464.0	3.813
1860	461.0	3.813
1980	459.0	3.812
2200	458.0	3.811
2320	457.0	3.810
2440	456.0	3.810
2560	455.0	3.809

TABLE F-1 (continued)

RESULTS OF THERMOGRAVIMETRIC ANALYSIS

Polyquinoxaline Run 3-2-5

Time sec	Temp °C	Weight mg
990	24.0	5.386
1230	366.0	5.227
1250	380.0	5.224
1260	386.0	5.223
1290	400.0	5.219
1350	413.0	5.215
1380	417.0	5.214
1410	419.0	5.213
1440	421.0	5.212
1560	419.0	5.210
1680	417.0	5.208
1920	411.0	5.205
2210	406.0	5.204

TABLE F-1 (continued)

RESULTS OF THERMOGRAVIMETRIC ANALYSIS

Polyquinoxaline Run 3-2-7

Time sec	Temp °C	Weight mg	Time sec	Temp °C	Weight mg
1570	27.5	6.644	9000	506.0	5.980
1740	509.0	6.371	9600	506.0	5.954
1800	525.0	6.367	10200	506.0	5.931
1860	527.0	6.363	10800	506.0	5.908
1920	525.0	6.358	11400	506.0	5.887
1980	522.0	6.355	12000	506.0	5.868
2040	520.0	6.351	12600	506.0	5.849
2100	519.0	6.347	13200	506.0	5.833
2400	514.0	6.329	13800	506.0	5.816
3000	508.0	6.295	14400	506.0	5.801
3600	507.0	6.260	15000	506.0	5.788
4200	506.0	6.226	15600	506.0	5.775
4800	506.0	6.193	16200	506.0	5.763
5400	506.0	6.158	16800	506.0	5.750
6000	506.0	6.128	17400	506.0	5.738
6600	506.0	6.095	18000	506.0	5.728
7200	506.0	6.064	18600	506.0	5.718
7800	506.0	6.034	19200	506.0	5.708
8400	506.0	6.005			

TABLE F-1 (Continued)

RESULTS OF THERMOGRAVIMETRIC ANALYSIS

Polyquinoxaline Run 3-2-9

Time sec	Temp °C	Weight mg	time sec	Temp °C	Weight mg
1380	23.0	5.968	1570	647.0	4.530
1420	586.0	5.796	1590	645.0	4.505
1440	614.0	5.725	1610	643.0	4.487
1460	630.0	5.415	1640	641.0	4.468
1490	642.0	4.845	1700	637.0	4.444
1510	646.0	4.695	1860	626.0	4.413
1530	647.0	4.613	2100	617.0	4.393
1550	647.0	4.565	2940	607.0	4.366

TABLE F-1 (Continued)

RESULTS OF THERMOGRAVIMETRIC ANALYSIS

Polyacrylonitrile Run 3-2-8

Time sec	Temp °C	Weight mg	Time sec	Temp °C	Weight mg
1380	22.0	4.891	1680	582.0	4.443
1440	334.0	4.792	1700	582.0	4.388
1460	421.0	4.790	1720	581.0	4.337
1480	479.0	4.787	1240	581.0	4.291
1500	517.0	4.775	1780	580.0	4.220
1530	554.0	4.756	1840	579.0	4.144
1560	571.0	4.730	1910	578.0	4.083
1580	576.0	4.204	2060	575.0	4.018
1600	580.0	4.665	2280	570.0	3.970
1620	581.0	4.618	3000	565.0	3.903
1640	582.0	4.563	3480	564.0	3.883
1660	582.0	4.503			

TABLE F-1 (continued)

RESULTS OF THERMOGRAVIMETRIC ANALYSIS

Advanced Polyquinoxaline Run 3-2-10

Time sec	Temp °C	Weight mg	Time sec	Temp °C	Weight mg
0	22.0	4.197	3440	621.6	3.169
1200	241.0	4.100	3560	640.0	3.069
1560	309.0	4.096	3700	661.0	2.997
1800	351.5	4.092	3800	676.0	2.962
2040	393.0	4.086	3860	685.0	2.941
2400	453.0	4.070	3920	694.0	2.924
2700	503.0	4.049	3990	704.5	2.902
2940	543.0	4.002	4050	714.0	2.883
3050	560.5	3.931	4110	724.0	2.861
3130	572.5	3.800	4180	735.2	2.835
3170	578.5	3.698	4280	750.6	2.796
3210	584.8	3.583	4480	780.2	2.726
3250	591.1	3.476	4740	821.0	2.677
3310	600.6	3.347	5070	870.5	2.643
3370	610.4	3.253	5340	910.0	2.621

TABLE F-1 (continued)

RESULTS OF THERMOGRAVIMETRIA ANALYSIS

Polyphenylene Run 4-2-2

Time sec	Temp °C	Weight mg	Time sec	Temp °C	Weight mg
0	22.0	5.108	240	569.0	4.973
80	387.0	5.082	300	575.0	4.954
100	451.1	5.059	360	376.0	4.942
130	508.0	5.030	420	576.0	4.931
150	531.0	5.017	540	575.0	4.918
180	551.0	5.000	780	573.0	4.897
190	557.0	4.990	2700	564.5	4.836
220	564.2	4.981			

TABLE F-1 (continued)

RESULTS OF THERMOGRAVIMETRIC ANALYSIS

Polyphenylene Run 4-2-3

Time sec	Temp °C	Weight mg	Time sec	Temp °C	Weight mg
0	22.0	5.986	200	606.0	5.770
70	404.0	5.925	210	609.0	5.764
100	506.0	5.871	220	611.0	5.758
130	562.0	5.832	230	612.0	5.753
150	583.0	5.811	240	613.0	5.748
160	590.0	5.801	250	614.0	5.744
170	596.0	5.793	270	615.0	5.737
180	600.0	5.785	300	617.0	5.726
190	604.0	5.778	420	618.0	5.700

TABLE F-1 (continued)

RESULTS OF THERMOGRAVIMETRIC ANALYSIS

Polyphenylene Run 4-2-1

Time sec	Temp °C	Weight mg	Time sec	Temp °C	Weight mg
930	150.0	6.410	4120	66.50	5.941
1530	220.0	6.406	4220	680.0	5.858
2250	359.0	6.355	4300	692.3	5.772
2580	415.0	6.321	4380	705.0	5.678
2880	465.0	6.282	4460	717.7	5.584
3120	504.5	6.250	4560	732.5	5.488
3360	545.5	6.203	4720	756.0	5.394
3520	570.8	6.168	4920	786.0	5.331
3700	599.3	6.122	5160	823.0	5.291
3920	635.0	6.047	5400	857.5	5.273
4020	650.0	6.005	5630	904.0	5.265

TABLE F-1 (continued)

RESULTS OF THERMOGRAVIMETRIC ANALYSIS

Polyimide Run 5-2-1

Time sec	Temp °C	Weight mg	Time sec	Temp °C	Weight mg
1620	319.0	9.443	3420	618.5	7.206
1740	340.5	9.438	3540	632.5	6.695
1860	361.0	9.436	3660	654.5	6.320
1950	382.0	9.430	3780	675.0	6.079
2100	402.5	9.416	3930	698.1	5.891
2220	423.0	9.395	4110	725.9	5.755
2370	447.5	9.353	4290	752.5	5.661
2520	472.3	9.302	4500	784.0	5.579
2670.	497.8	9.230	4680	811.0	5.531
2760	513.0	9.137	4920	840.0	5.489
2910	537.6	8.970	5220	870.0	5.458
3060	562.0	8.633	5430	902.0	5.435
3270	587.1	8.135	5450	920.0	5.421
3360	608.8	7.485			

TABLE F-1 (continued)

RESULTS OF THERMOGRAVIMETRIC ANALYSIS

Polyphenylene Run 4-2-5

Time sec	Temp °C	Weight mg	Time sec	Temp °C	Weight mg
0	22.0	5.233	140	863.0	4.250
60	550.0	5.130	180	884.0	4.230
90	702.0	4.550	240	892.0	4.219
100	760.0	4.350	300	895.0	4.209
120	844.0	4.275	540	895.0	4.178

TABLE F-1 (continued)

RESULTS OF THERMOGRAVIMETRIC ANALYSIS

Polyimide Run 5-2-2

Time sec	Temp °C	Weight mg	Time sec	Temp °C	Weight mg
1550	22.0	5.786	1860	488.0	5.600
1620	39.0	5.724	1890	492.0	5.590
1650	115.0	5.703	1920	495.0	5.581
1680	272.0	5.684	1950	497.0	5.573
1710	359.0	5.665	1980	498.0	5.565
1740	418.0	5.649	2010	498.0	5.557
1770	451.0	5.635	2040	498.0	5.551
1800	470.0	5.622	2100	498.0	5.539
1830	480.0	5.610	2400	495.0	5.496

TABLE F-1 (continued)

RESULTS OF THERMOGRAVIMETRIC ANALYSIS

Polyimide Run 5-3-7

Time sec	Temp °C	Weight mg	Time sec	Temp °C	Weight mg
0	22.0	10.458	380	569.0	9.165
180	539.0	9.925	410	569.5	9.085
200	548.0	9.856	450	570.0	8.997
220	555.0	9.766	510	569.0	8.884
240	560.0	9.685	660	569.0	8.683
260	564.5	9.590	840	569.0	8.517
280	566.0	9.505	1080	568.0	8.349
300	568.0	9.430	1260	5.675	8.250
320	568.0	9.354	1500	567.0	8.140
340	568.0	9.287			
360	568.0	9.224			

TABLE F-1 (continued)

RESULTS OF THERMOGRAVIMETRIC ANALYSIS

Polyimide Run 5-2-6

Time sec	Temp °C	Weight mg	Time sec	Temp °C	Weight mg
0	22.0	7.683	330	596.0	6.404
150	560.0	7.385	360	597.0	6.327
170	574.0	7.245	420	597.0	6.177
190	581.0	7.095	510	595.0	6.034
210	586.5	6.953	600	593.0	5 935
230	590.0	6.835	690	591.0	5.861
250	592.0	6.720	780	589.0	5.800
270	593.5	6.628	900	588.0	5.737
300	596.0	6.507	1020	586.0	5.686

TABLE F-1 (continued)

RESULTS OF THERMOGRAVIMETRIC ANALYSIS

Polyimide Run 5-2-5

Time sec	Temp °C	Weight mg	Time sec	Temp °C	Weight mg
0	23.0	5.489	3600	621.5	4.259
2100	389.5	5.461	3720	639.5	3.970
2280	409.5	5.456	3840	656.3	3.755
2400	430.0	5.444	3960	674.3	3.609
2520	449.5	5.428	4080	693.8	3.503
2840	468.5	5.408	4200	712.0	3.427
2760	487.6	5.381	4320	729.8	3.366
2880	507.8	5.342	4440	747.5	3.315
3000	527.8	5.285	4500	764.5	3.273
3120	546.8	5.190	4680	781.5	3.237
3240	565.5	5.041	5040	834.8	3.154
3360	584.5	4.836	5280	870.0	3.096
3480	603.0	4.563	5520	904.5	3.034

TABLE F-1 (continued)

RESULTS OF THERMOGRAVIMETRIC ANALYSIS

Polyimide Run 5-2-4

Time sec	Temp °C	Weight mg	Time sec	Temp °C	Weight mg
0	23.0	8.322	450	542.0	7.641
240	537.0	7.962	500	541.0	7.595
260	539.0	7.922	540	541.0	7.563
280	540.5	7.884	600	539.5	7.522
300	541.0	7.847	690	538.0	7.473
320	541.0	7.813	810	536.0	7.418
340	541.5	7.780	900	535.0	7.383
360	542.0	7.750	1080	534.0	7.321
400	542.0	7.697			

TABLE F-1 (continued)

RESULTS OF THERMOGRAVIMETRIC ANALYSIS

Polyimide Run 5-2-3

Time sec	Temp °C	Weight mg	Time sec	Temp °C	Weight mg
2400	23.0	8.304	2710	585.0	7.126
2500	493.0	8.165	2730	585.0	7.055
2530	534.0	8.064	2760	586.0	6.960
2550	551.0	7.975	2800	586.0	6.850
2570	563.0	9.865	2850	586.0	6.735
2590	570.0	7.736	2890	586.0	6.658
2610	575.0	7.605	2940	586.0	6.575
2630	579.0	7.486	3000	586.0	6.491
2650	581.0	7.379	3210	585.0	6.279
2670	583.0	7.289	3510	584.0	6.089
2690	584.0	7.205			

APPENDIX G
MASS BALANCE CALCULATIONS

In this appendix the results of elemental analyses conducted on virgin polymers and char residues are utilized to postulate the gaseous species evolved during pyrolysis.

UNCLASSIFIED
Security Classification

DOCUMENT CONTROL DATA - R & D

(Security classification of title, body of abstract and indexing annotation must be entered when the overall report is classified)

1. ORIGINATING ACTIVITY (Corporate author) University of Utah Salt Lake City, Utah 84112	2a. REPORT SECURITY CLASSIFICATION UNCLASSIFIED 2b. GROUP

3. REPORT TITLE

THERMAL DECOMPOSITION OF HIGH-TEMPERATURE RESISTANT POLYMERS

4. DESCRIPTIVE NOTES (Type of report and inclusive dates)
Scientific Interim

5. AUTHOR(S) (First name, middle initial, last name)
Norman W Burningham
J D Seader

6. REPORT DATE July 1970	7a. TOTAL NO. OF PAGES 286	7b. NO. OF REFS 50
8a. CONTRACT OR GRANT NO. F44620-68-C-0022 b. PROJECT NO. 9561 c. 61102F d. 681308	9a. ORIGINATOR'S REPORT NUMBER(S) UTEC TH 70-085 9b. OTHER REPORT NO(S) (Any other numbers that may be assigned this report) AFOSR 70-1936TR	

10. DISTRIBUTION STATEMENT
This document has been approved for public release and sale; its distribution is unlimited.

11. SUPPLEMENTARY NOTES TECH, OTHER	12. SPONSORING MILITARY ACTIVITY AF Office of Scientific Research (SREP) 1400 Wilson Boulevard Arlington, Virginia 22209

13. ABSTRACT

During this research work, the thermal response of several test materials was characterized by isothermal and dynamic thermogravimetric analysis. Pyrolysis gas analysis, infrared spectra analysis and elemental analysis were employed also to formulate a description of the thermal-degradation reaction. A new, systematic approach to the determination from dynamic TGA data of kinetic parameters describing pyrolysis was developed. The specific polymeric materials selected for evaluation in this program were chosen from those representing the forefront of high-temperature polymer technology. Samples of linear para-polyphenylene, polybenzimidazole, polyimide, phenylated polyquinoxaline and phenolic resins were tested.

In TGA experiments, material samples ranging in weight from 3 to 9 mg were heated in both flowing and non-flowing helium environments. In separate experiments, gaseous products of isothermal decomposition were collected and analyzed by the techniques of gas chromatography.

In order to overcome the limitations and inaccuracies of generally employed methods of TGA-data analysis, the quasilinearization numerical technique was introduced. This powerful analytical tool used data points directly and computed kinetic parameters based on a least-squares-optimized fit of the data. In this way, pyrolysis kinetic parameters were determined for polyphenylene, polyimide and polyquinoxaline. Similar parameters were not determined for phenolic and polybenzimidazole resins since the analytical method was not sufficiently developed to permit handling of their complex thermograms.

UNCLASSIFIED
Security Classification

KEY WORDS	LINK A		LINK B		LINK C	
	ROLE	WT	ROLE	WT	ROLE	WT
Thermal Decomposition						
High-Temperature Resistant						
Polymers						